Integrated Target Tracking and Weapon Guidance

Thesis submitted in accordance with the requirements of
the University of Liverpool for the degree of Doctor in Philosophy
by
James M. Davies

June 2013

Abstract

The requirements of a modern guided weapon will be established based on the current and perceived threats at the time the design is commissioned. However the design of a modern guided weapon is a long and expensive process which can result in the weapon entering service only for the original threat to have changed or passed, inevitably inducing a capability gap. The defence budgets of the major military powers such as the UK and USA continue to shrink. As a result the emphasis of military research is being placed on adapting current legacy systems to bridge these capability gaps. One such gap is the requirement to be able to intercept small relocatable, highly manoeuvrable targets.

It was demonstrated a number of years ago that the performance of a legacy weapon against manoeuvring targets could be potentially increased by retrofitting a data link to the weapon. The data link allows commands to be sent to the weapon in flight. The commands will result in the weapon executing one or more manoeuvres which will change the shape of the trajectory. This has the potential to improve the performance of current Advanced Anti-Armour Weapons (AAAW) against manoeuvring targets.

The issue which arises from data linking any weapon including an AAAW, is that the ability to shape the trajectory of the weapon will be limited due to the original design parameters of the non data linked system. Therefore in order to obtain the maximum performance increase, the trajectory shaping (retargeting) capability must be efficiently utilised over the duration of the weapon fly out.

It was postulated in this thesis that this could be achieved using an integrated fire control system which would seek to calculate an optimal shaped weapon trajectory. The optimal trajectory should maximise the ability of the weapon to respond to target manoeuvres, thereby improving the probability of a successful intercept occurring.

The potential effectiveness of an integrated fire control system was explored by

considering the scenario of a generic data linked AAAW which is to intercept a small highly manoeuvrable surface vessel.

A total of three integrated fire control systems were developed which calculated the optimal trajectory for different criteria.

The first system optimised the weapon trajectory considering multiple predicted target trajectories. Each trajectory had an associated probability. For a given weapon trajectory the seeker would be able to detect the target at one or more locations along certain predicted target trajectories. The sum of the probabilities associated with the detectable locations represented the total probability of intercept. The weapon trajectory was optimised by calculating the trajectory which achieved the maximum probability of intercept using simulated annealing and simple search optimisation algorithms.

The second system optimised the weapon trajectory considering only the most probable trajectory (M.P.T) from a distribution of predicted target trajectories. Appropriate commands were calculated such that a location along this M.P.T trajectory was detectable at some instant in time.

The third system presented in this thesis optimised the trajectory considering the maximum probability of intercept initially and then only the M.P.T trajectory later on in the engagement.

The three integrated systems and a Fire and Forget system were tested against 80 random target trajectories. In each of the integrated fire control systems, the performance of the AAAW against manoeuvring targets was significantly improved when compared to the Fire and Forget results.

Contents

List of Figures

List of Tables

List of Abbreviations

A.T.T	Able to Transmit
Bo	Boost Guidance Phase
C.T.L	Coordinated Turn Left
C.T.R	Coordinated Turn Right
C.V	Constant Velocity
D	Target Detectable
I.B.M	Intercept Before Manoeuvre
I.F.T.R	Inflight Trajectory Revision
Mi	Midcourse Guidance Phase
M.T	Manoeuvring Target
N.D	Not Detectable
N.A.T	Not Able to Transmit
N.M	Non Manoeuvring Target
M.P.T	Most Probable Trajectory
P.S.A	Predicted Scan Area
W.I	Weapon Initialisation
W.T	Weapon Terminal Guidance

S.A	Simulated Annealing
S.A.S.S	Simulated Annealing and Simple Search
S.A.M.P.T	Simulated Annealing and Most Probable Trajectory
S.S	Simple Search

Acknowledgements

I would like to thank my supervisor Dr Jason Ralph for his support, advice and encouragement for the duration of my PhD as well as the introduction to some excellent single malts.

Special thanks go to Dr Neil Oxtoby whose support and words of wisdom through the first two years of the PhD helped me to progress through some of the most difficult aspects of the research.

I am also grateful to Dr Ralph and the Department of Electrical Engineering for their financial support.

Last but not least, I would like to thank my parents for there support over the past 24 years, which has led me to achieve my goals.

Chapter 1

Introduction

World War II saw the first operational use of a guided weapon, when the German Luftwaffe successfully deployed the Fritz X radio controlled bomb against the Italian Battleship Roma on the 21st July 1943. The Fritz X was equipped with moveable control surfaces, which could be deflected by an operator sending control signals over a radio link. By deflecting the control surfaces the bomb could be steered onto the target thereby increasing the probability of a successful strike [1].

In the 70 years since the deployment of the Fritz X, guided weapon technology has advanced rapidly with an assortment of weapons being developed to fulfil a variety of roles and operational requirements across a wide range of launch platforms. The configuration of a guided weapon depends on a number of factors such as the desired weapon stand off range, operating conditions and launch platform.

For example, the Storm Shadow missile was developed as a long range, air launched cruise missile, which is deployed against high value targets. The long stand off range (maximum range at which the weapon can be launched such that it can reach its intended target [2]) allows the aircraft to engage a target beyond the engagement range of enemy air defence systems thereby increasing the survivability of the launch platform itself [3]. Another example of a guided weapon is the Sea Wolf missile system which is designed as a last resort naval point defence weapon to destroy enemy ships, aircraft and missiles [4].

The design of a new guided weapon can be incredibly expensive, with the weapon often taking many years to enter service after the initial specification was established. The specification will have been developed based on the current and anticipated threats and associated requirements at the time that the design was commissioned. However, the long design process of many systems can often result in the weapon entering service when the threat that was originally anticipated

has changed or disappeared.

The Brimstone Missile system for example, was originally selected to meet the RAF requirement for a long range Anti-Armour Weapon in 1997. This requirement was identified from the substantial use of tanks and armoured vehicles by Iraq forces during the 1st Gulf War. However the weapon only entered into service in 2005 after a development cost of £370 million [5], by which time the Gulf War was over.

Over the past few years a requirement to be able to intercept highly manoeuvrable relocatable targets has emerged [6], especially within Naval operations as demonstrated by the emergence of the small boat threat [7]. As the defence budgets of prominent military powers such as the UK and the USA continue to shrink, greater emphasis is being placed on adapting current legacy systems to respond to new operational requirements such as these.

In 2006, an Enhanced Paveway II (ePwyII) bomb was fitted with a data link and released from a Tornado GR4 aircraft [8]. In a standard ePwyII bomb the weapon would have followed a trajectory to a preset target location. The trajectory flown by the weapon would have been governed by the onboard guidance system.

However in this weapon trial the target co-ordinates where updated in flight using the data link. The bomb would then have performed one or more manoeuvres thereby changing the shape of its trajectory in order to reach the updated target location. The trial was successful, with the weapon successfully flying to the updated target location.

The demonstrated ability to shape the trajectory of an inflight data linked weapon has the potential to significantly increase the performance of some legacy systems to intercept highly manoeuvrable targets. One possible candidate for this type of approach is the Advanced Anti-Armour Weapon (AAAW).

Research is currently being conducted in the UK S.P.E.A.R program to add a data link to this type of weapon [9]. The issue which arises from data linking any weapon including an AAAW, is that the ability to shape the trajectory of the weapon will be limited due to the original design parameters of the non data linked system. Therefore in order to obtain the maximum performance increase, the trajectory shaping (retargeting) capability must be efficiently utilised over

the duration of the weapon fly out (maximum flight time of the weapon).

It is postulated in this thesis that this can be achieved through the use of an integrated fire control system. The system will seek to calculate an optimal shaped weapon trajectory which should maximise the ability of the weapon to respond to target manoeuvres thereby improving the probability of a successful interception occurring.

The potential effectiveness of an integrated fire control system is explored by considering the scenario of a generic data linked AAAW which is to intercept a small agile highly manoeuvrable surface vessel.

1.1 Structure of thesis

This thesis is divided into seven chapters :

- Chapter 2 - Weapon Model, describes the fundamental concepts associated with tactical missile design and the specification of the AAAW model.
- Chapter 3 - The Small Boat Threat, discusses a realistic target model representative of a small boat threat. A performance evaluation of the AAAW as a Fire and Forget system using 80 random target trajectories is provided.
- Chapter 4 - Integrated Tracking and Trajectory Prediction, describes the design and implementation of an integrated tracking and target trajectory prediction system
- Chapter 5 - Integrated System One (S.A.S.S), describes the design, implementation and results of the first integrated fire control system to be discussed in the thesis.
- Chapter 6 - Integrated System Two (M.P.T), describes the design, implementation and results of the second integrated fire control system to be discussed in the thesis.
- Chapter 7 - Integrated System Three (S.A.M.P.T), describes the design, implementation and results of the final integrated fire control system to be discussed in the thesis.
- Chapter 8 - Summary and Conclusions, presents a summary of the work discussed in this thesis. A number of conclusions from the results of this thesis are produced. Recommendations for further work are then provided.

1.2 Original contributions of this thesis

The contribution of this thesis is to demonstrate that an integrated fire control system can significantly improve the performance of a weapon against manoeuvring targets.

Though the focus of the research is the scenario of an AAAW intercepting a small boat, the techniques and systems discussed in the thesis can potentially be applied to a wide range of targets and weapon systems.

The results of this study are also relevant to current industrial programmes which are seeking to use Advanced Anti-Armour Weapons to intercept small boats [10].

Chapter 2

Weapon Model

The research discussed in this thesis is based around a fixed launcher Advanced Anti Armour Weapon (AAAW) which is simulated using the Matlab programming language. The AAAW model is classed as a tactical missile. The details surrounding the model itself and the justification for its selection in this particular project will become apparent later on in the chapter. However many of the concepts and much of the terminology surrounding tactical missiles will be unknown to the non expert. Therefore the purpose of this chapter is firstly to present a brief overview of these fundamental concepts such as aerodynamics, weapon guidance and control and rocket propulsion and then to outline the specifics of the model and its role within this research project, beginning with the definition of a missile.

2.1 The Main Components of a Tactical Missile

A missile can be defined as a self propelled aerospace vehicle designed for the purpose of inflicting damage on a designated target [11]. There are two main classes, strategic and tactical. Strategic missiles are long range weapons designed to inflict a significant amount of damage onto a target, with the most widely recognised form of strategic missile being the intercontinental ballistic missile (ICBM), which carries a high yield nuclear warhead. Tactical missiles are generally much smaller weapons, carrying conventional warheads and are used against specific threats such as aircraft, ships and enemy missiles.

The main components of a tactical missile consist of, the airframe and external control surfaces, payload, guidance computer and propulsion system. Tactical missiles are normally classified by their launch platform and intended target. Examples include, Air-to-Air such as the ASRAAM Advanced Short Range Air-to-Air missile [12] and Air-to-Surface, such as the Storm Shadow [3] air launched

cruise missile.

The AAAW model is of the tactical class, which having a fixed launcher system will always be launched at the same pitch, yaw (heading) and roll for each engagement. By considering a fixed launcher, the performance of the integrated fire control systems discussed in later chapters is then dependent only on the missile sizing and associated aerodynamic capability and the quality of the weapon trajectory optimisation methods.

2.2 Basic Aerodynamics and Fundamental Concepts

A dynamic model describes the motion of the missile within one or more degrees of freedom. Each degree of freedom describes either the translational or rotational motion of the airframe. The number of degrees of freedom used depends on the specific application of the model. The greater the number of degrees of freedom which are used to describe the motion, the more computationally intensive the model will be. This will be due to the increased number of equations required to be solved to model the airframe dynamics. The choice of model is therefore determined based on the user's requirements.

The dynamics of a missile airframe are normally modelled assuming rigid body dynamics [13] which for general spatial motion results in three translational and three rotational degrees of freedom. This is known as a Six Degrees of Freedom (6DoF) model.

In a 6DoF model the translational motion is described as translation in (X, Y, Z) with the rotational motion defined in terms of three angles (pitch θ, heading ψ and roll ϕ). However if only the longitudinal motion of the weapon was of interest e.g. in an assumed planar engagement, then the dynamics could be modelled using a 3DoF model [14], considering only the translation of the airframe in the X and Z axis and the weapon pitch.

Different combinations of translational and rotational motion can be used to define a variety of dynamic models. An overview of the most common dynamic models used in missile simulation today can be found in [15].

In this thesis the weapon is required to intercept a target which moves within the XY plane. The simulated engagements are therefore non planar, requiring

both longitudinal and lateral guidance commands to be generated. The weapon is a roll, stabilised missile, requiring roll stabilisation commands to be generated by the guidance computer. Therefore a full 6DoF model is required to model the motion of the missile airframe using three translational and three rotational degrees of freedom.

A 6DoF model requires the rate of change of both the translational and rotational degrees of freedom to be determined. The associated variables for the translational and rotational movement are the translational velocities and accelerations and the Euler angle rates.

The translational velocities (v_x, v_y, v_z) and accelerations (a_x, a_y, a_z) are relatively simple to determine, they are the first and second time derivatives of the airframe position in 3DoF. The Euler angle rates $(\dot{\psi}, \dot{\theta}, \dot{\phi})$ (defined in Earth-orientated axes) however are more complicated to determine. The Euler rates are functions of the angular velocities (P, Q, R) (defined in body orientated axes) and the weapon attitudes. The Euler rates are calculated using the following equations [16] :

$$\dot{\phi} = P + Q \sin\phi \tan\theta + R \cos\varphi \tan\theta. \tag{2.1}$$

$$\dot{\theta} = Q \cos\phi - R \sin\phi. \tag{2.2}$$

$$\dot{\psi} = Q \frac{\sin\psi}{\cos\theta} + R \frac{\cos\psi}{\cos\theta} \tag{2.3}$$

The dynamics of the missile are dependent on the aerodynamic forces and moments which act on the airframe during flight. The aerodynamic forces as well as the moments are produced by the variations in pressure and velocity due to the flow of air around the missile. The propulsive force (i.e thrust) is generated from the propulsion system on the missile.

In a 6DoF model, the aerodynamic forces are summed to produce the resultant aerodynamic force. The resultant aerodynamic force is resolved into parallel and perpendicular components to the direction of the free stream velocity, where the free stream velocity is defined as the velocity of the airflow (whose direction is parallel and opposite to the forward direction of flight) far ahead of the missile such that the air is not affected by the motion of the missile in the opposite direction [11]. The parallel and perpendicular components of the resultant force define three forces known as the Drag, Lift and Side Forces.

The **Drag** force is produced by the pressure and skin forces which act on the surface of the missile. It acts parallel to the free stream velocity [11].

The **Lift** force is produced by the pressure forces acting on the surface of the missile. It acts perpendicular to the velocity vector of the missile and to the free stream [11].

The **Side Force** is the component of the resultant aerodynamic force which acts perpendicular to the lift and drag forces [11].

Three moments consisting of the **Pitching**, **Yawing** and **Rolling** moments are also defined which are created by varying the aerodynamic load distribution on the airframe using a control scheme.

2.3 Axes Systems

There are three important axes systems which are used within missile flight simulation consisting of the Earth, Body and Wind axis systems.

The **Earth** axes is a right handed system [11] which is used to determine the true position of the missile at every time step during the simulation. The X and Y axes lie in the horizontal plane (X_e, Y_e), with the Z axis pointing vertically down in the direction of gravity (Z_e). The Earth axes system [17] is shown in Figure 2.1.

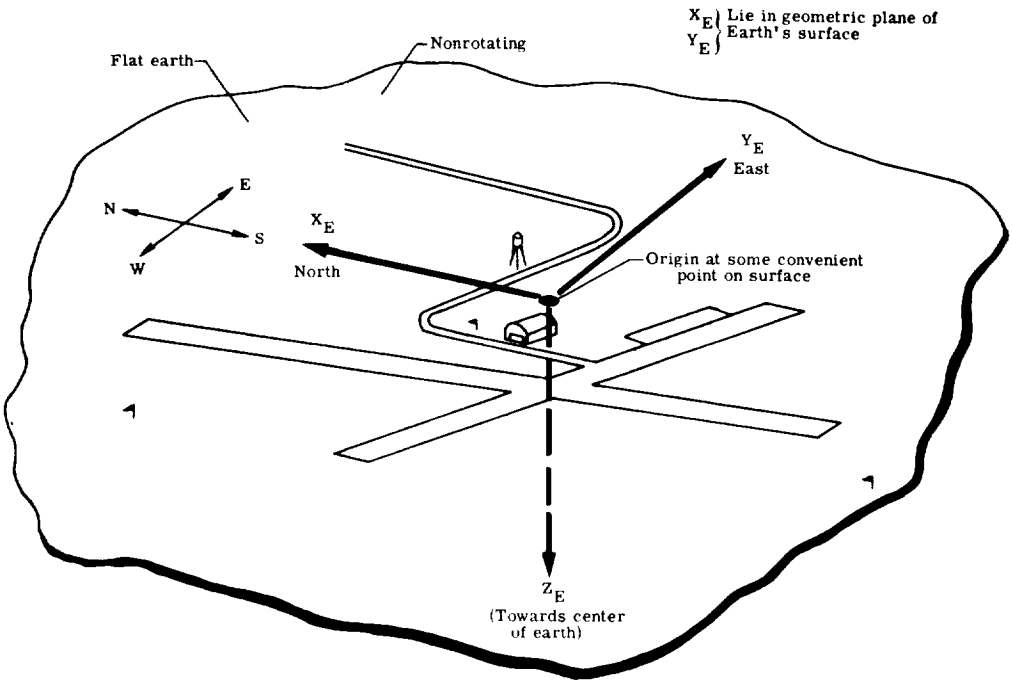

Figure 2.1: Earth Axes

The missile **Body** axes is a right handed system which is used for calculating the aerodynamic forces and moments, with an origin defined by the missile centre of gravity. The X axis coincides with the longitudinal axis of the missile (X_b). The positive Y axis is positive to the right and lies perpendicular to the X axis (Y_b). The Z axis is positive downwards (Z_b) and is perpendicular to the XY plane.

Three rotations are also defined within this axes system, which are known as the Roll ϕ, Pitch θ and Yaw ψ.

1. Roll is a rotation about the X_b axis.
2. Pitch is a rotation about the Y_b axis.
3. Yaw is a rotation about the Z_b axis.

The Body axes system [17] is shown for a generic aircraft in Figure 2.2.

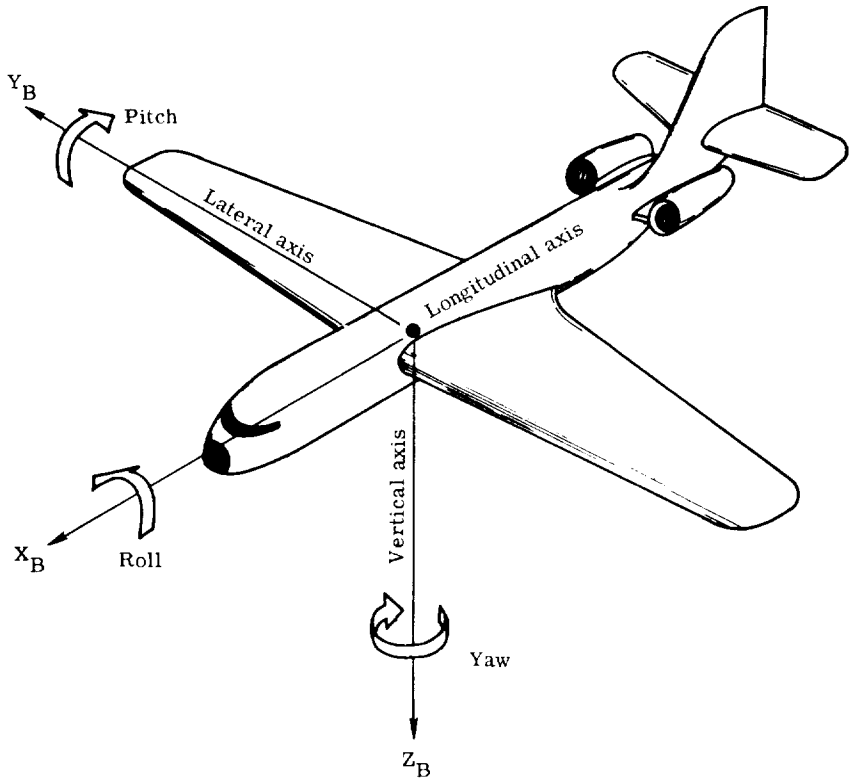

Figure 2.2: Body Axes

The **Wind** axes is right handed system which is used for the calculation of aerodynamic coefficients. The X axis in the system is positive in the direction of the free stream X_w. The Y axis is perpendicular to the X axis and positive to the right of the X axis Y_w and the Z axis is positive downwards perpendicular to the XY plane Z_w. The missile/aircraft centre of gravity lies at the origin of the axes system. The Wind axes is shown in Figure 2.3 [17].

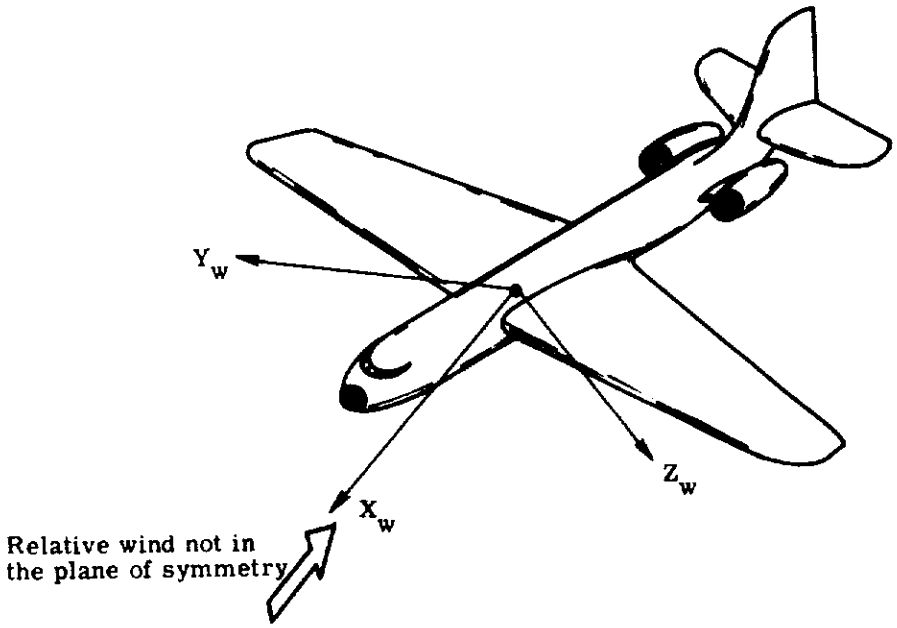

Figure 2.3: Wind Axes

During the missile simulation, variables such as the position and velocity in the Earth axes will be transformed into the Body axes position and velocity and vice versa. This is accomplished by multiplying the defined missile position vector in the Earth axes by rotation matrices in heading, pitch and roll about the body X axis, Y axis and Z axis respectively. Rotations in heading (ψ), pitch (θ) and roll (ϕ) are calculated as follows [13] :

$$\begin{pmatrix} X' \\ Y' \\ Z' \end{pmatrix} = \begin{pmatrix} \cos\psi & \sin\psi & 0 \\ -\sin\psi & \cos\psi & 0 \\ 0 & 0 & 1 \end{pmatrix} \begin{pmatrix} X \\ Y \\ Z \end{pmatrix} \tag{2.4}$$

$$\begin{pmatrix} X' \\ Y' \\ Z' \end{pmatrix} = \begin{pmatrix} \cos\theta & 0 & -\sin\theta \\ 0 & 1 & 0 \\ \sin\theta & 0 & \cos\theta \end{pmatrix} \begin{pmatrix} X \\ Y \\ Z \end{pmatrix} \tag{2.5}$$

$$\begin{pmatrix} X' \\ Y' \\ Z' \end{pmatrix} = \begin{pmatrix} 1 & 0 & 0 \\ 0 & \cos\phi & \sin\phi \\ 0 & -\sin\phi & \cos\phi \end{pmatrix} \begin{pmatrix} X \\ Y \\ Z \end{pmatrix} \tag{2.6}$$

The Earth coordinate system to Body coordinate system transformation matrix T_e^b is then expressed as the multiplication of the following matrices [15]:

$$\left(T_e^B\right) = \begin{pmatrix} 1 & 0 & 0 \\ 0 & \cos\phi & \sin\phi \\ 0 & -\sin\phi & \cos\phi \end{pmatrix} \begin{pmatrix} \cos\theta & 0 & \sin\theta \\ 0 & 1 & 0 \\ \sin\theta & 0 & \cos\theta \end{pmatrix} \begin{pmatrix} \cos\psi & \sin\psi & 0 \\ -\sin\psi & \cos\psi & 0 \\ 0 & 0 & 1 \end{pmatrix} \tag{2.7}$$

The axes systems used in the weapon model assumes that the earth is flat and static. While both of these assumptions are approximate, they only become a

problem if distances are long, i.e if the trajectory of an ICBM was to be determined the curvature of the earth and its rotation would have to be considered. The Advanced Anti Armour Weapon model used in this thesis has a range of less than 11000m therefore these approximations are acceptable.

2.4 Aerodynamic Force and Moment Equations

The forces and moments which act on the missile airframe, are calculated using the equations of motion for a rigid body. The use of a rigid airframe model is an approximation. An actual missile would flex slightly during flight. However the error induced in the calculated values for the forces and moments will only be very small as missiles are designed to withstand high lateral G-forces [13]. The use of a rigid body simplifies the calculation of the forces and moments considerably.

The **Drag** (F_x), **Side** (F_y) and **Lift** (F_z) forces are defined mathematically as [18] :

$$F_x = -qS(C_D \cos\alpha \cos\beta + C_Y \cos\alpha \sin\beta - C_L sin\alpha) - mg \sin\theta + T. \tag{2.8}$$

$$F_y = -qS(C_D \sin\beta - C_Y \cos\beta) + mg \cos\theta \sin\varphi. \tag{2.9}$$

$$F_z = -qS(C_D \sin\alpha \cos\beta + C_Y \sin\beta + C_L \cos\alpha) + mg \cos\varphi. \tag{2.10}$$

where :

q = Dynamic Pressure (Pa)

S = Reference Area (m^2)

T = Thrust (N)

m = Mass of the weapon (kg)

g = Gravity constant of 9.81 (m/s^2)

α = Angle of attack (rads)

β = Angle of side slip (rads)

C_D = Aerodynamic drag coefficient defined in the wind axis (dimensionless)

C_Y = Aerodynamic side force coefficient defined in the wind axis (dimensionless)

C_L = Aerodynamic lift coefficient defined in the wind axis (dimensionless)

The **Pitching** (M), **Yawing** (N) and **Rolling** (L) moments are defined as [18] :

$$M = qSbC_m. \tag{2.11}$$

$$N = qSbC_n. \tag{2.12}$$

$$L = qSbC_l. \tag{2.13}$$

where :

b = Reference length (m)

C_m = Aerodynamic pitching moment coefficent (dimensionless)

C_Y = Aerodynamic yawing moment coefficient (dimensionless)

C_L = Aerodynamic rolling coefficient (dimensionless)

The mathematical representation of the forces and moments has introduced a number of important quantities which must be properly defined and calculated such as, the definition of the reference area and length, the calculation of the dynamic pressure and angles of attack and side slip. The remainder of this section will provide a brief description of each of the quantities defined in the force and moment equations beginning with the reference area and reference length.

The **reference area** (S) for a missile is defined as the body cross-sectional area and the **reference length** (b) is defined as the mean missile diameter [19]. Conventionally for an aircraft model, the reference area is defined as a wing plan form area and the reference length is defined as the wingspan for the calculation of the lifting and yawing moments and the mean aerodynamic chord for the calculation of the pitching moment.

The **dynamic pressure** (q) is calculated from the total airspeed (V_a) and the atmospheric air density (ρ) in kg/m^3 at a height (h in metres) as follows [16] :

$$q = \frac{1}{2}\rho V_a^2 \tag{2.14}$$

The atmospheric air density is defined as [16] :

$$\rho = 1.225(1 - 2.18 \times 10^{-5}h)^{4.2586}. \tag{2.15}$$

The total airspeed is calculated as :

$$V_a = \sqrt{(u - u_g)^2 + (v - v_g)^2 + (w - wg)^2} \tag{2.16}$$

where (u, v, w) are the components of the missile velocity vector and (u_g, v_g, w_g) are the components of the local wind velocity vector.

In order for aerodynamic lift to be generated by the missile, it must achieve an angle of attack [15]. The **angle of attack** α is defined as :

$$\alpha = \arctan\left(\frac{w - w_g}{u - u_g}\right) \tag{2.17}$$

The **angle of sideslip** β can be thought off as the directional angle of attack and is calculated from the body X axis and the wind corrected velocity vector as follows :

$$\beta = \arcsin\left(\frac{v - v_g}{V_a}\right) \tag{2.18}$$

The angles of attack and sideslip appear in the force equations because the aerodynamic coefficients for Drag, Lift and Side force are often determined in the wind axes, however the force equations are solved within the body axes. The angles of attack and sideslip are used to correctly express the force coefficients in terms of the body axes instead of the wind axes

The **Aerodynamic coefficients** are used to calculate the aerodynamic forces and moments which act on the missile in flight [15]. They can be calculated from wind tunnel measurements or using analytical methods. The most common analytical method is to calculate stability derivatives which predict how the forces and moments which act on the airframe change as stability parameters such as the angle of attack are varied.

2.4.1 Calculation of Aerodynamic Coefficients

Each aerodynamic coefficient is defined by a set of stability derivatives which can be defined using a first order Taylor series expansion about a trim flight condition. A trim flight condition is a flight condition whereby the forces and moments on the missile sum to zero. The stability derivatives are then determined by considering all of the possible relationships which may exist between the force and moment coefficients and the parameters which affect the stability of the airframe, such as the angles of attack and sideslip. Before defining the aerodynamic coefficients, the calculation of a first order Taylor expansion [20] for a multivariate function is reviewed below :

1. Consider a real valued function in two variables $f(x, y)$ which is expanded about the points (a, b) respectively.

2. The Taylor series expansion of the first order would then be defined as :

$$f(x,y) = f(a,b) + \left[(x-a)\frac{\partial f}{\partial x} + (y-b)\frac{\partial f}{\partial y}\right] \tag{2.19}$$

3. If $a = 0$ and $b = 0$, then the expansion becomes :

$$f(x,y) = f(0,0) + \left[(x)\frac{\partial f}{\partial x} + (y)\frac{\partial f}{\partial y}\right] \tag{2.20}$$

4. This can be more compactly defined as :

$$f(x,y) = f_0 + f_x x + f_y y \tag{2.21}$$

The equations for each aerodynamic coefficient can then be defined as :

$$\begin{aligned} C_D = {} & C_{D_0} + C_{D_\alpha}\alpha + C_{D_\beta}\beta + C_{D_{\delta_p}}\delta_p + C_{D_{\delta_q}}\delta_q + C_{D_{\delta_r}}\delta_r + C_{D_{\delta_x}}\delta_x + ... \\ & C_{D_{\alpha^2}}\alpha^2 + C_{D_{\beta^2}}\beta^2 + C_{D_{\delta_p^2}}\delta_{p^2} + C_{D_{\delta_q^2}}\delta_{q^2} + C_{D_{\delta_r^2}}\delta_{r^2} + C_{D_{\delta_x^2}}\delta_{x^2} + ... \\ & \frac{S}{2V_a}[C_{D_{\dot\alpha}}\dot\alpha + C_{D_{\dot\beta}}\dot\beta + C_{D_p}P + C_{D_q}Q + C_{D_r}R] \end{aligned} \tag{2.22}$$

$$\begin{aligned} C_Y = {} & C_{Y_0} + C_{Y_\alpha}\alpha + C_{Y_\beta}\beta + C_{Y_{\delta_p}}\delta_p + C_{Y_{\delta_q}}\delta_q + C_{Y_{\delta_r}}\delta_r + C_{Y_{\delta_x}}\delta_x + ... \\ & C_{Y_{\alpha^2}}\alpha^2 + C_{Y_{\beta^2}}\beta^2 + C_{Y_{\delta_p^2}}\delta_{p^2} + C_{Y_{\delta_q^2}}\delta_{q^2} + C_{Y_{\delta_r^2}}\delta_{r^2} + C_{Y_{\delta_x^2}}\delta_{x^2} + ... \\ & \frac{S}{2V_a}[C_{Y_{\dot\alpha}}\dot\alpha + C_{Y_{\dot\beta}}\dot\beta + C_{Y_p}P + C_{Y_q}Q + C_{Y_r}R] \end{aligned} \tag{2.23}$$

$$\begin{aligned} C_L = {} & C_{L_0} + C_{L_\alpha}\alpha + C_{L_\beta}\beta + C_{L_{\delta_p}}\delta_p + C_{L_{\delta_q}}\delta_q + C_{L_{\delta_r}}\delta_r + C_{L_{\delta_x}}\delta_x + ... \\ & C_{L_{\alpha^2}}\alpha^2 + C_{L_{\beta^2}}\beta^2 + C_{L_{\delta_p^2}}\delta_{p^2} + C_{L_{\delta_q^2}}\delta_{q^2} + C_{L_{\delta_r^2}}\delta_{r^2} + C_{L_{\delta_x^2}}\delta_{x^2} + ... \\ & \frac{S}{2V_a}[C_{L_{\dot\alpha}}\dot\alpha + C_{L_{\dot\beta}}\dot\beta + C_{L_p}P + C_{L_q}Q + C_{L_r}R] \end{aligned} \tag{2.24}$$

$$\begin{aligned} C_m = {} & C_{m_0} + C_{m_\alpha}\alpha + C_{m_\beta}\beta + C_{m_{\delta_p}}\delta_p + C_{m_{\delta_q}}\delta_q + C_{m_{\delta_r}}\delta_r + C_{m_{\delta_x}}\delta_x + ... \\ & C_{m_{\alpha^2}}\alpha^2 + C_{m_{\beta^2}}\beta^2 + C_{m_{\delta_p^2}}\delta_{p^2} + C_{m_{\delta_q^2}}\delta_{q^2} + C_{m_{\delta_r^2}}\delta_{r^2} + C_{m_{\delta_x^2}}\delta_{x^2} + ... \\ & \frac{S}{2V_a}[C_{m_{\dot\alpha}}\dot\alpha + C_{m_{\dot\beta}}\dot\beta + C_{m_p}P + C_{m_q}Q + C_{m_r}R] \end{aligned} \tag{2.25}$$

$$\begin{aligned} C_n = {} & C_{n_0} + C_{n_\alpha}\alpha + C_{n_\beta}\beta + C_{n_{\delta_p}}\delta_p + C_{n_{\delta_q}}\delta_q + C_{n_{\delta_r}}\delta_r + C_{n_{\delta_x}}\delta_x + ... \\ & C_{n_{\alpha^2}}\alpha^2 + C_{n_{\beta^2}}\beta^2 + C_{n_{\delta_p^2}}\delta_{p^2} + C_{n_{\delta_q^2}}\delta_{q^2} + C_{n_{\delta_r^2}}\delta_{r^2} + C_{m_{\delta_x^2}}\delta_{x^2} + ... \\ & \frac{S}{2V_a}[C_{n_{\dot\alpha}}\dot\alpha + C_{n_{\dot\beta}}\dot\beta + C_{n_p}P + C_{n_q}Q + C_{n_r}R] \end{aligned} \tag{2.26}$$

$$C_l = C_{l_0} + C_{l_\alpha}\alpha + C_{l_\beta}\beta + C_{l_{\delta_p}}\delta_p + C_{l_{\delta_q}}\delta_q + C_{l_{\delta_r}}\delta_r + C_{l_{\delta_x}}\delta_x + ...$$
$$C_{l_{\alpha^2}}\alpha^2 + C_{l_{\beta^2}}\beta^2 + C_{l_{\delta_p^2}}\delta_{p^2} + C_{l_{\delta_q^2}}\delta_{q^2} + C_{l_{\delta_r^2}}\delta_{r^2} + C_{l_{\delta_x^2}}\delta_{x^2} + ...$$
$$\frac{S}{2V_a}[C_{l_{\dot\alpha}}\dot\alpha + C_{l_{\dot\beta}}\dot\beta + C_{l_p}P + C_{l_q}Q + C_{l_r}R] \quad (2.27)$$

The rotational derivatives such as $C_{D_{\dot\alpha}}$ are multiplied by $\frac{S}{2V_a}$ as these derivatives are taken with respect to this quantity where S is the reference area and V_a is the total airspeed of the missile [21]. The value of each stability derivative listed in equations 2.22-2.27 is provided in Table 1 of Appendix A. Stability derivatives with a value of 0 indicate that there is no significant relationship between the stability parameter and the respective coefficient. Stability derivatives with a non zero value are listed as the actual coefficient. This means that either a constant is known for that stability derivative or an expression is provided in [19] which can reliably predict the value of the derivative under various trim conditions.

The actual values of the non zero stability derivatives are sensitive and have therefore been omitted from the thesis.

It should be noted that there are a number textbooks for which expressions for non zero stability derivatives can be obtained (see references [11] and [15]), however [19] should be consulted in the first instance. This is because the text provides a number of reliable expressions for the calculation of several stability derivatives for the moment (C_l, C_m, C_n) and side force (C_Y) coefficient expressions as well as an in-depth calculation of the drag coefficient. The reliability of these expressions has been verified by comparing predicated values from this text to known parameters for a classified weapon model.

The expressions for the aerodynamic coefficients have introduced two important aspects of missile design and simulation. These consist of conventional weapon control indicated by the δ terms in the stability derivatives and the calculation of the drag coefficient. The δ terms in the stability derivatives represent control deflections for a weapon which uses a conventional aerodynamic control scheme, Section 2.4.1.1 provides a brief explanation of how the AAAW model is controlled in simulated flight using a fin control scheme. The calculation of the drag coefficient is briefly discussed in Section 2.4.2, this may be of interest to the reader in order to understand the parameters which the affect the drag on a missile airframe during flight.

2.4.1.1 Conventional Weapon Control

Conventional aerodynamic control of a tactical missile is often very different to that of an aircraft. Changes in the roll, pitch and yaw of an aircraft is achieved by using elevators, ailerons and rudders. However the attitudes of a tactical missile (which uses conventional aerodynamic control) are normally manipulated using external control surfaces of which there are three main types, consisting of canards, wings and fins.

Canards are small surfaces located at the front of the body, **wings** are larger surfaces located within the middle of the body and **fins** are small surfaces located at the rear of the body. Other control methods exist, such as, thrust vectoring and reaction jet control which manipulate the direction of the thrust produced by the rocket engine to achieve attitude changes. The choice of control scheme is dependent on a number of factors which are beyond the scope of this thesis, however an in-depth discussion of each control scheme is provided in [19] for the interested reader.

The simulated AAAW in this thesis utilises a conventional fin control scheme. A fin control scheme allows the guidance computer on the weapon to produce four control deflections, which consist of, a required change in pitch (δ_q), heading (δ_r), roll (δ_p) and drag (δ_x). Drag control is used in some Laser Guided Bombs to increase the amount of drag on the bomb to reduce the speed of descent. Drag control is not utilised in the guidance and control scheme of the AAAW model.

There are two possible fin configurations for conventional aerodynamic control consisting of (+) and (×) configuration. This particular weapon model uses a (+) configuration, as this is relatively simple to implement compared to (×). Figure 2.4 indicates how this fin configuration produces the required attitude changes. The fins are numbered in order to aid in discussing how the aerodynamic control [19] is achieved.

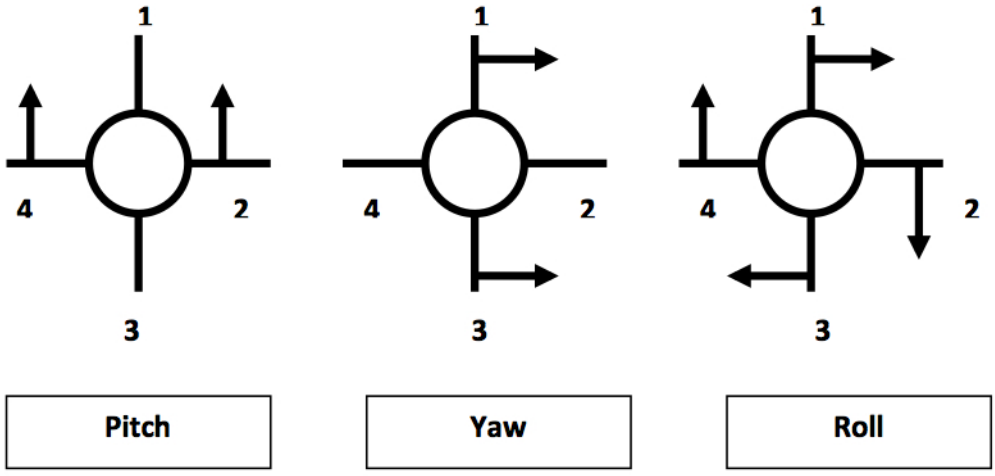

Figure 2.4: + configuration

In the simple case of (+) roll orientated weapon using four control surfaces (as in this model) [19], a pitching moment is created by deflecting fins 2 and 4 which results in a normal force in the direction of the required pitch. A yawing moment is created by deflecting fins 1 and 3 in alternative directions, inducing a side force into the desired yaw direction. A rolling moment is created by deflecting all 4 fins in either a clockwise or counter clockwise direction.

2.4.2 Coefficient of Drag Calculation

The coefficient of drag is the summation of the drag due to the body ($C_{D_{0body}}$) control surfaces ($C_{D_{0controlsurfaces}}$) and stabilising surfaces ($C_{D_{0stable}}$). Control and stabilising surfaces consist of wings, fins and canards. A missile can have either 1-3 sets of surfaces, for instance the Starburst missile system [19] has only canards and a tail. This section will explore the calculation of the drag due to the body and then due to the external control and stabilising surfaces.

2.4.2.1 Body Drag

The body drag consists of three parts, the drag due to the shock wave on the nose, the drag due to the body base and the drag due to the body skin friction.

The drag due to the shockwave on the nose is determined based on its geometry, namely the nose length (l_n), nose diameter (d_n), missile reference area (S_{ref}) and the nose tip cross-sectional area (S_{hemi}). The drag is also a function of the Mach

number (M) which is calculated as [15] :

$$M = \frac{V_a}{a} \tag{2.28}$$

where V_a is the missile airspeed and a is the speed of sound (which is 343.2 m/s at sea level and standard atmospheric pressure [15]). The drag due to the shockwave on the nose $C_{D_{0_{nose}}}$ can then be defined as [19] :

$$C_{D_{0_{nose}}} = \frac{3.6}{\left[(\frac{l_n}{d})(M-1)+3\right]}\frac{(S_{ref}-S_{Hemi})}{S_{ref}} + \frac{3.6}{\left[\frac{0.5}{M-1}+3\right]}\frac{S_{Hemi}}{S_{ref}} \tag{2.29}$$

It is worth mentioning that the drag due to the shockwave on the nose only becomes significant if the missile is travelling at supersonic speeds, it is relatively small for subsonic speeds.

The drag due to the body base depends on whether the missile is coasting or is powered and if the missile is at subsonic or supersonic speeds when the aerodynamic drag due to the body base is computed.

If the missile is travelling at supersonic speeds and is coasting then the drag due to the body base ($C_{D_{Base,Coast}}$) will be [19] :

$$(C_{D_{Base,Coast}}) = 0.25/M \tag{2.30}$$

If the missile is travelling at subsonic speeds and coasting then ($C_{D_{Base,Coast}}$) becomes [19] :

$$(C_{D_{Base,Coast}}) = 0.12 + 0.13M^2 \tag{2.31}$$

However if the missile is powered then the base drag is reduced by a factor of $(1 - A_e/S_{Ref})$ (where A_e is the effective nozzle area). The drag due to the body base ($C_{D_{Base,Powered}}$) then becomes [19]:

$$(C_{D_{Base,Powered}}) = (1 - A_e/S_{Ref})(0.25/M) \tag{2.32}$$

If the missile is travelling at subsonic speeds and is powered then the base drag becomes [19] :

$$(C_{D_{Base,Powered}}) = (1 - A_e/S_{Ref})(0.12 + 0.13M^2) \tag{2.33}$$

When the missile rocket engine is on, the base of the missile is at a high pressure therefore the base drag is low. Once the rocket engine cuts out the pressure drops resulting in low a pressure area being formed behind the missile. Hence this is

why the base drag is reduced at both subsonic and supersonic speeds during powered flight.

At subsonic speeds the pressure waves created by the missile passing through the air will be smooth and gradual. The air begins to move out of the way of the missile before the missile reaches it. Therefore at subsonic speeds, the more significant contribution to the body drag in respect of the skin friction and nose shockwave will be the skin friction.

The drag due to the skin friction is a function of the body length (l), dynamic pressure (q) and Mach number (M) and is defined as [19] :

$$C_{D_{0Body,Friction}} = 0.053(l/d)[M/(ql)]^{0.2} \tag{2.34}$$

As the missile accelerates to the speed of sound, shockwaves appear on the upper and lower surfaces. Once the missile reaches the speed of sound (Mach 1), the shockwaves will arrive at the trailing edge of the airframe. A bow shockwave will also form at the nose. As the missile then accelerates past the speed of sound, the shockwaves on the nose and trailing edge will become more oblique. The drag due to the shockwave on the nose will then become the most significant contribution to the missile body drag at higher than Mach 1 speeds.

2.4.2.2 Drag Due to Control Surfaces and Stabilising Surfaces

There are two components to the drag produced by the aerodynamic surfaces, these are the drag due to the shockwave and the drag due to the skin friction.

The drag due to the shockwave for an external aerodynamic surface is a function of the Mach Number (M), the specific heat ratio (γ), the leading edge sweep and thickness angles (δ_{LE}, Δ_{LE}), the thickness of the mean aerodynamic chord (t_{mac}), the span (b) and the number of the specific aerodynamic surfaces being considered (n_w).

Taking the wing as example, the drag due to the shockwave on the wing (if $M\cos\Delta_{LE} > 1$) is defined as [19]:

$$C_{D_{0_{wing,wave}}} = n_w \frac{2}{[(\gamma(M\cos\Delta_{LE})^2)]} \left\{ \left\{ \frac{[(\gamma+1)(Mcos(\Delta_{LE})^2]}{2} \right\}^{\frac{\gamma}{\gamma+1}} \right.$$
$$\left. \left\{ \frac{(\gamma+1)}{[2\gamma(M\cos\Delta LE)^2 - (\gamma-1)]} \right\}^{\frac{1}{\gamma-1}} - 1 \right\} \frac{sin^2\gamma_{LE}cos\Delta_{LE}t_{mac}b}{S_{ref}} \tag{2.35}$$

If $M_{\Delta LE} < 1$ then the drag due to the shockwave $C_{D_{0_{Wing,Wave}}}$ is 0.

The drag due to the wing friction $C_{D_{0_{Wing,Friction}}}$ is a function of the number of aerodynamic dynamic surfaces being considered (n_w), the length of the mean aerodynamic chord (C_{mac}), the dynamic pressure (q) and the wing platform and reference areas (S_W, S_{Ref}). It is defined as follows [19] :

$$C_{D_{0_{Wing,Friction}}} = n_w[0.0133/(qC_{mac})^{0.2}](2S_W/S_{Ref}) \tag{2.36}$$

Therefore the total drag due to the wings is equal to:

$C_{D_{0_{Wing}}}$=$C_{D_{0_{Wing,Wave}}} + C_{D_{0_{Wing,Friction}}}$

The weapon model in this thesis is fin controlled and uses fixed canards for airframe stabilisation. Therefore the total drag C_{D_0} due to the body and the aerodynamic surfaces is defined as [19] :

$$C_{D_0} = C_{D_{0_{body}}} + C_{D_{0_{canard}}} + C_{D_{0_{fins}}} \tag{2.37}$$

The calculation of the aerodynamic drag coefficient concludes the discussion of the concepts and equations associated with the 6DoF dynamic model. The following sections will discuss the propulsion, warhead, guidance and control considerations.

2.5 Warheads

There are a variety of warheads available which can be used in complex weapons, with the most common warheads being blast effect, fragmentation, shaped charge and explosive pellet [22]. In this model it is assumed that the weapon is fitted with a fragmentation warhead. This is a warhead, which on detonation, sends out pellets at high velocity from a central blast point in a circular band [11]. This type of warhead is representative of missiles such as Hellfire II which can be outfitted with this type of munition. The size of the warheads employed in this type of weapon is unknown and would be classified anyway. However the effect of a fragmentation grenade such as the M67 can be found in open source literature [23]. This grenade has a blast radius of 15m. A missile would most likely be capable of carrying a larger warhead so for this model a conservative blast radius of 15m is used. A simulated engagement is then classed as successful if the final range of the missile to target is within 15m.

2.6 Propulsion

There are a variety of propulsion technologies which can be utilised in the design of a tactical missile. The main technologies are Turbofan/TurboJet, Ramjet and Solid Fuel Rockets [15]. Turbofan/Turbojet engines are the oldest form of air breathing jet engine and are most commonly used for subsonic cruise missiles. For missiles which travel at supersonic speeds of between Mach 2.5 and Mach 5, ramjet technology becomes preferable. However ramjets work by using the engine's forward motion to compress incoming air. Therefore they cannot produce thrust at zero airspeed. In order to utilise a ramjet system, the missile must first be boosted to the ramjet take over speed using a rocket engine. The weapon model in this thesis is assumed to use a solid fuel rocket engine, to reflect the fact, that for the purposes of small to medium tactical missiles, solid fuel rocket motors are most often used. This is due to their simplicity, reliability and ability to produce thrust across the entire Mach range [19]. It is also very simple to produce a varying thrust profile.

Solid fuel rocket engines, like all rocket engines, work on the same Newtonian principle that "to every action, their is an equal and opposite reaction". The propellent in solid rockets consists of fuel and oxidiser. The fuel and oxidiser mix and burn at high pressure within the propellent storage casing, creating a fluid exhaust in the form of a hot gas. The gas is passed through a supersonic propelling nozzle which uses the heat energy of the gas to accelerate the exhaust to a very high speed. The reaction to this produces thrust pushing the engine in the opposite direction.

Some weapons will have a varying thrust profile such as constant thrust or boost sustain thrust. In a solid fuel rocket engine, this is simple to achieve. The gas produced from the combustion chamber is a function of the burn area of the propellent. A large burn area results in more gas and hence greater thrust and vice versa, the change in burn area over time (burn rate), produces the required time varying thrust profile. To change the burn area, a cavity of different shapes such as a wagon wheel or star can be drilled through the centre of the propellent creating various thrust profiles.

Solid fuel rocket motors with propellent cross section shapes are radial burning engines, which means that the propellent is burnt from inside of the relevant shape outwards [24]. A progressive burn is achieved using a tubular shape, in this case the surface area of the propellent increases with burn time. The greater

the surface area of the burnt propellent, the greater the thrust produced.

Star and rod-and-tube cross section shapes are designed to produce the same burning surface area over the duration of the burn time, resulting in a constant thrust. A multi-fin shape is designed to produce a boost-sustain profile, which is achieved from the initial burn surface area increasing rapidly over a given burn time. The burn area will then stabilise and remain constant for the remainder of the propellent burn time.

In terms of modelling the rocket engine for the weapon model, the important concept is the specific impulse. The specific impulse I_{sp} of a rocket engine is a measure of how energetic the propellent or propellent combination is for that particular engine [24]. It is defined as the thrust (T) per unit mass flow ($\dot{m}g$) of propellant (at the Earth's surface) as follows :

$$I_{sp} = \frac{T}{\dot{m}g} \tag{2.38}$$

It is given in units of seconds, with typical values for solid fuel rockets being of the order 250s [19]. The AAAW model has a boost-coast profile, which is simply implemented as the rearrangement of the above equation :

$$T = I_{sp}\dot{m}g \tag{2.39}$$

The boost phase has a duration of 3s and boosts the missile to speeds of over Mach 2.

2.7 Guidance and Control

A missile guidance system can be divided into three distinct phases, known as the boost, midcourse and terminal phases [11]. In the boost phase, the missile accelerates from its launch platform. During the midcourse phase, the guidance system will make minor modifications to the trajectory of the missile in order to keep the target within the intercept capability of the weapon. In the terminal guidance phase, the weapon will lock on to the target and will perform rapid manoeuvres to intercept the target.

There are four main types of guidance systems employed in modern tactical missiles [15]. These consist of Command, Beam-Riding, Semi-active Homing and Active Homing guidance. The choice of guidance system on the missile will depend on a variety of factors such as the intended targets the missile is designed to engage and the cost of the weapon and launch platform.

2.7.1 Command Guidance

Commanded missiles are guided by commands transmitted from the ground via a command link [25]. The missile and target are tracked by a measurement system such as radar [15]. A guidance computer then calculates the required accelerations and associated control commands required to steer the missile onto a collision course with the target. This type of guidance is referred to as command-to-line-of-sight, the midcourse part of the trajectory will normally be optimised to avoid excessive accelerations in the terminal phase of the engagement [26]. It should be noted that commanded missiles do not have their own seekers they can only execute orders, therefore their accuracy depends on the precision of the tracking system.

2.7.2 Beam Rider

A beam rider system consists of a missile with an on-board seeker, and a launch platform which has a radar or laser source [11]. The radar or laser source detects and tracks the target and launches the missile to engage. The seeker onboard the missile determines whether the missile lies within the centre of the beam. If the missile does not lie within the centre of the beam then its on-board guidance computer will apply controls to realign the missile with the target. As all the required information is extracted directly from the radar, there is no requirement for a command link which results in this type of system being relatively simple to implement. However the missile will often be forced to follow a trajectory that will require strong accelerations in the terminal phase, even if the target itself has not performed evasive manoeuvres [26].

2.7.3 Semi-active Homing

Homing guidance is the most common and modern form of missile guidance in use today. There are three primary forms of homing guidance consisting of semi-active, active and passive guidance [11]. In a semi-active system the target will be illuminated by a radar on the launch platform. The missile is launched and a passive seeker on the missile detects and tracks the signal scattered off the target. Unlike beam riding systems, the missile does not have to remain within the radar beam. Because of this, proportional navigation is often exploited (Proportional Navigation is discussed in detail in Section 2.8.1 of this Chapter). The disadvantage of using a semi-active homing system is that the target has to be constantly illuminated for the duration of the engagement. This is especially dangerous for an aircraft launching an air-to-air missile as the aircraft must keep approaching the target at which point the enemy may also launch a missile.

2.7.4 Active and Passive Homing

To overcome the constant illumination issue found in semi-active homing missiles, active seekers have been developed. Active homing missiles have a seeker which is both a transmitter and detector of radiation, with the most common form being radar [11]. An active homing missile will often have a two phase guidance system. In the first part of the engagement i.e the midcourse phase, the missile will be guided to the target using either command or inertial guidance. Once the target is within range of the seeker, the seeker will lock onto the target and proceed to the terminal phase of the trajectory often using a proportional navigation guidance law [26].

There are two disadvantages to this type of system. The first is that active homing missiles are considerably more expensive than other types of weapon. The second is that because the missile seeker is a transmitter as well as receiver, the target will often be able to detect that the missile is locked onto it, therefore covert operation will not be possible.

A passive homing missile works much the same way as an active homing missile, however the seeker is only a detector of radiated energy from the target. For example an infrared homing missile is a system which locks onto the heat generated by a target such as in the anti air role, where the missile locks onto the heat produced by the aircraft's engines.

2.8 AAAW - Guidance System

The weapon model in this thesis is classed as an active homing system, utilising a proportional control scheme and a radar seeker to detect and track targets. The guidance system is activated once the weapon has left the launcher. The missile will first climb to a predefined ride height (boost phase), at which point the midcourse guidance phase will begin. The weapon will now be unpowered and will therefore coast for the remainder of the flight. At a weapon range from launch of 3000m the radar seeker will be turned on. The seeker will now be in target detection mode which means it will scan for a potential target.

The guidance computer in the midcourse phase is required to generate airframe accelerations which will roll stabilise the weapon, maintain the desired ride height and a specified heading. The accelerations are then produced by deflecting the appropriate controls surfaces. The weapon will scan for a target up to a maximum weapon range from launch of 10000m.

On the successful detection of a target the seeker will enter the tracking mode and the weapon will begin the terminal guidance phase. The accelerations applied during this guidance stage will cause the weapon to lose altitude. The commanded accelerations will also manoeuvre the weapon to maintain the target within the seeker scan area during this final guidance phase. This is because the seeker is used to determine the position and velocity of the target which are required in order to calculate the appropriate accelerations. The accelerations for the terminal guidance stage are calculated using a Proportional Navigation (PN) law.

2.8.1 PN Guidance Law

Proportional navigation (PN) is the most widely used guidance law in use today [27]. The basic principle of PN guidance is to generate a missile acceleration "which will nullify the line-of-sight (LOS) rate between the target and intercepter [27] ", where the line of sight $\vec{R}_{LOS}$ is defined as vector between the position of the intercepter ($\vec{R}_i$) and the position of the target ($\vec{R}_T$).

$$\vec{R}_{LOS} = \vec{R}_T - \vec{R}_i \tag{2.40}$$

The guidance law [28] can then be expressed as :

$$\vec{a}_c = \frac{N}{R^2}((\vec{R}_{LOS} \times \vec{V}_C) \times \vec{V}_i) - \vec{g} \tag{2.41}$$

where $\vec{a_c}$ is the required airframe acceleration,$\vec{V}_C$ and $\vec{V}_i$ are the closing velocity and intercepter velocity respectively, N is the navigation constant and R is the range from the weapon to the target. The gravity bias term $\vec{g}$ insures that the "intercepter is not pulled under the target in the terminal phase of the engagement" [28].

2.9 Fire and Forget AAAW Operation

The AAAW model used in this research was originally designed to be representative of a Fire and Forget Anti-Tank weapon for an unrelated project. The weapon can either be launched on or off-boresight. An **on-boresight** launch is simple, the weapon will maintain the same yaw angle as the launcher once separation has been achieved. An **off-boresight** launch consists of the weapon executing a turn right or left after separation which will place the missile on a new heading. The new heading is referred to as the off-boresight angle O_b and is calculated as :

$$O_b = \psi + \Delta\psi \tag{2.42}$$

where ψ is the missile launcher yaw angle and $\Delta\psi$ is the required missile yaw change. The missile launcher heading and off-boresight angle are set at the beginning of the flight simulation. In this research, the missile launcher heading is always set at 0° to represent a fixed launcher situation. This means that the initial yaw of the missile before a potential off-boresight command is initialised as 0°.

If an off-boresight launch is simulated then the off-boresight command is executed by the weapon control system once the simulation clock reaches 1s. This time delay simulates the weapon clearing the launcher. The respective off-boresight angle is then achieved using a yaw control, which requires the deflection of two fins as previously shown in Figure 2.4.

In order to achieve a required fin deflection, gas is expended from a small tank on the missile which in turn moves the fin. The weapon has a limited amount of gas. Therefore the fins can only be deflected a limited number of times during the course of the missile flight. However the fins are responsible for the control of the weapon during all three guidance phases. Because of this, the weapon is restricted to a maximum launch off-boresight angle of 40° to ensure that the fins can deflected a sufficient number of times in order to facilitate weapon control during the midcourse and terminal guidance phases. The 40° limit was imposed in the original design specification. The AAAW can be launched with an off-boresight angle in the range of ±40°.

As the weapon in this case is simulated as a Fire and Forget system, no further off-boresight commands can be transmitted to the weapon once the simulation has begun. The weapon seeker is aligned to the centre of the missile airframe. The choice of an on-boresight or off-boresight launch will then dictate where the seeker will scan for a potential target.

2.9.1 Scan Area Prediction

In the weapon model the seeker, is simulated as a radar spot on the ground which is scanned back and forth continuously. The seeker scan will scan a limited area (within the xy plane) in front of the weapon as it flies. Only targets which have been successfully detected within the scan area at a given scan time can therefore be engaged and potentially intercepted by the AAAW. The x and y bounds of the seeker scan area are a function of the ride height (R_h), missile heading (ψ), the seeker depression angle (θ_d) and the positive and negative seeker sweep angle limits ($\pm\alpha$). Each of these parameters is depicted in the diagram shown in Figure 2.5.

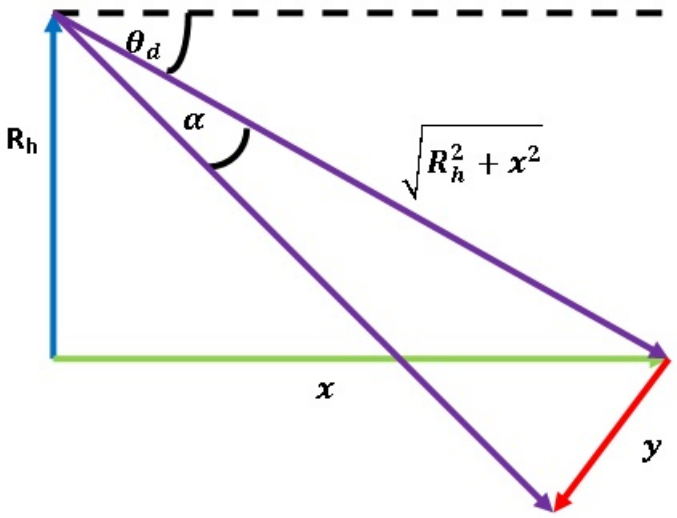

Figure 2.5: Scan Pattern Calculation

The coordinate limits of the scan area can then be calculated using equations 2.43 and 2.44 respectively.

$$x = x_1 = x_2 = R_h \tan(90 - \theta_d) \tag{2.43}$$

$$y_{\pm} = (\sqrt{x^2 + R_h^2}) \tan(\pm\alpha) \tag{2.44}$$

In order to account for the heading of the missile, the x and y seeker limits are assembled as a vector and rotated using the following matrix :

$$\begin{bmatrix} cos\psi & -sin\psi \\ sin\psi & cos\psi \end{bmatrix}$$

The scan pattern width dictated by the x and y limits can be tuned by varying the seeker sweep angle limits ($\pm\alpha$) and the ride height of the weapon. The typical scan pattern width is value of between 120-180m. Over the flight period the weapon seeker will end up scanning a large continuous area. This is demonstrated in Figure 2.6 for an off-boresight command of 0°.

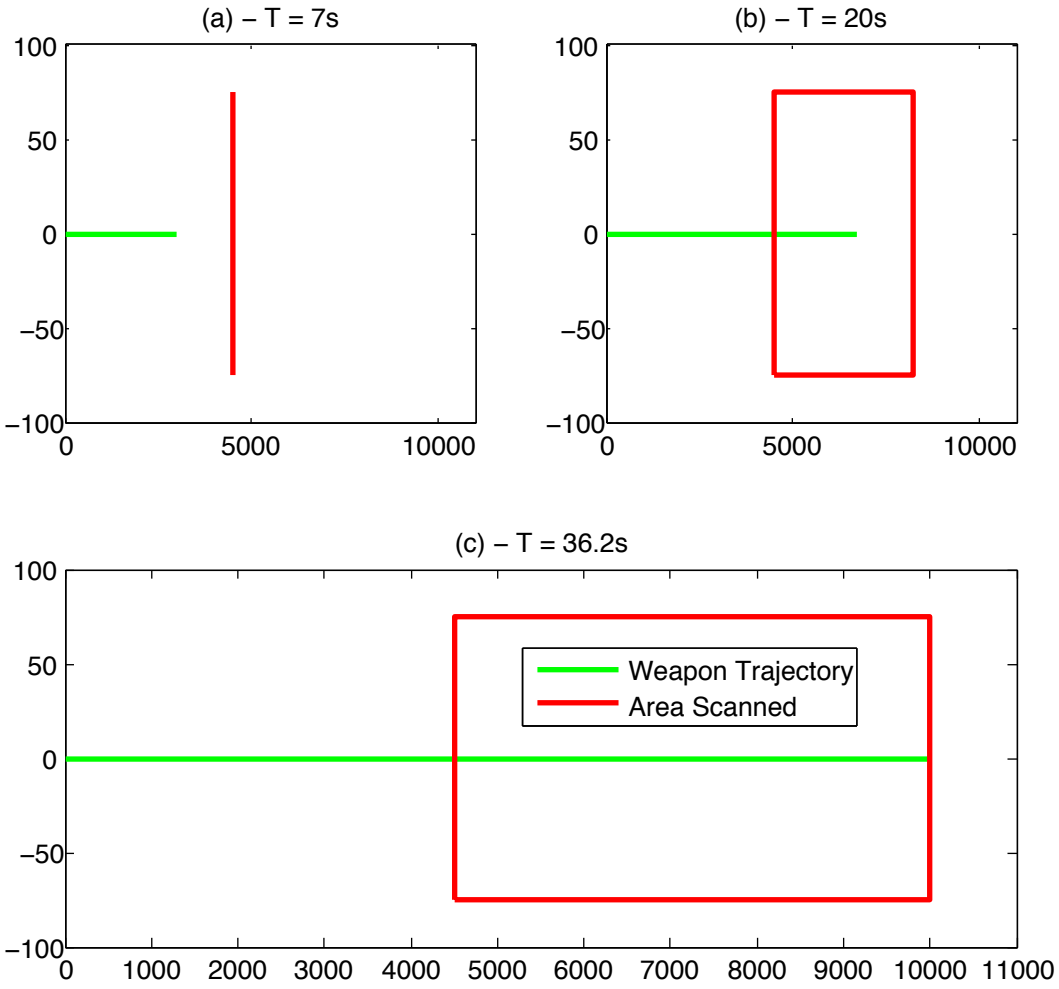

Figure 2.6: Scan Pattern Calculation

In Figure 2.6 (a), the weapon range from launch is 3000m and therefore the seeker has been activated. In Figure 2.6 (b), the weapon has been in flight for 15s and, as can be seen from the plot, a large area has now been scanned by the seeker. In Figure 2.6 (c), the weapon has been in flight for 36.2s and is now 10000m from the launch point. The seeker has therefore been deactivated. It can be seen, from the Figure that applying an off-boresight angle will therefore change where the seeker will scan for a target for the duration of the weapon fly out.

The weapon model is implemented as a series of mathematical functions which are programmed using the Matlab language. Each function such as the 6DoF model or guidance algorithm is defined within an individual Matlab file. The trajectory of the weapon is then determined from the integration of the equations of motion (equations 2.8-2.13) using a fixed time step of 0.005s. The time step has been fixed at 0.005s to be representative of the operating frequency of a modern

weapon INS guidance system such as the Novatel UIMU-LN200 [29]. This system has an operating frequency of 200Hz which is equivalent to an integration period of 0.005s. The calculation of a weapon trajectory and associated scan area takes approximately 3s based on the PC specification outlined in Appendix B.

2.9.2 On or Off-Boresight Launch Selection Criteria

The AAAW model was originally designed to be initialised at the point that a target had been detected from a separate sensor system. The target range, speed and heading of the threat where therefore known. In order to launch the weapon, an appropriate off-boresight angle (if required) is determined by considering a predicted target trajectory and the weapon reachable set.

2.9.2.1 Target Trajectory Prediction

As the weapon model was developed to be representative of in service Anti-Armour Weapons, it was therefore designed to engage the type of targets that this class of weapon would be deployed against operationally. Anti-Armour weapons are used to engage targets which normally travel relatively slowly and in straight lines and/or constrained to terrain features such as roads [30]. Examples of this type of target are vehicles such as Main Battle Tanks, Air Defence Units and Armoured Personnel Carries.

The weapon has a maximum flight time of approximately 40s, so will therefore engage the target in a short space of time.

The predicated target trajectory is calculated by assuming that the target will maintain the detected heading and speed for a duration of 40s, in essence the target will travel in a straight line. As the manoeuvrability of targets such as a Main Battle Tank is poor compared to the weapon, then even if the target does manoeuvre it will not significantly deviate from the predicted trajectory over such a small time period.

Once the predicted trajectory has been determined the appropriate off-boresight angle (if required) can be calculated by using the reachable set.

2.9.2.2 Reachable Set Calculation

Each off-boresight angle will result in the seeker scanning a given area over the flight time of the weapon. The weapon model can be set to fly at an off-boresight angle of $\pm 40^{\circ}$ (as the weapon heading is initialised as 0°). By calculating the

seeker scan area for each off-boresight angle value and joining the respective scan areas together results in the reachable set of the weapon. The reachable set represents the maximum detection boundaries of the seeker and is shown Figure 2.7.

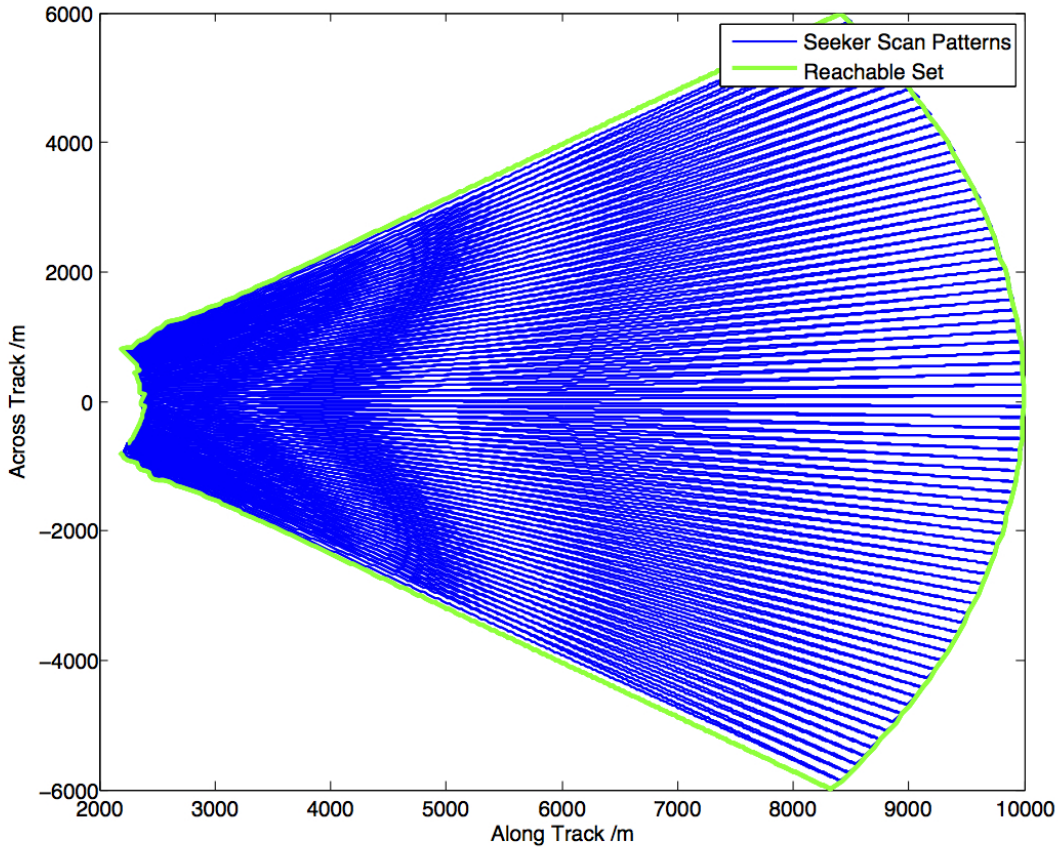

Figure 2.7: Reachable Set with a Missile Launcher Heading of 0°

In order for the weapon to intercept a target, the target must have one or more points along its trajectory whereby it can be detected by the seeker within the boundaries of the reachable set.

2.9.2.3 Combination of Reachable Set and Predicted Target Trajectory

Some or all of the predicted trajectory will intercept the reachable set area. In order to determine whether an off-boresight angle is required each seeker scan area is compared with the predicated target trajectory, beginning with the scan area associated with an off-boresight launch of $-40°$.

The off-boresight angle is incremented in steps of 1° until one or more valid detection points are determined for a given scan area. A valid detection point is simply when the target at a given time step will lie within the area being scanned by the weapon at the same time step. This requirement is depicted in Figure 2.8.

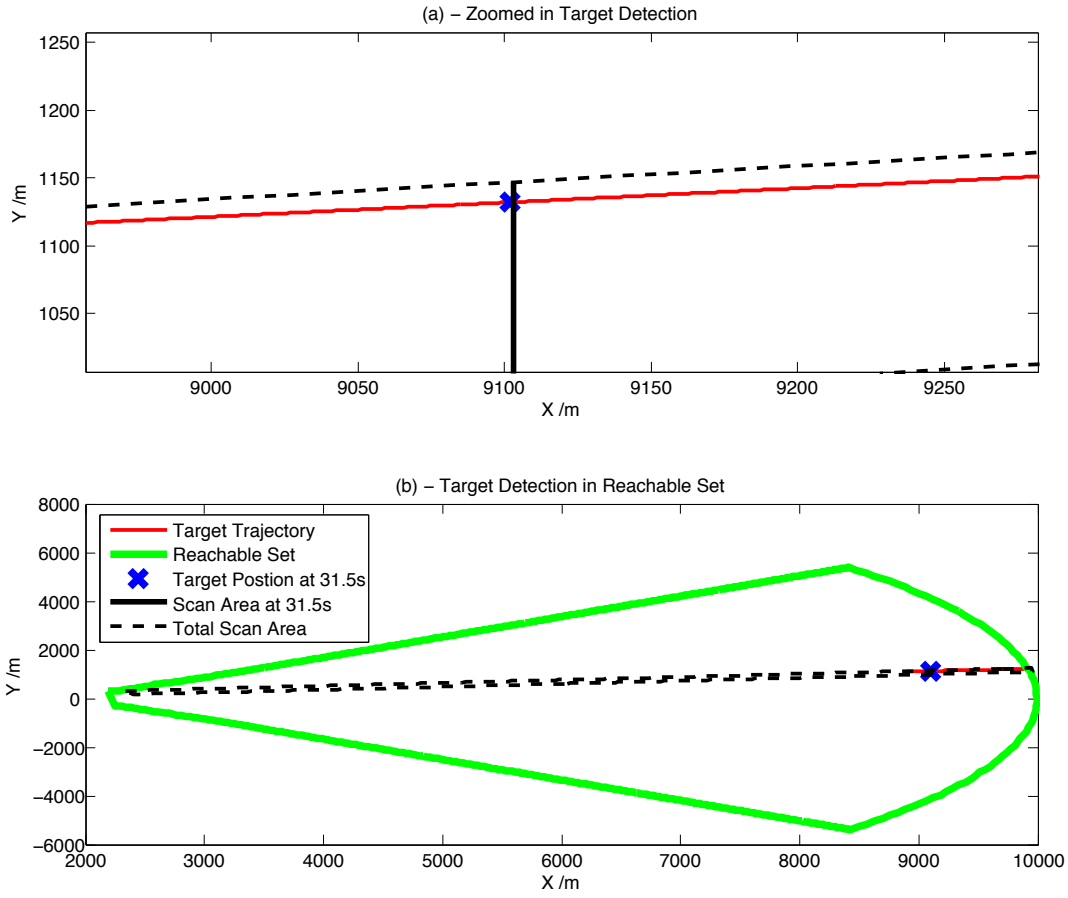

Figure 2.8: Determination of Detectable Location within the Reachable Set

In Figure 2.8, the initial target position has been set at the Cartesian $[x(0), y(0)]$ co-ordinate of $[9920, 1218]$. The velocity of the target is $26m/s$ which is representative of the maximum road speed of a modern light tank such as the FV 107 in service with the British Army [31], the velocity components $[v_x(0), v_y(0)]$ are $[-25.85, -2.717]$. The predicted trajectory is then calculated using the following expression :

$$\begin{bmatrix} x \\ v_x \\ y \\ v_y \end{bmatrix} (t + dt) = \begin{bmatrix} 1 & dt & 0 & 9 \\ 0 & 1 & 0 & 0 \\ 0 & 0 & 1 & dt \\ 0 & 0 & 0 & 1 \end{bmatrix} \begin{bmatrix} x \\ v_x \\ y \\ v_y \end{bmatrix} (t) \tag{2.45}$$

where t = the prediction time and dt is the prediction time step. The matrix within this expression is a constant velocity model [32]. A target which obeys this model will, maintain the same velocity for the 40s period hence the prediction of a non manoeuvring target trajectory. A time step (dt) of 0.005s is used to define the target at each point along the predicted trajectory. This time step is used to match the integration time for the weapon model. Based on the predicted trajectory, an off-boresight angle of 7° has been determined. This will result in a target detection by the seeker at 31.5s provided that the target follows the constant velocity prediction.

A flow diagram of the simulation of the Fire and Forget (F.F) AAAW engaging a target is shown in Figure 2.9.

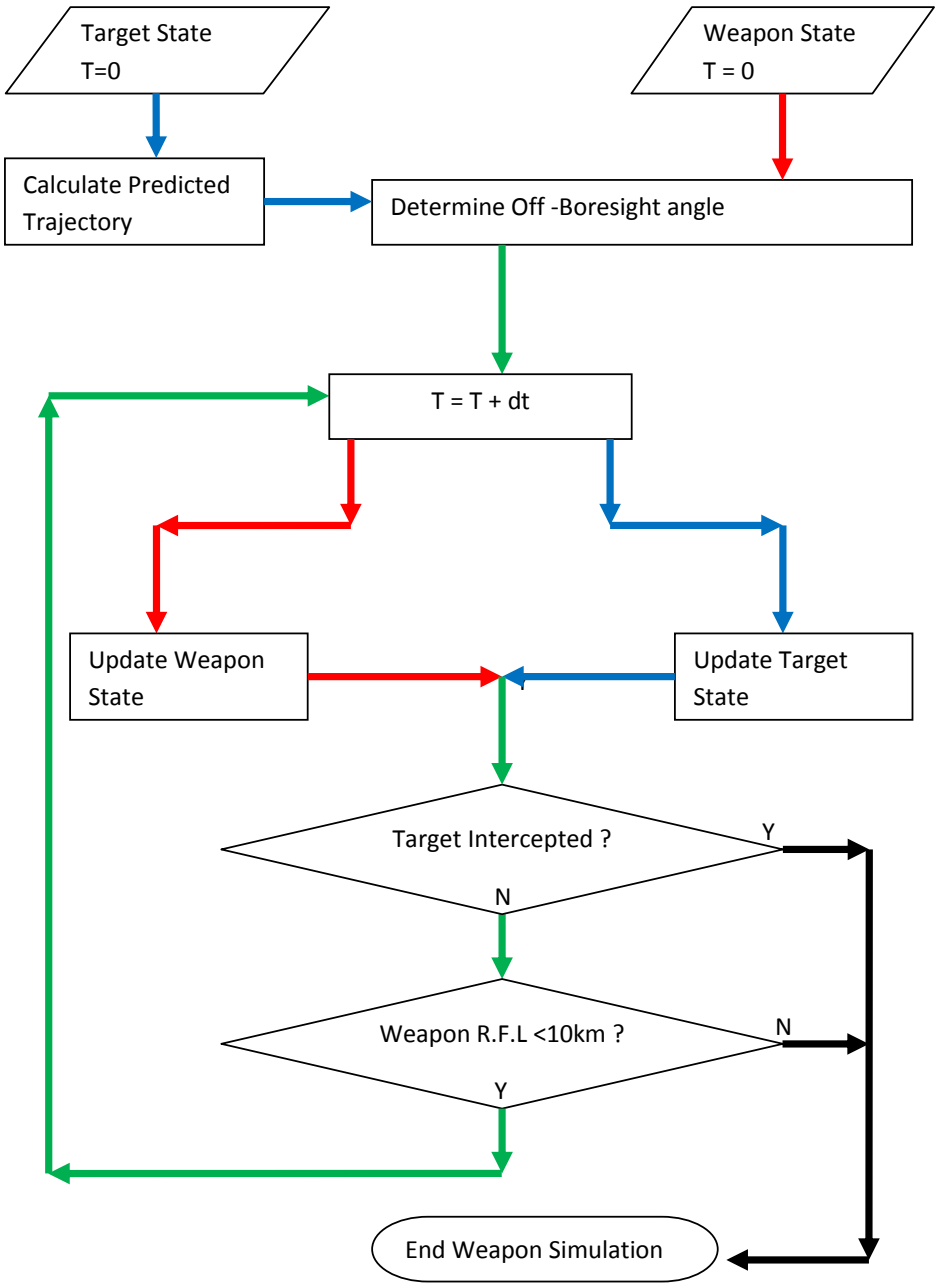

Figure 2.9: Fire and Forget AAAW flow diagram

The target state at T= 0 is the initial position and velocity at the beginning of the simulation. The weapon state at T= 0 is the launch, position and attitudes of the weapon. The simulation will continue until either the weapon range from launch (R.F.L) exceeds 10km, which will coincide with the seeker being turned off, or the target is intercepted based on the conditions described previously.

2.9.3 Fire and Forget AAAW Demonstration

In order to demonstrate how the AAAW model engages a typical non manoeuvring target, a simulation was performed with the target following the predicted trajectory determined in section 2.9.2. The results of the simulation are displayed using various plots in Figures 2.10 and 2.11.

In Figure 2.10 (a) the trajectory of the missile during the boost (W.T.B), midcourse (W.T.M) and terminal (W.T.T) guidance phases is shown.

In Figure 2.11 (a) the target detectability during the three guidance phases is shown. A state of N.D means that the target is not detectable by the seeker, in that the target does not lie in the area being scanned by the seeker at that point in time. A state of D means that the target is within the scan area of the weapon and is detectable. The seeker mode during the three guidance phases is depicted in Figure 2.11 (b). The seeker is either off (S/O), in detection mode (S/D) or in tracking mode (S/T).

The weapon altitude, speed, heading and range is shown for the boost (Bo), midcourse (Mi) and Terminal (Te) guidance phases.

The time that the weapon spends in each guidance phase is also depicted in Figure 2.10 (c).

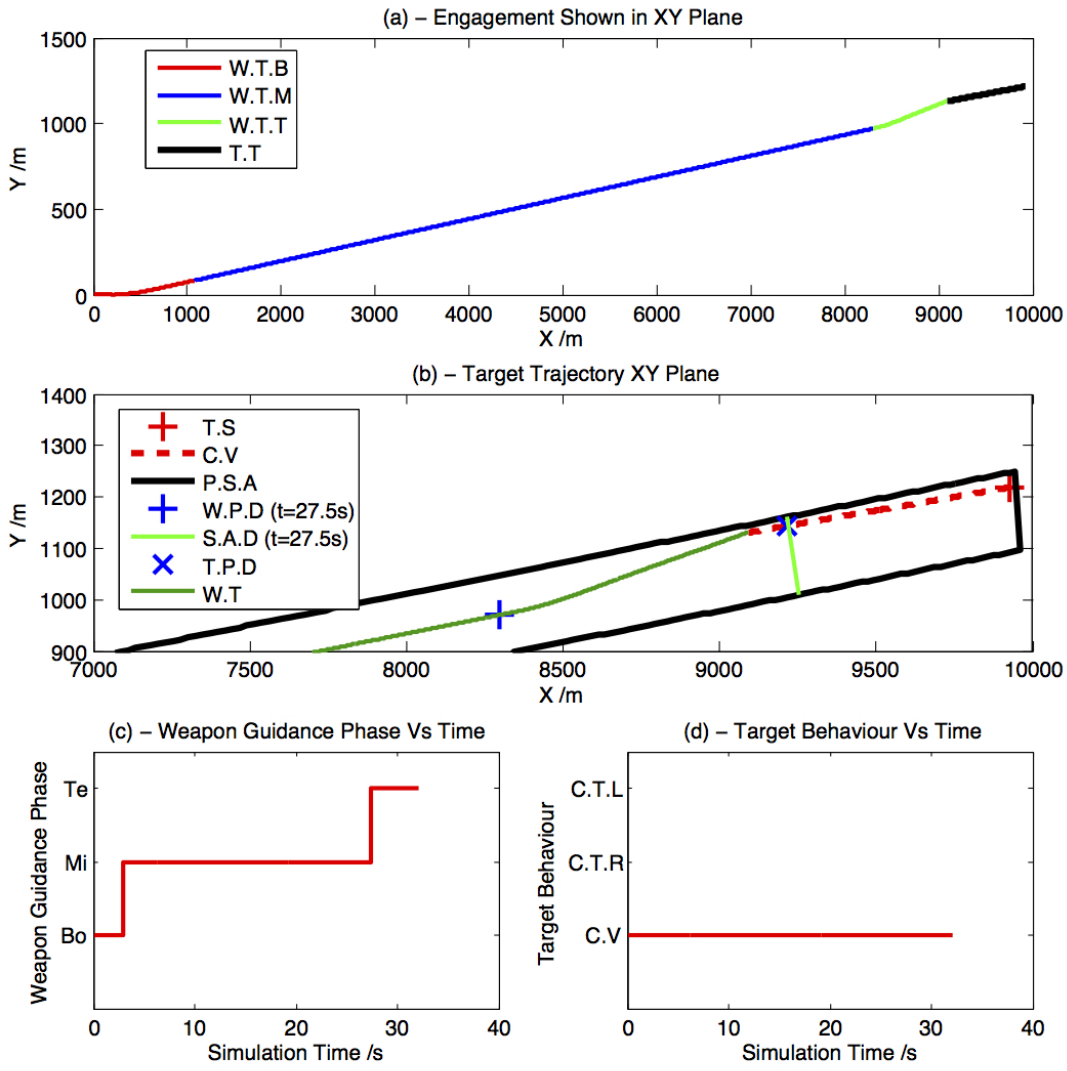

Figure 2.10: AAAW successful direct attack strike, (plot set 1)

As can be seen from Figure 2.10 (a) and (c) the weapon spends the majority of the simulated flight in the midcourse guidance stage. The target behaviour over the flight time of the weapon is depicted in Figure 2.10 (b) and (d). The target maintains a constant heading from the initial target location (T.S) which can be described as the target obeying a constant velocity model (C.V). The target is detected within the area being scanned by the seeker at 27.5s (S.A.D) due to the missile position at that point in time (W.P.D). The trajectory of the weapon and the predicted scan area for an off-boresight command of 7° is also shown in this plot which are labeled as P.S.A and W.T respectively.

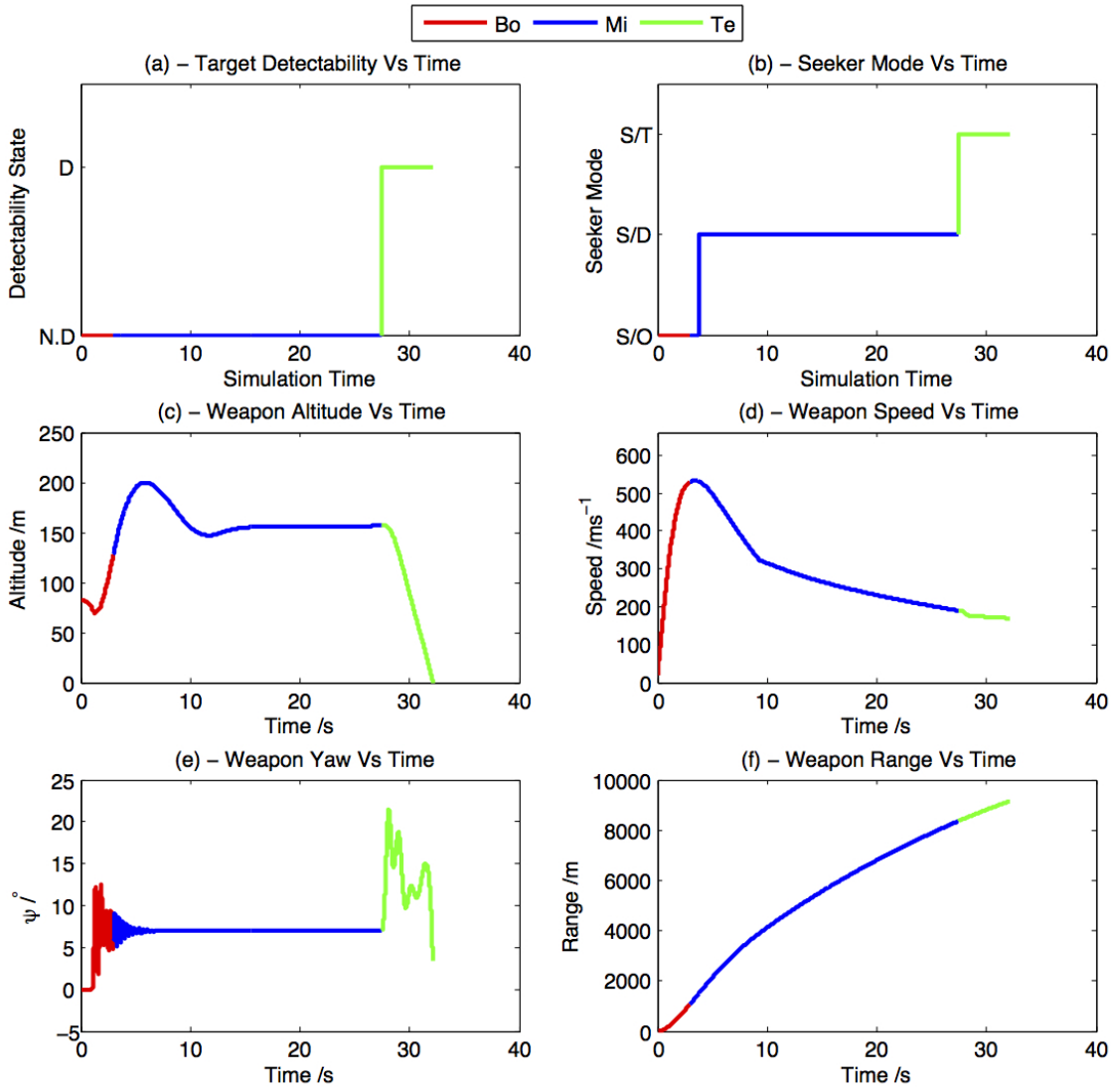

Figure 2.11: AAAW successful direct attack strike (plot set 2)

The seeker is in the detection mode during the midcourse guidance phases. As can be seen from Figure 2.11 (b) the seeker entering the tracking mode and the weapon beginning the terminal guidance phase happens simultaneously. The weapon altitude and yaw plots depicted in subplots (c) and (e) respectively indicate an underdamped control law.

The suggestion of an underdamped control law is apparent from the time taken for the altitude to settle to the desired ride height and the slightly erratic weapon yaw angle during the application of the off-boresight command. In a real world system the guidance system would be tuned to ensure the controls where prop-

erly damped. However the guidance system was never developed to be a perfect control system and it is an internal property of the (legacy) system being studied.

The underdamped control does not pose an issue in this research for a number of reasons. The first reason is that the weapon is a considerable distance from the target at launch it will only engage the target in the later part of the trajectory so the effect of the time taken for the ride height to settle is inconsequential as the ride height is stable from approximately 11s onwards. The effect of the yaw instability is only a potential issue when an off-boresight command is executed, however the yaw angle stabilises within less than 2s from an off-boresight command being enacted. Furthermore the observed instability in the terminal guidance phase is to be expected as the weapon will execute a number of rapid manoeuvres during this guidance phase.

The weapon simulation ends at the point that the altitude reaches zero. The engagement is classified as successful if the final range of the weapon to the target is less than the blast radius of the warhead (15m). Even with an underdamped control law the weapon range to the target at the point that this simulations ended is 2.73m which is well within the blast radius of the fragmentation warhead.

The underdamped control law will also effect the seeker scan area as dictated by equations 2.43-2.44. However the oscillations that will be observed in any calculated scan pattern (see Figure 2.7) will be accounted for when determining the off-boresight command required for a target interception. Therefore the performance of the weapon due to the underdamped control law is unaffected.

2.10 Chapter Review

This chapter has discussed the various concepts and theories surrounding the components of a modern missile system. The specific parameters of an Advanced Anti-Armour Weapon to be used in this research have been discussed. The analysis of the trajectory of the weapon in a typical non manoeuvring target engagement indicated that the weapon has an underdamped control law which results in oscillations in the calculated scan area.

The oscillations are accounted for when determining the off-boresight angle required for the interception for a non manoeuvring target and therefore do not impact the performance of the weapon against non manoeuvring targets. The

oscillations will also be accounted for in any system which shapes the trajectory and scan area in response to a manoeuvring target. Therefore the underdamped control law will not impact upon the performance of the weapon to intercept manoeuvring targets in any integrated fire control system proposed in this thesis.

Chapter 3

The Small Boat Threat

Though AAAWs such as the Brimstone and Hellfire missiles were primarily developed to engage targets with relatively poor manoeuvrability, research is now being conducted to determine whether these systems can be deployed against more challenging targets. A new role foreseen for these systems is in the defence of high value maritime military assets, such as aircraft carriers, against the small boat threat [33]. The small boat threat encompasses four main scenarios which consist of using a boat to [34] :

1. Act as a waterborne improvised explosive device.
2. Smuggle weapons including WMDs into a country's port, the ship itself could be used as a platform for denotation for some smaller nuclear weapons.
3. Conduct piracy operations such as those often reported off the coast of places such as Somalia.
4. Conduct stand off attacks i.e. Man Portable Air Defence System attacks

However in terms of the threat against high value maritime assets, two highly problematic behaviours in particular have been identified based on research carried out at the Naval Postgraduate School in the USA [35]. The behaviours consist of either attacking the asset (ship) or harassing it in an effort to distract the ship for an attack by some other craft or vehicle. In both behaviours the assumption is made that the target will use its maximum dynamic capability at all times in order to accomplish the goals of each behaviour.

If the boat attacks, then it will follow a trajectory which will bring it towards the ship in order to mount to some form of assault. In an attack scenario the boat will seek to reach its target in the shortest time possible. This will be to minimise the time that the ship has to form a defensive response in order to intercept the boat and prevent the attack.

If the intent of the boat is to distract the ship, then it will initially travel sufficiently close to the ship to gain attention. However it is then likely to perform several manoeuvres in order to make the task of tracking it as difficult as possible.

The actual definition of a small boat varies slightly for different countries. For instance, the United States Department of Homeland Security describes a small boat as any vessel used for commercial or recreational purposes less than 300 gross tons [7].

What the small boat threat represents in essence is a small, fast and agile target. This is a type of target which this Fire and Forget AAAW model (and AAAWs in general) was not originally designed to engage.

3.1 Small Boat Target Model

The first step in the research is to develop a target model which is a realistic representation of a boat suitable for a small boat attack. The performance of the current Fire and Forget AAAW model can then be evaluated against this type of target.

3.1.1 Boat Specification

The target model in this thesis is representative of fast attack craft in service today, such as the Royal Marines MK3 Rigid Raider [36], as this type of craft is a possible candidate for a small boat attack. This is because they are fast, highly manoeuvrable and potentially difficult to track due to their small size. As such, the dynamic capability of the target consists of [36] :

1. A maximum speed of 50 knots which is equivalent to $26m/s$.
2. A turning radius of 150m. At the maximum speed, this allows turns of approximately 0.5g to be executed which is equivalent to a turn rate of $10^{\circ/s}$

The target model is used to calculate a realistic trajectory for the small boat to follow over a maximum simulation period of 40s i.e. the maximum flight time of the weapon. At each point in time for a given trajectory, the target is constrained to follow one of three behaviours which consist of :

1. The boat is traveling at its maximum speed of 50 knots at a constant heading.

2. The boat is turning right at a turn rate of $10°/s$.

3. The boat is turning left at a turn rate of $10°/s$

By constraining the target to using its maximum speed and turn capability, the performance of the AAAW and any future systems is then evaluated based on a realistic small boat threat.

3.1.2 Random Target Trajectory Generation

As the boat is capable of performing both direct and manoeuvring attacks, the behaviour of the boat for a given target trajectory is therefore determined at random using the following process.

1. The AAAW can only intercept a target which lies within its reachable set. The boundaries of the reachable set as determined by off-boresight angles of $+40°$ and $-40°$ coincide with a target range of 10000m and a polar angle of $\pm 35°$. Real world sensor systems such as radar describe the position of a target in terms of a range and bearing. The polar angle limits and the equivalent bearings are shown in Figure 3.1

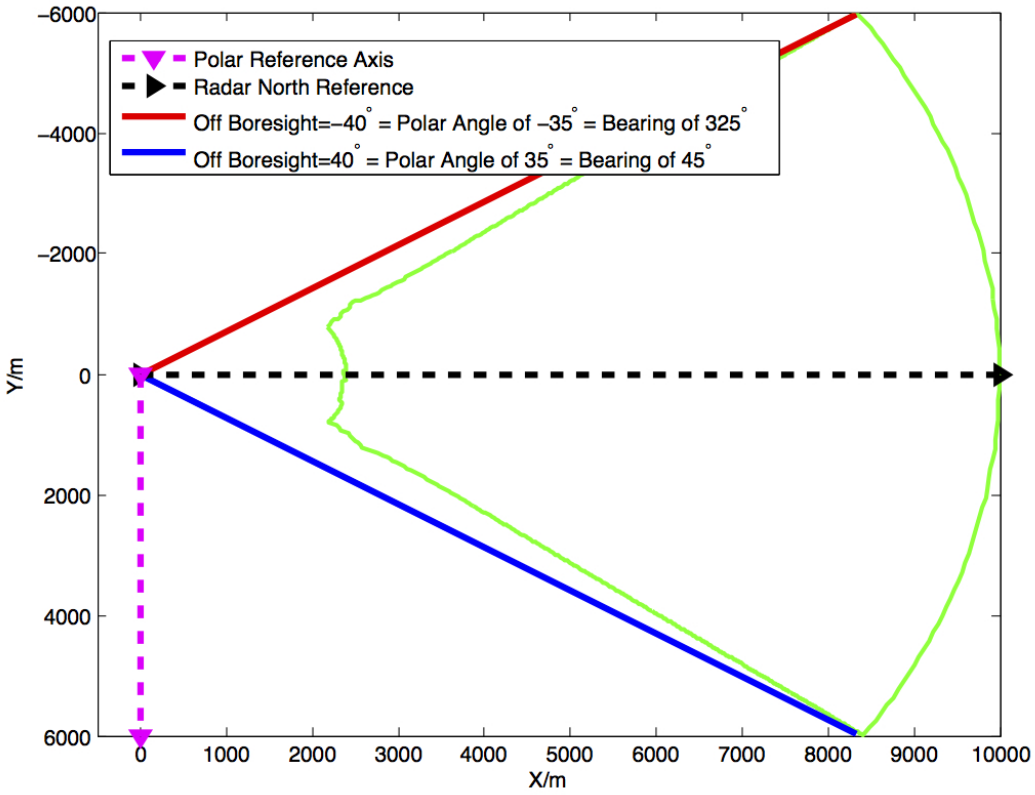

Figure 3.1: Off-boresight and equivalent Polar and Bearing angles

The range of the target is set at the maximum detection and engagement range of the weapon of 10000m. An initial polar angle (θ) is then randomly generated using the following expression :

$$\theta = -35 + 70A \tag{3.1}$$

where A $\sim U(0,1)$. The polar coordinates are then converted into their Cartesian equivalent which results in an initial target position which lies within the reachable set of the weapon.

2. A target heading ψ is then determined as :

$$\psi = 0 + 360A \tag{3.2}$$

The maximum target speed and generated heading are then used to determine the velocity components (v_x, v_y). The cartesian position and velocity components are assembled as a target state vector $X(0) = [x, v_x, y, v_y]$

3. A target behaviour (b) is then determined using the following expression which produces an integer value of either 1, 2 or 3 :

$$b = 1 + 2A \tag{3.3}$$

A value of 1 is a continuation of the current heading. A value of 2 or 3 is turn to the right or left respectively.

4. A duration time for the behaviour (b_d) of between 5s and maximum time of 40s is then determined as :

$$b_d = 5 + 35A \tag{3.4}$$

5. The initial state vector, behaviour decision value and the behaviour duration time are then passed as inputs to a function which calculates the target trajectory produced under those conditions for the behaviour duration b_d using the following expression :

$$X(T + dt) = F(b)X(T) \tag{3.5}$$

where :

T = Current trajectory calculation time

dt = Trajectory calculation time step (0.005s)

$X(T)$ = State vector of the target at the calculation trajectory time (T)

$F(b)$ = The dynamic model associated with behaviour decisions 1-3.

The dynamic models F(1), F(2), F(3) are defined as [32] :

$$F(1) = \begin{bmatrix} 1 & dt & 0 & 0 \\ 0 & 1 & 0 & 0 \\ 0 & 0 & 1 & dt \\ 0 & 0 & 0 & 1 \end{bmatrix} \quad F(2/3) = \begin{bmatrix} 1 & \frac{sin(\omega dt)}{\omega} & 0 & \frac{-1-cos(\omega dt)}{\omega} \\ 0 & cos(\omega dt) & 0 & -sin(\omega dt) \\ 0 & \frac{1-cos(\omega dt)}{\omega} & 1 & \frac{sin(\omega dt)}{\omega} \\ 0 & sin(\omega dt) & 0 & cos(\omega dt) \end{bmatrix}$$

where ω is the turn rate, F(2) is a target coordinated turn to the right (C.T.R) therefore the turn rate is set as $+10°/s$. Matrix F(3) is a coordinated turn to the left (C.T.L), with an associated turn rate of $-10°/s$.

At the end of the behaviour duration time, the trajectory calculation time (T) is compared with the maximum flight time of 40s. If they are equal, then the trajectory calculation process ends. If not, steps 3-5 of the process are repeated with the updated state vector now defined at $X_b(T = b_d)$ used as the input to Equation 3.5.

The process continues until the target trajectory time is equal to 40s. A flow diagram of the trajectory calculation process is provided in Figure 3.2

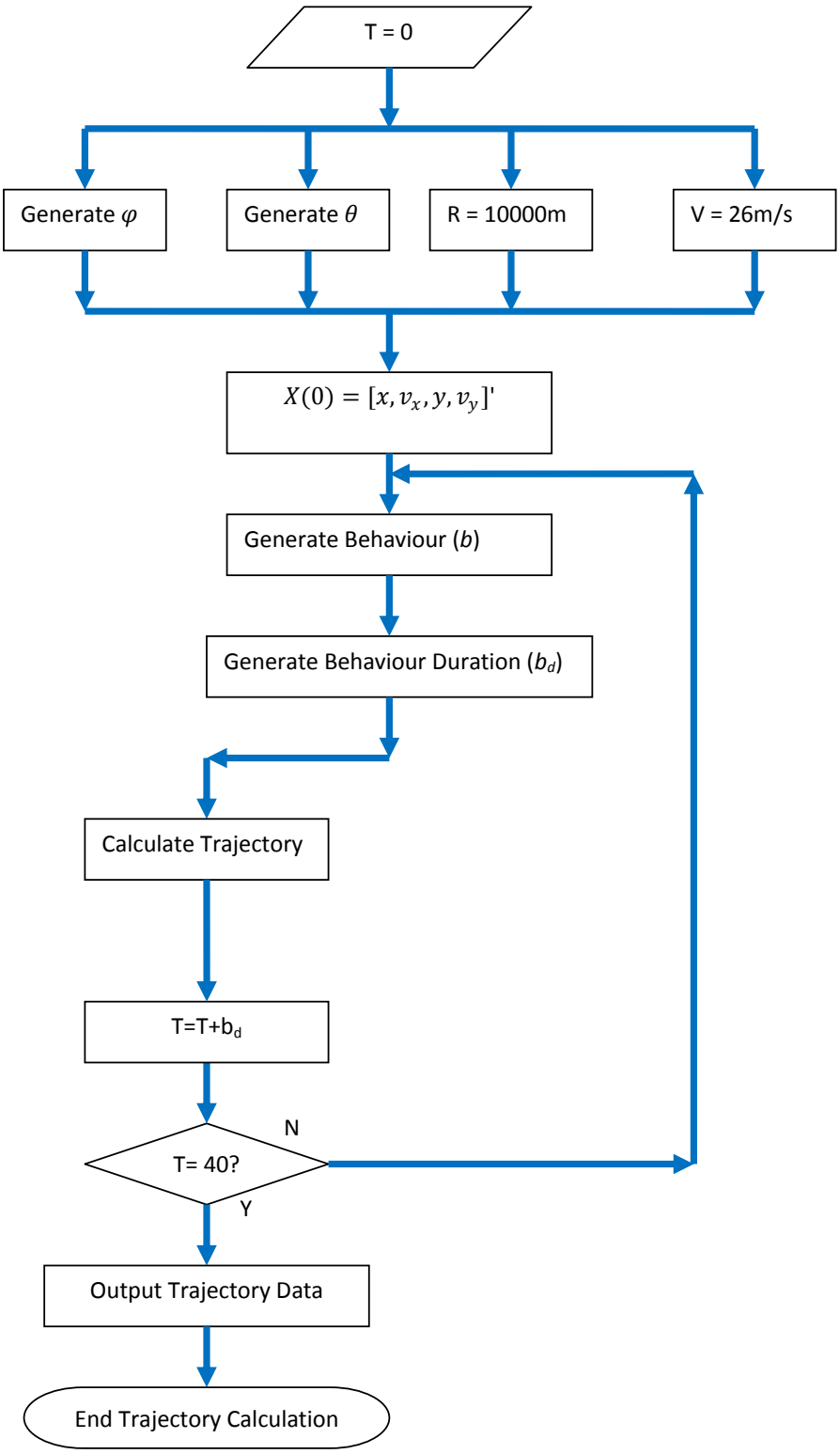

Figure 3.2: Random Trajectory Calculation Flow Diagram

In order to develop an accurate performance assessment of the AAAW model against this type of target, only trajectories whereby the target could be detected

at a point within the reachable set should be considered. To determine whether a valid detection location exists for given random target trajectory, the position of the target trajectory at each point in time is compared with the reachable set area at the same point in time. A valid detection will occur when the target lies within the reachable set defined at the same point in time. This requirement is shown in Figure 3.3.

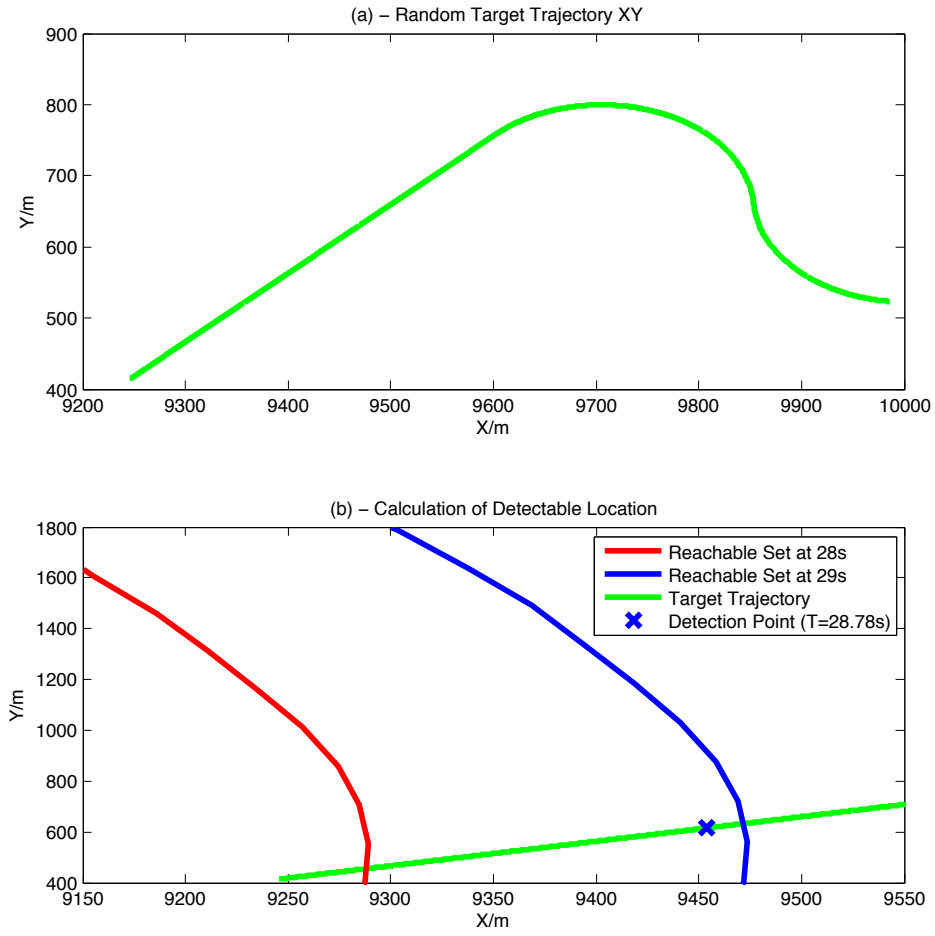

Figure 3.3: Determination of valid detection point for a randomly generated target trajectory

For this particular trajectory a valid target detection location was determined at a position of [9460,628] at a scan time of T=28.7s. If the randomly generated target trajectory does not have a valid target detection location, the trajectory is discarded. The trajectory calculation process can be repeated for any number of desired target trajectories. Each target trajectory is calculated within the Earth axes system

In order to asses the overall performance of the weapon against a small boat, 80 random trajectories were generated using the target model. The trajectories produced by the model encompass a variety of scenarios. The behaviour of the target for each trajectory can then be characterised by calculating the area under the curve bounded by the target line of sight $\vec{R}_{LoS}$ and the actual target trajectory as follows:

1. The target line of sight $\vec{R}_{LoS}$ between the target location at $T = 0s$ $\vec{R}_{in}$ and the location of the target at $T = 40s$ $\vec{R}_{end}$ is determined as :

$$\vec{R}_{LoS} = \vec{R}_{end} - \vec{R}_{in} \tag{3.6}$$

   The target line of sight (LoS) represents the non manoeuvring trajectory the target would follow to arrive at the same location at $T = 40s$.

2. Each location along the generated target trajectory has a Cartesian coordinate (x, y) which is defined at a given point in time, $\vec{R}_t(T)$. The distance, $d(T)$ between the target position at time T and the line of sight is calculated as :

$$d(T) = \frac{|\vec{R}_{LoS} \times (\vec{R}_t(T) - \vec{R}_{in})|}{|\vec{R}_{LOS}|} \tag{3.7}$$

   The distance at each time step is representative of the magnitude of the deviation from a non manoeuvring trajectory, brought about by the target behaviour up to that point in time. The calculation of distance is depicted in Figure 3.4 to aid in the understanding of the significance of the computed distance.

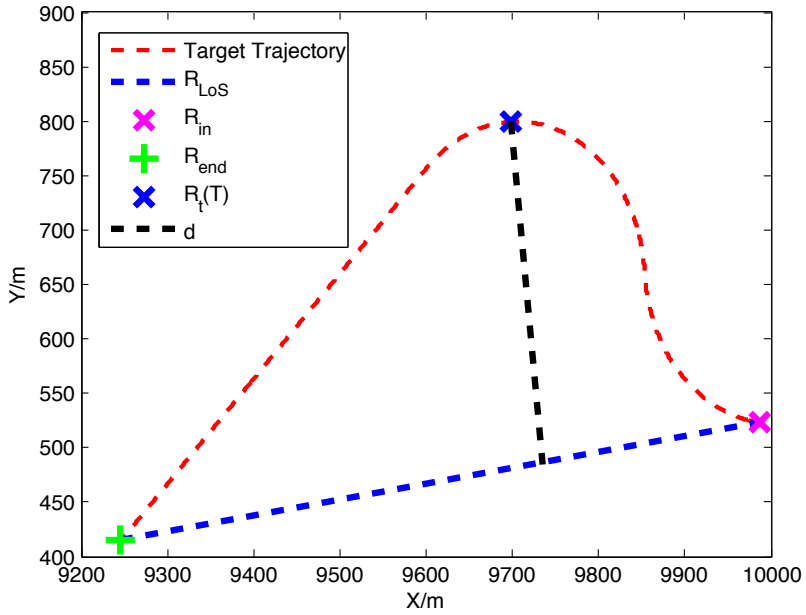

Figure 3.4: Calculation of deviation from LoS

3. The area (A) is then the total deviation of the target from the non manoeuvring trajectory (LoS) for the 40s period. It is calculated as the summation of each deviation (distance) value defined at time steps (dt) of 0.005s as follows :

$$A = \sum_{T=0}^{T} d(T) \tag{3.8}$$

An area value of $0m^2$ coincides with a non manoeuvring target with an area value greater than $0m^2$ characterising a manoeuvring target trajectory. The area due to the target deviation from the LoS for each randomly generated trajectory is shown in Figure 3.5.

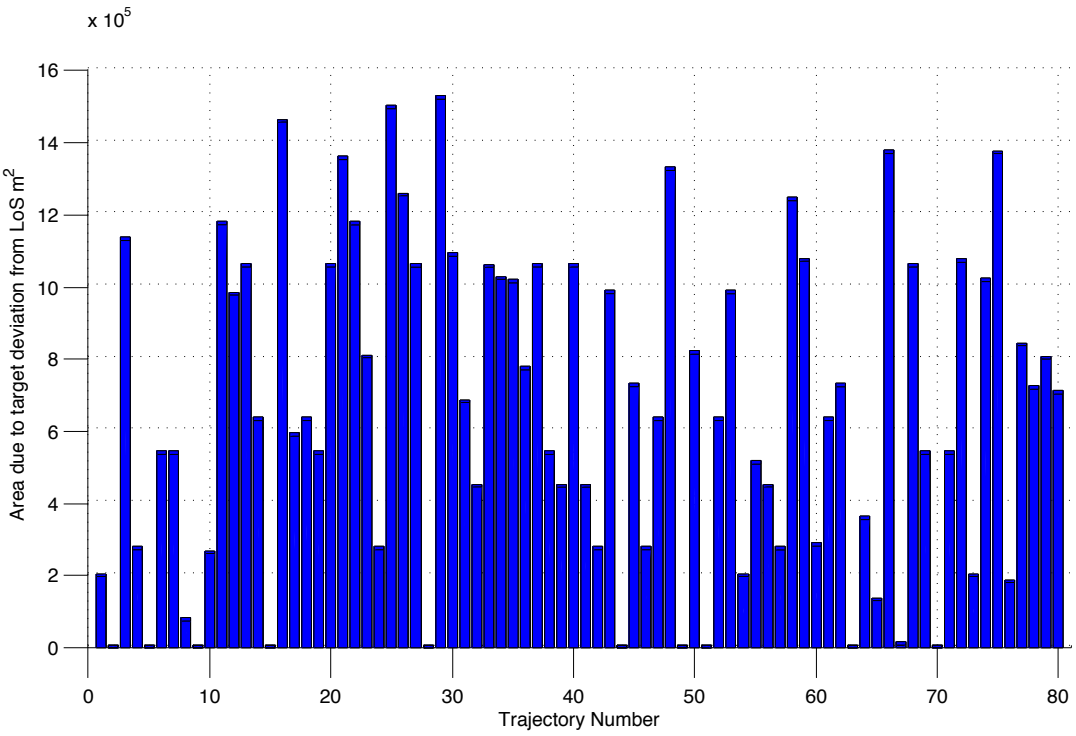

Figure 3.5: 80 Random Target Trajectories

The size of the deviation brought about by a manoeuvre is dependent on the duration and whether it results in the target then traveling in a direction which takes it further away or brings it closer to the LoS. The area will therefore increase as the target spends a greater proportion of the 40s trajectory travelling in a direction away from the LoS. The effect of different manoeuvres on the size of the area is shown in Figures 3.6 and 3.7.

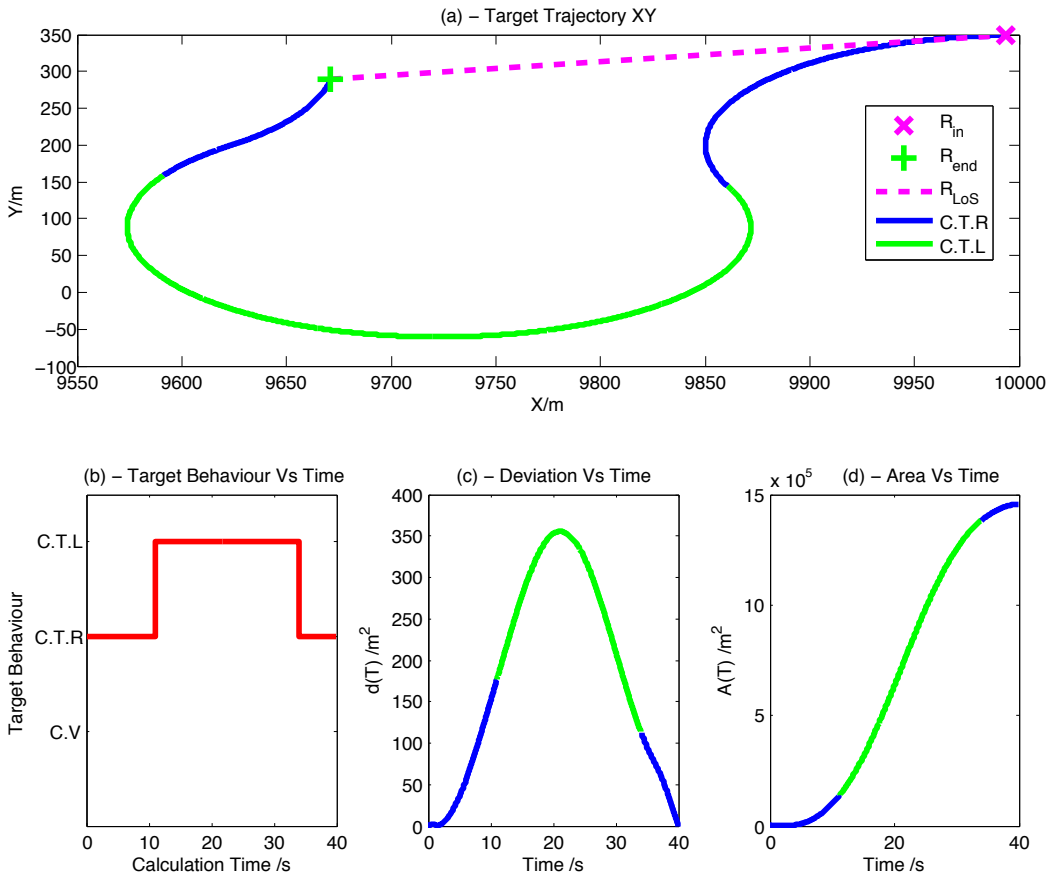

Figure 3.6: Determination of valid detection point for a randomly generated target trajectory

The plots shown in Figure 3.6 are generated from the data produced for trajectory number 16 (Figure 3.5). For this trajectory the target was initialised at a position of [9994,349]. It then executed a 11s turn right, before performing a turn to the left which had a duration of 25s. At T = 36s, it began a turn to the right which was terminated when the trajectory calculation clock reached T = 40s. As can be seen from Figure 3.6 (c) the deviation of the target increases rapidly from T= 0, to T= 22s as the target is moving in a direction away from the line of sight. The deviation then starts to reduce as the effect of the remaining target motion is to bring the target closer to the line of sight.

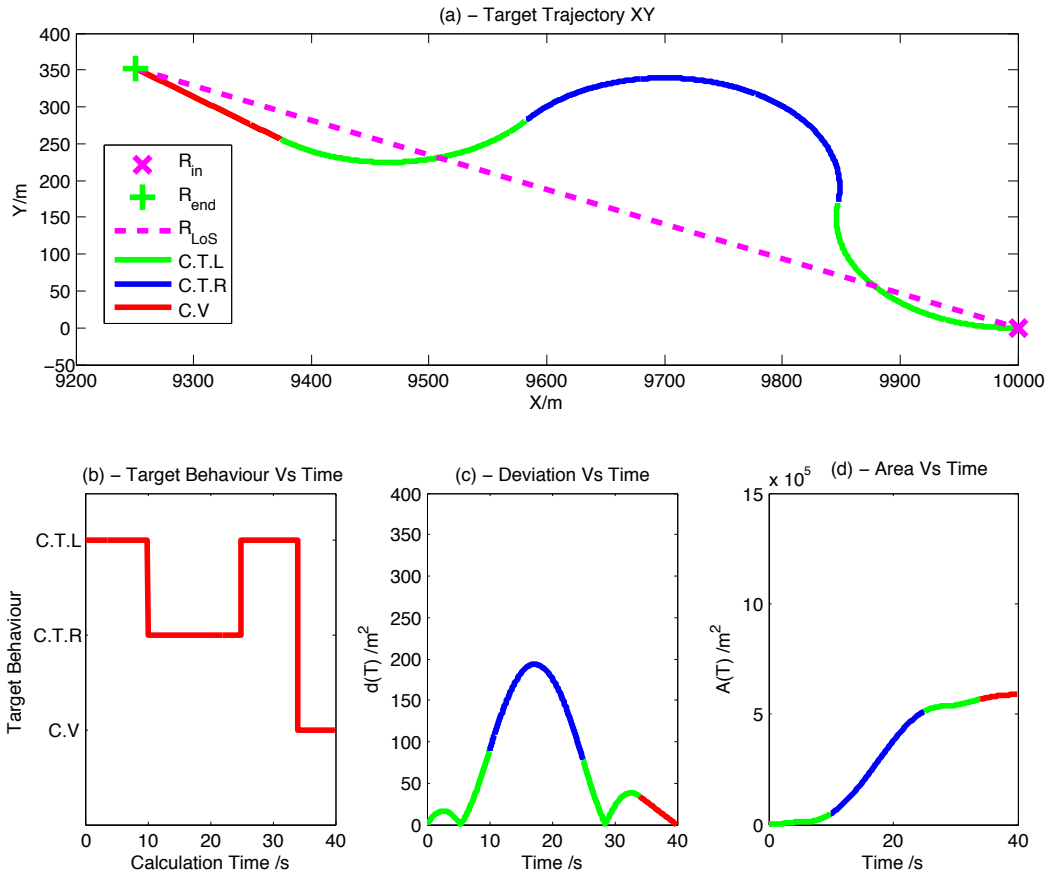

Figure 3.7: Determination of valid detection point for a randomly generated target trajectory

The plots shown in Figure 3.7 are generated from the data produced for trajectory number 17 (Figure 3.5). For this trajectory the target was initialised at a position of [10000,0], it then executed a 10s turn left, before performing a 15s turn right. At T=25s, the target began a 9s turn to the left before continuing on the resultant heading for 6s. As can be seen from Figure 3.7 (d), though the target performs 3 turns just as in the case of Figure 3.6, the actual area due to the deviation brought about these manoeuvres is smaller.

3.1.3 Fire and Forget AAAW Benchmark

The Fire and Forget AAAW was tested against the 80 random trajectories produced by the target model. The weapon successfully intercepted 47 targets and failed to intercept 33 targets. The 33 failed intercepts, can be described as obeying 1 of 3 failure modes, which are defined as:

Failure Mode 1 states that the manoeuvring target has not been detectable within the scan area at any point in time. This is due to the calculation of a weapon trajectory and thereby scan area based on the assumption of a non manoeuvring target trajectory.

Failure Mode 2 applies to both manoeuvring and non manoeuvring targets. In this failure mode, the target **has** been detectable within the scan area of the weapon at a given point in time. However the seeker has failed to recognise the valid target and has therefore not entered the tracking mode. Due to the detection failure, the weapon does not then enter the terminal guidance phase resulting in the target not being intercepted.

Failure Mode 3 again applies to both manoeuvring and non manoeuvring targets. In this failure mode, the target is detectable within the seeker scan area. The seeker recognises the valid target and transitions into the tracking mode. The weapon then begins the terminal guidance phase, however the guidance fails to reduce the weapon range to the target to less than 15m, which is the warhead blast radius. The target in this case escapes the effect of the warhead and is therefore not intercepted.

Each failed intercept in the case of this Fire and Forget system is classed as Failure Mode 1. An example of this Failure is provided in Figures 3.8 and 3.9. The target in Figure 3.8 was initialised at a position $[x, y]$ of $[10000, 350]$, with a velocity $[v_x, v_y]$ of $[-25.6, -3.6]$. Based on this initial state a predicted non manoeuvring target trajectory was determined. An off-boresight angle of 2° was calculated to achieve a target detection by the weapon seeker. At T=0s, the target began an 8s turn to the left. The target then maintained the new heading as result of the turn for 8s. At T=16s, the target began a 23s turn to the right.

The weapon trajectory during the boost (W.T.B) and midcourse guidance phases (W.T.M) is provided in Figure 3.8 (a) as well as the target trajectory (T.T). The target start location is shown in Figure 3.8 (b) along with the weapon trajectory (W.T) and the predicted scan area (P.S.A).

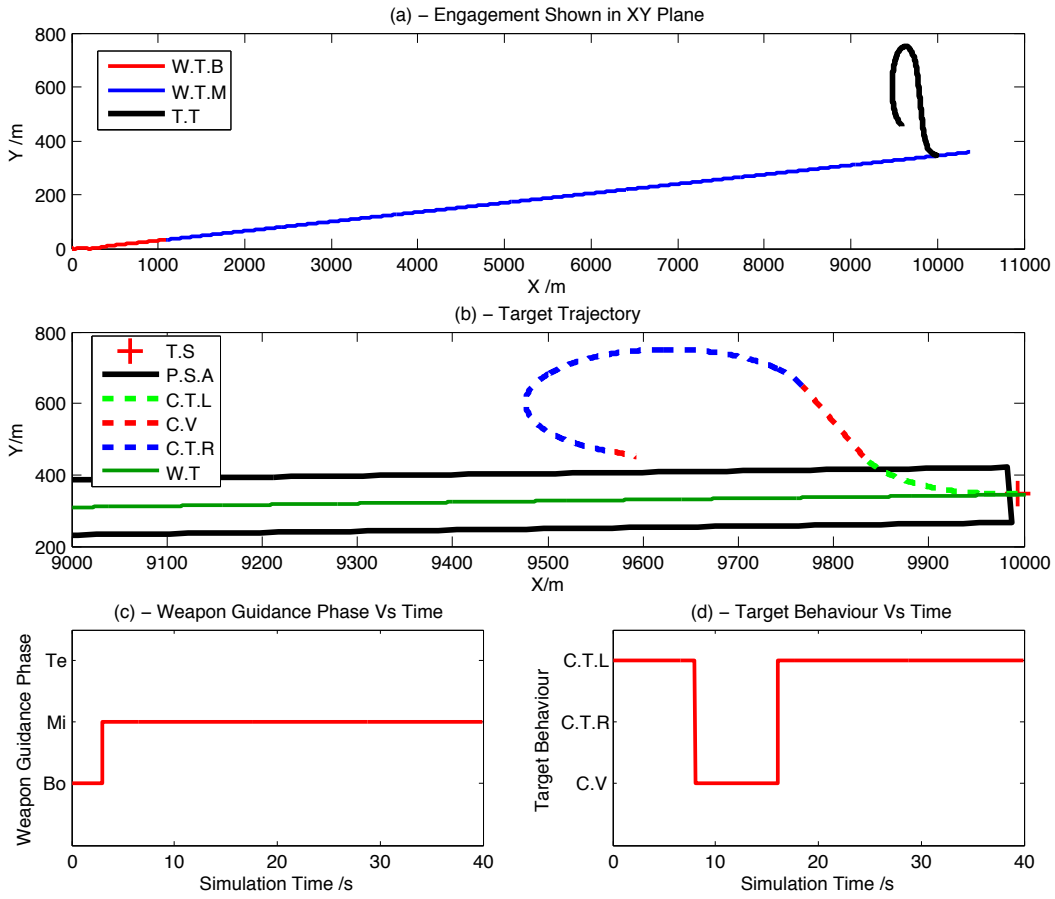

Figure 3.8: Manoeuvring Target Miss by F.F AAAW (plot set 1)

The initial 8s turn to left, results in the target following a trajectory which takes it out of the predicted scan area. The trajectory followed by the target over the remaining 32s, does not bring the target back into the weapon scan area. Therefore the target does not become detectable. As a result, the seeker does not transition into the tracking mode and the weapon does not enter the terminal guidance phase. As can be seen from Figure 3.9 (b) and (f), once the weapon range from launch reaches 10000m, the seeker transitions into the off-mode (S/O).

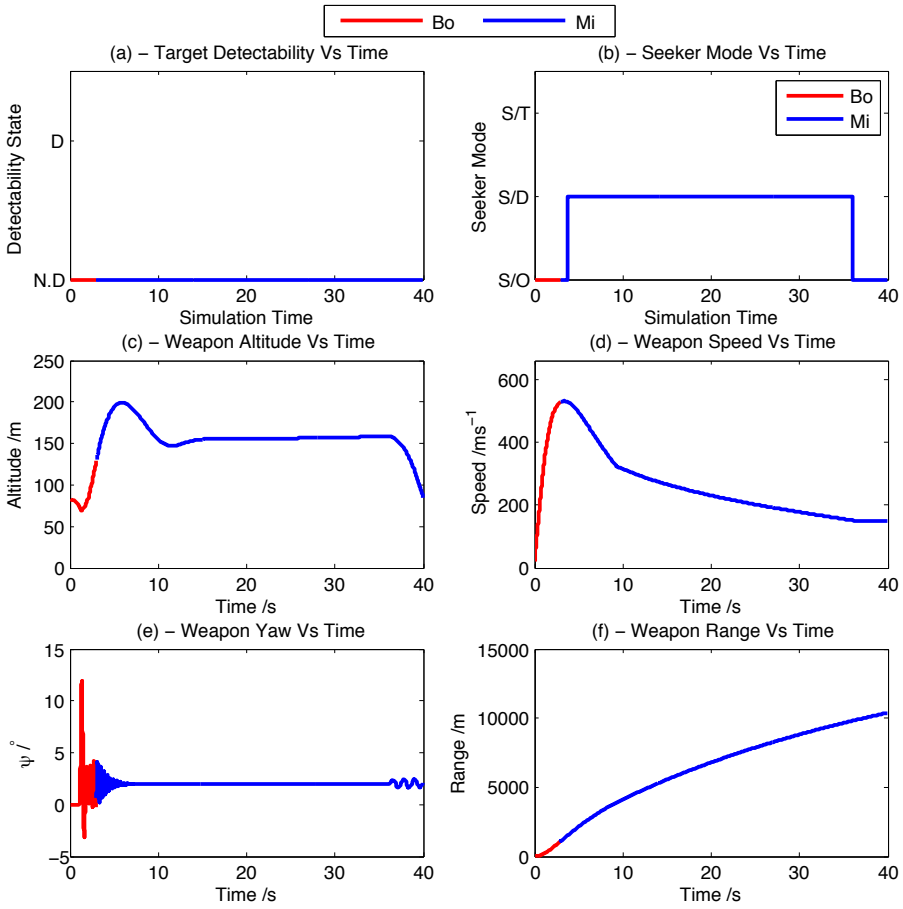

Figure 3.9: Manoeuvring Target Miss by F.F AAAW (plot set 2)

The results of the 80 simulated engagements are presented in Figure 3.10. The area due to the target deviation in each engagement is determined based on the observed behaviour up until the point of interception or T=40s if the weapon failed to intercept the target.

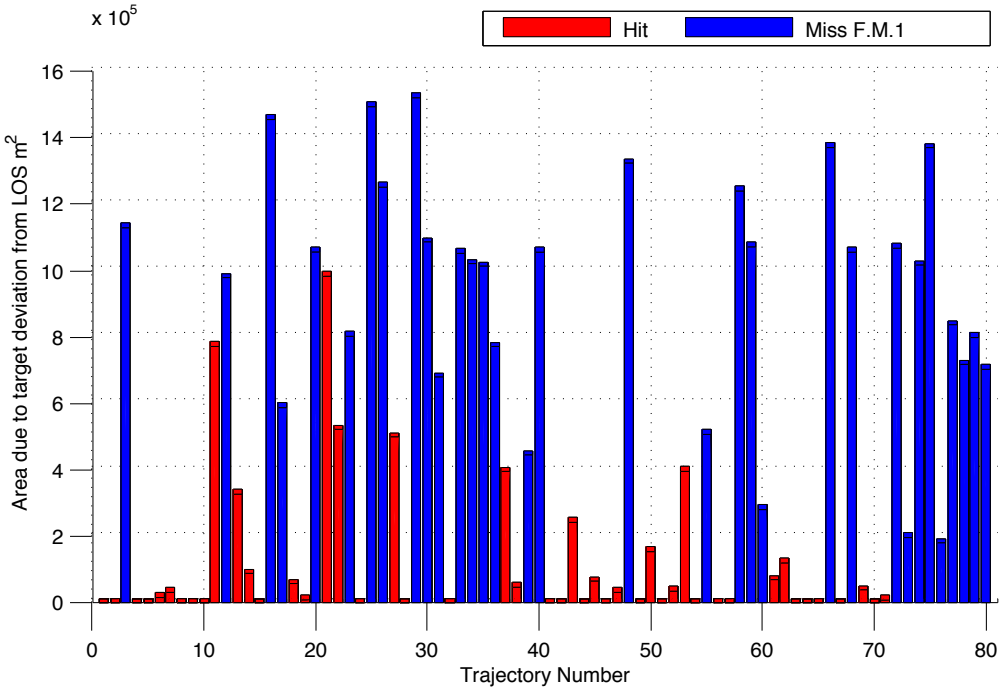

Figure 3.10: Fire and Forget AAAW Results

Of the 80 trajectories generated by the target model, 14 would be classed as non manoeuvring targets, in that no manoeuvres where executed by the target for the duration of the 40s weapon fly out. 6 trajectories generated by the model consisted of non manoeuvring behaviour for the majority of the simulation and then the execution of a late turn.

In these 6 trajectories it is possible to intercept the target based on the prediction of a non manoeuvring target in the F.F system before the target is able to manoeuvre. In this and future chapters, this type of trajectory will be referred to as a possible intercept before manoeuvre (I.B.M) target.

The remaining 60 target trajectories are manoeuvring targets (M.T), whereby the target will perform one or more manoeuvres such that the target can not be intercepted before the first manoeuvre occurs. The performance of the weapon against the three types of trajectories produced by the model is summarised in Table 3.1

N.M	I.B.M	M.T
14/14	6/6	27/60

Table 3.1: Fire and Forget (F.F) System Results

For each of the manoeuvring target intercepts, the weapon will have maintained a constant heading up until the point the target is detected, which means the seeker will have scanned only a limited area. The conditions for an intercept of a manoeuvring target will therefore be very restrictive and can be explained by considering trajectory 21 using Figures 3.11 and 3.12.

In the engagement depicted in Figure 3.11, the target was initialised at a position $[x, y]$ of $[10000, 530]$, with a velocity $[v_x, v_{y]}$ of $[-25.8, 2.7]$. Based on this initial target state a predicted non manoeuvring trajectory was determined. An off-boresight angle of 4° was calculated to achieve a target detection by the weapon seeker.

At T=0s, the target began an 8s turn to the left, at T=8s, the target began a 13s turn to the right. From T=21s until detection by the seeker at T=28.5s the target maintained the new heading, obeying a constant velocity model. The target trajectory in the xy plane is depicted in Figure 3.11 (b). The weapon trajectory, position, scan area at the detection point and the predicted scan area are also plotted and are labelled as W.T, W.P.D, S.A.D and P.S.A respectively.

In Figure 3.12, (a) the detectability of the target is plotted against time. If the target follows the predicted trajectory, then it should be detected within part of the total predicted scan area at some point in time. If the target manoeuvres, it will then potentially follow a trajectory which takes it out of the predicted scan area making it undetectable by the seeker. Even if the target then manoeuvres further and arrives back in the predicted scan area, it may not lie within the predicted scan area at the correct point in time and will still be undetectable.

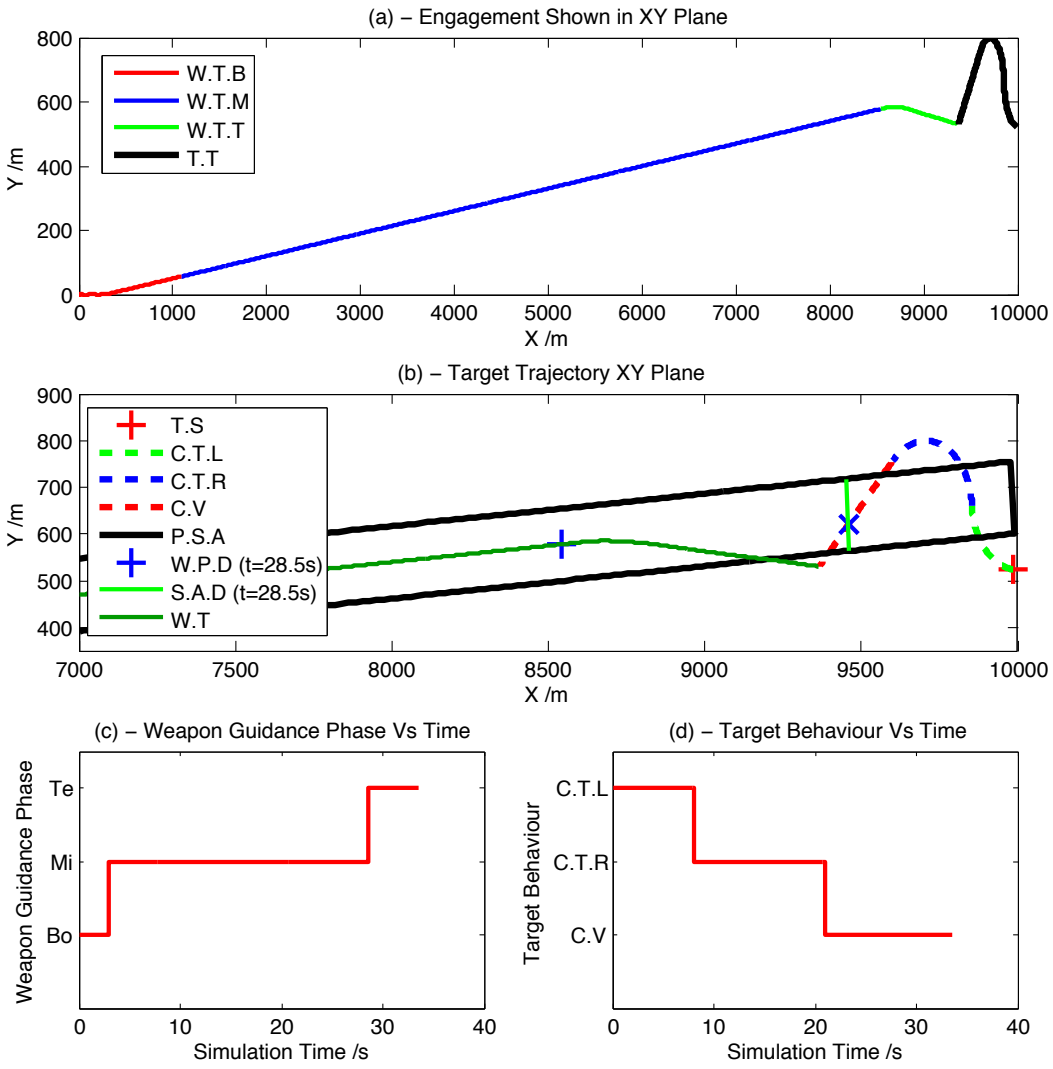

Figure 3.11: Successful Manoeuvring Target Intercept by F.F AAAW (plot set 1)

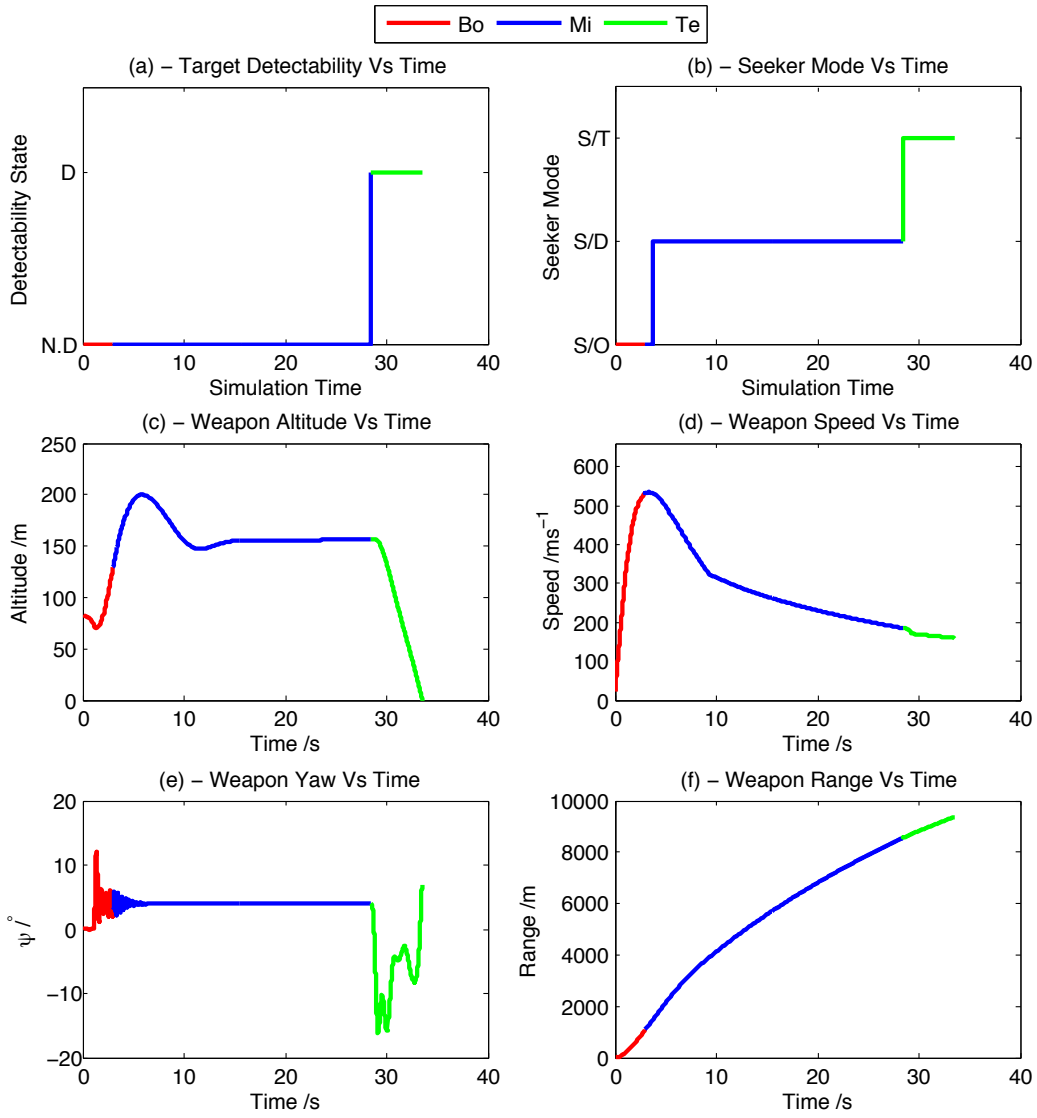

Figure 3.12: Successful Manoeuvring Target Intercept by F.F AAAW (plot set 2)

In this trajectory the target has manoeuvred in and out of the predicted scan area. During both the left and right turns the target is undetectable by the weapon seeker. However the target becomes detectable by the seeker at T=28.5s as it lies within the area being scanned by the seeker at that instant in time.

3.2 Data Link AAAW

For each of the failed intercepts, the target had performed one or more manoeuvres. Each of the 33 failed engagements were classed as Failure Mode 1. The performance of the AAAW against manoeuvring targets can therefore be considered limited at best.

Current UK defence programs such as the Selective Precision Effects at Range (S.P.E.A.R) package are exploring the use of data links with Advanced Anti-Armour Weapons such as the Brimstone Missile system [9]. In essence a data link allows a weapon to be retargeted in flight either by sending new target data or off-boresight commands. If a target was tracked after the weapon was launched then feasibly a weapon could be retargeted in response to detected target behaviours. This will enhance the performance of the weapon against manoeuvring targets. The information transmitted using the data link will depend on the specific guidance system used on the weapon.

In the case of this weapon model, a data link will allow off-boresight commands to be transmitted to the weapon in flight. The application of an off-boresight command will change the weapon heading and therefore the area scanned over the simulated flight period. Two or more off-boresight angle commands will therefore create a shaped weapon trajectory and scan area.

In section 2.9, the off-boresight angle, O_b was defined as follows :

$$O_b = \psi_L + \Delta\psi \tag{3.9}$$

where ψ_L was the initial launcher yaw angle and $\Delta\psi$ was the yaw angle which was limited to an absolute maximum value of 40°. A data linked AAAW can receive a number of off-boresight commands during the flight. Each off-boresight angle transmitted to the weapon after launch can then be defined as :

$$O_b = \psi_w + \Delta\psi \tag{3.10}$$

where ψ_w is the current missile heading (yaw angle) and $\Delta\psi$ is the required missile heading change. The limitation of a maximum absolute heading change of 40° still applies. Therefore, for a weapon which is able to receive a number of off-boresight commands, the absolute sum of the changes required for each off-boresight command must not exceed 40°. This can be stated mathematically considering n off-boresight commands O_b with each command requiring a heading change $\Delta\psi_b$ as follows :

$$\sum_{b=1}^{b=n} |\Delta\psi_b| \leq 40^\circ \tag{3.11}$$

Each off-boresight command sent to the weapon which is not equal to the previous command will reduce the size of the heading change which can be applied for future off-boresight commands. This can be demonstrated considering the trajectory and subsequent plots presented in Figure 3.13.

The trajectory of the weapon was shaped at four points in time. At T=0s an off-boresight command of 5° was supplied to the weapon while in the launcher. At T=10s, T=15s and T=25s, off-boresight commands of 15°, 0° and 10° were sent to the weapon (simulating the transmission over a data link).

The four off-boresight commands required heading ψ_b changes of 5°, 10°, −15° and 10° which are shown in Figure 3.13 (b). The absolute sum of these heading changes is 40°.

In Figure 3.13 (d) the heading change capability spent is labelled as H.C.S and the maximum heading angle which can be applied for remaining off-boresight commands is labeled as H.C.R.

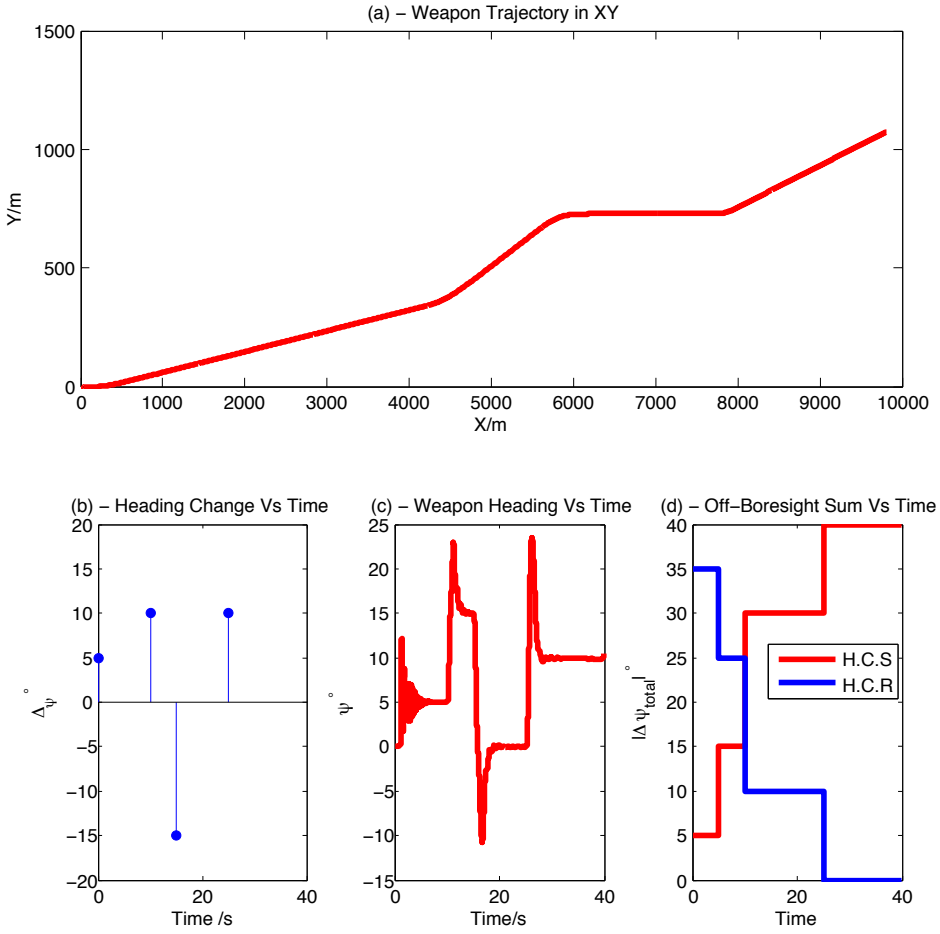

Figure 3.13: Example of a Shaped AAAW Trajectory

After 25s the absolute maximum cumulative heading change of 40° has been reached which means that the weapon cannot receive any further off-boresight commands after this point in time

3.3 Proposal for an Integrated Fire Control System

The ability to retarget the weapon in flight has the potential to increase the performance of the weapon against manoeuvring targets. As demonstrated in Figure 3.13, the weapon can only be retargeted a limited amount, which is specified by the maximum cumulative absolute heading change of 40°.

In order to maximise the ability of the weapon to intercept a manoeuvring target, the limited retargeting capability must be utilised efficiently over the simulation period. In that, it should be possible to retarget the weapon sufficiently at any point in time, in response to a detected target manoeuvre. This thesis proposes that this requirement can be achieved from the calculation of an optimal shaped weapon trajectory in each engagement. This trajectory can be calculated using an integrated fire control which considers four questions :

1. What is the current behaviour of the target?
2. What is the possible future behaviour of the target?
3. What is the maximum allowable yaw change ?
4. What is the optimal trajectory based on the answers to questions 1-3?

An integrated fire control system consists of three fundamental aspects, target tracking, target behaviour prediction and weapon trajectory optimisation. The Fire and Forget approach only considers one possible target trajectory i.e. a non manoeuvring target, but the target could follow a variety of trajectories during the weapon fly out. If the target is tracked after the weapon launch, its behaviour can then be monitored.

The behaviour can then be used to update the current single prediction or calculate a number of potential future target trajectories. By using a more advanced behaviour prediction, the future optimal weapon trajectory can then be updated in response.

A general flow diagram of an integrated fire control system is provided in Figure 3.14.

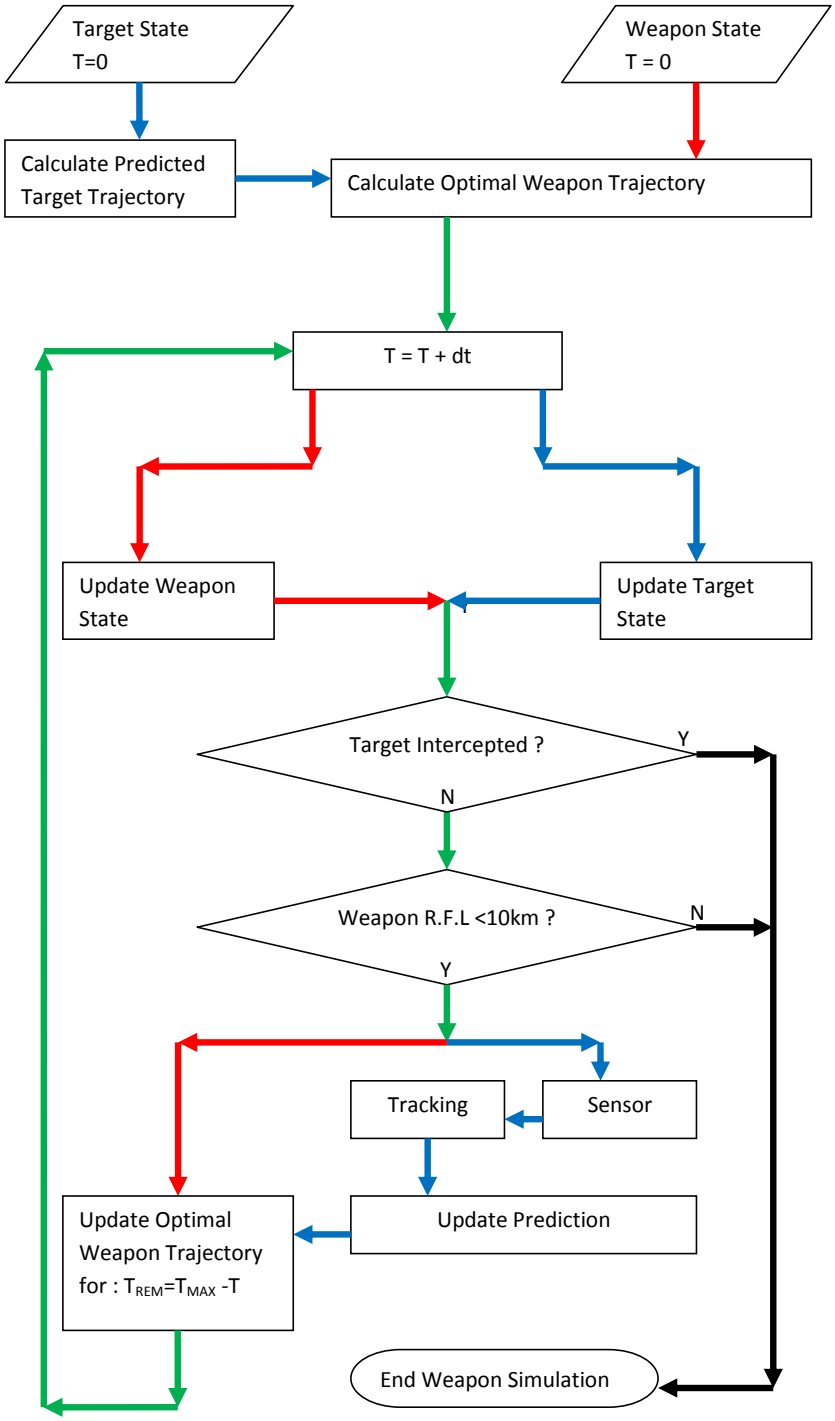

Figure 3.14: Flow Diagram of an Integrated Fire Control System

3.4 Chapter Review

This chapter has evaluated the performance of the existing Fire and Forget AAAW model against a fast agile surface vessel which is able to manoeuvre at several points in time during the weapon fly out. The performance of the weapon against non manoeuvring targets was excellent. The AAAW successfully intercepted all 14 of the non manoeuvring targets generated by the target model. This was to be expected given the original design specification of the AAAW which is based on non manoeuvring targets. The AAAW was also able to intercept 6 targets which would have performed a manoeuvre later in the simulation, had the intercept not occurred.

The weapon successfully intercepted 33 of the 60 manoeuvring targets generated by the model.

The chapter highlighted that current UK research programs are exploring the use of data links with this type of weapon. The data link allows the weapon to receive off-boresight commands in flight in order to shape the trajectory of the weapon. This has the potential to significantly improve the performance of the weapon against manoeuvring targets. Here, performance is measured by the number of manoeuvring targets, the weapon is able to intercept over a number of simulated engagements. The greater the number of intercepts, the greater the performance of the weapon.

The level to which the performance can be increased, is limited by the trajectory shaping capability. This limitation is due to the original design specification of the AAAW, such as the number of times the fins can be deflected and a maximum cumulative off-boresight angle of 40°.

It was postulated that in order to achieve the maximum performance increase, the limited trajectory shaping (retargeting) capability would have to be efficiently utilised over the course of the weapon fly out. This could be achieved using an integrated fire control system.

Chapter 4

Integrated Tracking and Trajectory Prediction

The ability to shape the trajectory and scan area of the weapon will not improve the performance of the AAAW against a manoeuvring target if the only predicted target behaviour considered is that of a non manoeuvring target. Therefore, in order to utilise this capability effectively and improve the performance of the weapon, a wide range of possible target trajectories must be considered. A method can then be established to calculate the optimal weapon trajectory based on a given set of performance criteria, considering the widest range of possible target trajectories.

If the target is tracked after the initial detection, the information obtained regarding its behaviour, such as whether it has manoeuvred, can be used to update the possible future trajectories. The optimal weapon trajectory can be revised considering the updated predicted target trajectories. By doing this the performance of the weapon against manoeuvring targets should improve. In that the number of manoeuvring targets intercepted by the AAAW should increase.

The combination of the information obtained from the tracking system with a realistic target model can be referred to as an integrated tracking and trajectory prediction system. This system underpins the three integrated fire control systems described in Chapters 5 and 6. This chapter consists of three parts, the first part presents a model which can be used to determine the possible trajectories that the target may follow over a 40s weapon flight period. The second part of the chapter discusses the development of a tracking system which is capable of successfully tracking a small manoeuvrable boat. The final part of this chapter discuses how the tracking and prediction model are integrated in order to improve the quality of the target trajectory prediction over the weapon fly out.

4.1 Target Trajectory Prediction

It is standard practice to define an exclusion zone around naval military assets [37]. Unauthorised ships which then enter the zone can and will be fired upon [38]. In this thesis, the exclusion zone will be considered as the reachable set of the AAAW, the intent of a target entering the reachable set will be unknown. The target may or may not have electronic capability which allows it to determine if it is being tracked by the high value asset that the AAAW is protecting. There is no military doctrine available for the target, which means that the trajectory cannot be predicted based on a set of known rules. As such, the future trajectory of the target is also unknown. However, provided that the target always follows a trajectory which allows it to be detected within a scan area determined by a prediction of a non manoeuvring target, then this lack of information would not pose a significant problem. However, this constraint severely limits the performance of the AAAW to intercept manoeuvring targets.

It is possible to predict the potential trajectories that the target could follow over a potential 40s engagement by considering the target as obeying one of three behaviours at each point in time which consist of the target :

1. Travelling at its maximum speed (obeying a constant velocity model)
2. Performing a turn to the right at its maximum turn rate (obeying a coordinated turn model).
3. Performing a turn to the left at its maximum turn rate (obeying a coordinated turn model)

The constraints on the target behaviour are based on the assumptions outlined in the research carried out by the Navel Research Institute in relation to the small boat threat [35]. The target can transition between behaviours over the flight time of the weapon. The integrated fire control systems will seek to shape the trajectory of the weapon based on the predicted target trajectories. In order for a shaped weapon trajectory to be effective, the approximate minimum time that the target would spend in each behaviour to allow it to escape the seeker scan area determined for a non manoeuvring target, for part of, or all of the weapon fly out must be calculated.

This time can be calculated approximately considering a target position at a detection of [10000,0]. The scan area of the weapon over a 40s flight will then be evenly distributed either side of the target position as shown in Figure 4.1 (a). In this scenario, there is no advantage to the target turning left or right.

The time taken for the target to achieve a lateral distance of greater than half of the seeker width based on a turn followed by constant velocity motion is then a reasonable approximation to this behaviour duration. This is because target turns of a shorter duration will produce trajectories which are closer to the non manoeuvring target trajectory. These targets would be less problematic, reducing the effectiveness of the prediction.

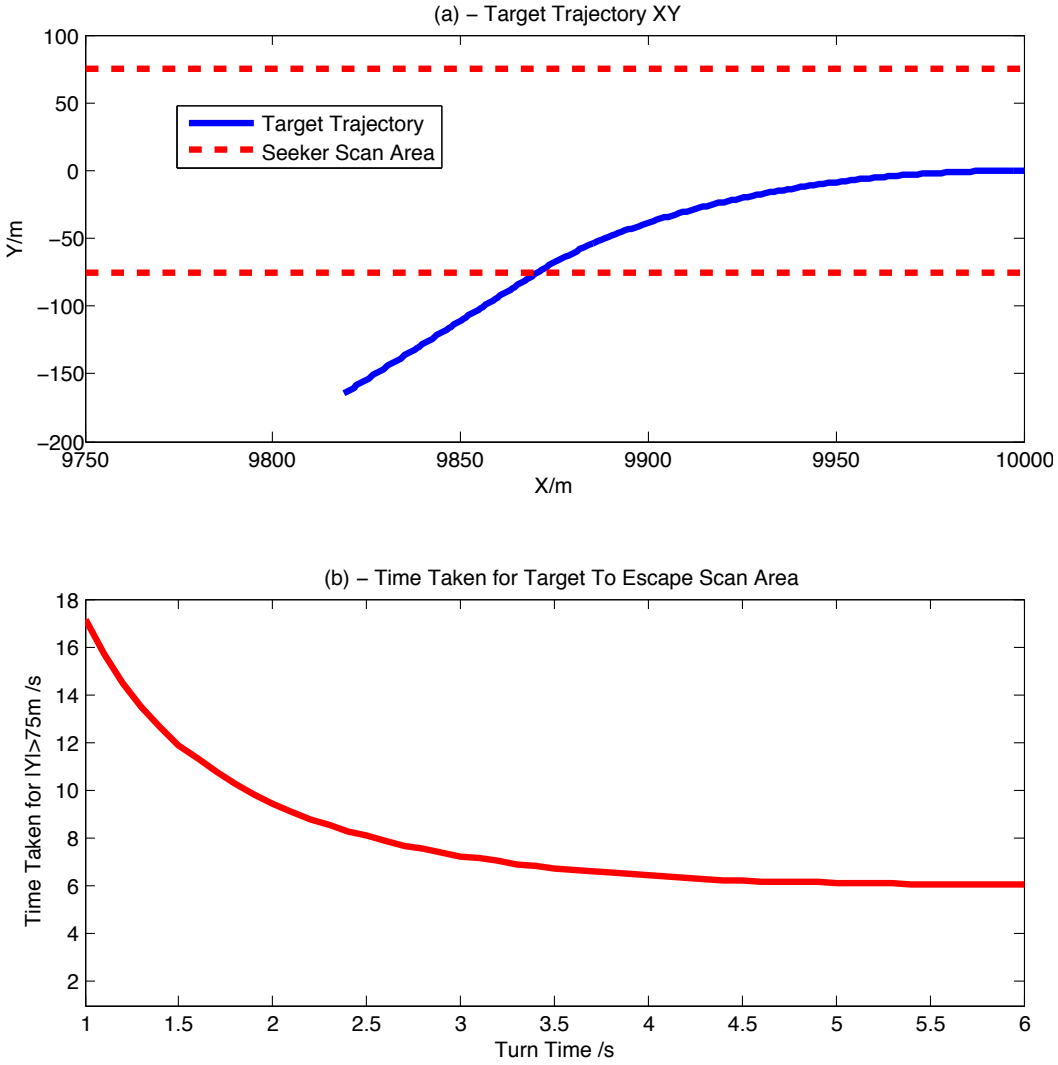

Figure 4.1: Calculation of Behaviour Time for Target Trajectory Prediction

From Figure 4.1 subplot (b) it is apparent that the most appropriate behaviour duration time is 5s. This is because a turn of less than 5s increases the time taken for the target to escape the seeker scan area and a turn duration of longer than 5s does not reduce this escape time. A turn/manoeuvre duration of 5s is therefore a reasonable approximation to use to predict the various trajectories.

Each target behaviour can be represented as a state which is assigned an integer value in the range of 1-3 as follows:

1. A state value of 1, is a 5s continuation of the previous target heading at maximum velocity.

2. A state value of 2, is a 5s turn to the right at a turn rate of $10°/s$

3. A state value of 3, is a 5s turn to the left at a turn rate of $10°/s$

A continuation of the previous target heading at maximum velocity is calculated using a constant velocity model (F_{CV}). A turn to the right (F_{CTR}) or left (F_{CTL}) is calculated using a co-ordinated turn model [32]. The transition matrix required for each of these dynamic models have been defined mathematically in Section 3.1.2

Each possible target trajectory is then simply a combination of 8, 5s state transitions which occur from an initial target state at a range of 10000m. For instance, a 5s turn to the right from launch by the target followed by 35s of continuing along the new heading would be defined in state transitions as 21111111.

The model predicts a total of 6561 (3^8) possible trajectories that the target could follow during the weapon fly out, including a non manoeuvring trajectory. The model is designed to be initialised from a target state observed from an initial radar detection. In order to show the complexity of the initial prediction trajectory distribution, the distribution of potential target trajectories has been calculated from an initial state of [10000,-26,0,0]' and is shown in Figure 4.2.

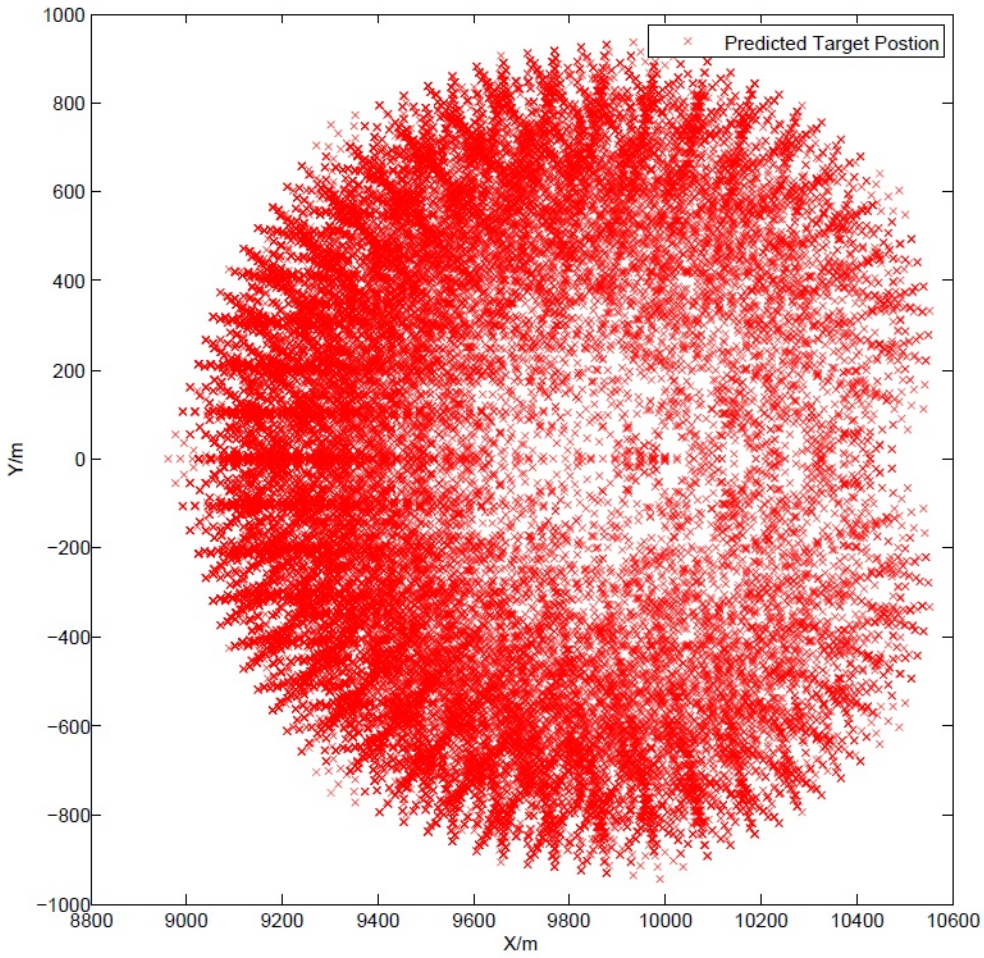

Figure 4.2: Distribution of Predicted Trajectories

Due to the large number of possible trajectories calculated by the model, it can be difficult to understand the time aspect of the trajectory distribution considering only this figure. Therefore Figure 4.3 is also provided which displays three trajectories predicted by the model. The trajectories are colour coded to show the 8 states which form each predicted trajectory and the time period associated with that particular state.

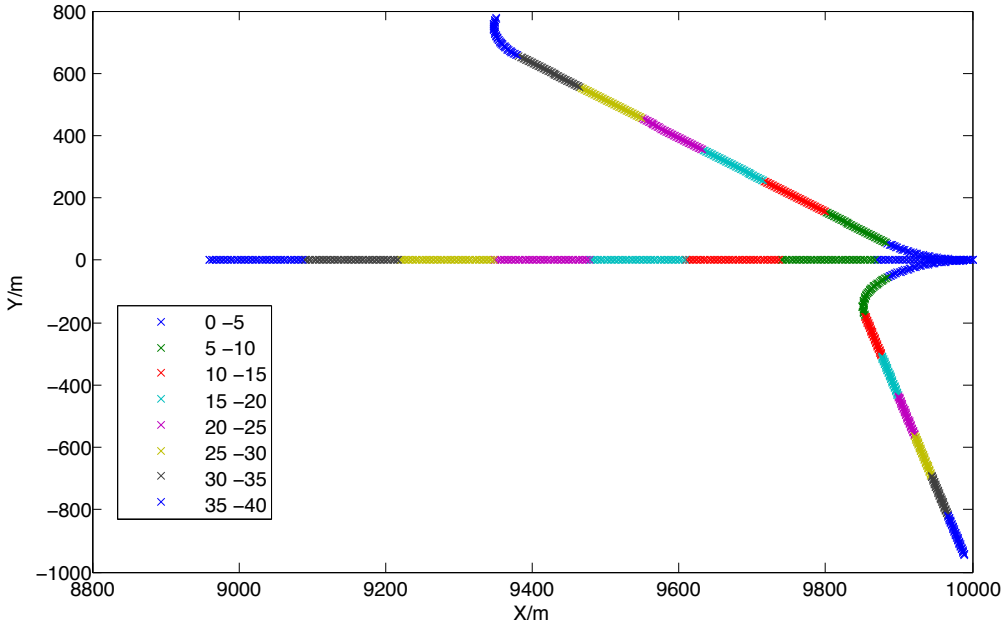

Figure 4.3: Selected Predicted Target Trajectories

The scan area associated with a given shaped trajectory would only be able to overlap part of the predicted trajectory distribution. In order to be able to optimise the weapon trajectory in the integrated fire control systems, the probability of the target following each of these approximate predicted trajectories during each 5s interval must be calculated.

4.2 Calculation of Associated Trajectory Probabilities

A target following one of the predicted trajectories will be within 1 of 3 states at each point in time. As each state has a duration of 5s, the target will therefore perform 8 state transition states (or steps) for a 40s target trajectory prediction. A state transition also includes transitions whereby the target remains in the current state.

As the military doctrine of the target is unknown, the most suitable approximation for the target behaviour is therefore a random process. In addition, it is assumed that the future state transitions of the target are independent of the past sequence of state transitions (Markov assumption [32]).

Based on this set of approximations, the probability of the target following any

one predicted trajectory during each 5s time period, can be calculated by modelling the behaviour of the target as a Markov Chain as follows:

1. Let $S = \{S_1, S_2, S_3\}$ be the possible target states and $\vec{P}_n = [p_1, p_2, p_3]'$ be the vector of probabilities of each state at step n. The probability p_i is then the probability that the target is in state S_i at step n.

2. The conditional probability p_{ij} that the target will be in state S_j at step $n+1$, provided it was in state S_i at step n is then defined as :

$$p_{ij} = P(X_{n+1} = S_j | X_n = S_i) \tag{4.1}$$

   where X_{n+1} and X_n denote the future and present state respectively.

3. The associated transition matrix P which contains all the conditional probabilities for the chain is then defined as:

$$P = \begin{bmatrix} p_{11} & p_{12} & p_{13} \\ p_{21} & p_{22} & p_{23} \\ p_{31} & p_{32} & p_{33} \end{bmatrix} \tag{4.2}$$

4.2.1 State Probability and Transition Matrix Calculation

In order to determine the state probabilities, the minimum time that the weapon seeker will be on and therefore in the detection mode before turning off must first be considered. The seeker will be on and in the detection mode while the weapon's range from launch is less than 10km.

The time taken for the weapon to achieve this range to turn off is primarily dependent on whether the weapon executes one or more off-boresight commands during the flight. Each off-boresight command will increase the weapon deceleration rate with greater yaw changes increasing the deceleration rate further. As the weapon speed then decreases, the time taken to achieve a range from launch of 10000m will therefore increase. The effect on the time taken for the weapon to achieve the turn off-range by the application of an off-boresight command is demonstrated in Figure 4.4.

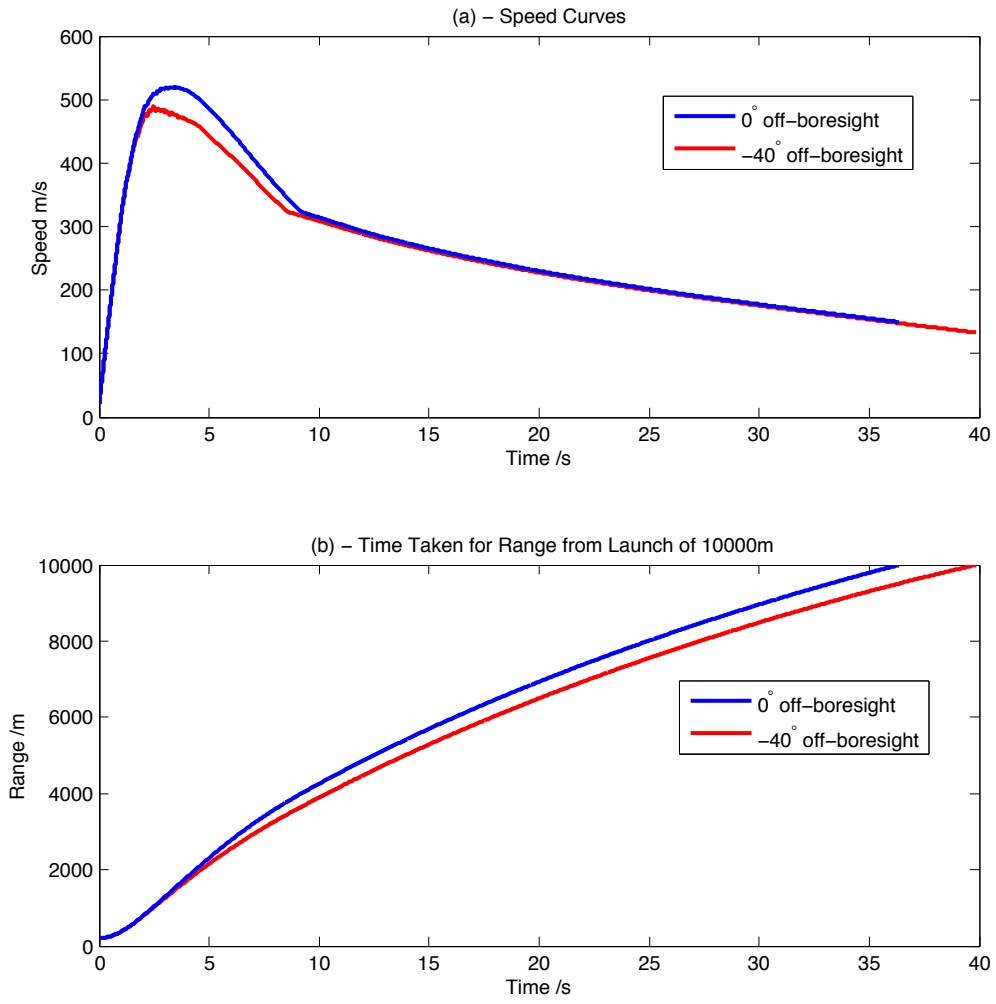

Figure 4.4: Speed Curve comparison of off-boresight angles of 0° and −40°

The speed and range graphs displayed in Figure 4.4 (a) and (b) are calculated with an launch off-boresight angle of 0° and −40° respectively. If the weapon is launched with an off-boresight angle of 0° it will reach the turn of range at T=36.8s. If the weapon is launched with an off-boresight angle of −40° it will reach the turn of range at T = 39.8s. In Figure 4.5, the seeker turn off time as a function of the launch off-boresight angle is shown.

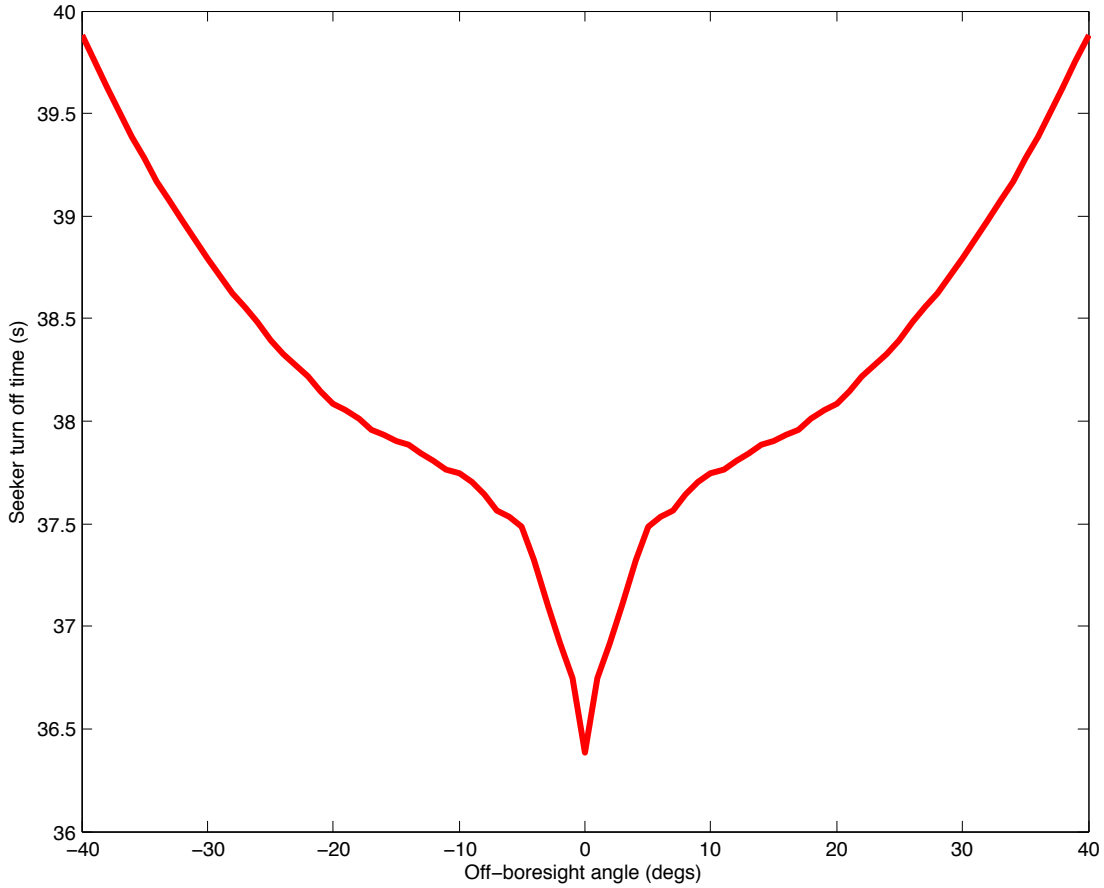

Figure 4.5: Seeker turn off time as a function of the launch off-boresight angle

Increasing the absolute value of the launch off-boresight angle increases the seeker turn off-time. The same effect can be achieved by sending off-boresight commands to the weapon once it is in flight. As can be seen from Figure 4.5, the time at which the seeker turns off varies from approximately T=36.2 to T=39s. It can therefore be confidently assumed that the seeker should be on for 35s of flight, regardless of the manoeuvres performed by the weapon. This minimum seeker time is equivalent to 7 state transitions for each predicted target trajectory. At T = 35s, there will be 3^7 possible target locations with an associated discrete probability distribution. Assuming that the seeker does not detect the target untill T=35s, then the state probability values can be tuned based on what the probability distribution would be at T=35s.

There is an equal probability that the target will turn right or left (P_2, P_3), therefore the three state probabilities can be determined using the following equation :

$$[P_2/P_3] = \frac{1 - P_1}{2} \tag{4.3}$$

Decreasing the probability of state 1 P_1 will increase the probabilities of P_2 and P_3. As the probabilities of P_2 and P_3 increase the total probability distribution at 35s will spread out. The state probabilities are calculated by considering the ideal case whereby the initial target location at T=0s is at the centre of the scan area associated with a predicted non manoeuvring target. The scan area will therefore overlap the middle of the predicted target distribution at T=35s as shown in Figure 4.6 (a).

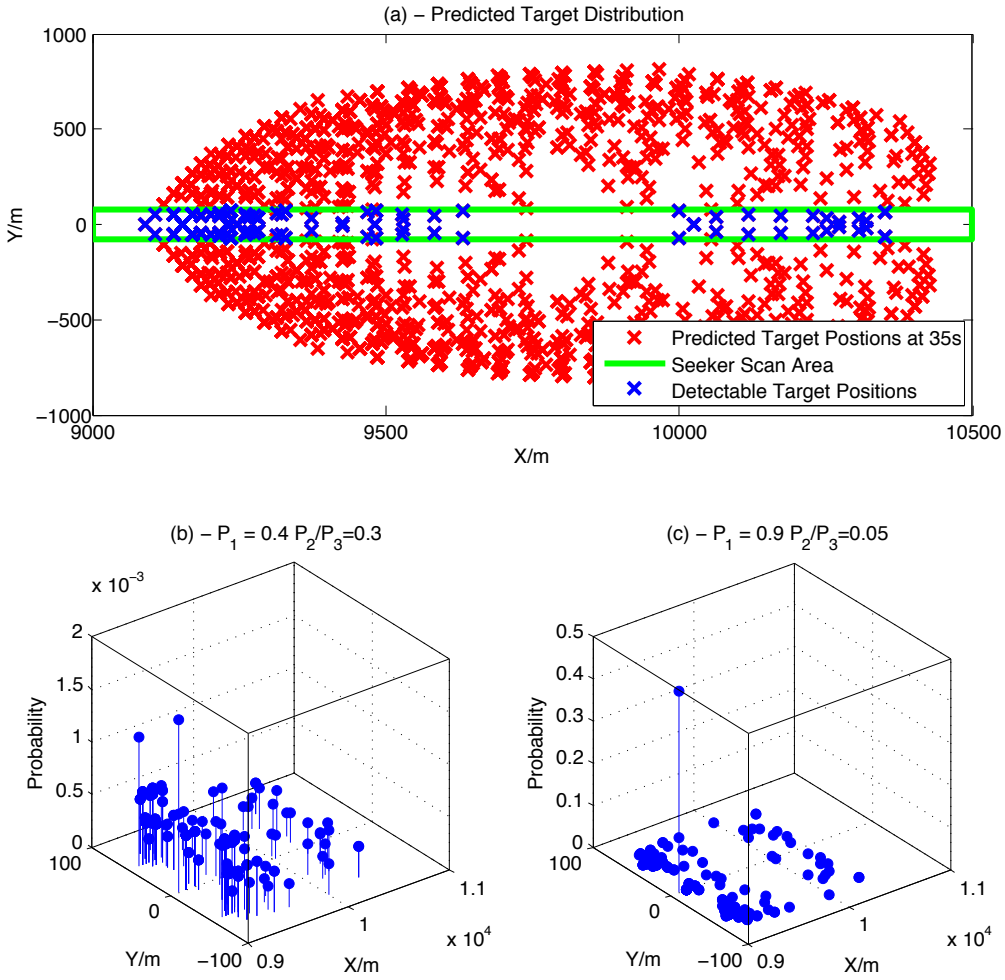

Figure 4.6: Predicted target locations at 35s

If $P_1 = 0.9$, $P_2/P_3 = 0.05$. then the scan area associated with a non manoeuvring target prediction results in a total probability of intercept of 0.46. However this probability of intercept is due to the high peak associated with a non manoeuvring prediction which is shown in subplot (c). The probabilities of the remaining target positions are negligible in comparison due to the shape of the probability distribution.

Any shaped trajectory and scan area generated by an integrated system will therefore be heavily biased towards the non manoeuvring trajectory and the limited number of other predicted target positions, which can be detected by focusing the seeker scan area over the non manoeuvring probability peak. An integrated solution will therefore not achieve a significant improvement in the performance of the AAAW to intercept a manoeuvring target. If the probability of state 1 is reduced, the significance of the bias towards a non manoeuvring target is decreased which can be demonstrated using Figure 4.7.

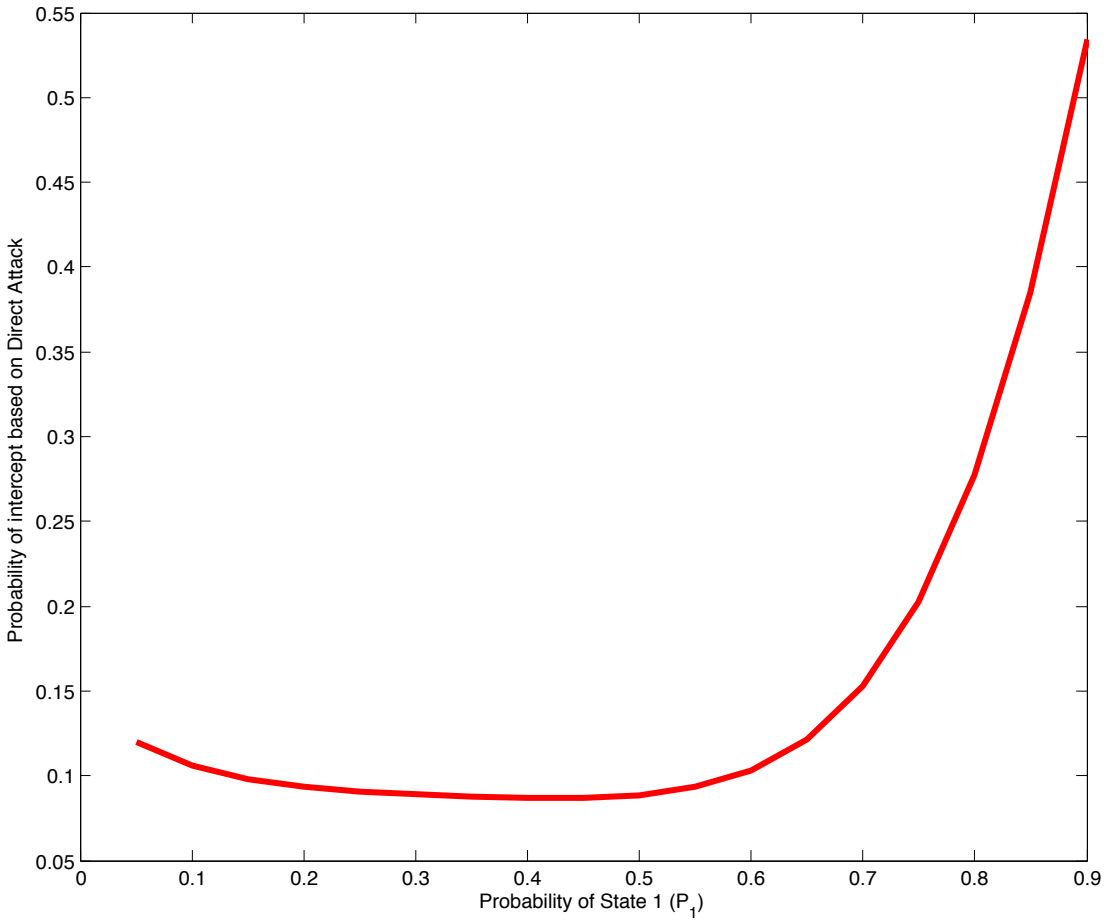

Figure 4.7: Total probability of intercept considering only the scan area associated with a direct attack

As shown in the Figure, the bias towards the non manoeuvring trajectory reaches a minimum level at a P_1 of 0.4. If the probability of state 1 is reduced further, then a bias towards manoeuvring targets starts to appear. This will have the opposite effect of biasing the trajectory solution towards a manoeuvring target trajectory, reducing the performance of an integrated system against a non manoeuvring target. As the possibility of a non-manoeuvring attack still exists

then any integrated system should be capable of intercepting this type of attack and other target behaviours. Therefore the probability of each state was set as $\vec{P}_n = [0.4, 0.3, 0.3]'$ with the associated transition matrix P calculated as:

$$P = \begin{bmatrix} 0.4 & 0.3 & 0.3 \\ 0.4 & 0.3 & 0.3 \\ 0.4 & 0.3 & 0.3 \end{bmatrix} \tag{4.4}$$

4.3 Sensor Selection - Pulsed Radar

The first part in the development of a simulated tracking system is the selection of an appropriate sensor input. The sensor will provide a series of noisy measurements for the target which are then processed by the tracking system.

There are a variety of sensor systems employed across, land, sea and air domains. These range from electro-optical systems, which sense radiation in the ultra-violet, visible and infrared portion of the electromagnetic spectrum, to systems like pulsed and continuous wave radar.

For target detection at sea, the target will most likely be detected at a low grazing angle (angle between the horizontal and a radar ray path). Electro-optical systems detect a lot of background clutter from the sea at low grazing angles. The background clutter in electro-optical systems consists of, saturation (sensor output does not change with increased radiance) and false alarms (detection of a non present target), which are due to the reflected solar radiation. [39]. As electro-optical systems are passive, it is very difficult to separate foreground objects from background clutter on the horizon easily.

Radar systems perform considerably better at low grazing angles. The background clutter due to the large return echoes observed from the sea is also much easier to separate from the target. This is because, the target will normally be moving, therefore Doppler processing can be used to separate out the echoes and detect the target. [40]

A pulsed radar system was chosen to be modelled in order to produce the noisy measurements. This is because a radar system will perform well at low grazing angles, with a further benefit that the range of the target is very easy to determine using a pulsed system [41].

4.3.1 Radar Theory

Radar uses radio waves to detect the presence and position of both friendly and hostile objects, this is what is known as radio detection and ranging [41], i.e (RADAR). The principle of radar is fairly simple. An antenna radiates electromagnetic energy in the form of radio waves which will scatter off anything which it encounters such as land, sea and man made objects such as aircraft and ships. A radio receiver (which can be the same antenna) detects reflected energy and after amplification and signal processing of the received echoes, information such as the range, bearing etc. of the target can be determined. There are a variety of radar systems employed in both military and civil applications. The two fundamental radar technologies in radar system design for target detection are Pulsed and Continuous wave.

Pulsed Radars transmit a pulse and then wait for the return signal. Though relatively complicated to manufacture, the target range can be easily calculated by measuring the time delay from the pulse being transmitted and the detection of the reflected pulse [42].

Continuous wave radars transmit a continuous signal. Because of this the target range cannot be calculated by measuring a time delay. However continuous wave radars are capable of determining the velocity of the target accurately and their range is only limited by the broadcast power level, making them ideal candidates for things like early warning systems.

For the purposes of this research, the radar model is representative of a short range pulsed radar system such as the Man-portable Surveillance and Target Acquisition Radar (MSTAR) which is used by the British Army for the detection of helicopters, vehicles and infantry. A pulsed radar model was selected because pulsed systems like MSTAR [43] have a strong track record in short range surveillance.

4.3.2 Noisy Measurement Generation

Pulsed radar systems describe the position of an object in 3D space in terms of Range (R), Bearing (θ) and Elevation (ψ). As the radar model is only operating over a short range, a flat earth approximation is used [44]. The implication of this approximation, is that if the radar were looking down at the sea at a given depression angle, the grazing angle can be taken as equal to the depression angle. For simplicity, the radar is assumed to be operating at sea level. Therefore, the

grazing angle can be taken as 0°. The position of the target is then described just in terms of range and bearing.

A radar system would detect clutter produced by the backscatter of the transmitted signal by elements of the sea surface. The clutter would be observed as a large background echo, which would be far greater in size than the return echo from the target. The level of clutter is dependent on the sea state, i.e. whether the sea was smooth or rough and on the size of the grazing angle. As the sea state worsens and the grazing angle increases, the amount of clutter detected increases [40]. Modelling the sea state and the associated clutter is highly complex and beyond the scope of this thesis. Therefore the sea state and associated clutter are ignored in this model.

Based on these approximations, the noisy measurements are generated by firstly converting the Cartesian coordinates (x_t,y_t) of the trajectory data supplied by the target model into a true range R_t and true bearing θ_t which are achieved using the following expressions :

$$R_t = \sqrt{(x_t - x_r)^2 + (y_t - y_r)^2} \tag{4.5}$$

$$\theta_t = atan\frac{(y_t - y_r)}{(x_t - x_r)} \tag{4.6}$$

The standard deviation of the measurement noise in range and bearing is then calculated, with the noises in the range and bearing measurements assumed to be normally distributed with a respective mean of the true range and true bearing.

The standard deviation of the measurement noise for the range is a function of the signal-to-noise-ratio (SNR), the speed of light (c) and the radar bandwidth (B) and can be defined as follows [41] :

$$\sigma_R \simeq \frac{c}{2B\sqrt{2 \times SNR}} \tag{4.7}$$

The standard deviation of the measurement noise for the bearing is a function of the radar beam width ($\Delta\theta$) and the signal to noise ratio and is defined as [41] :

$$\sigma_\theta \simeq \frac{\Delta\theta}{2 \times SNR} \tag{4.8}$$

Normally distributed random noise values for both the range R and bearing θ are calculated (δR, $\delta\theta$). The range R_m and bearing θ_m measurements are then defined as

$$R_m = R_t + \delta R \tag{4.9}$$

$$\theta_m = \theta_t + \delta\theta \tag{4.10}$$

with the final Cartesian position measurements (x_m, y_m) then calculated as :

$$x_m = x_r + R_m cos(\theta_m) \tag{4.11}$$

$$y_m = y_r + R_m sin(\theta_m) \tag{4.12}$$

Equations 4.7 and 4.8 have introduced a number of the important radar concepts used to create the model such as the signal to noise ratio (SNR) and bandwidth (B). Parameters such as these are optimised in the design of a radar system or the creation of a mathematical model. As such they require an in-depth explanation which is provided in the following section of this chapter.

4.4 Radar Model Design

The mathematical model of the radar system is based on the radar equation [41]. All calculations, in the model are performed by considering a radar with a single antenna to transmit and receive. Sections 4.4.1-4.4.2 present the derivation of this equation and further radar concepts. Section 4.4.3 presents the specification of the final radar model and the associated noise standard deviations for the range and bearing measurements.

4.4.1 Radar Equation Derivation

The first part of the derivation is to calculate the power density per unit area or power flux (P_{Fl}) at the target from the radar installation. It is assumed that the radar antenna has a peak power output P_t and that the power is concentrated towards the target.

The power flux at the target is a function of the peak output power P_t, the area of the sphere (at the end of the antenna) through which the power must pass and the gain factor (G_t) associated with the geometry of the transmitting antenna design. The power flux at the target (P_{ft}) can therefore be defined as :

$$P_{ft} = \frac{P_t G_t}{4\pi R^2} \tag{4.13}$$

The gain factor of the transmitter antenna is a function of the wavelength of the transmitted radio waves (λ) and the effective area of the transmitter (A_e). It is defined as :

$$G_t = \frac{4\pi A_e}{\lambda^2} \tag{4.14}$$

The wavelength is a function of the operating frequency (f) and the speed of light (c) and is calculated as

$$\lambda = \frac{c}{f} \tag{4.15}$$

The next step is to consider the power re-radiated by the target. Transmitted radio waves will be reflected off any object encountered. Each object, including the target and surrounding clutter, will intercept some of the incident power and re-radiate it back towards the radar. The amount of incident power intercepted and reflected by an object is what is known as the radar cross section (σ) of that particular object. Therefore the power re-radiated (P_{rr}) towards the radar due to the radar cross section of the target is calculated as

$$P_{rr} = \frac{P_t G_t \sigma}{4\pi R^2} \tag{4.16}$$

The reflected power intercepted by the antenna is a function of the effective area of the antenna and the spread of the power over a sphere of area $4\pi R^2$ on its return path, as well as some losses in the system (L). The power intercepted at the antenna P_{IA} becomes :

$$P_{IA} = \frac{P_t G_t G_r \sigma \lambda^2 L}{4\pi^3 R^4} \tag{4.17}$$

The final step is to consider the background noise (N). For all practical radars the noise will be dominated by internal noise produced by thermally excited electrons. The noise is a function of the Boltzmann constant (k), the system temperature T_0 and the radar bandwidth (B) and is calculated as [40]:

$$N = kT_0B \tag{4.18}$$

The final radar equation then becomes :

$$SNR = \frac{P_t G_t G_r \sigma \lambda^2 L}{4\pi^3 R^4 N} \tag{4.19}$$

The radar equation is often used to find one unknown [41], for the purposes of this research it was used to calculate a required transmitter power for a given set of design parameters. For further information on the derivation of the radar equation, see references [45] and [42].

4.4.2 Operating Frequencies, Pulse Width, Bandwidth

Before proceeding to discuss the specification of the radar model and the calculation of the required transmitter power. It is first worth exploring in greater detail the significance of the selection of the radar operating frequency, pulse width and bandwidth.

4.4.2.1 Operating Frequency

The operating frequency of the radar is an important design consideration in any radar system as it directly influences the angular resolution (beamwidth) of the radar beam, the dimensions of the transmitter and the efficiency of the propagation of the radio waves through the medium [41]. The angular resolution ($\Delta\theta$) of a radar beam is defined as :

$$\Delta\theta = \frac{\lambda}{d} \tag{4.20}$$

where λ is the wavelength and d is the diameter of the antenna.

A higher operating frequency results in a smaller beamwidth and therefore a better angular resolution. However at lower frequencies the propagation of the radio waves through the medium is more efficient but larger antennas are required. Short range surveillance radars such as the British MSTAR system [43] operate in the I and J bands (8-20 GHZ).

4.4.2.2 Pulse width and Bandwidth

The selection of the pulse width is an important factor in the design of a pulsed radar system. It dictates the range resolution (ΔR), bandwidth and the sampling frequency for a given range to be surveyed. The range resolution dictates how far apart two targets must be in order to be recognised as two separate targets. It is a function of the pulse width (τ) and the speed of light (c) and is defined as :

$$\Delta R = \frac{c\tau}{2} \tag{4.21}$$

As can be seen a shorter pulse width gives an improved range resolution. However, to survey the same area as a longer pulse width requires a faster sampling frequency resulting in increased computational load on the digital signal processing component of the radar system. A shorter pulse width results in a higher bandwidth (as bandwidth is defined as) :

$$B = \frac{1}{\tau} \tag{4.22}$$

The higher the bandwidth for a given SNR, the smaller the standard deviation of the measurement noise in terms of the range measurement. However a higher bandwidth also increases the noise in the system, reducing the SNR.

It is easy to see the difficult balance that must be achieved by a radar engineer when optimising the operating frequency, pulse width and bandwidth.

4.4.3 Calculation of Transmitter Power

The first step in the calculation of the transmitter power is to set a reasonable radar detection range. This can be accomplished by considering a real world scenario, in that the integrated fire control system for the AAAW would be part of a much larger multilayered defensive system [46].

The radar model described in this chapter would be known as a fire control radar, as it is responsible for supplying target measurements to a weapon fire-control system. A ship would most likely utilise a variety of systems for long range threat detection such as continuous wave radar [41]. On the detection of a target, the fire control system for the AAAW would be activated. However sufficient time would have to be allowed in order to steer the fire control radar onto the target. The specific timing details for this type of multilayered defence system are not available within open source literature, therefore a reasonable time and associated detection range has to be approximated.

The target has a maximum speed of 26m/s and the AAAW has a maximum seeker target detection range of 10000m. Based on these parameters the detection range of the radar was set at 10500m. This would allow allow a minimum time of just under 20s to steer the radar onto the target, which should be a reasonable allocation of time.

As the pulsed radar is therefore operating over a short range, a J-Band operating frequency of 20Ghz is selected which results in a respective wavelength of 0.015m. In order to achieve good range resolution a short pulse width of $1\mu s$ was selected. This results in a bandwidth of 1MHz and an associated noise level of 144dBW.

The next step is to consider the radar cross section of the target. In a real would scenario, the radar cross section of the boat (target) would vary based on a number of parameters. It is a highly complicated issue which is beyond the scope of this research. However approximate constant values for various target types are provided in [41]. A small boat has an approximate radar cross section of $1m^2$ or 0dB [41].

For a target with a cross section of 0dB, the SNR for reliable detection was set at 30dB [41]. The final variable in the model to be determined is the antenna diameter which was selected to be 2m [41]. The transmitter power can then be

calculated from a rearrangement of the radar equation as follows :

$$P_t = \frac{SNR4\pi^3 R^4 N}{G_t G_r \sigma \lambda^2} \tag{4.23}$$

After substituting the values defined from the specification provided earlier, a peak power of 70W was obtained. The standard deviation of the measurement noise in respect of the range (σ_r) and bearing (σ_θ) at the maximum detection range was calculated as 3.037m and 1.2149×10^{-4} rads respectively.

Changing the parameters of the radar model specification will change the noise values obtained. However these values have been verified against open source parameters for in service radars such as MSTAR [43] and the Ranger R4. The radar model therefore represents a realistic model suitable for this research. In an operational radar such as these systems, the transmitter power would most likely be reduced using techniques such as pulse integration, which integrates a number of lower power pulses to produce the equivalent transmitter power.

4.5 Stochastic Estimation

Measurements generated by any sensor will be noisy. The factors which control the level of noise in a radar system have been discussed in detail in the preceding Section. Once noisy measurements are available, whether modelled in the case of this research, or within a real world system, the next issue to address is how to estimate the state of the target at each point in time. A general approach known as stochastic methods can be used for the purposes of estimation. Stochastic methods estimate an unknown target state assuming that the measurement noise is either statistical in nature or can be modelled as such [47]. They often make use of state-space models.

An overview of the principle of state space models as well as important statistical concepts are discussed in the following sections.

4.5.1 State-space models

State-space models are a convenient mathematical notation for estimation and control problems. State-space models can be used to describe many processes in the world from biological systems to processes in economics and physics [48]. By deriving a mathematical system model to represent the process, the tools of mathematics can be used to obtain information about the process and potentially control it.

There are two types of system model, linear and non-linear. Most real processes are non-linear. However the mathematics required to describe a non-linear process are often highly complex. Therefore many non linear processes are often approximated as a linear system as the mathematics required to define a linear process are often simpler than that of non linear processes [48].

The state of a system is expressed as a state vector, with the variables within the state vector describing the dynamic state of the system at a particular instant in time. A state space model contains two equations consisting of the system and measurement equations. The system equation is a mathematical model which predicts the evolution of the system subject to a defined dynamic model and external influences such as system inputs. The system equation will normally be an incomplete characterisation of the system. Therefore, a process noise is also used to account for modelling inaccuracies.

The measurement equation describes how the variables in the state vector are related to the noisy observed measurements, where each measurement will be the true system state with some added unknown noise which is often due to inaccuracies in the sensor. Estimating the future state of a system using only noisy measurements will often be ineffective for most tracking problems. In order to produce a more reliable prediction of the future state of the system, predictive filters can be used.

Predictive filters estimate the optimal state of a system by using a mathematical model of the dynamics of the systems to propagate the state and the associated uncertainties [49]. The propagated state is then combined with the best information available from the measurements. There are numerous filter types available with each one being appropriate for a certain type of uncertainty representation and dynamic model.

The predictive filter used in this thesis is a Kalman filter which represents uncertainties as Gaussian random variables (justification of a Kalman filter is provided in Section 4.6). In order to understand how the filter works, the fundamental statistical concepts related to the Kalman filter are firstly reviewed, with the general mathematical representation of a state space model then provided.

4.5.2 Statistical Concepts

There are four main statistical concepts which must be understood in order to fully understand how the Kalman filter works. These consist of the mean, standard deviation and variance of a scalar random variable as well as the covariance of two scalar random variables which are defined as follows :

The expected value (E) [32] of a scalar random variable (x) which is more commonly known as the mean $\bar{x}$ is defined as

$$\bar{x} = E[x] = \int_{-\infty}^{\infty} xp(x)dx \tag{4.24}$$

The second central moment [32] or variance (σ^2) is then defined as

$$\sigma_x^2 = E[(x - \bar{x}^2)] = \int_{-\infty}^{\infty} (x - \bar{x}^2)p(x)dx \tag{4.25}$$

with the square root of the variance yielding the standard deviation (σ_x)

$$\sigma_x = \sqrt{\sigma_x^2} \tag{4.26}$$

In a multivariate case i.e two scalar random variables (x_1, x_2) with respective means of $(\bar{x_1}, \bar{x_2})$ a covariance matrix is obtained [32] as

$$cov(x_1, x_2) = E[(x - \bar{x_1})(x - \bar{x_2})] \tag{4.27}$$

The Kalman filter describes uncertainties using Gaussian random variables. This means that the random variables has a probability density function $p(x)$ defined as :

$$p(x) = \frac{1}{\sqrt{2\pi\sigma_x}} exp^{-\frac{(x-\bar{x})^2}{2\sigma_x^2}} \tag{4.28}$$

The Gaussian distribution is one of the most historically popular probability distributions used in modelling random systems. It is a special distribution because it appears many random processes which occur in nature appear to be Normally distributed or very close to it. Under some moderate conditions it can even be proved that a sum of random variables with any distribution will tend towards a normal distribution. This property is stated formally by the central limit theorem [50].

4.5.3 State-space model mathematical representation

The concept of state space can be explained by considering a moving object. The variables which represent the dynamical motion of the system i.e. position and

velocity are defined by a sequence of states which can be collated into a state vector $x(k)$. The state vector can then be used to define the dynamical state of the system at each time step (k). The evolution of the system state over time is then predicted by the **system** equation. The system equations defined in this thesis are direct discrete-time models as such they have the following general form [32] :

$$x(k+1) = F(k)x(k) + G(k)u(k) + \Gamma(k)v(k) \tag{4.29}$$

where $F(k)$ is state transition matrix and $v(k)$ is a white process noise which enters through a noise gain Γ [32]. The process noise accounts for inaccuracies in the system model. It has an associated covariance matrix $Q(k)$. $u(k)$ represents a set of assumed known controls with an associated input gain $G(k)$ [51].

The **measurement** equation describes the relationship between the predicted state vector $x(k)$ obtained from the system equation and the observed measurement $z(k)$. The observed measurement will be the true state of the system with the addition of a unknown noise $w(k)$ which is defined mathematically as :

$$z(k) = H(k)x(k) + w(k) \tag{4.30}$$

where $H(k)$ is measurement matrix used to selected the measured states from the state vector.

The system and measurement equations which define the state-space model form the basis of virtually all linear predictive filters.

The Kalman filter was chosen as the fundamental component of the tracking algorithm in this thesis because linear target dynamics are assumed and the measurement noise produced by the radar model is white and Gaussian distributed. The Kalman filter under these conditions will provide the optimal state estimate [48]. In cases where the process model is not strictly linear, and can not be successfully approximated as such, other filters exist such as the Extended Kalman Filter [52], Unscented Kalman Filter [53] and the Particle filter [54].

4.6 Kalman Filter

The Kalman filter is a predictive filter which was introduced by Rudolf Kalman in 1960 [55]. It is an algorithm that has been employed in various applications from process control to stock price prediction [56].

The filter estimates the instantaneous state of a linear dynamical system using measurements corrupted by Gaussian white noise which are linearly related to the system state [57]. It is a recursive filter which minimises the mean square estimation error without direct observation of the system state.

There are several good explanations of the Kalman filter available such as those found in [55, 58, 59]

The notation for the filter algorithm provided in the following section is the same as used in reference [32] which can be consulted for further information on the implementation of the Kalman Filter.

4.6.1 Kalman Filter Algorithm

1. The first step in the algorithm is to initialise the estimated state $\hat{x}(0|0)$ and associated estimated state covariance $P(0|0)$. The initial estimated state can be obtained using some preliminary measurements.

2. The predicted state $\hat{x}(k+1|k)$ is obtained from a given system model as :

$$\hat{x}(k+1|k) = F(k)\hat{x}(k|k) + G(k)u(k) \tag{4.31}$$

   where $F(k)$ is a state transition matrix which predicts how the system should evolve from state to state and $G(k)$ is an input gain associated with a set of known controls $u(k)$.

3. The predicted measurement $\hat{z}(k+1|k)$ is then calculated from the predicated state as :

$$\hat{z}(k+1|k) = H(k+1)\hat{x}(k+1|k) \tag{4.32}$$

   where $H(k+1)$ is a measurement matrix which will select the predicted states which will be measured at $k+1$.

4. The updated estimated state covariance matrix $P(k+1|k)$ is then calculated as :

$$P(k+1|k) = F(k)P(k|k)F(k)' + Q(k) \tag{4.33}$$

   where $Q(k)$ is the process noise covariance matrix which represents the inaccuracies in the assumptions made when characterising the dynamics of the target for the system model.

5. The measurement prediction covariance $S(k+1)$ is then determined from the predicted state covariance $P(k+1|k)$, the measurement matrix $H(k+1)$ and the actual measurement covariance matrix $R(k+1)$. The measurement

covariance matrix is determined from the properties of the noise associated with the measurement sensor. The measurement prediction covariance is calculated as :

$$S(k+1) = H(k+1)P(k+1|k)H(k+1)' + R(k+1) \tag{4.34}$$

6. The Kalman Gain $W(k+1)$ is then determined, with the associated matrix constructed in such a way as to minimise the covariance of the expected errors in the predicted state as follows :

$$W(k+1) = P(k+1|k)H(k+1)'S(k+1)^{-1} \tag{4.35}$$

7. A new measurement is obtained $z(k+1)$ from the sensor and the predicted state is updated from the innovation $\nu(k+1)$ and the filter gain $W(k+1)$. The updated state estimate $\hat{x}(k+1)(k+1)$ is calculated as :

$$\hat{x}(k+1|k+1) = \hat{x}(k+1|k) + W(k+1)\nu(k+1) \tag{4.36}$$

where :

$$\nu(k+1) = z(k+1) - \hat{z}(k+1|k) \tag{4.37}$$

8. The final step in the filtering process is to update the estimated state covariance matrix as :

$$P(k+1|k+1) = [I - W(k+1)H(k+1)]P(k+1|k) \tag{4.38}$$

where I is the identity matrix.

The filter is computationally simple consisting of only three main steps; measurement, innovation and prediction [51]. A simple tracking problem utilising a Kalman filter is provided in the following section in order to give a clearer understanding of the principle of operation of the filter algorithm.

4.6.2 Kalman Filter Simple Example

A target begins with an initial state $X(0) = [x, v_x, y, v_y]$ of $[10000, -25.8, 1220, 2.7]'$. It moves at constant velocity for 35s. At T=35s, the target begins a 5s turn to the right. Appropriate noisy measurements of the target position are produced using the pulsed radar model. A simple Kalman filter utilising a constant velocity model [32] is used to track the target for a 40s time period. The state transition matrix, $F(k)$ can be derived from the following equations of motion :

$$x(k+1) = x(k) + v_x(k)t \tag{4.39}$$

$$v_x(k+1) = v_x(k) \tag{4.40}$$

which yields the transition matrix :

$$F(k) = \begin{bmatrix} 1 & dt & 0 & 0 \\ 0 & 1 & 0 & 0 \\ 0 & 0 & 1 & dt \\ 0 & 0 & 0 & 1 \end{bmatrix} \tag{4.41}$$

The measurement matrix $H(k)$ is calculated to select the target states which are measured (i.e. the cartesian position in $[x, y]$) and is defined as :

$$H(k) = \begin{bmatrix} 1 & 0 & 0 & 0 \\ 0 & 0 & 1 & 0 \end{bmatrix} \tag{4.42}$$

with the covariance matrices of the estimation error $P(0|0)$ and measurement error $R(0|0)$ [32] initially defined as :

$$P(0|0) = \begin{bmatrix} 1 & \frac{1}{dt} & 0 & 0 \\ \frac{1}{dt} & \frac{2}{dt^2} & 0 & 0 \\ 0 & 0 & 1 & \frac{1}{dt} \\ 0 & 0 & \frac{1}{dt} & \frac{2}{dt^2} \end{bmatrix} \cdot (\sigma^2) \tag{4.43}$$

$$R(0|0) = \begin{bmatrix} 1 & 0 \\ 0 & 1 \end{bmatrix} \cdot (\sigma^2) \tag{4.44}$$

The system transition matrix assumes that the target is moving at constant velocity during each finite time step (dt). However, for most real world applications the target motion may suffer from some small fluctuations (accelerations). The process noise covariance matrix $Q(k)$ represents the inaccuracy in assuming constant target motion.

$$Q(k) = \begin{bmatrix} \frac{1}{4}dt^4 & \frac{1}{2}dt^3 & 0 & 0 \\ \frac{1}{2}dt^3 & dt^2 & 0 & 0 \\ 0 & 0 & \frac{1}{4}dt^4 & \frac{1}{2}dt^3 \\ 0 & 0 & \frac{1}{2}dt^3 & dt^2 \end{bmatrix} \cdot \sigma_v^2 \tag{4.45}$$

The σ_v term within the process noise covariance matrix represents the standard deviation of the perturbations i.e. the typical acceleration of the target between time steps. The typical accelerations will often be unknown, therefore the value of σ_v becomes a design parameter which is tuned to produce the best tracker performance. An increase in the value of this design parameter results in an increase within the expected errors in the prediction step of the filter [51]. It should be noted that the covariance matrix in this form will only work for fixed time steps.

In this particular example a small value of $0.1m/s^2$ was chosen as it is assumed that the target velocity will vary only a very small amount.

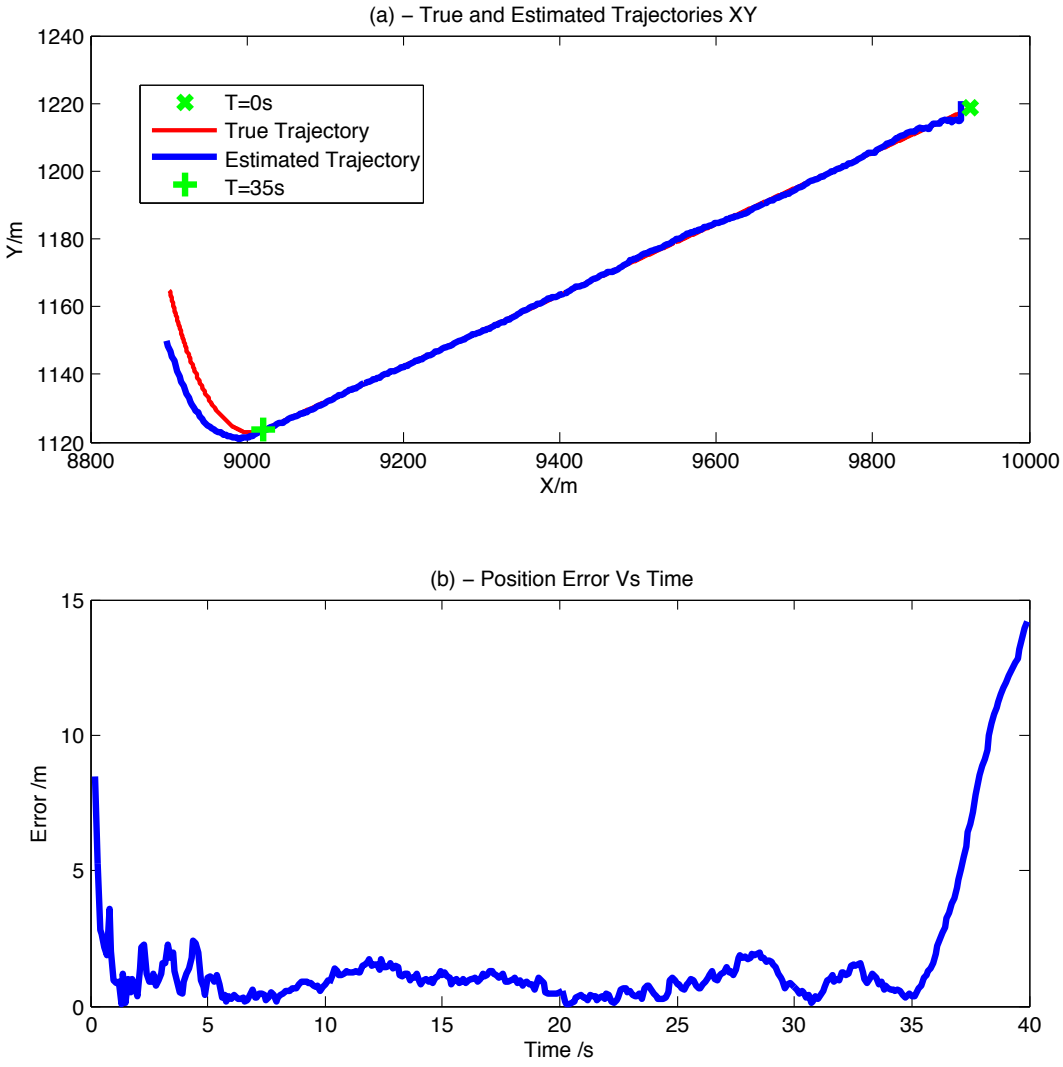

Figure 4.8: Kalman Filter Example

During the non manoeuvring motion of the trajectory, the Kalman filter performs well, shown by the small error in the estimated position depicted in Figure 4.8 However once the target begins the turn, the error rapidly increases. This is due to the mismatch between the assumed target dynamics in the filter (i.e. the constant velocity model) and the actual target dynamics of a turn at T=35s onwards. The poor performance of a single Kalman filter in respect of a manoeuvring target is a common issue. Several algorithms have been developed to improve the ability of the Kalman filter to track a manoeuvring target. These algorithms are discussed in detail in the next Section of this Chapter.

4.7 Manoeuvring Target Tracking (MTT)

There are two significant issues which all target tracking algorithms must seek to overcome; the measurement origin uncertainty and the target motion uncertainty [60]. The measurement origin uncertainty arises because a measurement produced by any sensor system may have originated from another source instead of the object of interest (target). For instance if the sensor system is a radar, then measurements could originate from background clutter and false alarms. Numerous techniques have been developed to understand and overcome this uncertainty. The reader is directed to [61] and [62] for further information.

The target motion uncertainty arises due to the fact that the target may undergo a known/unknown manoeuvre starting and ending at unknown points in time. When the target manoeuvres, a mismatch will exist between the assumed modelled dynamics i.e. the transition matrix used in the state equation in the Kalman filter and the actual target dynamics [63]. For instance, if the Kalman filter uses a constant velocity model with a low process noise and the target performs a co-ordinated turn, then a large mismatch will exist between the estimated state of the target and the actual state of the target.

In order to improve the performance of the Kalman filter to track a manoeuvring target, there are two fundamental approaches available. These consist of Adaptive Estimation and the Multiple Model Approach.

4.7.1 Overview of Adaptive Estimation

Adaptive Estimation makes use of both estimation and decision in order to track a manoeuvring target [64]. It is discussed in varying degrees of detail in references [65–70].

The mismatch between the assumed target dynamics and the actual target dynamics will result in a poor track being produced by the filter. Adaptive estimation techniques attempt to compensate for the mismatch by adapting the state estimate in some way from decisions made about the behaviour of the target. Normally the start and end time of a particular manoeuvre are used in order to make the decision to adapt the state estimate. A variety of techniques exist in this area with the three most common being, Adjustable Level of Process Noise, Input Estimation and Variable State Dimension. These are the techniques which are discussed in this chapter assuming a Kalman filter is being used to track the target.

4.7.2 Adjustable Level of Process Noise

The covariance of the process noise (Q) is used to represent the inaccuracies associated with the assumptions made about the behaviour of the target in the prediction step of the filter [51].

A target manoeuvre will result in a large innovation, as there will be a significant mismatch between the true and estimated target dynamics. The adjustable level of process noise approach assumes that the effect of the large innovation on the state estimate can be compensated for by scaling the process noise level covariance by a predefined factor, or by switching to a higher process noise covariance matrix. Once the manoeuvre terminates the process noise covariance matrix is either scaled down or the filter switches to a lower predefined process noise covariance matrix.

The upward and downward adjustments of the process noise covariance level are performed from the detections of the onset and termination of the manoeuvre.

There are a variety of manoeuvre detections techniques which can be used to detect the manoeuvre onset and termination [65], [71], the most common choice is a simple chi-square test [72].

There is a significant amount of literature utilising this technique in a variety of applications [65], [66] [73]. The reason for the choice of the test indicated in the reviewed literature is the simplicity in its implementation. The test is also reliable provided that the individual terms of the test can be assumed to be independent and Gaussian in nature [64] (which is normally acceptable based on the Central Limit Theorem).

The test can be applied in this research to determine whether there is statistical evidence to suggest that the results of the successful manoeuvring intercepts achieved by a data linked AAAW in a given integrated fire control system are due to chance alone.

4.7.3 Input Estimation

Input Estimation assumes that a manoeuvring target can be described as a linear system which is being driven by an unknown input, over a particular time window [32]. This can be stated mathematically as :

$$x(k+1) = F(k)x(k) + G(k)u(k) + \Gamma(k)v(k) \tag{4.46}$$

where $u(k)$ represents an unknown input with an associated gain $G(k)$, $v(k)$ is a process noise with associated gain Γ(k) and a covariance matrix $Q(k)$. The estimate produced by the filter will initially be reliable up until the target manoeuvre.

During the manoeuvre, the filter will be mismatched to the actual target behaviour. The error in the estimate will increase significantly. Input estimation seeks to correct the state estimate by estimating the unknown input during the manoeuvre time window.

There have been numerous papers on tracking published which make use of the input estimation technique such as [74–76]. The algorithm can be briefly summarised as :

1. A filter with an input $u(k)$ of 0 is used to estimate the state during the manoeuvre based on an original assumed system model such as a constant velocity model.

2. The target manoeuvre will result in a large innovation for the mismatched filter, which can then be considered as "a linear measurement of the input with additive zero-mean white noise with covariance equal to the filter's innovation covariance [32]" .

3. Assuming that the manoeuvre started at the beginning of an assumed sliding time window and that it can be represented as a constant unknown input, then the input itself can be estimated using the method of Least Squares.

4. The size of the estimated input (e.g. acceleration) is then compared against the standard deviation of the measurement to determine whether the size of the input is statistically significant. If the size of the input is significant then the state estimate produced by the mismatched filter is corrected with the effect of the estimated input from the start of the assumed time that the manoeuvre began.

The reader is directed to either, [64] or [32] for a more in depth explanation of the algorithm.

4.7.4 Variable State Dimension (VSD)

The Variable State Dimension approach is the the last of the three adaptive estimation techniques to be discussed in this thesis. The VSD considers the manoeuvre as an inherent part of the target dynamics.

While the target is not manoeuvring, the filter operates using a quiescent state model. A manoeuvre detection results in the filter switching to an augmented state model which consists of further state components. The target is then tracked with the augmented model until another decision is made to revert back to the quiescent model. A summary of the algorithm is provided below :

1. The filter is initialised with a quiescent state model, the filter uses this state model during the non manoeuvring part of the target motion.

2. A target manoeuvre is detected when a fading memory average of the normalised innovations exceeds a predefined threshold.

3. The detection of a manoeuvre results in the estimator switching to an augmented model which incorporates additional state components.

4. The filter switches back to the quiescent model when a manoeuvre is declared terminated. This is when the extra estimated state components of the augmented model become statistically insignificant.

4.7.5 Review of Techniques

Though each algorithm described in this chapter can be used to track a manoeuvring target, each one has a number of drawbacks which limits the effectiveness of the algorithm for a MTT problem. The adjustable level of process noise approach is very simple to implement, however the calculated equivalent noise is highly non stationary which makes it unsuitable for most MTT problems. Assuming the input is constant in the case of the input estimation algorithm, limits again this algorithm's applicability to most MTT problems. The variable state dimension approach is the best of the three algorithms. It is the most flexible but relies more heavily on good manoeuvre detection [64] for MTT problems, than the other techniques. Due to the greater dependency of VSD on good manoeuvre detection, relatively few examples of this approach where found utilising this approach for tracking a manoeuvring target [77, 78] compared to the other algorithms. A more widely used approach in terms of tracking a manoeuvring target is Multiple Model Methods which is the subject of the next section of this chapter.

4.8 Multiple Model (MM) Methods

In general the most effective way of describing manoeuvring and non-manoeuvring target motion is to use different motion models. For instance the motion of a civil-

ian aircraft in the horizontal plane can be described by a nearly constant velocity model for when the aircraft is maintaining its current heading with turns characterised by a coordinated turn model [79].

One of the most common approaches to target tracking in the presence of motion uncertainty is the Multiple Model (MM) method. This is evidenced by the wide range of literature available on manoeuvring target tracking utilising this technique [80–93]. The first approach to this algorithm was the static multiple model estimator. It uses a number of models, each matched to a filter to represent possible system behaviours (e.g. manoeuvres). These various behaviours are commonly referred to as system modes. The early results of the static multiple model estimator provided good results for systems with a time invariant unknown or uncertain system mode. However the static approach has been proven ineffective for handling a manoeuvring target tracking problem in which the system undergoes frequent transition between system modes [60, 70].

It was not until 1988 when the highly cost-effective Interacting Multiple Model (IMM) [94] estimator was developed that the multiple model approach became an effective method for tracking a manoeuvring target.

One of the most significant properties of the IMM which makes it such an effective approach for manoeuvring target tracking is its ability to get around the difficulty of the target model uncertainty [95].

In approaches prior to this and especially in decision-based methods, only the estimate produced from one filter at any point in time was considered. The accuracy of the tracker is then heavily dependent on correct behaviour detection.

The IMM estimator uses multiple models and generates a state estimate by combining the state estimates produced from each filter within a given bank of models. By weighting these estimates, improved tracker performance against manoeuvring targets is established without the strong reliance on correct target model detection. Due to this property, the IMM was identified as the most suitable algorithm to use with the tracking system developed for the current project.

4.8.1 IMM Algorithm Overview

Based on known or assumed parameters governing the nature of the expected motion of the target, a number of models are defined. The IMM then assumes that, at each point in time, the target will follow one of the predefined models.

Each model is matched to a filter, which run in parallel. The state estimate produced after each cycle of the algorithm (i.e. at the end of each time step) is a weighted sum of the individual filter estimates [32].

1. The first step in one cycle of an IMM estimator which consists of n filters running in parallel with associated mode probabilities μ_i (where $i, j = 1 : n$) is to compute the mixing probabilities $\mu_{i|j}$ as follows :

$$\mu_{i|j}(k-1|k-1) = \frac{1}{\bar{c}_j} p_{i|j} \mu_i(k-1) \tag{4.47}$$

where $\bar{c}_j = \sum_{i=1}^{n} p_{i|j}\mu_i(k-1)$ and $p_{i|j}$ is the Markov chain transition probability between modes.

2. A mixed state estimate $\hat{x}^{0j}$ and covariance are then calculated which are used as the input for each filter along with the measurement $z(k)$ in order to yield the respective estimated states $\hat{x}^j(k|k)$ and estimated covariances $P^j(k|k)$. The calculation of the mixed state estimate and covariance for each filter is performed as follows :

$$\hat{x}^{0j}(k) = \sum_{i=1}^{n} \hat{x}^i(k-1|k-1)\mu_{i|j}(k-1|k-1) \tag{4.48}$$

$$P^{0j}(k-1|k-1) = \sum_{i=1}^{n} \mu_{i|j}(k-1k-1)\{P^i(k-1|k-1) + [\hat{x}^i(k-1|k-1) - \hat{x}^{0j}(k-1|k-1)] \cdot [x^i(k-1|k-1) - \hat{x}^{0j}(k-1|k-1)]'\} \tag{4.49}$$

3. After the n filters have been applied the mode probabilities are then updated as follows :

$$\mu_j(k) = \frac{1}{c}\Delta_j(k)\bar{c}_j \tag{4.50}$$

where c is a normalisation constant defined as $c = \sum_{j=1}^{n} \Delta_j(k)\bar{c}_j$ and Δ_j is a likelihood function defined as $\Delta_j(k) = \mathcal{N}[z(k); \hat{z}^j[k|k-1; \hat{x}^{0j}(k-1|k-1)], S^j[k; P^{0j}(k-1|k-1)]]$

4. The final step at the end of the filter cycle is to compute the combined state estimate $\hat{x}(k|k)$ and associated covariance $P(k|k)$ which are calculated as :

$$\hat{x}(k|k) = \sum_{j=1}^{n} \hat{x}(k|k)\mu_j(k) \tag{4.51}$$

$$P(k|k) = \sum_{j=1}^{n} \mu_j(k)\{P^j(k|k) + [\hat{x}^j(k|k) - \hat{x}(k|k)][\hat{x}^j(k|k) - \hat{x}(k|k)]'\} \tag{4.52}$$

As can be seen from the stated equations, the IMM is computationally simple. A major advantage of this approach is that the algorithm is modular in nature meaning that, filters can be modified, added, removed or replaced without a complete redesign of the algorithm [96]. It is therefore possible to optimise the models required to track a particular type of target.

Further explanation of the IMM algorithm can be found in reference [97].

4.8.2 IMM Design Considerations

As with any system, in order to obtain the best results, there are a series of design considerations which need to be taken into account [98], such as :

1. The required level of accuracy in estimating the position and velocity of the target.
2. The speed at which target manoeuvres are detected and terminated.
3. The complexity of the IMM implementation.

The performance of the IMM is generally dependent on two main design parameters; the model selection and the Markov chain transition probabilities.

4.8.2.1 Model Selection

When selecting the models to be used in the IMM algorithm, both the complexity and quality of the models need to be considered. If the IMM algorithm uses Kalman filters then some of the most widely models [32,99] are constant velocity, constant acceleration and co-ordinated turn.

An extensive literature review showed that dynamical models are commonly defined in discrete-time. This is based on the assumption that with most sensor systems, measurements are often only available at a certain sample rate. The models defined in this thesis are all in discrete time. The reader is referred to [32, 99] for other types of model.

The general definition of a discrete time equation for the non manoeuvring models is a function of the current state $x(k)$, the state transition matrix $F(k)$, a process noise $v(k)$ and the gain vector Γ and is calculated as :

$$x(k+1) = F(k)x(k) + \Gamma v(k) \tag{4.53}$$

A **constant velocity model** has a state vector in two dimensions of $x(k) = [x, v_x, y, v_y]'$, where x, y are the position of the target in the x axis and y axis

respectively and v_x, v_y are the associated velocity components of the target. The state transition matrix $F(k)$ and gain vector Γ are defined as :

$$F(k) = \begin{bmatrix} 1 & dt & 0 & 0 \\ 0 & 1 & 0 & 0 \\ 0 & 0 & 1 & dt \\ 0 & 0 & 0 & 1 \end{bmatrix} \quad \Gamma = \begin{bmatrix} \frac{1}{2}dt^2 \\ t \\ \frac{1}{2}dt^2 \\ t \end{bmatrix}$$

The process noise $v(k)$ in this case is a zero mean white acceleration sequence, with the covariance of the process noise is computed as [32]:

$$Q(k) = \begin{bmatrix} \frac{1}{4}dt^4 & \frac{1}{2}dt^3 & 0 & 0 \\ \frac{1}{2}dt^3 & dt^2 & 0 & 0 \\ 0 & 0 & \frac{1}{4}dt^4 & \frac{1}{2}dt^3 \\ 0 & 0 & \frac{1}{2}dt^3 & dt^2 \end{bmatrix} \cdot \sigma_v^2 \tag{4.54}$$

Though the target is assumed to be travelling at constant velocity, its motion will be subject to small perturbations [51]. For example, the motion of an aircraft is subject to effects such as turbulence and drag. In order to account for these effects, a small value of σ_v is selected, where σ_v represents the standard deviation of the perturbations, i.e. the typical fluctuations in velocity between time steps.

A **constant acceleration model** has a state vector in two dimensions of $x(k) = [x, v_x, a_x, y, v_y, a_y]'$ where x and y are the position of the target in the x and y axes, v_x and v_y are the associated velocities and a_x and a_y are the acceleration components of the target. The state transition matrix $F(k)$ and gain vector Γ are defined as [32]:

$$F(k) = \begin{bmatrix} 1 & dt & \frac{1}{2}dt^2 & 0 & 0 & 0 \\ 0 & 1 & dt & 0 & 0 & 0 \\ 0 & 0 & 1 & 0 & 0 & 0 \\ 0 & 0 & 0 & 1 & dt & \frac{1}{2}dt^2 \\ 0 & 0 & 0 & 0 & 1 & t \\ 0 & 0 & 0 & 0 & 0 & 1 \end{bmatrix} \quad \Gamma = \begin{bmatrix} \frac{1}{2}dt^2 \\ dt \\ 1 \\ \frac{1}{2}dt^2 \\ dt \\ 1 \end{bmatrix}$$

The process noise $v(k)$ in this case is a zero mean white sequence, the acceleration is a discrete-time Wiener process. The covariance of the process noise is computed

to be [32]:

$$Q(k) = E[\Gamma v(k) v(k) \Gamma'] = \begin{bmatrix} \frac{1}{4}dt^4 & \frac{1}{3}dt^3 & \frac{1}{2}dt^2 & 0 & 0 & 0 \\ \frac{1}{2}dt^3 & dt^2 & dt & 0 & 0 & 0 \\ \frac{1}{2}dt^2 & dt & 1 & 0 & 0 & 0 \\ 0 & 0 & 0 & \frac{1}{4}dt^4 & \frac{1}{3}dt^3 & \frac{1}{2}dt^2 \\ 0 & 0 & 0 & \frac{1}{2}dt^3 & dt^2 & dt \\ 0 & 0 & 0 & \frac{1}{2}dt^2 & dt & 1 \end{bmatrix} \sigma_v^2 \qquad (4.55)$$

In this case, it is assumed that the target is travelling with a constant acceleration. However, the accelerations will be subject to small fluctuations. A small value of σ_v is selected to account for this.

A **coordinated turn model with a known turn rate** has a state vector in two dimensions of $x(k) = [x, v_x, y, v_y]'$ where x and y are the position of the target in the x and y axes and v_x and v_y are the associated velocity components of the target. The state transition matrix $F(k)$ and vector Γ are defined as [100] :

$$F(k) = \begin{bmatrix} 1 & \frac{sin(\omega dt)}{\omega} & 0 & \frac{-1 - cos(\omega dt)}{\omega} \\ 0 & cos(\omega dt) & 0 & -sin(\omega dt) \\ 0 & \frac{1 - cos(\omega dt)}{\omega} & 1 & \frac{sin(\omega dt)}{\omega} \\ 0 & sin(\omega dt) & 0 & cos(\omega dt) \end{bmatrix} \quad \Gamma = \begin{bmatrix} \frac{1}{2}dt^2 \\ t \\ \frac{1}{2}dt^2 \\ t \end{bmatrix}$$

The covariance of the process noise is computed as [32] :

$$Q(k) = \begin{bmatrix} \frac{1}{4}dt^4 & \frac{1}{2}dt^3 & 0 & 0 \\ \frac{1}{2}dt^3 & dt^2 & 0 & 0 \\ 0 & 0 & \frac{1}{4}dt^4 & \frac{1}{2}dt^3 \\ 0 & 0 & \frac{1}{2}dt^3 & dt^2 \end{bmatrix} \cdot \sigma_v^2$$

In this case it is assumed the target is performing a coordinated turn, however the turn will often not be perfectly co-ordinated. A small value of σ_v is selected to account for the modelling error.

If the turn rate is unknown then the state vector and state transition matrix

can be augmented to estimate the turn rate. This is accomplished by the use of an extended Kalman filter, the reader is directed to [99] for further information. The choice and number of models used is an important consideration in the design of the algorithm. It could be assumed that increasing the number of models will lead to greater accuracy in the estimate produced as more of the potential maneuvers the target could perform are covered. However it should be noted that the more models that are used, the higher the computational load and the stronger the competition between modes, with no guarantee of increased accuracy [98].

4.8.2.2 Markov Chain Transition Probabilities

The Markov transition probabilities represent an assumed probability that the system model will switch (transition) from one model to another. The values are calculated to approximately match the expected time the system spends in each mode [99]. The transition probabilities are often tuned by performing a number of Monte Carlo simulations.

The selection of the probabilities results in a trade-off between the peak estimation errors at the onset of a target manoeuvre and the maximum reduction of the estimation errors during uniform motion [70]. If the desired result is that the filter detects and transitions between modes quickly (i.e. a highly adaptive filter) then high transition probabilities should be selected. However, this will result in low smoothing and higher errors when tracking uniform target motion. This is because the IMM is more likely to transition in and out of the manoeuvring mode during the uniform target motion as the behaviour of the IMM will be much more volatile.

4.8.3 IMM Implementation

The IMM for this research has a state vector defined in two dimensions which tracks position and velocity.

The state vector is mathematically defined as $x(k) = [x, v_x, y, v_y]$ with an associated measurement matrix $H(k)$ defined by equation 4.42.

Three Kalman filters are used within the IMM algorithm which have the following specifications :

1. Filter 1 uses a constant velocity state transition matrix (F_{CV}) defined as :

$$F_{CV} = \begin{bmatrix} 1 & dt & 0 & 0 \\ 0 & 1 & 0 & 0 \\ 0 & 0 & 1 & dt \\ 0 & 0 & 0 & 1 \end{bmatrix}$$

2. Filter 2 uses a coordinated turn right state transition matrix (F_{CTR}) defined as :

$$F_{CTR} = \begin{bmatrix} 1 & \frac{sin(\omega dt)}{\omega} & 0 & \frac{-1-cos(\omega dt)}{\omega} \\ 0 & cos(\omega dt) & 0 & -sin(\omega dt) \\ 0 & \frac{1-cos(\omega dt)}{\omega} & 1 & \frac{sin(\omega dt)}{\omega} \\ 0 & sin(\omega dt) & 0 & cos(\omega dt) \end{bmatrix}$$

3. Filter 3 has a co-ordinated turn left state transition matrix (F_{CTL}) defined as :

$$F_{CTL} = \begin{bmatrix} 1 & \frac{sin(-\omega dt)}{-\omega} & 0 & \frac{-1-cos(-\omega dt)}{-\omega} \\ 0 & cos(-\omega dt) & 0 & -sin(-\omega dt) \\ 0 & \frac{1-cos(-\omega dt)}{-\omega} & 1 & \frac{sin(-\omega dt)}{-\omega} \\ 0 & sin(-\omega dt) & 0 & cos(-\omega dt) \end{bmatrix}$$

where dt = radar sampling period, and ω = turn rate of $10°/s$ ($\approx 0.5g$).

The three filters have a matrix representing the covariance of the process noise, $Q(k)$ with an associated process noise of $\sigma_v = 0.1\ m/s^2$. This reflects the assumption that the modelling error is relatively small where :

$$Q(k) = \begin{bmatrix} \frac{1}{4}dt^4 & \frac{1}{2}dt^3 & 0 & 0 \\ \frac{1}{2}dt^3 & dt^2 & 0 & 0 \\ 0 & 0 & \frac{1}{4}dt^4 & \frac{1}{2}dt^3 \\ 0 & 0 & \frac{1}{2}dt^3 & dt^2 \end{bmatrix} \cdot \sigma_v^2$$

The preceding discussion on state estimation assumed that the measurements in x and y where uncorrelated. Due to this assumption, the initial covariance in the error in the state estimate $P(0|0)$ and in the measurement $R(0|0)$ could be

initially defined easily as :

$$P(0|0) = \begin{bmatrix} 1 & \frac{1}{dt} & 0 & 0 \\ \frac{1}{dt} & \frac{2}{dt^2} & 0 & 0 \\ 0 & 0 & 1 & \frac{1}{dt} \\ 0 & 0 & \frac{1}{dt} & \frac{2}{dt^2} \end{bmatrix} \cdot (\sigma^2) \quad R(0|0) = \begin{bmatrix} 1 & 0 \\ 0 & 1 \end{bmatrix} \cdot (\sigma^2)$$

where σ = the standard deviation of the measurement error. However the error in measurements of the position in x and y, produced by a radar system /model as in this research are correlated as they are the cartesian equivalent of the radar range and bearing. The covariance matrices for the error in the state estimate and measurement for correlated measurement errors are initialised using equations 4.58-4.60 [101, 102], provided that :

$$\frac{R\sigma_\theta^2}{\sigma_r} < 0.4 \tag{4.57}$$

Equations 4.58-4.60 are functions of the range (R), bearing (θ) and the standard deviation of the range (σ_R) and bearing errors (σ_θ) and are defined as :

$$\sigma_x^2 = \sigma_R^2 \cos^2\theta + R^2\sigma_\theta^2 \sin^2\theta \tag{4.58}$$

$$\sigma_y^2 = \sigma_R^2 \sin^2\theta + R^2\sigma_\theta^2 \cos^2\theta \tag{4.59}$$

$$\sigma_{xy} = (\sigma_R^2 - R^2\sigma_\theta^2) \sin\theta \cos\theta \tag{4.60}$$

As the radar model used to generate noisy measurements meets this requirement, the covariance of the state estimate error $P(0|0)$ and measurement error $R(0|0)$ can then be initially defined using the following matrices [101] :

$$P(0|0) = \begin{bmatrix} \sigma_x^2 & -\frac{\sigma_x^2}{dt} & \sigma_{xy} & -\frac{\sigma_{xy}}{dt} \\ -\frac{\sigma_x^2}{dt} & \frac{2\sigma_x^2}{dt^2} & -\frac{\sigma_{xy}}{dt} & \frac{2\sigma_{xy}}{dt^2} \\ \sigma_{xy} & -\frac{\sigma_{xy}}{dt} & \sigma_y^2 & -\frac{\sigma_y^2}{dt} \\ -\frac{\sigma_{xy}}{dt} & \frac{2\sigma_{xy}}{dt^2} & -\frac{\sigma_y^2}{dt} & \frac{2\sigma_y^2}{dt^2} \end{bmatrix} \quad R(0|0) = \begin{bmatrix} \sigma_x^2 & \sigma_{xy} \\ \sigma_{xy} & \sigma_y^2 \end{bmatrix}$$

where dt= the radar sample period = 0.1s.

The filters are initialised using the first two measurements produced by the radar model, with mode probabilities set at 0.4 for the constant velocity filter (mode

1) and 0.3 for the right and left co-ordinated turn models (modes 2 and 3). To ensure the IMM transitions quickly between modes, the Markov chain transition matrix $[p_{i|j}]$ is set at :

$$p_{i|j} = \begin{bmatrix} 0.99 & 0.005 & 0.005 \\ 0.005 & 0.99 & 0.005 \\ 0.005 & 0.005 & 0.99 \end{bmatrix}$$

These values where obtained using a Monte Carlo tuning method. A range of 0.8 and 0.99 was used for the largest probability in the chain transition matrix, with the remaining probabilities calculated using equation 4.3. 100 runs were performed for each possible matrix combination with the matrix provided in this thesis yielding the best overall performance in terms of the state transition time.

Normally, the IMM would produce the state estimate and mode probabilities for the length of the tracking time after initialisation without interference. However, in this particular algorithm, the mode probabilities are reset at each 5s time interval. This is to reflect the assumption within the target trajectory prediction model that the future behaviour is independent of past events.

Shown in Figure 4.9 is a typical target trajectory with the estimated trajectory overlaid. The target begins with an initial target position of (10000, 350). It performs a left coordinated turn lasting 8s and then continues on its current bearing. At T=16s it begins a coordinated turn to the right lasting 24s. Ground truth data has been calculated for the trajectory and is provided in Figure 4.10 with the mode probabilities presented in Figure 4.11.

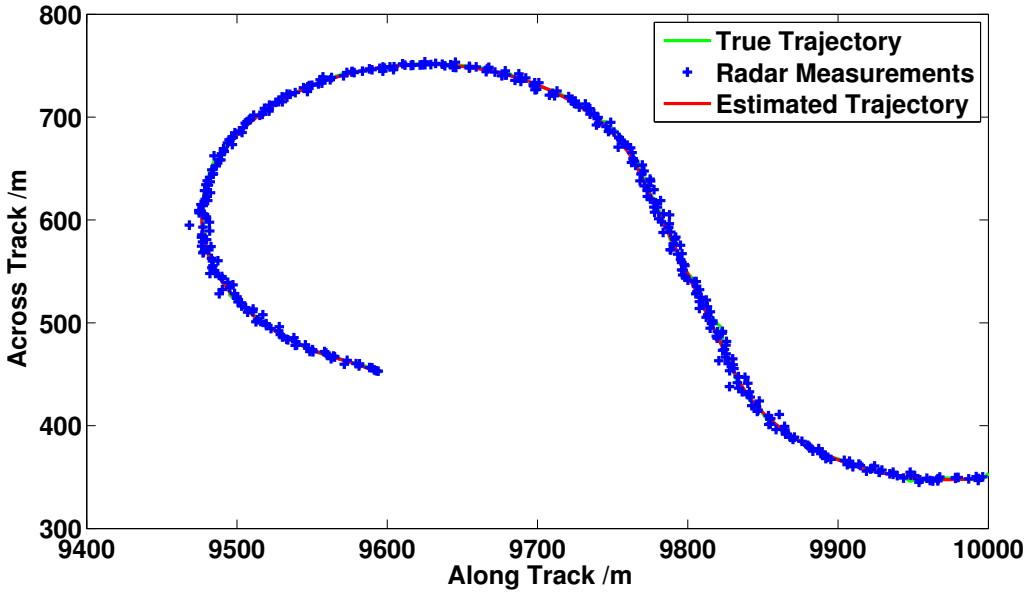

Figure 4.9: Typical Target Trajectory

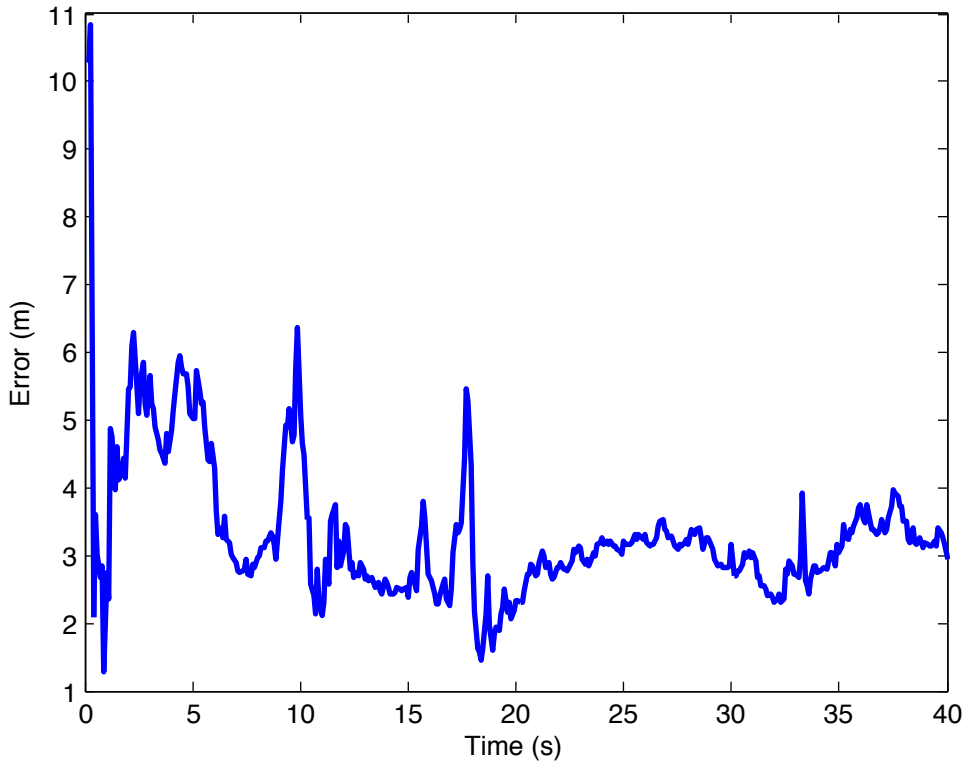

Figure 4.10: Ground Truth Data for a Typical IMM Run

As can be seen in Figure 4.10, for this particular trajectory and associated measurements, the IMM produced an accurate target track even with the high Markov

transition probabilities.

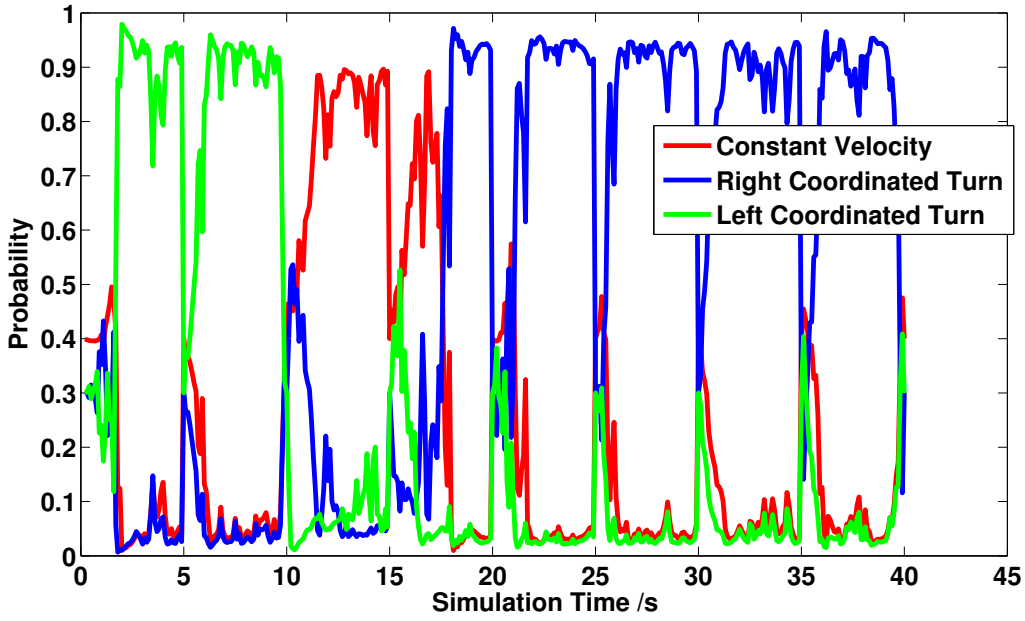

Figure 4.11: Associated Mode Probabilities

The purpose of the tracking algorithm and specifically the IMM is to detect the target behaviour in order to be able to update the distribution of possible target trajectories. Though ground truth data has been presented, the focus of the reliability of the IMM is on its ability to correctly detect the target behaviour at each point in time for any given set of data.

4.8.4 Reliability Testing

The reliability was quantified using the results of 100 random target trajectories and associated radar measurements. The mode probability data provided in Figure 4.11 can be used to help explain the reliability analysis.

1. The random target model records both the target state in each trajectory and start and end time of each behaviour. For this particular case (i.e. Figure 4.9) the following information is attached to the true trajectory data :

State	3	1	2
Start Time	0	8	16
End Time	8	16	40

Table 4.1: True State Data for a Typical Random Target Trajectory

2. For each trajectory produced by the random trajectory generator, noisy measurement data was generated using the pulsed radar model.

3. The IMM algorithm was then run with a mode detection threshold of 0.85 set. If a mode probability either reached or peaked above this threshold the mode was recorded and the time at which it occurred. For this particular trajectory the following detections where made :

Detection Time	1.8	6.2	11.5	18	21.2	25.7	31.2	35.9
State	3	3	1	2	2	2	2	2

Table 4.2: IMM Mode Detection Data for a Typical Random Target Trajectory

4. The final step is to consider what the estimated behaviour could be for the 3 possible behaviour states. From the results of the simulations the following confusion matrix is obtained :

Actual/Estimated	C.V	C.T.R	C.T.L
C.V (State 1)	505	8	1
C.T.R (State 2)	0	187	1
C.T.L(State 3)	0	4	94

Table 4.3: IMM Confusion Matrix for 100 Random Target Trajectories

The low number of incorrect behaviour detections indicate that the IMM algorithm is very reliable if a manoeuvre detection threshold of 0.85 is used. However by considering a variable threshold and using a Receiver Operating Characteristic (ROC) curve the most appropriate threshold can be determined.

4.8.5 ROC Curve Analysis

The ROC curve was first used during the second world war for the analysis of radar signals before it was eventually employed in signal detection theory [103]. The ROC curve requires two quantities to be calculated, Sensitivity and Specificity.

The Sensitivity is the proportion of the true positives (mode 2 or mode 3 detected) given that the target is manoeuvring.

The Specificity is the proportion of the true negatives (mode 1 is detected) given that the target is not manoeuvring.

$$\text{Sensitivity} = \frac{\text{Number of True Positives}}{\text{Number of true positives} + \text{Number of false negatives}} \tag{4.61}$$

$$\text{Specificity} = \frac{\text{Number of True Negatives}}{\text{Number of true negatives+Number of false positives}} \tag{4.62}$$

The ROC curve is a then a plot of the true positive rate (Sensitivity) as a function of the false positive rate (1-Specificity) at different detection thresholds. An ideal tracker (classifier) will have a true positive rate of 1 and a false positive rate of 0 at some threshold. The ROC curve shown in Figure 4.12 is calculated using a mode threshold range of of $0.3 - 0.9$.

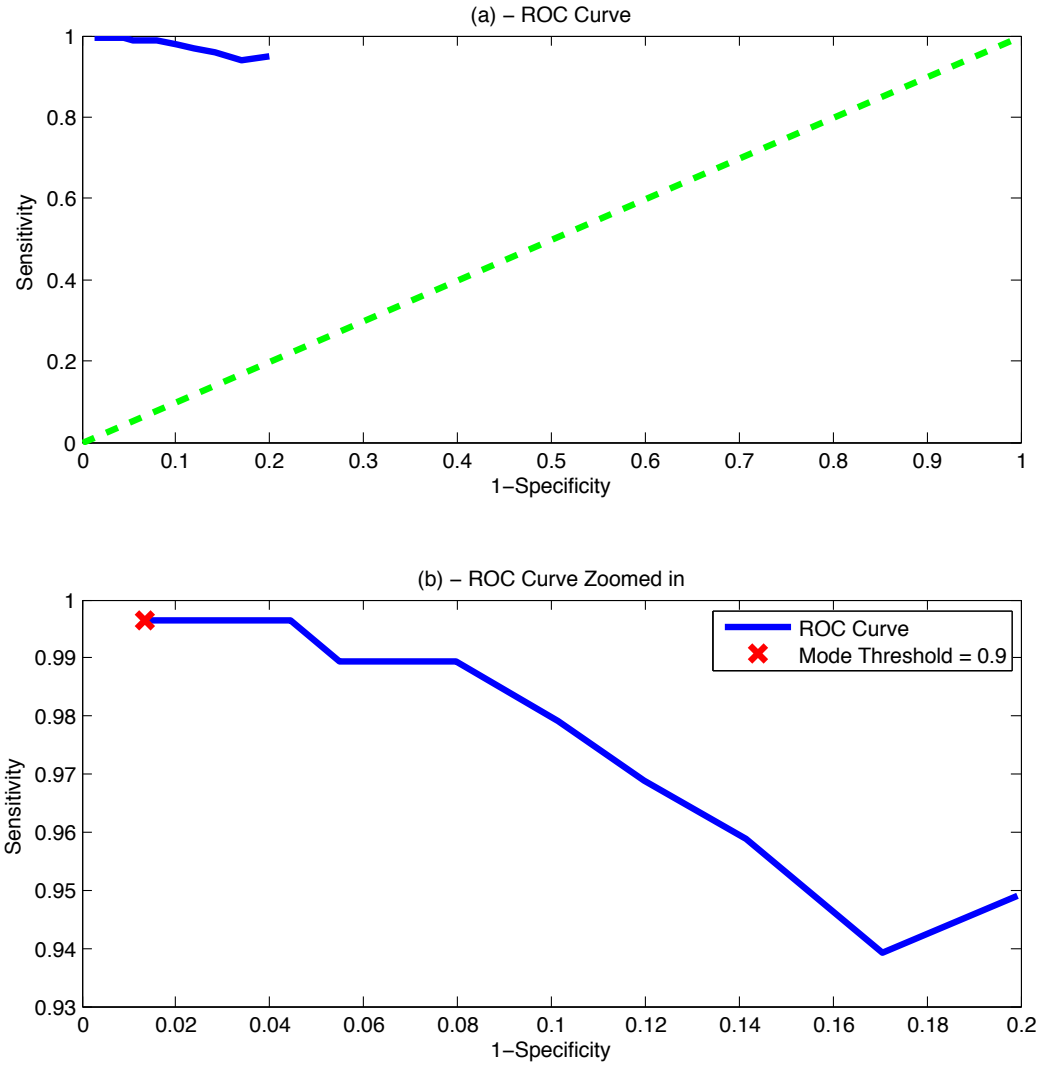

Figure 4.12: ROC Curve Based on 100 runs

The ROC curve indicated that a mode threshold of 0.9 gives almost perfect classifier performance based on 100 random runs. Due to this result, a mode threshold of 0.9 is utilised in the final IMM implementation. The average mode transition time for the implemented IMM algorithm was calculated to be 1.4s. The ROC curve analysis and confusion matrix indicated that the IMM was reliable and suitable for integration with the target trajectory prediction model.

4.9 Tracking and Prediction - Integrated System

In each integrated fire control, the initial distribution of possible target trajectories will be calculated and the associated probabilities based on the first pulsed radar measurements. There will initially be 6561 predicted trajectories that the target could follow over the 40s period. However the possible target trajectories will be eliminated as information about the behaviour of the actual target (i.e. the small boat) is obtained using the IMM estimator. The elimination of the predicted trajectories is performed considering two possible situations over each 5s state transition period.

1. If during a state transition period, mode 2 or 3 rise above the threshold value of 0.9 then the assumption is made that the turn has a duration of 5s and that the turn began at the start of the state transition period. An example would be that mode 2 (turn to the right) peaks above the threshold at T=3s. The assumption is then made that the turn began at T=0s and will end at T=5s. Trajectories predicted by the initial model at T=0s, which do not feature this behaviour are then eliminated.

   A flag is then set within the relevant code which prevents further trajectory limitations from either mode 2 or mode 3 peaking again above the threshold during the same time period. The flag is reset at the beginning of the next state transition period, i.e. between T=5s and T=10s.

2. If mode 2 or mode 3 do not peak above the threshold during a state transition period, then the assumption is made that the target continued along its original heading at its maximum speed for that time period. Trajectories which feature a turn either right or left during that particular state transition period are eliminated. An example of this would be between T=15s and T=20s neither mode 2 or mode 3 peak above 0.9. At T=20s predicted trajectories whereby the target turns right or left during this period are then eliminated.

After each predicted trajectory elimination, the probabilities are recalculated. The probabilities of the remaining predicted target trajectories will increase as the prediction model predicts a smaller and smaller time period into the future.

A flow diagram of the integrated tracking and prediction system which reduces the predicted trajectories has time progresses is shown in Figure 4.13. Rs in the diagram denotes the radar sample period and T_1 and T_2 define the current state transition time window. As the average mode settling time in the IMM is 1.4s no eliminations are made in the first 1.4s of the state transition time period.

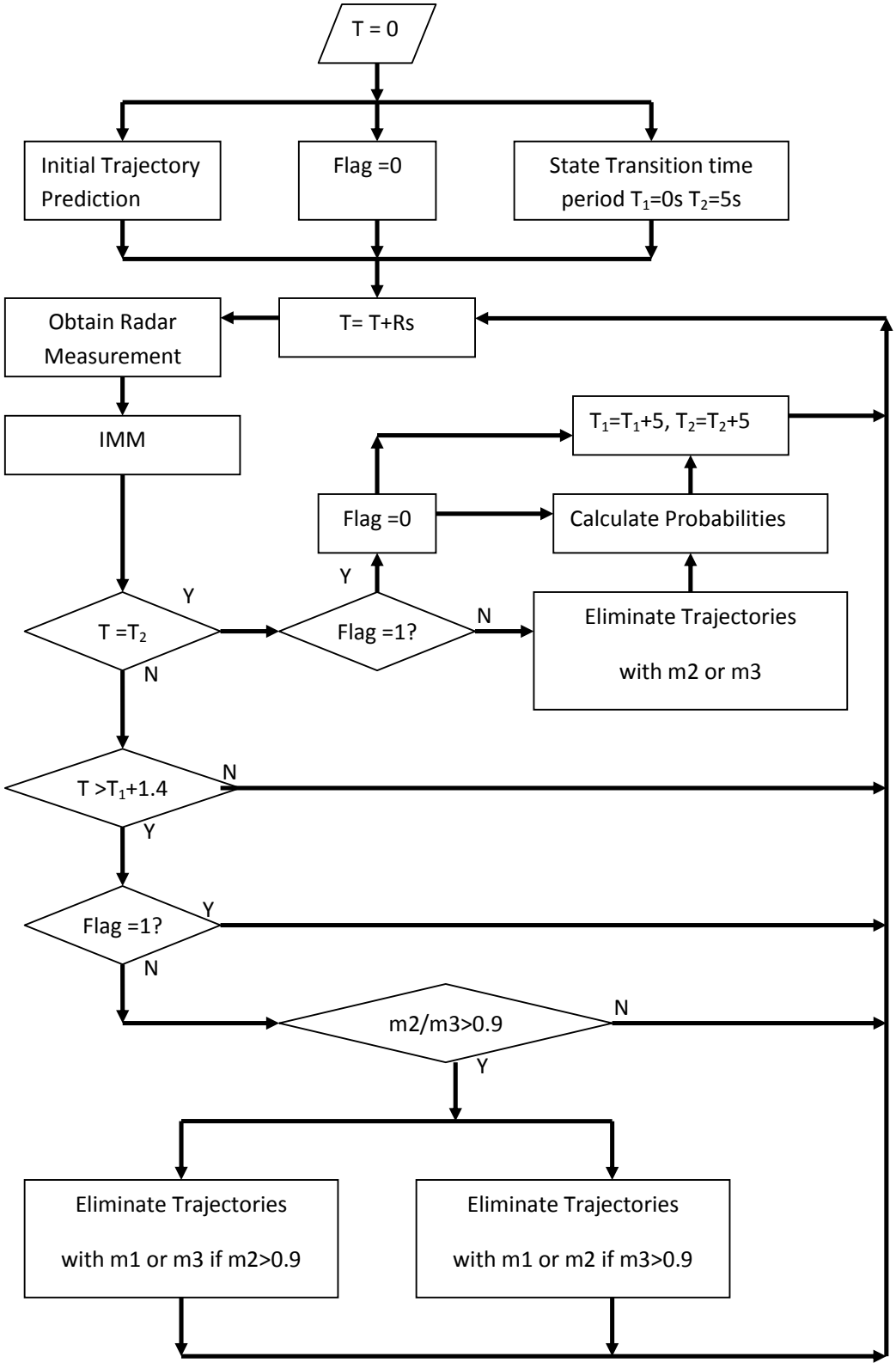

Figure 4.13: Flow diagram for the integrated tracking and prediction system

The trajectory elimination process depicted in this figure will continue to propa-

gate within the integrated fire control systems until the simulation clock reaches T=40s or the weapon successfully detects the target.

An example of the predicted trajectory elimination process is provided in Figure 4.14

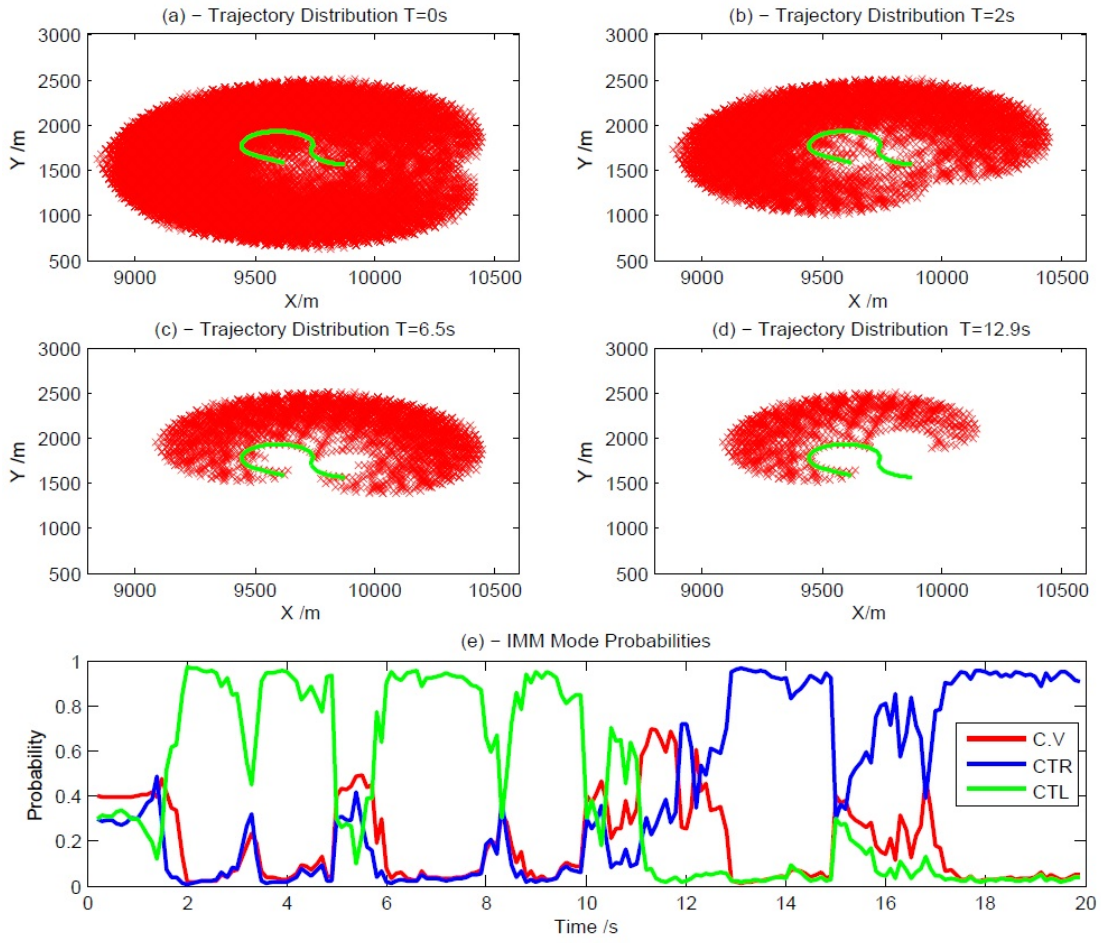

Figure 4.14: Example of Elimination of Predicted Trajectories by the Integrated Tracking and Prediction System

A random trajectory generated by the target model in Chapter 3 is shown in green in Figure 4.14 (a)-(d). The initial distribution of predicted trajectories is provided in Figure 4.14 (a), with the mode probabilities of the IMM provided in Figure 4.14 (e). At T=2s, T=6.5s and T=12.9s, manoeuvres were detected by the IMM as indicated by the plot of the coordinated turn right (C.T.R) and left mode probabilities (C.T.L). The appropriate trajectories were eliminated at these manoeuvre detection times. As information is obtained about the target behaviour, the predicted target distribution becomes a better predictor of the actual target behaviour. This improved prediction can be observed in the Figure.

4.10 Chapter Review

This chapter has covered several important aspects of research which are important in the design of the different systems described later in this thesis. Firstly a method for calculating the various trajectories the target could follow over a 40s engagement was discussed. By using a Markov chain, the probability of the following any one trajectory at each point in time was calculated.

The components of a tracking system which uses a radar for the sensor input was then discussed. The literature reviewed indicated that a Kalman filter based IMM estimator would be a suitable algorithm which could be used to track a potentially manoeuvring target.

The chapter concluded by discussing the integration of the tracking algorithm and target trajectory model. By integrating the two systems, the target trajectory prediction will become a more accurate predication as the engagement progresses.

Three integrated fire control systems are presented in Chapters 5, 6 and 7. The initial distribution of predicted target trajectories and subsequent updated distributions, calculated by the system discussed in this chapter, are used for the determination of the optimal weapon trajectory under different criteria, within each of the fire control systems.

Chapter 5

Integrated System One - Trajectory Optimisation By Simulated Annealing and Simple Search (S.A.S.S)

The scan area associated with a shaped weapon trajectory will only be able to overlap part of a distribution of possible target trajectories. One or more of the overlapped trajectories will have a detectable position. Each detectable position will have an associated probability. Therefore the sum of the probabilities for all detectable positions/locations is then the total probability of intercepting the target for that particular shaped weapon trajectory.

It is postulated that for a given distribution of target trajectories, there will be a maximum probability of intercept which can be achieved from shaping the weapon trajectory. A weapon trajectory which achieves this maximum intercept probability can be considered optimal.

The optimal trajectory should maximise the ability of the weapon to respond to any target manoeuvres detected by the IMM. As more information is obtained about the target behaviour, possible target trajectories are then eliminated from the distribution. The optimal trajectory will then be revised as more information is obtained and the distribution of the possible target trajectories reduces in size. The weapon should fly a heading which reduces the range of the weapon to the target. The target should then, at a given point in time, lie within the seeker scan area. If a successful detection is made, the terminal guidance phase will be triggered and the weapon will attempt to intercept the target.

5.1 Determination of Detectable Target Locations

In order to calculate the intercept probability for a given weapon trajectory, the locations within the distribution of predicted trajectories overlapped by the associated scan area must be determined. Two possible methods were developed to achieve this. The first method considers the problem in 3 dimensions (3D) and the second considers the problem in 2 dimensions (2D).

5.1.1 Detectable Target Location Determination in 3D

The seeker scan area can be split up into a series of planes where each plane is the area produced by the xy coordinates of the seeker scan pattern defined at two points in time (t_1, t_2). The planes are calculated sequentially and are determined on a one second time interval. The xy co-ordinates for each predicted target trajectory are sampled at one second intervals. A 3D intercept can then be calculated by considering a plane from the seeker scan pattern and a line produced by two points from a given predicted trajectory, as follows :

1. The (x, y, t) co-ordinates for the seeker scan patterns defined at (t_1, t_2) can be used to calculate the equation of the plane which can be represented as

$$Ax + By + Ct + D = 0 \tag{5.1}$$

2. For a given predicted target trajectory for the same time interval, two points (m_1, m_2) can be extracted which are used to calculate the equation of a line as follows:

$$m = m_1 + u(m_2 - m_1) \tag{5.2}$$

   where $m_1 = [x_1, y_1, t_1]'$, $m_2 = [x_2, y_2, t_2]'$

3. The equation of the line defined by (m_1, m_2) is then substituted into the equation of the plane and the intercept (u) calculated as :

$$A(x_1 + u(x_2 - x_1)) + B(y_1 + u(y_2 - y_1)) + C(z_1 + u(t_2 - t_1)) + D = 0 \tag{5.3}$$

A further step verifies that the intercept (xy) coordinates are enclosed by the bounds of the seeker scan area. If they are enclosed by the seeker area a detectable target location has been found.

A diagram showing this process is displayed in Figure 5.1.

The plane is the seeker scan pattern defined between 28 and 29s for a given weapon trajectory. Two intercepts have been calculated which indicate two possible predicated target trajectories which have a detectable location.

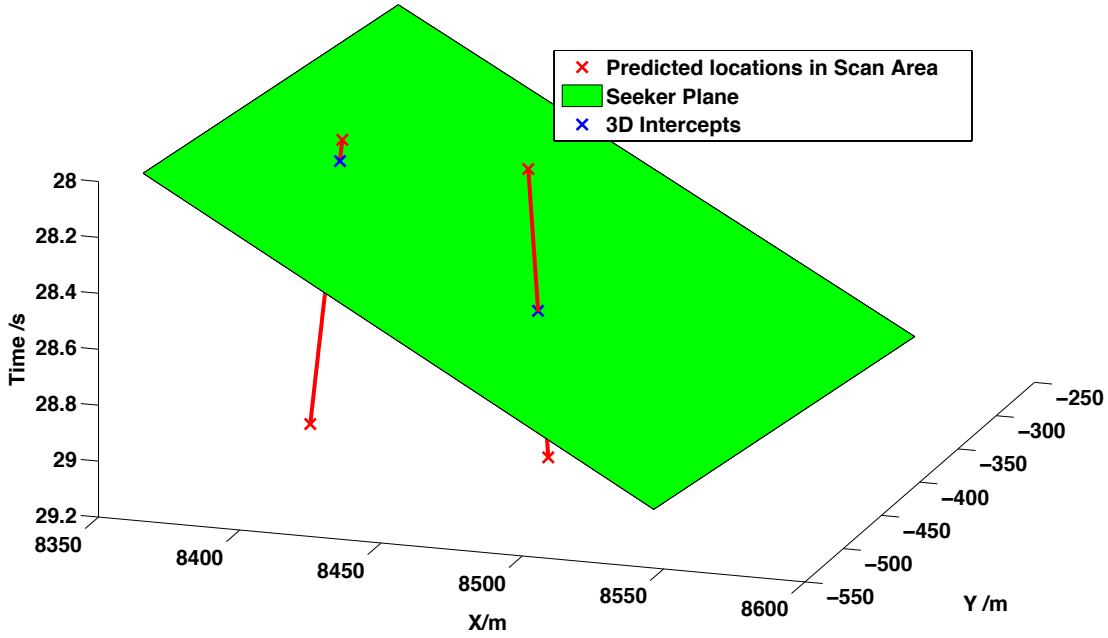

Figure 5.1: Detectable predicted target locations determined using the 3 dimensional method

This method can be very time consuming. If there is a large number of possible target locations enclosed by the seeker scan area, it can take up to 60s to determine which of the target locations are detectable for one shaped trajectory. An optimisation algorithm will have to consider a large distribution of possible weapon trajectories therefore a computationally faster solution was required.

5.1.2 Detectable Target Location Determination in 2D

The 2D method consists of separating the seeker scan pattern area into a series of individual areas between two consecutive time steps, i.e. the area between 1-2s, then 2-3s, 3-4s etc. The predicted target trajectories which are then enclosed by this seeker area can then be divided up into the xy coordinates associated with each set of time steps. If the predicted target data defined between each set of consecutive time steps is enclosed by the seeker scan defined by the same time steps then detectable target locations have been found.

The ability of this method to correctly determine the same trajectories which have a detectable location (as calculated using the 3D method) has been verified

by performing a number of trials using different weapon trajectories and various predicted target trajectory distributions. In each case the same trajectories with detectable locations were identified using this method. An example of this verification is provided in Figure 5.2

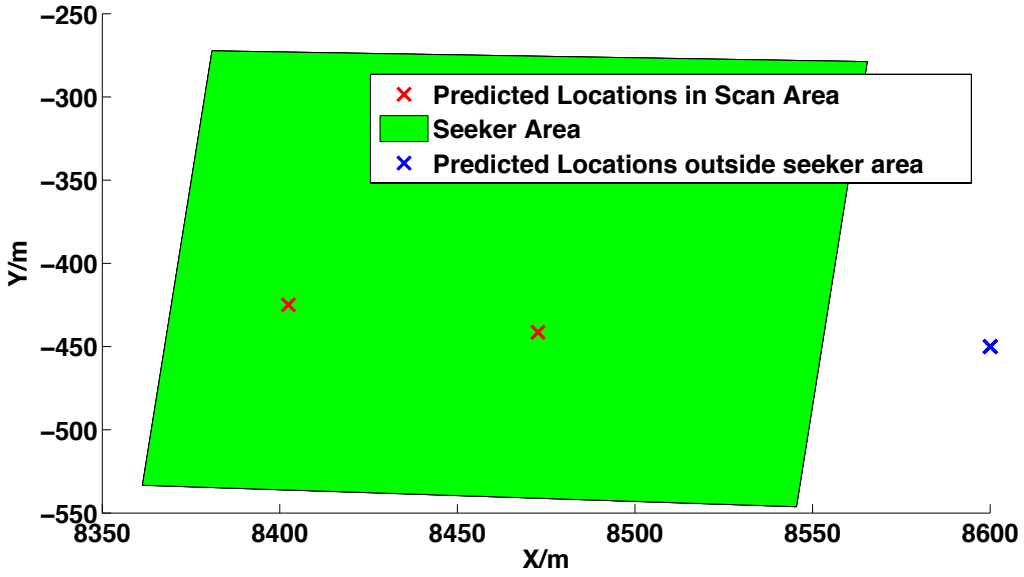

Figure 5.2: Detectable predicted target locations determined using the 2 dimensional method

As can be seen in the figure, the same two trajectories with a detectable location have been identified using this method.

The 2D method is considerably faster with the time taken to determine the detectable locations depending on the number of possible target locations which lie within the seeker area. The calculation of the detectable locations can take on average between 0.08s for a small number of possible locations up to 1s for a greater number of possible target locations. Therefore this method is used to determine the detectable target locations for each shaped weapon trajectory.

The possibility exists that the same predicted target trajectory could have more than one location whereby the target could be detected by the weapon seeker at different instants of time. More than one probability value for that particular trajectory would then be included in to the calculation of the total probability of intercept. This would overweight that particular weapon trajectory in an optimisation process which would reduce the performance of that algorithm.

To ensure the correct intercept probability for each generated weapon trajectory

is established the following checks are made:

1. Each trajectory has an associated label, if two or more points of the same trajectory lie within a particular interval i.e. they have the same label only one point will be counted.

2. The labels of each potential intercept are also compared to each other to ensure that only one potential intercept is determined for a given predicted trajectory.

For example, if the potential detectable locations had labels of 1111, 11112 then only the data of 11112 would be counted. The label of 1111 states that the target continues on its current heading for 4 state transitions. The label of 11112 states that the target continues on its current heading for 4 state transitions and then performs a coordinated turn to the right. The first label specifies a part of a predicted trajectory which is the same trajectory as label 2. Label 2 is a later point in time. This is the target that the weapon would actually engage, as the later target position associated with this point in time is closer to the weapon launch point. Therefore label 1 is discounted from the calculation of the intercept probability.

If a very agile missile was used, which could miss the target defined at label 2 and hit the target defined at label 1, then the case would have to be reconsidered. However the missile is assumed not to be sufficiently agile to achieve this and therefore the discounting of label 1 stands.

5.2 Optimal Trajectory Calculation Formulated as an Optimisation Problem

The intercept probability obtained for a given weapon trajectory will depend on the off-boresight command combination and the time steps that those commands are transmitted to the weapon. In order to determine the optimal trajectory, a variety of possible shaped weapon trajectories must be considered. Each proposed trajectory should be generated under the same set of constraints which consist of:

1. The number of off-boresight commands which are used to shape the trajectory.

2. The time steps at which the off-boresight commands are transmitted to the weapon.

Each proposed weapon trajectory will result in an intercept probability of between 0 and 1. The total set of calculated intercept probabilities will form a discrete probability distribution which will have a global maximum indicating the optimal weapon trajectory. The trajectory optimisation process will be required to determine an optimal trajectory for the weapon to follow, which is dependent on the application of n off-boresight commands.

Each off-boresight command is comprised of the weapon heading ψ and a required heading change $\Delta\psi$ and is defined as:

$$O_b = \psi + \Delta\psi \tag{5.4}$$

The sum of the absolute heading (yaw) changes associated with n off-boresight angles for a given shaped trajectory must not exceed 40° therefore the optimisation problem can be defined mathematically as:

$$\begin{aligned} &\underset{O_b \ldots O_{b_n}}{\text{argmax}} \quad P(O_{b_1} \ldots\ldots O_{b_n}) \\ &\text{subject to} \quad \sum_{i=1}^{n} |\Delta\psi_i| \leq 40 \end{aligned} \tag{5.5}$$

The maximisation of equation 5.5 can be achieved using a variety of computational optimisation algorithms e.g. [104–106]. To discuss every suitable algorithm would take up a thesis of several hundred pages. The following section provides an overview of the main optimisation algorithms which are suitable for this particular problem.

5.3 Computational Optimisation Literature Review

The algorithms detailed in this chapter can be classed as either Derivative-Based, Derivative-Free or Metaheuristic [107]. There are a number of texts available which discuss computational optimisation techniques. The reader is directed to references [107–109] for more in depth explanations than those provided herein.

5.3.1 Derivative-Based

Derivative-Based algorithms (also known as gradient-based algorithms) are very efficient local search algorithms for convex functions which are used in many applications [110, 111]. They use the information of derivatives to determine either the minimum or maximum of the function. In order to be used successfully the objective function (i.e. the function to be optimised) must be sufficiently smooth

such that the first (and more often than not the second) derivatives can be calculated.

Newton's Method is one of the most popular gradient-based algorithms. The method utilises both the first and second derivatives of a function and an initial starting point to determine the location of the optimal solution. The optimal solution will be either the maximum or minimum value of the function depending on the optimisation problem. The iterative procedure for this method can be derived as follows [112] :

1. For a given multivariate objective function $f(x)$, a starting point (x_t) is selected (x_t will be a vector of n variables).

2. A quadratic approximation for the objective function $f(x)$ is constructed using a second order Taylor series which matches the first and second derivatives of the objective function at that given point, which is defined mathematically as :

$$f(x) = f(x_t) + \nabla f(x_t)\Delta x + \frac{\Delta x^T H f(x_t)\Delta x}{2} \tag{5.6}$$

   where $\Delta x = (x - x_t)$, $\nabla f(x_t)$ is the gradient of the objective function which is determined for n variables of a multivariate function as :

$$\nabla f(x_t) = \begin{bmatrix} \frac{\partial f}{\partial x_1}(x) \\ \vdots \\ \frac{\partial f}{\partial x_n}(x) \end{bmatrix} \tag{5.7}$$

   and H is the Hessian matrix of the objective function which is calculated as :

$$H = \nabla^2 f(x) = \begin{bmatrix} \frac{\partial^2 f}{\partial x_1^2}(x) & \cdots & \frac{\partial^2 f}{\partial x_1 \partial x_n}(x) \\ \vdots & \cdots & \vdots \\ \frac{\partial^2 f}{\partial x_n \partial x_1}(x) & \cdots & \frac{\partial^2 f}{\partial x_n^2}(x) \end{bmatrix} \tag{5.8}$$

3. The right hand side of equation 5.6 is in quadratic form ($q(x) = \frac{x^T}{2} H(x) + b^T x + c$), assuming that the Hessian matrix (H) is positive definite then the next step is to find a vector which minimises the right hand side. This is accomplished using the following expression :

$$x = x_t - H(x_t)^{-1} \nabla f(x_t) \tag{5.9}$$

4. Equation 5.9 forms the basic iterative procedure for Newton's Method, however, a step size term α is normally added to the formula which controls the

rate of convergence. Therefore the final equation for **Newton's Method is defined as** :

$$x_{t+1} = x_t - \alpha H^{-1}(x_t)\nabla f(x_t)) \tag{5.10}$$

where (x_{t+1}) is the current estimated position of the optimal solution.

The step size in equation 5.10 is carefully chosen, as a small value will result in slow convergence towards the local optimum whereas a high value will produce a fast convergence but may cause the algorithm to overshoot the optimum point.

The iterative process is performed until the stopping criterion ϵ is reached. The stopping criterion will be the accuracy required in the estimate of the location of the actual optimal solution. The following expression is used to assess whether the iterative procedure should stop :

$$|x_{t+1} - x_t| < \epsilon \tag{5.11}$$

It is worth noting that if the original objective function to be optimised is quadratic, then Newton's Method will yield the optimum solution in one step. The process will provide the exact position of the optimal solution. If the original objective function is not quadratic then the process will produce an approximate position of the optimal solution of the function [112].

5.3.2 Derivative-Free

The Derivative-Based algorithms discussed in the preceding section are efficient for continuous functions. However, they are memoryless, in the sense that they do not use information obtained from past iterations to shape the future search. They also often experience slow convergence near the local optimum. They have the added issue that they can become unstable if discontinuities are present. To improve the efficiency around discontinuous functions and the convergence rate, a derivative-free algorithm can be used. One of the earliest and most popular types of this algorithm is the Hookes-Jeeves pattern search [113], which also forms the basis of many modern pattern search algorithms.

The Hookes-Jeeves algorithm utilises the history of past iterations to produce a new search direction. The algorithm consists of two types of moves, exploratory and pattern. The algorithm begins by defining an initial base point b_t, and setting an initial step length (α). Each variable in the function is incremented by the step length in the positive direction first and then in the negative direction (if necessary). The objective function is evaluated for the incremented value of each variable. This is what is known as the exploratory move. If any move for each

variable decreases the value of the objective function (minimisation problem), the move is considered a success and the variable value is retained.

Once each variable has been considered the new base point b_{t+1} will be established, provided $b_{t+1} \neq b_t$. If $b_{t+1} = b_t$ then the step length will be reduced and the process repeated.

If the exploratory move has been successful then the base point will be moved along the direction which produced the greatest decrease in the objective function. A set of exploratory moves are then performed around the updated base point b_{t+1}. If one or more exploratory moves reduces the value of the objective function, then the pattern move is successful and a new base point is found b_{t+2}. However if the pattern move fails a new set of exploratory moves with a reduced step length are performed about b_{t+1}.

Iterations of this algorithm continue until a defined tolerance ϵ is met which is normally when the step length of each variable reaches a specified small value.

5.3.3 Metaheuristic

The Derivative Based and Derivative-Free algorithms discussed are all deterministic, in that that they have no random components. These algorithms are efficient if the function being optimised has only one optimum. However they show poor performance in finding a global optimum in a complex function which has multiple maxima and minima.

The final type of optimisation strategy to be discussed in this thesis is Metaheuristic algorithms which are a powerful set of algorithms that are often inspired from nature [107]. There are a diverse range of Metaheuristic algorithms such as ant and bee algorithms and particle swarm. This chapter discusses two prominent techniques, Genetic Algorithms and Simulated Annealing. These algorithms are the most well understood and reviewed within the combinational optimisation literature, hence there inclusion in the thesis.

5.3.3.1 Genetic Algorithms

Genetic Algorithms are an optimisation technique pioneered by J.Holland and several collaborators during the 60's and 70's. The algorithms are based on the abstraction of Darwin's evolution of biological systems. There are three main components or genetic operators in a genetic algorithm consisting of, crossover,

mutation and selection of the fittest [107]. Each potential solution to the optimisation problem is encoded in a string called a chromosome. New solutions are generated by applying the genetic operators, to produce the following results :

1. A crossover of two parent strings will produce offspring i.e. new solutions. This is performed by swapping genes of the chromosomes. Crossover has a typical probability of between 0.8-0.95 of producing a new solution.

2. A mutation is performed by flipping some digits of a string, the typical probability of generating a new solution is somewhere in the range of 0.001-0.05.

3. The new solutions produced by crossover and mutation are then selected according to their fitness, which results in only the best solutions remaining in the population. Sometimes the best solutions will be passed onto the next generation without much change (elitism).

5.3.3.2 Simulated Annealing

Simulated Annealing (SA) was developed by Kirkpatrick et al. in 1983 [114]. The idea of SA comes from a paper published by Metroplis et al in 1953 [115], which simulated the cooling of a material in a heat bath (commonly known as annealing). If a solid is heated past its melting point and then allowed cool, the structural properties of the solid will depend on the rate of cooling in that :

- A slow enough cool rate will result in large crystals being formed.

- A fast cool rate will result in crystals being formed which contain imperfections.

The algorithm presented by Metropolis simulated the material as a system of particles and the associated cooling process. The cooling process is simulated by gradually lowering the temperature until the system converges to a steady frozen state. Kirkpatrick et al. took the idea of the Metropolis algorithm and applied it to optimisation problems. The idea being to search for feasible solutions and converge to an optimal solution. The algorithm itself can be explained as :

1. Generate an initial random solution and calculate the value of the objective function.

2. Generate another random solution and calculate the value of the objective function. If the value of the objective function is lower for the new solution than the previous solution (minimisation problem) automatically accept

this new solution, otherwise calculate the probability P of accepting a worst solution as:

$$P = exp\left(\frac{-c}{t}\right) \tag{5.12}$$

where c = the change in the objective function and t = the current temperature. A random number, Rn between (0,1) is generated. The worse solution will then be accepted or rejected based on whether the probability of accepting a worse solution is greater or less than the generated random number using the following criteria:

- If $P > Rn$ then accept the worse solution.
- If $P < Rn$ then reject the worse solution.

The probability of accepting a worse solution is a function of the temperature as well as the change in the value of the objective function. As the temperature is lowered the probability of accepting a worse move is reduced. This is the same as gradually moving to a frozen state in physical annealing.

The performance of the Simulated Annealing algorithm is dependent on the cooling schedule which consists of four components :

- Starting Temperature - This must be hot enough to allow nearly any random solution to be considered. If this is too low, the end solution will be same or very close to the starting solution.
- Final Temperature - Often the final temperature is set at zero, however this can lead to the algorithm having to run a lot longer than required.
- Temperate Decrement and Iterations at each temperature - After establishing a start and end temperature a method needs to be found to lower the temperature. This is normally dependent on the algorithm performing a certain number of iterations at each temperature. The number of iterations should be high enough such that the algorithm reaches equilibrium at each temperature value. Their are many different ways of decrementing the temperature. The best results from the authors experience are often obtained using a geometric decrement $t = \alpha t$ where $\alpha < 1$

This section of the thesis has given a broad overview of computational optimisation and some of the main algorithms in use today. It is apparent from the techniques reviewed in this section, that when using any optimisation technique, the problem to be solved must be clearly identified and a thorough design specification produced in order to determine the most appropriate optimisation method to use.

5.4 Selection of Simulated Annealing Algorithm

In 1975, Kenneth Alan De Jong produced a PhD thesis which analysed the performance of a class of genetic adaptive systems [116]. Within the thesis, De Jong proposed five functions which could be used to benchmark the performance of the genetic algorithms. The benchmark functions consisted of the Sphere, Rosenbrock, Step, Quartic and Foxholes functions. The difficulty in optimising each function varied from easy in the case of the Sphere function to very difficult in the case of the Foxholes function. The Sphere function is very easy to optimise, because it is smooth, unimodal and has a definite optima and minima. However, the Foxholes function has many local optima which means that optimisation algorithms can become stuck at the first optima that they find.

In 2002, J.G. Digalakis et al. proposed a further 8 algorithms which could be used for the purposes of benchmarking optimisation algorithms each with a specific difficulty. The focus of this paper was once again on the performance of Genetic Algorithms. However, the same functions can be used to test performance of other types of optimisation algorithm [117].

It would appear from these references and associated works [107, 108, 114] that the choice of optimisation algorithm in any problem should be determined based on the difficulties envisaged from the complexity of the function which is to be optimised. If the function has similar characteristics to the Sphere optimisation problem then a simple algorithm such as Newton's method will be sufficient to either maximise or minimise the function.

If the function has many local optima such as the Foxholes function, then Metaheuristic algorithms such as Simulated Annealing and Genetic Algorithms are the most appropriate algorithm to use, as identified by the previous literature review.

For this particular optimisation problem, the complexity of the intercept probability distribution must be considered in order to determine what type of optimisation algorithm is required i.e. does the distribution have a single global maxima or are their a large number of local maxima as in the Foxholes function?

The trajectory of the weapon may be potentially shaped by the integrated fire control system at several points in time. However it is very difficult to visualise the intercept probability distribution in more than 3 dimensions. The complexity of the intercept probability distribution will therefore be evaluated considering

two possible trajectory shaping approaches. In the first approach, a single off-boresight angle will be applied at various points in time. In the second approach, two off-boresight angles will be transmitted to the weapon at fixed points in time. In both cases, the distribution of possible target trajectories and associated probabilities is calculated from an initial target state $[x, v_x, y, v_y]'$ of [10000,-26,0,0]'. The intercept probability distributions for each approach are displayed in Figures 5.3 and 5.4 respectively.

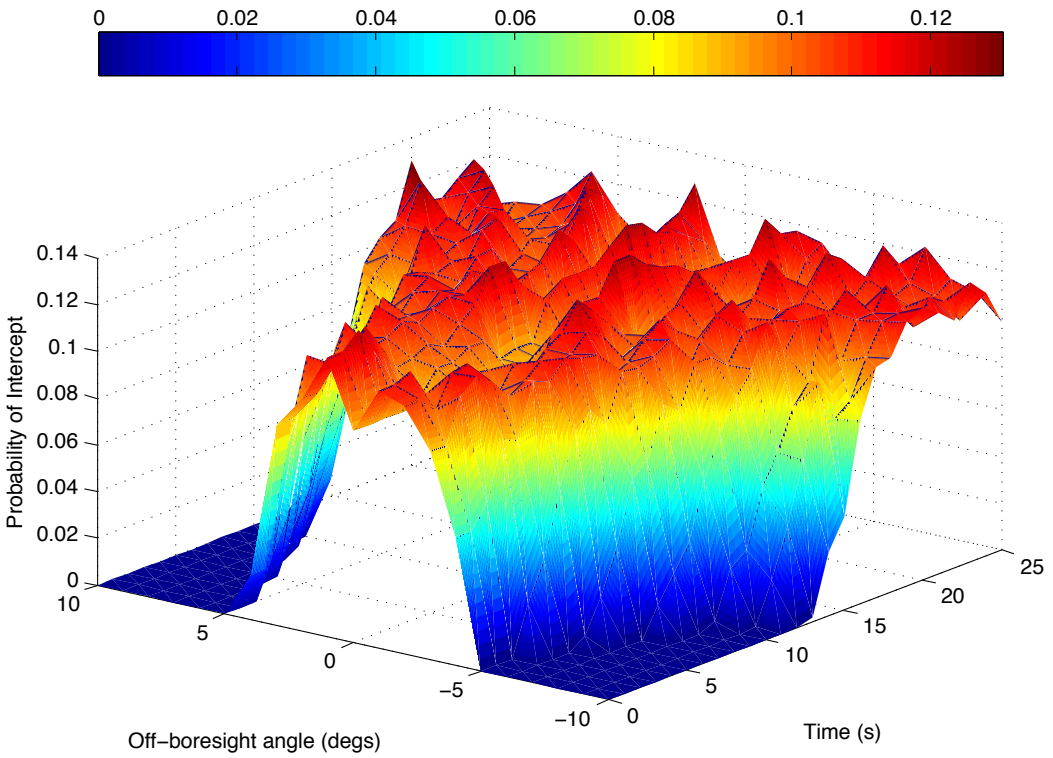

Figure 5.3: Intercept Probability Distribution for a Single Off-boresight Angle Applied at Times T=0s....T=25s

In Figure 5.3 an off-boresight command $\pm 10°$ was initially programmed into the weapon at T=0s, the process was repeated increasing the off-boresight angle by $1°$ for each off-boresight angle in this range. The process was then repeated by transmitting the off-boresight command to the weapon at T=1s, T=2s....T=25s.

In Figure 5.4, two off-boresight commands are used to shape the trajectory of the weapon. The first command is programmed into the weapon at T=0s, which is when the weapon is still on the launcher. The second command is transmitted to the weapon at T=10s. The off-boresight commands are an integer value in the range of $\pm 10°$.

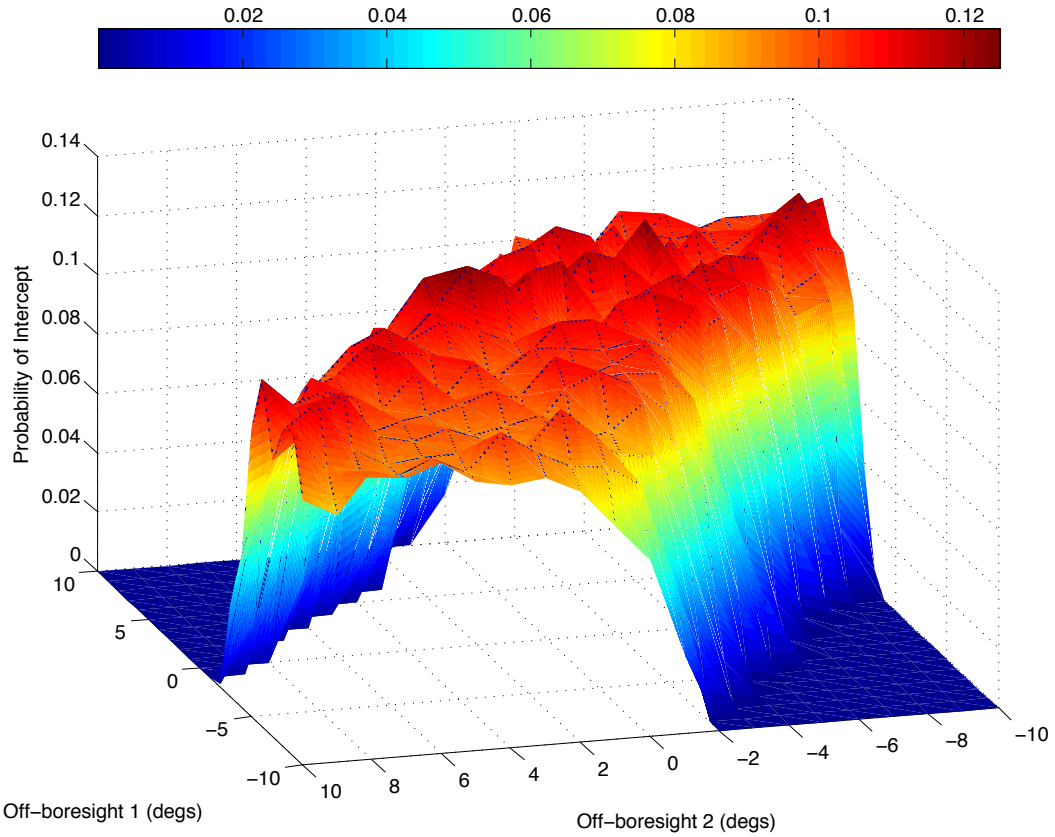

Figure 5.4: Intercept Probability Distribution for Two Off-boresight Angles Applied at T=0s and T=10s

In both figures, the intercept probability distribution has a large number of local maxima. As the number of off-boresight commands increases the complexity and the number of local maxima in the intercept probability distribution will most likely also increase. This is because their will be greater variation in the possible shaped weapon trajectories that can be generated.

The greater variation would allow a larger number of trajectories within the predicted target distribution to be overlapped by the weapon scan area. This increases the likelihood of being able to detect the target along more possible trajectories, resulting in an increased number of local maxima within the intercept probability distribution.

It is therefore evident that a Metaheuristic optimisation algorithm is required as both Derivative and Derivative-free optimisation algorithms will become stuck in local maxima of the intercept probability distribution. The literature review

identified two potential Metaheuristic algorithms which could be used for this particular optimisation problem, Simulated Annealing (SA) and Genetic Algorithms (GA).

Simulated Annealing was selected for the following reasons :

1. If the algorithm is correctly tuned i.e. sensible values are used for the start and end temperature and an appropriate cooling schedule determined the global optimum should be obtained.

2. The time taken for a genetic algorithm to find an optimal solution is generally longer than using a simulated annealing process [118].

5.5 Simulated Annealing Cooling Schedule Tuning

In order to calculate the optimal weapon trajectory, the simulated annealing algorithm will evaluate the intercept probability associated with a set of randomly generated weapon trajectories. If the optimisation algorithm is to work effectively, it must be correctly tuned. This requires a suitable cooling schedule to be developed. In an ideal situation, the algorithm would be tuned based on actual weapon trajectory data and the complete predicted trajectory distribution.

The calculation of a weapon trajectory and associated seeker scan area takes approximately 3s. The time taken for the determination of the target intercept probability for a weapon trajectory varies on average between 0.08s and 1s. Therefore the maximum time taken to complete both processes for a single weapon trajectory could be 4s.

It is apparent that attempting to tune the simulated annealing algorithm based on actual data would take an extremely long time. The process can be expedited by tuning the algorithm based on a function of the same characteristics.

The weapon seeker should be on and able to detect a valid target up to T=35s. If the assumption is then made that the weapon will detect the target at T=35s, then the probability distribution associated with the predicted target trajectories can be approximated to be representative of the intercept probability distribution that would be observed based on actual weapon trajectory data. The complexity of this distribution is then a reasonable approximation on which to tune the algorithm. The simulated annealing algorithm can then tuned by considering

the problem of finding the global maximum of the distribution. Each probability value in the distribution can be assigned a number which results in 2187 possible solutions. The simulated annealing process is then performed by generating random numbers in the range of 1-2187.

The first stage of the tuning process is then to develop a benchmark simulated annealing algorithm which will achieve a 100% success rate i.e. identify the global optimum each time the optimisation algorithm was run. The parameters of the benchmark algorithm where set as follows :

1. Start Temperature = 1, End Temperature = 0.01 (unitless in simulated annealing, Kelvin in physical annealing)
2. Number of runs at each temperature = 100
3. Temperate Decrement T = 0.99T

A start temperature of 1 was selected to ensure initially that nearly any random solution could be considered by the algorithm, thereby preventing it from becoming stuck in a local optimum or producing a solution close to the initial guess. The maximum probability of intercept which can physically be obtained by the seeker area overlap is 1. Therefore, this also represents the maximum logical starting temperature which could be used. A final temperature of 0.01 was selected because at a suitably low temperature the probability of the simulated annealing process accepting a worse solution is almost the same as the temperature being equal to 0. It is not normally required to allow the algorithm to run to a temperature of 0 [114].

A geometric temperate decrement with a high value of $\alpha = 0.99$ was selected as this would reduce the temperature of the algorithm very slowly. From the literature reviewed earlier in this chapter, it is apparent, that as long as the algorithm temperature is cooled very slowly and the algorithm reaches equilibrium at each temperature level, then it should always find the optimal value.

The number of runs was selected as 100 as this is a high number of runs for a very slow cooling schedule thereby allowing the algorithm to reach equilibrium at each temperature level. The algorithm was run 100 times and each time, the maximum value of the probability distribution was found. As a 100% success rate was obtained first time from this algorithm no further work was required on this benchmark algorithm.

Though the algorithm had a 100% success rate, each simulation required 45900 iterations. If this algorithm where used in practice it would take 51 hours for one optimisation process to run which is calculated as:

$$\text{Run Time} = \frac{45900 \times 4}{60 \times 60} \tag{5.13}$$

The trajectory optimisation algorithms developed in this thesis are not required to run in real time. The purpose of the thesis is to demonstrate the general concept of an integrated fire control system which uses a trajectory optimisation process and the associated benefits in terms of an increase weapon performance against manoeuvring targets.

In order for sufficient data to be collected to analyse the performance of the integrated fire control systems, a shorter run time for the simulated annealing optimisation algorithm is required.

The optimisation process can be expedited by changing the parameters of the cooling schedule such as reducing the number of iterations performed at each temperature level. Though this will speed up the optimisation process, the consequence will be a reduction in the reliability of the algorithm.

The optimisation algorithm is to be integrated with the tracking and prediction system discussed in Chapter 4. The IMM component of that system is not 100% reliable therefore it is unrealistic to use an optimisation process which is extremely computationally heavy which achieves 100% reliability when the rest of the system will not be at this level of performance. Therefore the simulated annealing algorithm was tuned such that it gave an acceptable success rate (in this case a reliability of greater than 90%) but was significantly computationally faster . The tuned algorithm completes in 5 hours as appose to 51 hours for the untuned benchmark algorithm.

5.5.1 Start and End Temperature

The first step in the tuning process is to consider the effect of the starting temperature on the reliability of the algorithm. A temperature range of 1-0.05 was chosen, this is due to the fact that the variation in the maxima of the probability distribution is 1 therefore 1-0.05 represents a sensible temperature range.

A step size between trial values of 0.05 was selected. By using a small step size, an accurate assessment can be made of the effect of the starting temperature. The algorithm was run 100 times at each starting temperature with the end temperature at 10 % of the start temperature, 100 runs is both a reasonable amount of data to collect and is also computationally efficient. The results of this tuning process are shown in the next figure :

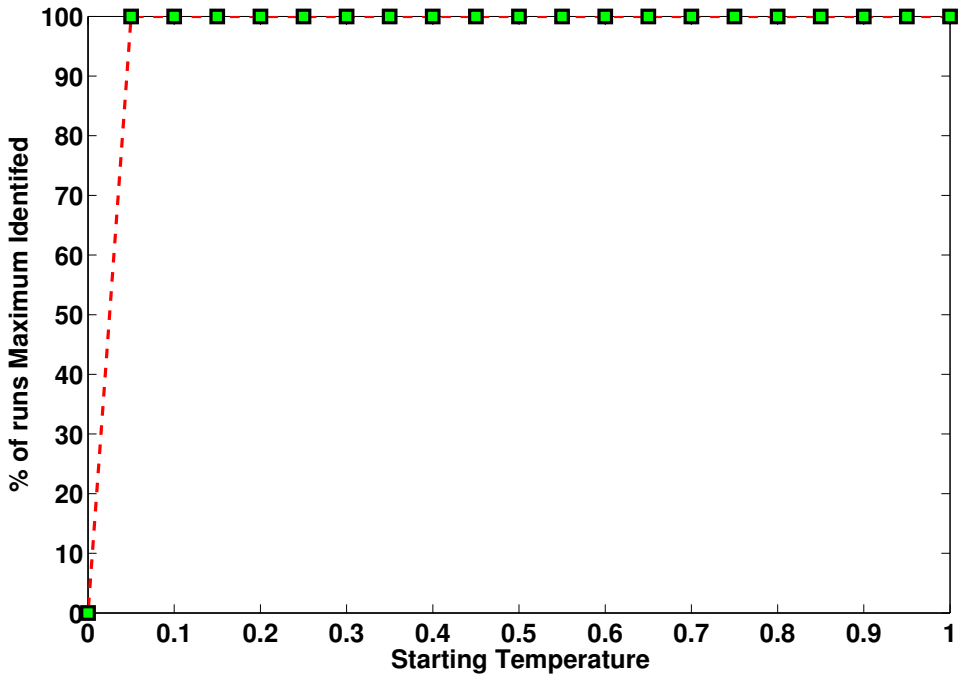

Figure 5.5: Effect of starting temperature on Simulated Annealing Performance

As can be seen from the figure, a starting temperature as low as 0.05 could be used and 100% reliability still be achieved. However, a starting temperature of 0.1 was actually selected. A starting temperature of 0.1 ensures that the simulated annealing algorithm should always be able to escape local optima at least in the initial stages of the algorithm. In any case, a temperature higher than this offers no greater reliability.

5.5.2 Number of Runs

The next stage of tuning is to consider the effect on the reliability of the algorithm of the number of runs performed at each temperature. With a starting temperature of 0.1 and an end temperature of 0.01. The same cooling schedule as in the benchmark example was also used. The range of the number of runs at each temperature was set between 5 and 100. The upper limit of 100 was chosen as the benchmark algorithm was 100 % reliable with this number of runs. The lower

limit of 5 was selected as this in theory would calculate an optimum quickly but would result in poor performance in terms of reliability, as the algorithm would not have sufficient amount of iterations at each temperature to reach equilibrium. As in the previous tuning process the algorithm was run 100 times, the results of this experiment are shown in Figure 5.6.

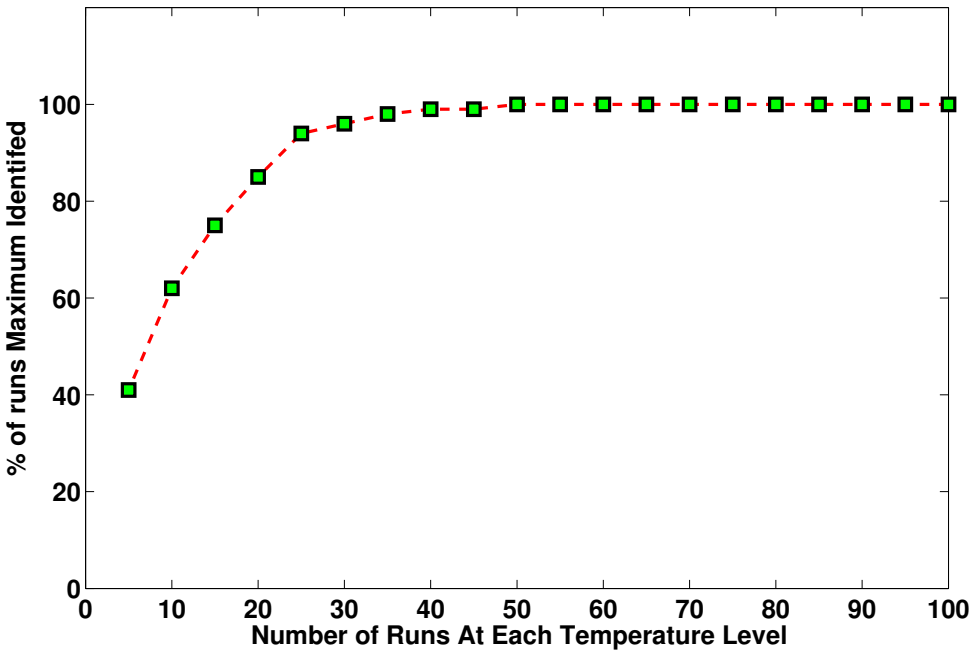

Figure 5.6: Effect of Number of Runs at each Temperature on Simulated Annealing Performance

Based on the results of this tuning process a value of 30 iterations at each temperature was selected. This is due to the fact that the algorithm with this level of runs has a reliability of over 95%, with a significant reduction in the computation time to find the maximum. A value of 35 runs upwards improves the overall performance of the algorithm in terms of correctly identifying the global maximum by 1-7 %. However the computation load is also increased due to the greater number of iterations performed at each temperature level.

5.5.3 Temperature Decrement

The final step in the algorithm tuning is consider the cooling constant. As in the benchmark a geometric temperate decrement T=αT was used, where α represents the cooling constant. A lower cooling constant will result in a faster algorithm however it will be less reliable. From the authors experience, a cooling constant of between 0.8-0.99 produced acceptable reliability for other simulated

annealing algorithms. This range was chosen to tune this particular algorithm. 100 simulations where performed for each cooling constant value. The results are shown in Figure 5.7. A starting temperature of 0.1 was used with a respective end temperature of 0.01, 30 runs where performed at each temperature level.

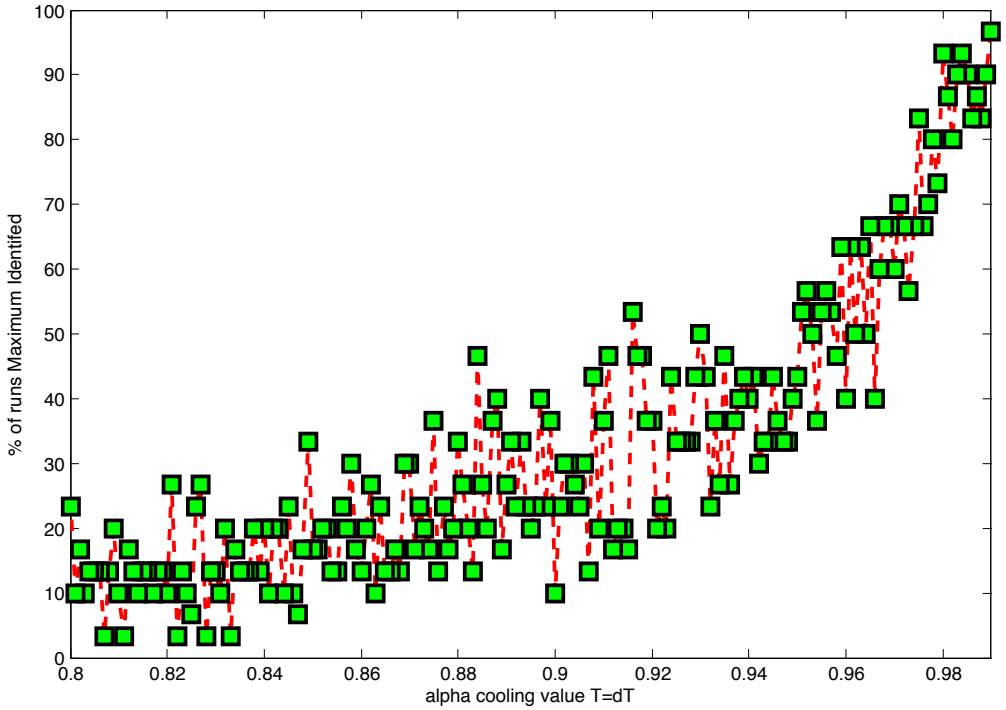

Figure 5.7: Effect of Cooling Constant on Simulated Annealing Performance

The higher the cooling constant, the greater the number of iterations performed in each run of the algorithm, increasing the computational requirements. A cooling constant of 0.98 resulted in the algorithm calculating the global maxima in 93 cases. Therefore this cooling constant value was selected for the final simulated annealing implementation.

The selection of the cooling constant marked the end of the tuning process and resulted in the following final specification for the actual algorithm to be used consisting of :

1. Start temperate of 0.1
2. End temperate of 0.01
3. 30 iterations at each temperature level
4. Cooling constant α of 0.98

A simulated annealing algorithm with this specification requires 3420 iterations to complete the optimisation process. This means that based on current computational limits, the process will complete within approximately 5 hours; a significant reduction in computation time from the benchmark algorithm proposed earlier in this chapter. If the trajectory calculation time is neglected, the simulated annealing algorithm can calculate the optimal trajectory within a few μs.

If an integrated system was deployed operationally which utilised this simulated annealing process, sufficient computing power would be made available to calculate the required trajectories for the optimisation process in real time.

The simulated annealing algorithm has been tuned considering a 2 dimensional problem. However the calculation of an optimal trajectory will be a higher dimensional problem. Therefore the performance of this algorithm was evaluated further by considering the problem of determining the maximum intercept probability of the complicated surface shown in Figure 5.4.

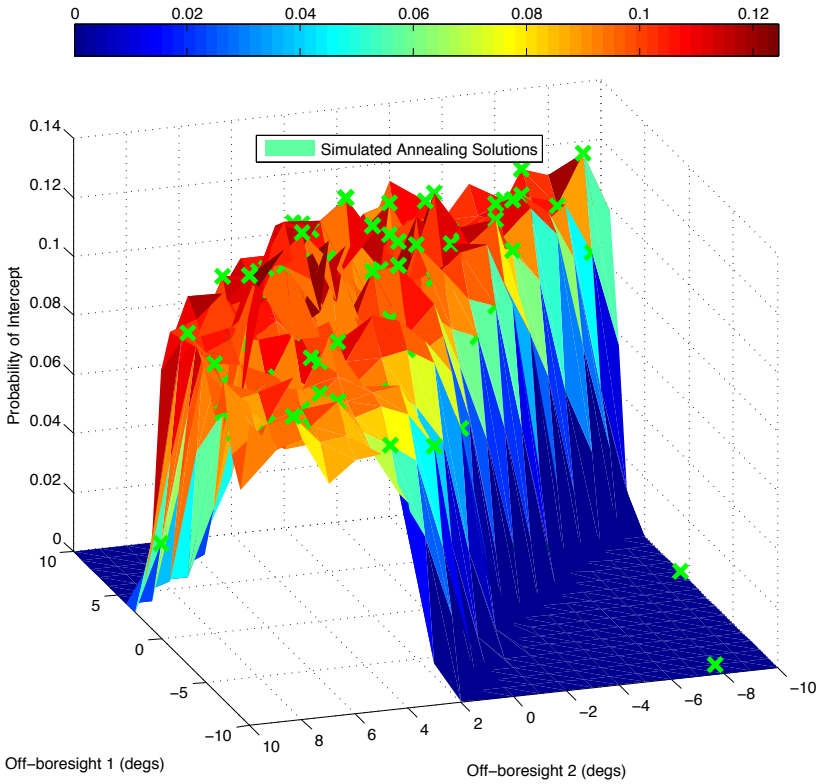

Figure 5.8: Simulated Annealing - Example Path Taken in a 3 Dimension Optimisation Process

The optimisation process was performed 100 times. On each occasion, the maximum probability of intercept found by the algorithm was recorded.

An exhaustive search was performed separately to determine what the actual maximum intercept probability was i.e. the global maximum. On each occasion, the global maximum was achieved. The path taken by the simulated annealing progress for one of the runs is shown in Figure 5.8.

The results of this simulation indicate that the simulated annealing algorithm should be reliable if applied to a higher dimension problems such as the calculation of the optimal weapon trajectory.

The algorithm calculated the global maximum in 93 trials of the cooling constant tuning process and on 100 occasions in the 3 dimension problem. The point estimate of the minimum reliability of the algorithm $\hat{p}$ would therefore be calculated as 0.93. However, there will be a margin of error in this reliability estimation which can be determined from the calculation of the 95% confidence interval as:

$$\hat{p} - E < p < \hat{p} + E \tag{5.14}$$

where E is the standard error which is calculated as:

$$E = 1.96\sqrt{\frac{\hat{p}\hat{q}}{n}} \tag{5.15}$$

The margin of error at 95% confidence is calculated as ±5%. Therefore at 95% confidence the reliability of the simulated annealing algorithm should be at least 88% but could be as high as 98%. The algorithm therefore displays sufficient reliability for implementation within the integrated fire control system discussed in this thesis.

5.6 Simple Search Optimisation

The trajectory of the weapon in this fire control system will be optimised using both the simulated annealing algorithm discussed in the previous section and a simple search approach. Trajectory optimisation by simple search consists of calculating the maximum probability of intercept based on the application of a single off-boresight command.

At any given point in time during the weapon fly out, there will be a maximum yaw change $|\delta\psi_{max}|$ which can be used to off-boresight the weapon. This allows two off-boresight limits $[O_{b_1}, O_{b_2}]$ to be defined as :

$$O_{b_1} = \psi + |\Delta\psi_{max}| \tag{5.16}$$

$$O_{b_1} = \psi - |\Delta\psi_{max}| \tag{5.17}$$

The intercept probability for each off-boresight command $P(O_b)$ can then be calculated in 1° steps from $O_{b_1} - O_{b_2}$. The simple search algorithm will seek to determine the off-boresight angle which results in the maximum probability of intercept. The calculation of this off-boresight angle can be mathematically defined as:

$$\begin{aligned} &\underset{O_b}{\text{argmax}} \quad P(O_b) \\ &\text{subject to} \quad \mathrm{O}_b \in (O_{b_1}, O_{b_2}] \end{aligned} \tag{5.18}$$

In the simulated system, this is achieved by calculating the probability of intercept for each possible off-boresight command. The off-boresight command that achieves the maximum probability of intercept is then transmitted to the weapon at that time step. The weapon will then apply appropriate controls to achieve the off-boresight heading.

5.7 Trajectory Optimisation Proposed Approach

In order to develop the final integrated fire control system, the number of off-boresight commands which can/will be used to shape the weapon trajectory must be established. The first off-boresight command is programmed into the weapon while on the launcher at T=0s. Subsequent commands will be transmitted to the weapon over the data link. The time steps at which the off-boresight commands will be transmitted will depend on the information obtained about the target from the tracking and prediction system. The appropriate number of off-boresight commands which should be used to shape the weapon trajectory over the flight period, can be established by considering the fire control system as operating in two phases during a simulated engagement. These phases consist of:

1. Weapon initialisation at T=0s.

2. In-flight trajectory revision.

At T=0s, the target will have entered the exclusion zone i.e. it will lie within the reachable set of the weapon. Any vessel which would have approached that exclusion zone would be warned to leave. Therefore, the logical assumption will be made that the target will have deliberately entered that zone and is seeking to attack the ship [38]. The trajectory of the weapon should therefore be shaped considering an attack by the target. As discussed by [35], in an attack, the target will want to minimise the time taken to reach the ship. In the most simple case it would favour a direct attack but it may have to manoeuvre for a number of reasons such as to achieve a specific attack heading.

The probabilities of the predicted target distribution which will be defined at this time step will initially weight the probability of a non manoeuvring target trajectory higher than the other trajectories thereby reflecting this assumption.

From Chapter 3, it is apparent that the seeker of the weapon should be on for 35s of flight, therefore the integrated fire control system should seek to shape the trajectory of the weapon such that the target should be detected at the latest in the 30-35s time interval.

The integrated tracking and prediction system will provide 6 updates in this time period. If the target performs a direct attack, then these updates (which will include an updated distribution of possible target trajectories and associated probabilities) will occur every 5s. It could be concluded that the trajectory should be therefore be shaped based on 7 off-boresight commands, which would initially be transmitted to the weapon at 5s intervals to coincide with the tracking and prediction system updates. However revising the trajectory at this update rate if the target has not manoeuvred could be inefficient in terms of the cost to the maximum heading change which can be applied at subsequent off-boresight commands.

Each off-boresight command which is not equal to the previous off-boresight requires a heading change. Though the new off-boresight heading will not be achieved instantly, the size of the maximum heading change which can be used in subsequent commands is reduced instantly within the fire control system.

If the target has not manoeuvred then the change in the probability distribution will be only be minor, especially in the early stages of the engagement. It is therefore unlikely that the optimal trajectory would need to be significantly revised at 5s time intervals. The maximum heading change capability would be better preserved in case the target does perform a manoeuvre. Therefore 4 off-boresight commands will be initially used to shape the trajectory of the weapon which are calculated considering that they will be transmitted to the weapon at T=0s, T=10s, T=20s and T=30s.

It is expected that the intercept probability distribution which will be associated with these trajectory constraints will have a large number of local maxima based on Figures 5.3 and 5.4. The simulated annealing algorithm is therefore used at the initialisation stage to determine the optimal weapon trajectory based

on an assumed complicated intercept probability distribution.

Once the weapon has left the launcher, the system will then enter the in-flight trajectory revision phase. The process by which the trajectory of the weapon is revised during this phase depends on how the target behaves over the flight time of the weapon. If the target obeys the assumption of a direct attack, then the trajectory will be revised at T=10s and T=20s using the simulated annealing process. If the weapon seeker has not detected the target prior to T=30s, then the trajectory at T=30s will be fine-tuned using a simple search algorithm. The simple search algorithm will seek to determine the appropriate off-boresight command to be applied at T=30s, considering only a very small number of remaining possible target trajectories.

If the target manoeuvres during the weapon fly out, then the in-flight trajectory revision phase will optimise the trajectory in a variety of ways, depending on the duration and number of the manoeuvres, using both the simulated annealing and simple search algorithms.

The initial calculation of the optimal trajectory and subsequent revision due to different target behaviours will be discussed in detail in Sections 5.8 and 5.9 respectively. However the integration of the weapon data link and the trajectory and prediction system is discussed first in order to aid the reader's understanding of the whole system in later sections.

5.7.1 Data Link and Tracking and Prediction System Integration

The data link is assumed to be an on-demand service. This means that the weapon could technically receive any number of off-boresight commands over the fly out. The off-boresight commands could be transmitted at any given point in time. However, as the weapon is to be deployed within an integrated fire control system, the data link capability is restricted. New off-boresight commands will only be transmitted by the fire control system if an optimisation process has been performed. An optimisation process will be performed based on the updated target trajectory prediction. The off-boresight commands will therefore be transmitted at the same time step that the tracking and prediction system produces updated target behaviour and an optimisation process has been performed.

The time taken for the optimisation process algorithm to run is neglected. The assumption is made if the system was deployed operationally, sufficient comput-

ing power would be available to complete the optimisation process in real time.

As the tracking system can only make one manoeuvre detection in a 5s period or update considering constant velocity behaviour, the fire control system will only be able to transmit one off-boresight command to the weapon in each 5s period. As the IMM has an average settling time of 1.4s, off-boresight commands will only be transmitted after the first 1.4s of each state transition period.

5.8 Fire Control System Implementation - Weapon Initialisation

At T=0s, the distribution of predicted target trajectories will be calculated from an initial target state with components $[x, v_x, y, v_y]'$. Each predicted target trajectory will be calculated for a maximum weapon flight duration of 40s. For the optimisation algorithm to be effective, each random weapon trajectory used to determine the intercept probability must have a scan area which overlaps part of the predicted target trajectory distribution. If the target trajectory distribution is compared with the reachable set of the weapon, it is apparent that it will only occupy a very small part of the reachable set. An example of this comparison is shown in Figure 5.9 with an initial target state of [10000,-26,350,0]'.

The target distribution in this case is actually bounded by an area defined from a trajectory with an off-boresight angle of 9° which is applied to the weapon at T=0s, and a trajectory with an off-boresight angle of -5° which is applied at the same time step. Only trajectories where the weapon seeker area will be enclosed by these boundaries over the distribution of predicted target trajectories will be capable of achieving an intercept probability. The area bounded by two trajectories calculated from respective off-boresight commands applied at launch can be defined as the feasible trajectory solution area.

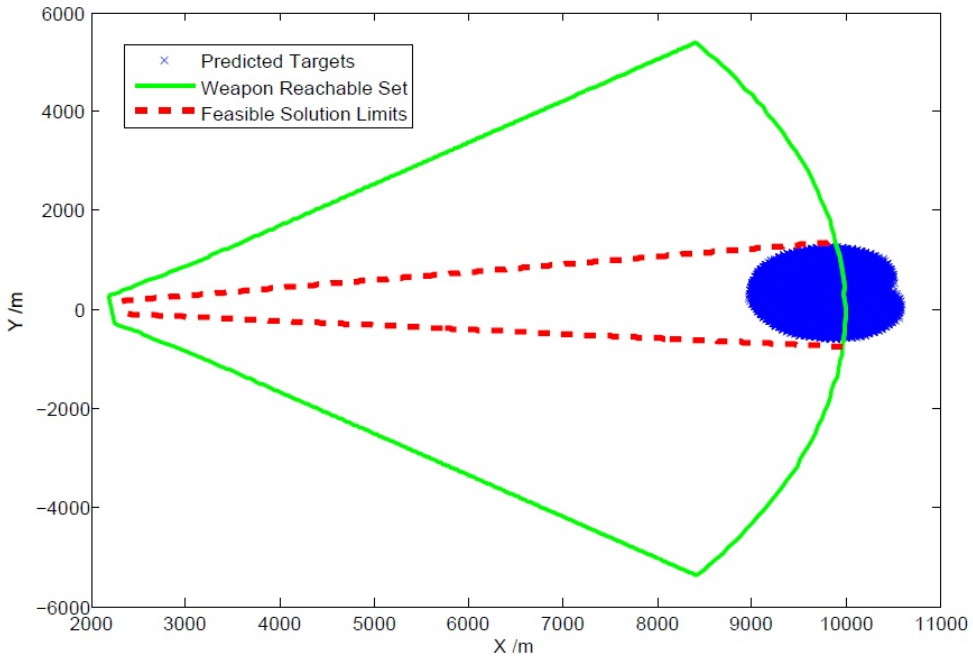

Figure 5.9: Feasible Trajectory Solution Area

The first stage of the weapon initialisation process in the fire control system is to calculate the feasible solution area for each target trajectory distribution which is performed as follows:

1. The reachable set of the weapon is overlaid on the distribution of predicted target trajectories. The number of individual target locations which form each predicted target trajectory, that are enclosed by the boundaries of the reachable set is determined.

2. The reachable set is bounded by trajectories with respective initial off-boresight commands of $\pm 40°$ which are programmed into the weapon while on the launcher.

3. The number of target locations is then re-evaluated based on a reachable set which is bounded by weapon trajectories with off-boresight commands of $39°$ and $-40°$. If the number of target locations is the same, the process is repeated reducing the positive off-boresight command trajectory in steps of $1°$, i.e. producing a reachable set defined by $38°$, $-40°$, $37°$, $-40°$. The process continues until the number of target locations is below the initial value defined from a full reachable set.

4. The process is then performed considering a reachable defined by the boundaries of off-boresight trajectories $40°$, $-39°$, the same procedure is followed

but with with the negative off-boresight command increased in steps of 1°, i.e 40°, −38° etc.

The final off-boresight limits which define the feasible solution area are then ±1° of the calculated boundaries in the respective direction. Once the feasible solution area has been calculated, 3420 weapon trajectories are randomly generated based on 4 off-boresight commands which are applied at T=0s, T=10s, T=20s, T=30s. In order for the random trajectories to lie within the feasible solution area, each off-boresight command is then generated between the limits of the feasible solution area. An example of the calculation of the random weapon trajectories is shown in Figure 5.10.

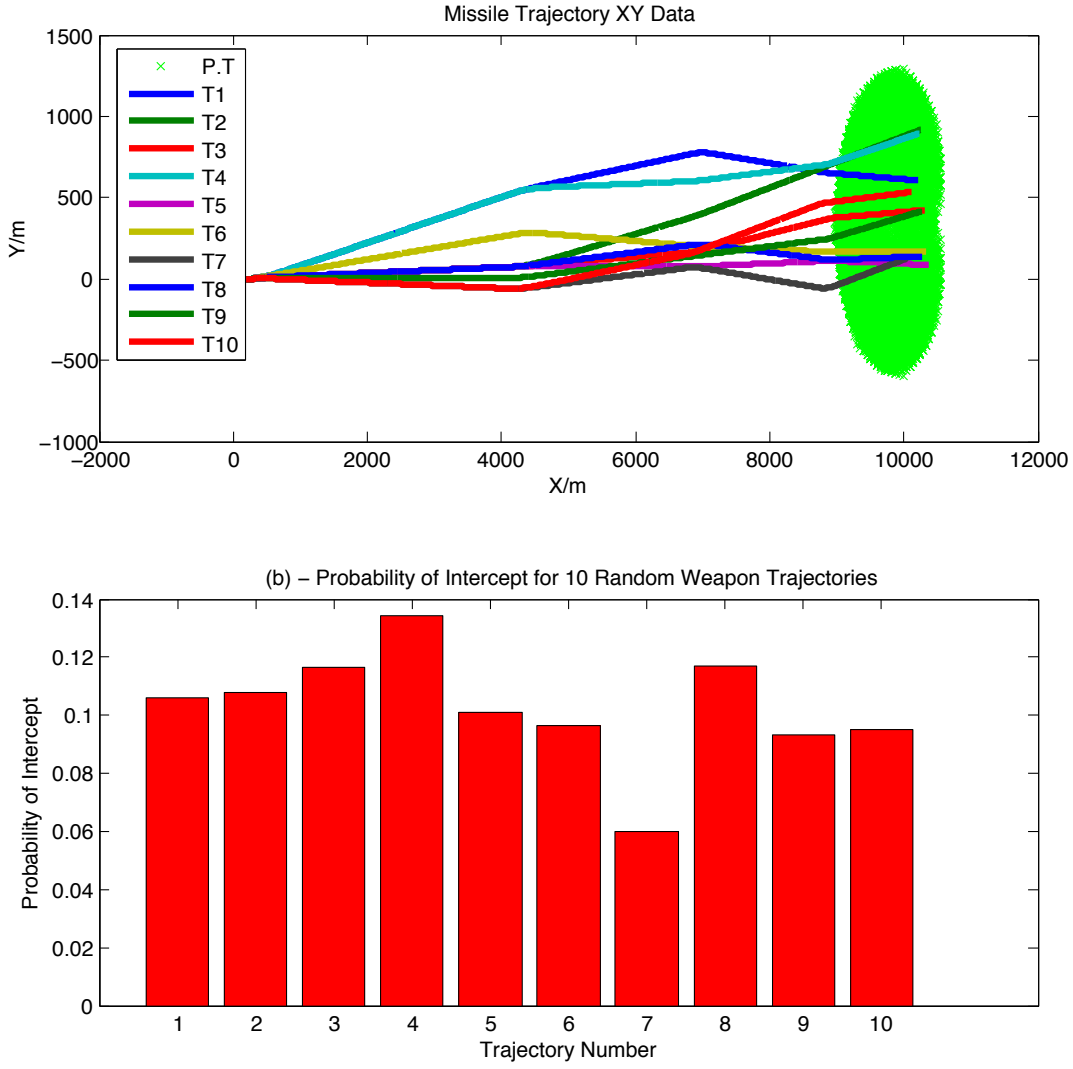

Figure 5.10: Feasible Trajectory Solution Area

The distribution of predicted trajectories in Figure 5.9 resulted in a feasible solution area defined by off-boresight commands of 9° and −5°. Random weapon

trajectories are then calculated by generating 4 off-boresight commands which will each have a random value between $-5°$ and $9°$. The off-boresight commands will be applied at T=0s, T=10s, T=20s and T=30s. 10 example trajectories generated under these conditions are shown in Figure 5.10 (a). In Figure 5.10 (b) the probability of intercept obtained for each of the 10 generated trajectories is displayed. By generating trajectories using these off-boresight constraints, each weapon trajectory has an associated target intercept probability > 0.

Once the random weapon trajectories have been generated, the last stage of the weapon initialisation phase is to run the simulated annealing optimisation algorithm to determine the initial optimal weapon trajectory.

The simulated annealing algorithm will optimise the trajectory based on the target trajectory distribution up to a prediction time of 35s as this is the maximum time by which it can confidently be assumed that the seeker will actually be on. The assumption is made that provided a target detection is made up to 35s, a successful interception will occur within the remaining 5s of the 40s flight time of the weapon.

The results of a simulated annealing optimisation run for this particular distribution of target trajectories are presented in Figure 5.11

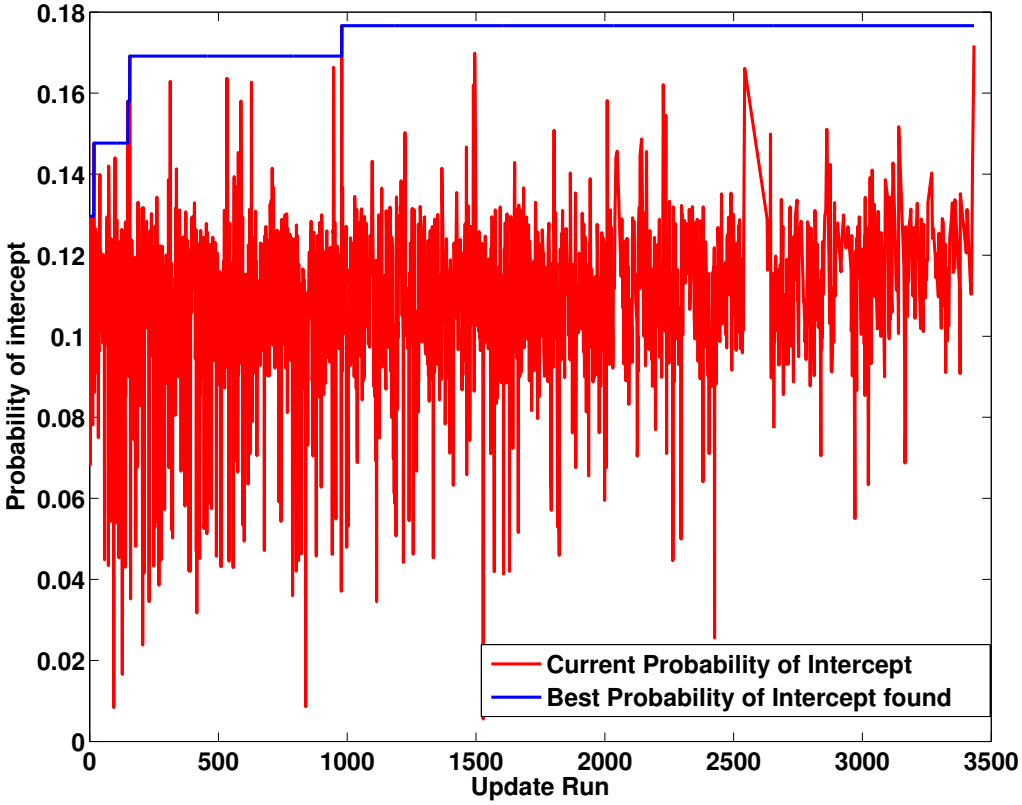

Figure 5.11: Typical Simulated Annealing Results at Weapon Initialisation

The probability of intercept for the initial optimal weapon trajectory will be fairly small at T=0s as indicated by Figure 5.11. This is due to a significant prediction into the future of the target behaviour, resulting in a large distribution of possible target trajectories with associated lower probability peaks. As more information is obtained about the target through manoeuvre detections, possible target trajectories will be eliminated resulting in a smaller probability distribution with larger peaks. The simulation begins with the first off-boresight angle programmed into the weapon at T=0s.

5.9 In-flight Trajectory Revision

The optimisation of the weapon trajectory after the weapon has left the launcher, is dependent on how the target behaves and if manoeuvres are detected by the IMM component of the integrated tracking and prediction system. Each off-boresight command transmission will include a revision of the current and future commands associated with the optimal trajectory. The times at which the trajectory is revised can be described considering either:

1. 0 manoeuvres are detected by the IMM.

2. 1 or more manoeuvres are detected by the IMM.

5.9.1 In-flight Trajectory Revision, 0 Manoeuvre Detections

The trajectory will be revised at T=10s, (which will coincide with the transmission of off-boresight command 2), T=20s, and T=30s. Simulated annealing is used to determine the optimal trajectory at T=10s and T=20s. At T=10s and T=20s, 2 or more off-boresight commands will be used to calculate each proposed weapon trajectory. This will result in a complicated intercept probability distribution. The simulated annealing algorithm will therefore be the appropriate optimisation algorithm, to determine the maximum probability of intercept and the associated optimal weapon trajectory.

At T=30s, the simple search algorithm is used to fine tune the trajectory provided a successful target detection has not already been made.

The data link activity for a non manoeuvring target trajectory is provided in Figure 5.12. The data link at each time step will be in one of two states which consist of, able to transmit (A.T.T) and not able to transmit (N.A.T).

The transmission times of each off-boresight command coincide with either a trajectory revision completed using simulated annealing (R.S.A) or simple search (R.S.S). Three trajectory revisions are shown on the data link. The initial optimal trajectory, and associated first off-boresight command would be programmed into the weapon while it is on the launcher.

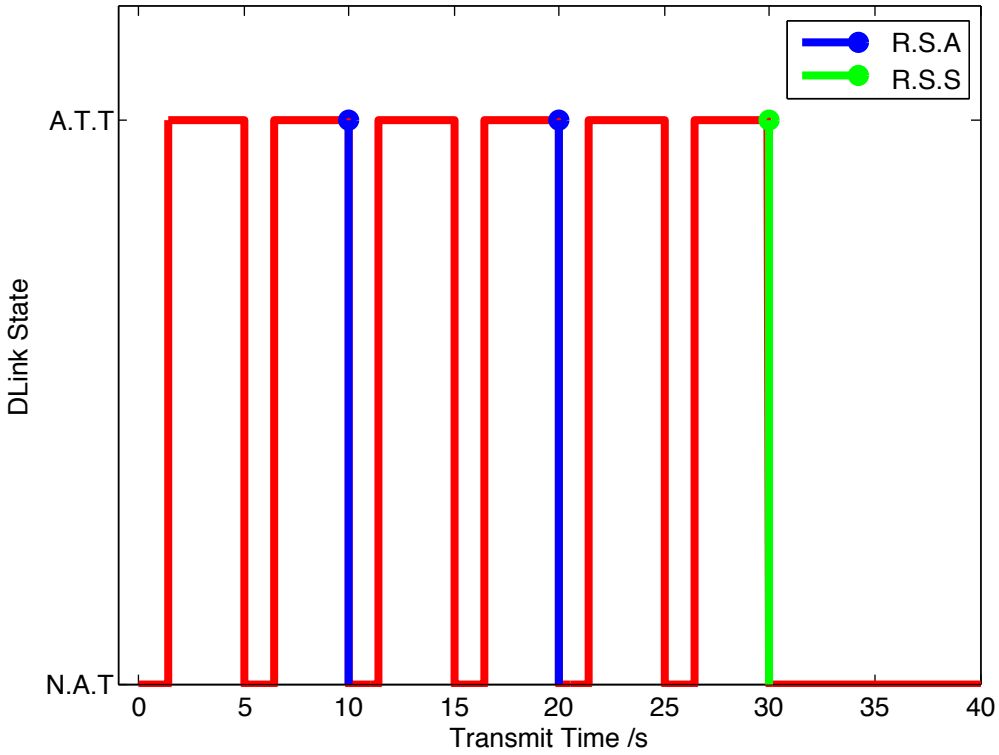

Figure 5.12: Data Link Activity for 0 Manoeuvre Detections by the IMM

The simple search algorithm is used at T=30s as only a very small number of possible target trajectories will remain. An intercept should occur within the next 5s therefore only one off-boresight command will be considered in the optimisation process. There will only be a limited number of off-boresight commands which could be applied at this point. The intercept probability distribution will cover only a small region of space in the xy plane which can be effectively evaluated using a simple search algorithm, which, in essence, will simply perform an exhaustive search.

Both optimisation algorithms have been developed considering that the final off-boresight command will occur either at T=30s or in the interval T=25s-30s. In the case that 0 manoeuvres are detected by the IMM, the data link will be deactivated at T=30s after the transmission of the final off-boresight command. As can be seen in Figure 5.12, the fire control system is unable to transmit over the data link after T=30s. This is shown as a data link state of not able to transmit (N.A.T).

5.9.2 In-flight Trajectory Revision, Manoeuvres Detected

The trajectory will be revised twice using simulated annealing and one or more times using the simple search approach. The final number off-boresight commands used to shape the trajectory will be either 4 or 7.

If a manoeuvre detection occurs between off-boresight commands which will be updated using simulated annealing then, the trajectory revision using simulated annealing will be brought forwards in time to the detection time step. For example, consider a manoeuvre detection which occurs at T=12.5s. This detection is between off-boresight command 2 at T=10s and off-boresight command 3 at T=20s. The trajectory revision at these time steps would be completed using a simulated annealing optimisation process. The simulated annealing process performed at T=20s, would now be performed at T=12.5s. If no further manoeuvre detections are made, then the simple search algorithm will be used to fine tune the trajectory at T=30s provided no target detection is made by the seeker. This is illustrated in Figure 5.13 which provides the data link activity for one manoeuvre detected at 12.5s.

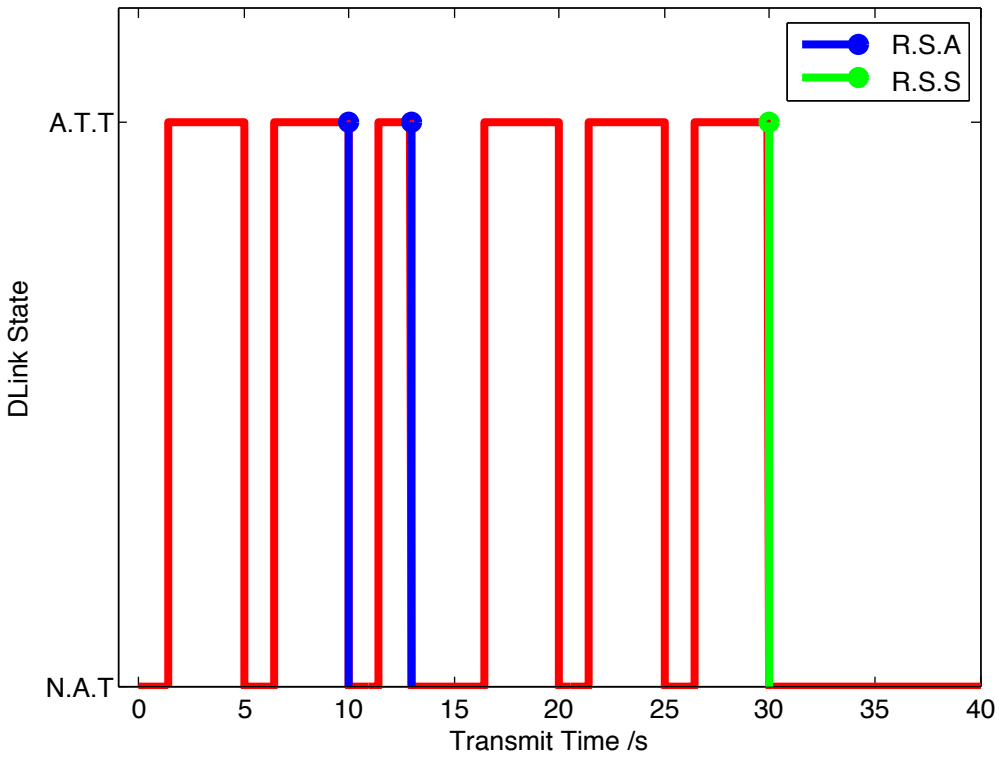

Figure 5.13: Data Link Activity for 1 Manoeuvre Detection by the IMM

If further manoeuvre detections are made after the third trajectory revision has

been completed using the simulated annealing algorithm, the trajectory will be revised using simple search for each subsequent detection. This algorithm is used due to the assumptions made when optimising the trajectory using simulated annealing.

Initially it was assumed that the target would attack the ship, which would potentially entail a small number of short manoeuvres. However the target (the small boat) would seek to spend the duration of the engagement not manoeuvring, in order to minimise the time that the ship would have in order to defeat the attack. The trajectory was therefore optimised considering that three trajectory revisions based on 4 off-boresight commands would be sufficient.

However if the manoeuvre detections exhaust the initial 3 revisions then the trajectory must still be revised. Further off-boresight commands are now required for the trajectory revision which the simulated annealing algorithm was not optimised to consider. Therefore the fire control system naturally defaults to the simple search algorithm for the remainder of the weapon flight.

To illustrate how the two optimisation processes would be used if multiple target manoeuvres are detected, the data link activity for 4 manoeuvre detections is depicted in Figure 5.14.

In this particular example, manoeuvres were detected at T=13.4s, T=17.3s, T=22.1s and T=27s. The optimal trajectory was revised using simulated annealing and off-boresight commands 2 and 3 where subsequently transmitted to the weapon using the data link at T=13.4s and T=17.3s. The trajectory was then revised at T=22.1s and T=27s using the simple search algorithm. The data link transitions into the N.A.T state at T=27s, instead of T=30s. The weapon trajectory in this case would have been shaped using 5 off-boresight commands.

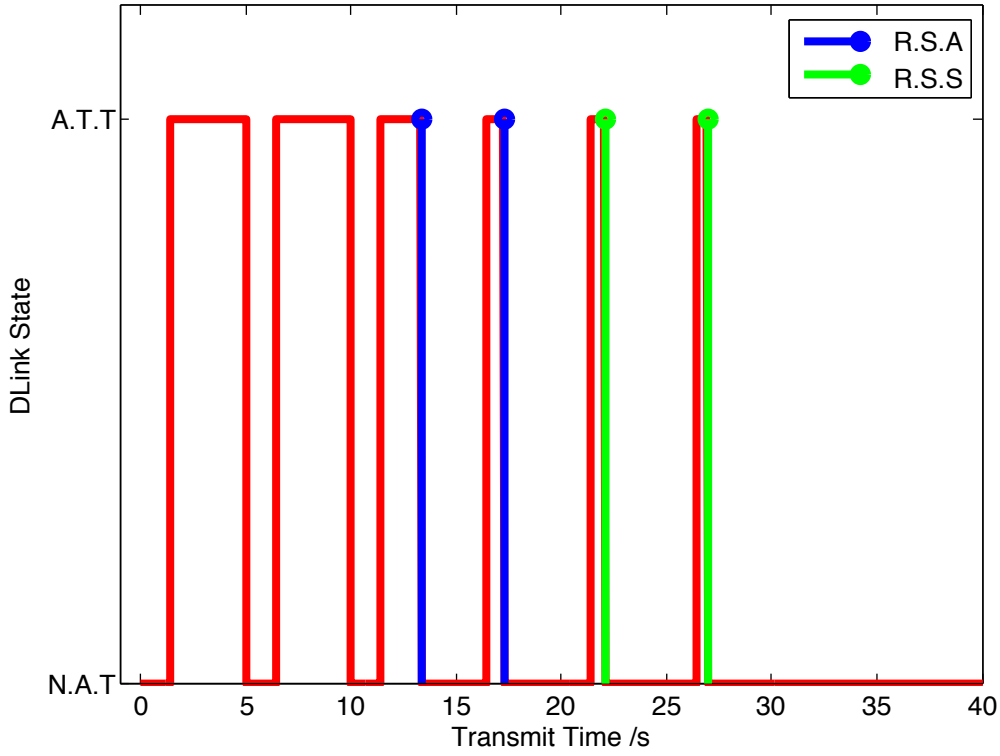

Figure 5.14: Data Link Activity for 4 Manoeuvre Detections by the IMM

5.9.3 Trajectory Revision using Simulated Annealing and Simple Search

On each occasion that the trajectory of the weapon is revised using the simulated annealing algorithm, the following process is performed.

1. The distribution of possible trajectories will firstly be updated based on either the detection of a manoeuvre or a 5s period of assumed constant velocity behaviour. The appropriate trajectory eliminations will be made and the associated probabilities recalculated using the Markov Chain.

2. The new off-boresight limits which the remaining trajectory distribution is enclosed by will be calculated using the same method as outlined in Section 5.8

3. 3420 random target trajectories will be calculated for the appropriate number of off-boresight commands remaining.

4. The simulated annealing optimisation algorithm will be performed based on the updated trajectory distribution and the generated target trajectories.

An example of a revision of the optimal trajectory using the simulated annealing algorithm is shown in Figures 5.15 and 5.16.

The weapon trajectory (W.T), scan area (S.A) and predicted target location distribution (P.T.D) are shown in the figure.

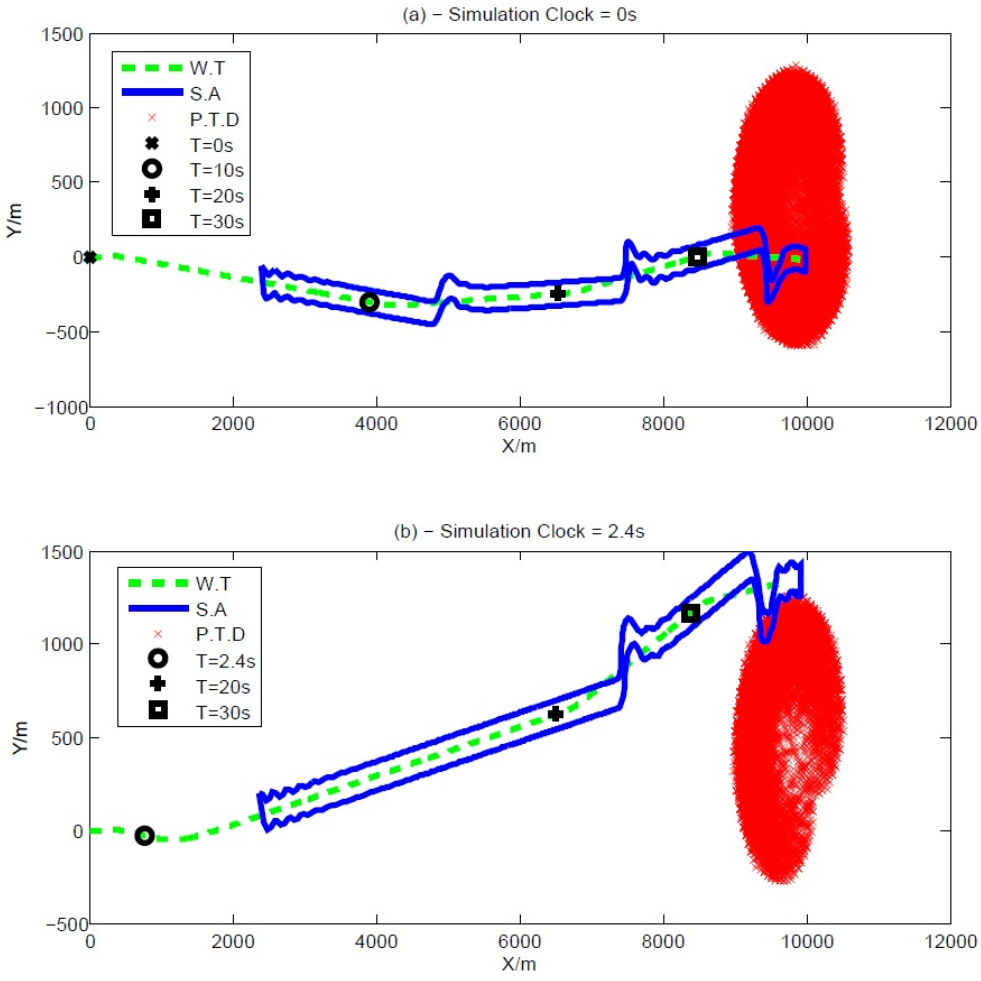

Figure 5.15: Optimal Weapon Trajectories and Associated Scan Areas Calculated by Simulated Annealing at T=0s, and T=2.4s

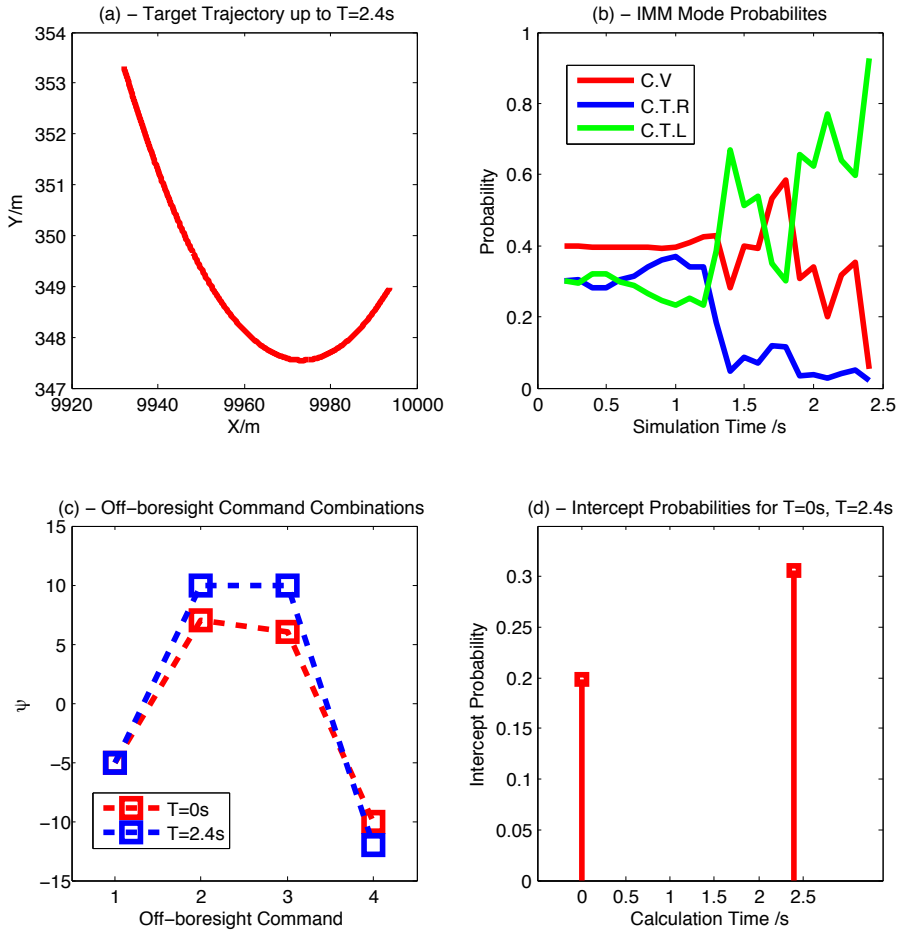

Figure 5.16: Assorted Data for Trajectory Revision in Figure 5.15

In the simulation depicted in Figures 5.15 and 5.16, the target had an initial state at T=0s of [10000,-25.6, 350, -3.6]' which was determined from the pulsed radar model. The optimal trajectory calculated by the simulated annealing algorithm is depicted in Figure 5.15 (a). The probability of target intercept was determined to be 0.2 which is indicated in Figure 5.16 (d).

The target then began a turn to the left. At T=2.4s, the IMM mode probability of the coordinated turn left model peaked above 0.9s, which triggered a weapon trajectory update. The revised weapon trajectory calculated by the simulated annealing process at T=2.4s is shown in Figure 5.15 (b). The maximum probability of intercept was determined to be 0.32 by the simulated annealing process if the weapon now flew the revised trajectory.

Trajectory revision using the simple search algorithm is performed in much the same way :

1. The distribution of possible trajectories will firstly be updated based on either the detection of a manoeuvre or a 5s period of assumed constant velocity behaviour. The appropriate trajectory eliminations will be made and the associated probabilities recalculated using the Markov Chain.

2. The new off-boresight limits which the remaining trajectory distribution is enclosed by will be calculated using the same method as outlined in Section 5.8

3. The trajectory for each possible off-boresight command is calculated, as is the associated probability of intercept. The off-boresight command with the largest maximum probability of intercept will be transmitted to the weapon at the required time.

Though the first off-boresight command will be programmed into the weapon at launch, the command will not be executed by the weapon until separation has occurred from the launcher. A time delay of 1s is utilised in the code to simulate the separation. The fire control system will enter the in-flight trajectory revision phase at the transmission time of off-boresight command 2.

5.9.4 Example Engagement

In order to understand how the various components of this integrated fire control system function to achieve an intercept, an example engagement is depicted in Figures 5.17 and 5.18 respectively.

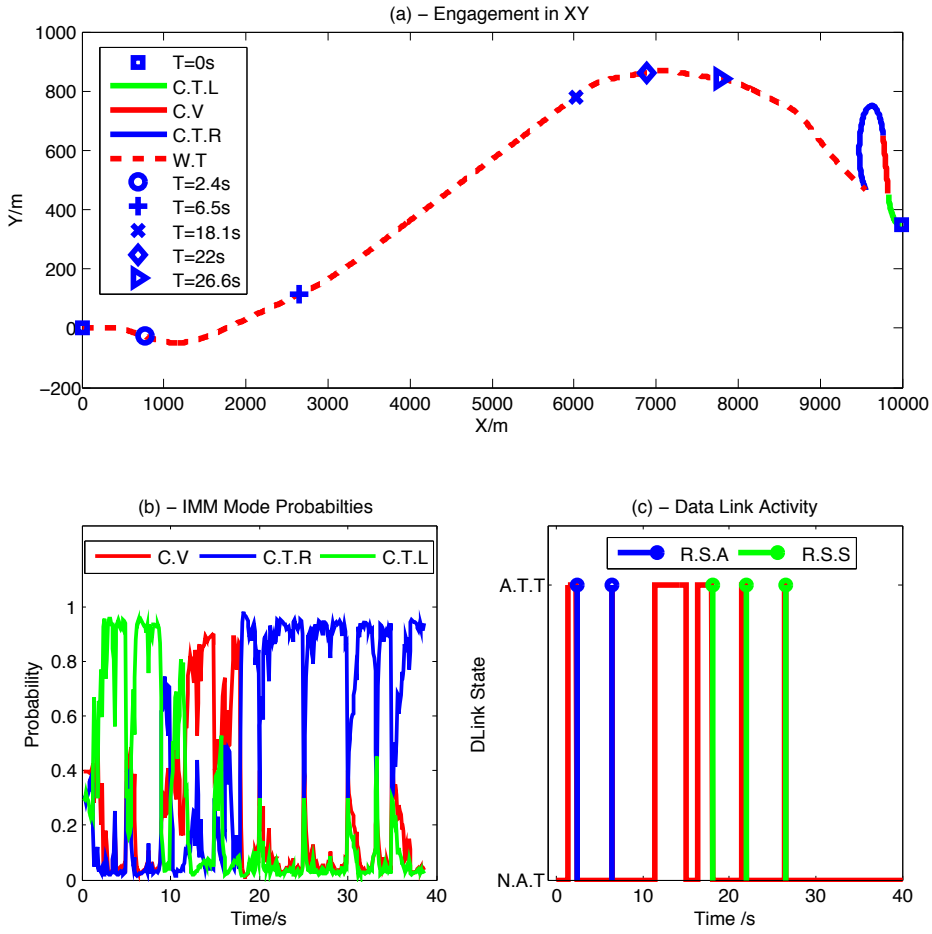

Figure 5.17: S.A.S.S - Example Engagement Plot Set 1

The target had an initial state at T=0s of [10000,-25.7, 350,-3.6]'. It then performed a turn to the left until T=8s. Between T=8s and T=16s, the target continued on the new heading achieved by the 8s turn. Between T=16s and the point of interception at T=38.65s, the target turned to the right. 5 manoeuvre detections were made by the IMM between T=0s and T=30s. The optimal trajectory calculated at T=0s was revised using the simulated annealing process at the manoeuvre detection points of T=2.4s (shown in Figure 5.15) and T=6.5s. The IMM made 3 further detections at T=18.1s, T=22s and T=26.6s. The trajectory of the weapon was revised using the simple search algorithm at each of these time steps. The trajectory of the weapon and target in the XY plane are depicted in Figure 5.17 (a).

The mode probabilities for the IMM and the data link activity is depicted in subplots (b) and (c). The phases of the fire control system are shown Figure 5.18 (f). The weapon initialisation, inflight trajectory revision and weapon terminal guidance phases are abbreviated as W.I, I.F.T.R and W.T.G respectively.

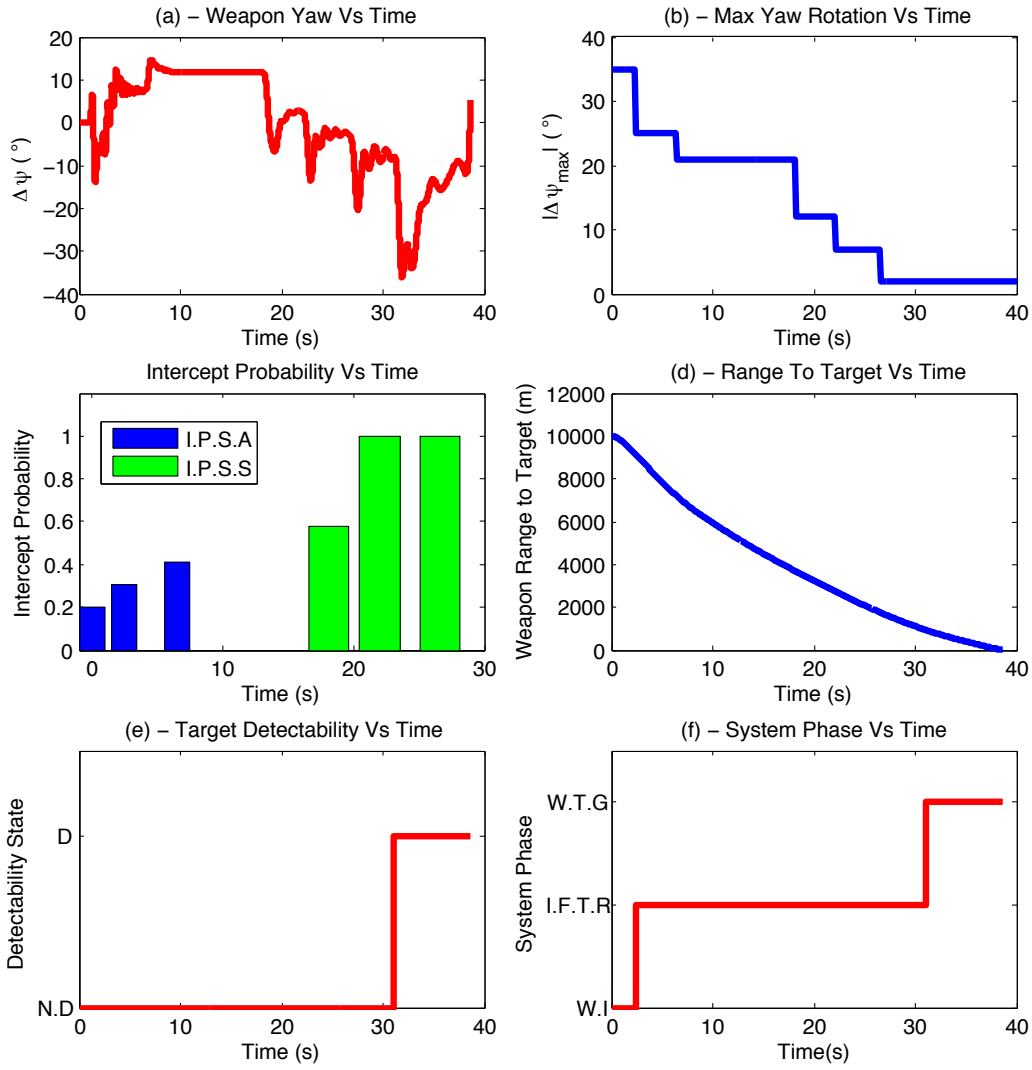

Figure 5.18: S.A.S.S Example Engagement Plot Set 2

The heading of the weapon and the maximum yaw change which can be applied at each time step is depicted in Figure 5.18 (a) and (b). Though each off-boresight command is transmitted instantly to the weapon at each trajectory update point, the desired off-boresight heading is not achieved immediately. However the maximum yaw change which can be applied in subsequent off-boresight commands is reduced instantly by the fire control system as shown in Figure 5.18 (b).

As time progresses and more information has been obtained about the target, the intercept probability increases as shown in Figure 5.18 (c). In this particular engagement an intercept probability of 1 was achieved, however this is calculated based on a predicted target behaviour. An intercept probability of 1 will not guarantee that the target will be intercepted. Though it should be highly probable that a successful detection will occur, provided of course that the correct trajectories have been eliminated by the combined tracking and prediction system.

In Figure 5.18 (d), the weapon range to the target is plotted over the duration of the engagement time period. Though very little information is known about the target in the initial stages of the engagement, calculating a weapon trajectory based on a prediction has resulted in the weapon flying a trajectory which continually reduces the range to the target at each point in time. For a successful detection to occur, the weapon must fly close enough to the target such that it is within the seeker detection range. A typical value for which is 1500m. Provided that the target then lies within the area being scanned by the weapon, once this range has been achieved, a successful detection should then be made. In this particular example the detection occurs at 31.5s. At which point the fire control system will relinquish control of the weapon. The weapon will have then entered the terminal guidance phase .

The target in this engagement did not comply with the initial predictions of 5s state transitions, however a successful interception has still been achieved.

5.10 Performance Evaluation

The integrated fire control system was benchmarked against the same initial 80 trajectories generated for the Fire and Forget performance evaluation in Chapter 3. The results of which would then indicate whether the performance of the AAAW was improved against manoeuvring targets if a data link and integrated fire control system were utilised.

The results of the simulated engagements are shown in Figure 5.19 (in subsequent chapters, the system will be referred to using the abbreviation of S.A.S.S, short for Simulated Annealing and Simple Search)

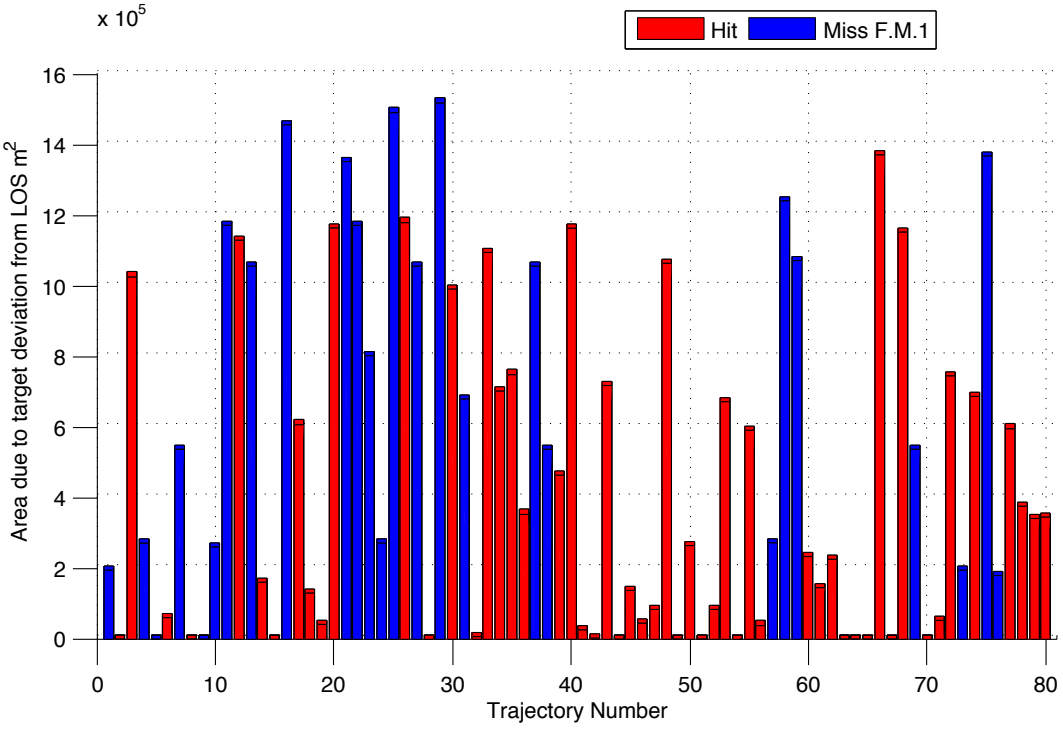

Figure 5.19: S.A.S.S results

The area due to the target deviation shown in Figure 5.19 is calculated using equations 2.51 and 2.54 with $\vec{R}_{in}$ either taken as the final location of the target at the point of interception or at T=40s. Out of the 80 engagements simulated, the weapon successfully intercepted 54 targets and failed to intercept 26. Just as in Chapter 2, missed targets by the weapon in the integrated fire control system can be considered as either Failure Mode 1, 2 or 3. However Failure Mode 1 in this case describes a failure of the integrated fire control system to calculate a trajectory which would result in the target being detectable within the weapon scan area at some instant in time.

The performance of this system against each of the three types of target trajectory generated by the model is presented in Table 5.1 along with the Fire and Forget (F.F) results obtained in Chapter 3.

System	N.M	I.B.M	M.T
S.A.S.S	12/14	1/6	41/60
F.F	14/14	6/6	27/60

Table 5.1: S.A.S.S and F.F Results

Each of the 26 failed intercepts are classed as Failure Mode 1. Of the 41 manoeuvring targets intercepted in the S.A.S.S system, 18 of the targets where also intercepted by the F.F system. The S.A.S.S system intercepted 23 manoeuvring targets which the F.F system failed to intercept and failed to intercept 9 targets which the F.F system successfully intercepted.

Though the F.F system intercepted 27 manoeuvring targets, the constraints for a successful intercept in this system are very limited, as discussed in Chapter 3. The constraints must be considered when comparing the results with the integrated system proposed in this Chapter.

In each of the successful intercepts in the S.A.S.S system, the trajectory has been shaped in response to target manoeuvres in order to improve the probability of a successful detection and engagement. Therefore the results of the S.A.S.S system indicate that this system overall offers a superior performance against manoeuvring attacks compared to the F.F system. The performance against non manoeuvring targets remains excellent as out of the 14 non manoeuvring target trajectories generated, 12 targets where successfully intercepted. However the performance of the F.F system against non manoeuvring targets was superior. The AAAW in the case of the F.F system successfully intercepted all 14 of the non manoeuvring targets.

5.10.1 Test for Statistical Significance - Chi Square χ^2 Test

The integrated system was developed to improve the performance of the weapon against manoeuvring targets, Though the results of the trials indicate that superior performance against manoeuvring attacks is obtained using this system, the possibility that the observed results are due to chance alone must be considered.

In order to determine whether this is the case, a test for statistical significance can be used. In this thesis, a Chi square test is used due to its simplicity and its recognised reliability in a variety of applications from manoeuvre detection in target tracking to drug trial analysis [72].

A Chi test requires the formation of a null hypothesis and the calculation of the χ^2 value. The probability of that value can then be obtained from look up tables or calculated in Matlab. Normally, a probability of 0.05 is then used for a comparison. If the computed probability is less than this value, then there is little statistical evidence to suggest that the results are due to chance. A probability value higher than this would indicate that there is statistical evidence to suggest that the results are due to chance alone.

The following statistical assumptions are made when using this test:

1. The sampling population is random, e.g. the patients of a clinical trial are selected from the wider population at random.

2. The variables of the trial are independent.

The assumptions are satisfied as the trajectories are randomly generated and in each simulated engagement the weapon can either hit or miss the target (independent variable). As only two possible outcomes exist for each simulated engagement, the engagements can actually be classed as Bernoulli trials.

The process for completing the Chi square test is as follows :

1. The results of the F.F and S.A.S.S system are collected into an observed table (O):

System	Hits	Misses	Total
F.F	27	33	60
S.A.S.S	41	19	60
Totals	68	52	120

Table 5.2: Observed Data

2. The expected values are then calculated as shown in the expected table (E) below :

System	Hits	Misses	Total
F.F	34	26	60
S.A.S.S	34	26	60
Totals	68	52	120

Table 5.3: Expected Data

3. The difference between the observed values and expected values is the calculated, the sum of which produces the χ^2 statistic.

$$\chi^2 = \sum_{n=1}^{4} \frac{(O_n - E_n)^2}{E_n} \tag{5.19}$$

4. The calculation of the probability of the null hypothesis being true requires the number of degrees of freedom (v) to also be determined which is simply defined as :

$$v = (m-1) \times (n-1) \tag{5.20}$$

where m is the number of rows in the observed table and n is the number of columns in the observed table. The number of degrees was calculated as 1.

5. The probability associated with this Chi squared value for the given number of degrees of freedom can be looked up in a table [72]. The Chi-square probability value for the S.A.S.S system was calculated as 0.01.

As the calculated probability is below that of statistical significance (p), the results of the S.A.S.S trials can be considered to be a reliable representation of the performance of the system. The result of the χ^2 test therefore supports the initial conclusion that the integrated system discussed in this chapter will improve the performance of the AAAW to intercept manoeuvring targets. However it is worth exploring the possible reasons why the system failed to intercept the 2 non manoeuvring targets, 5 I.B.M targets and 19 manoeuvring target trajectories.

5.11 Failure Analysis

In order to understand why the integrated system failed to achieve an intercept, firstly requires the behaviour of the IMM component of the system in each simulated engagement to be considered. In each simulated engagement, the integrated tracking and prediction system provided 6 updates.

The detections made by the IMM algorithm during each simulated engagement are shown in Figure 5.20.

The detections by the IMM and the actual target behaviour are described in the legend. The first letter of the legend label is the actual target behaviour which consists of Constant Velocity (C), Right Turn (R) and Left Turn (L). The second letter is the detection made by the IMM during each update.

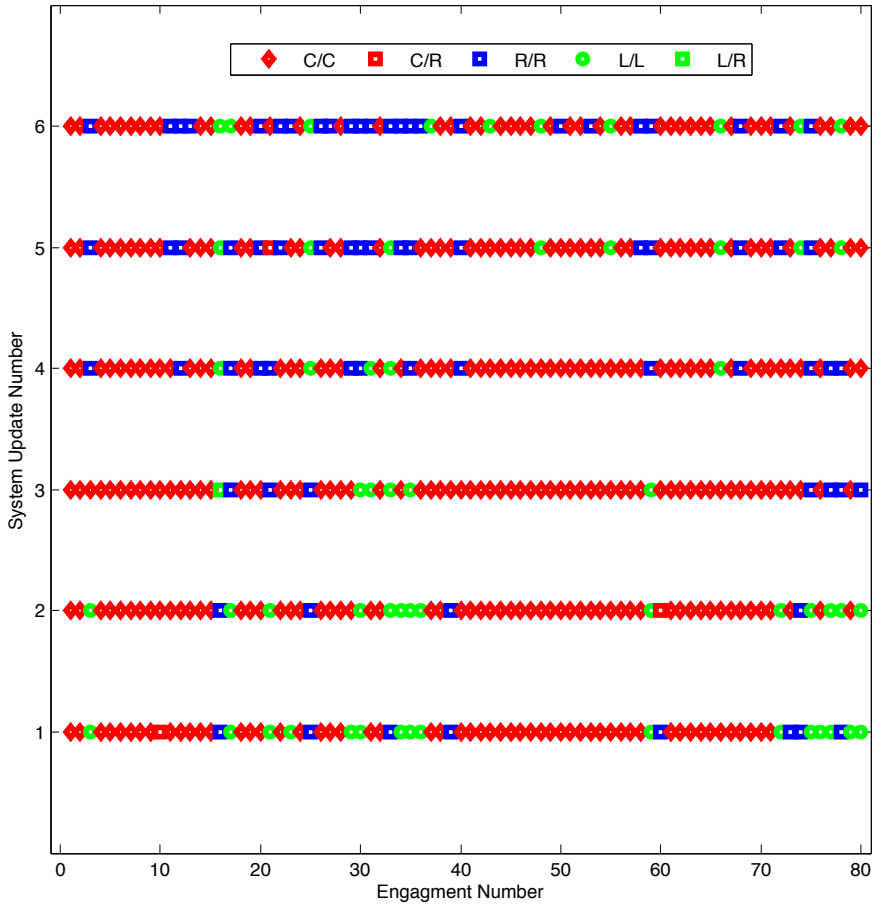

Figure 5.20: IMM Detections for each Simulated Engagement

The IMM component of the system produced a total of 4 incorrect detections which occurred in 4 engagements where the target had manoeuvred. The incorrect detections are shown in Figure 5.21.

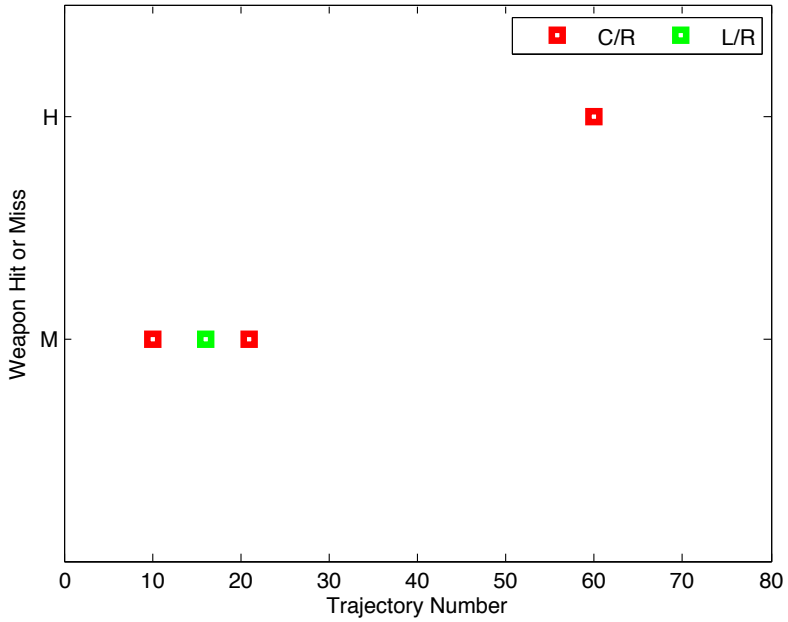

Figure 5.21: IMM Miss Detections

Three of the incorrect detections have potentially contributed to a failure by the fire control system to calculate a weapon trajectory which would result in an engagement. However in one engagement the IMM has failed but a successful intercept has still been achieved.

5.11.1 Non Manoeuvring Target Fails

The IMM failures did not occur in the 2 failed interceptions of non manoeuvring targets by the integrated fire control system. The failure in the system in these cases can therefore only be attributed to the trajectory optimisation process, specifically the simulated annealing optimisation step. If the target has not manoeuvred then the maximum probability of intercept will be achieved by a seeker scan area which allows a location on the most probable trajectory (non manoeuvring target) to be detectable and along one or more possible target trajectories.

As no manoeuvre detections were made, the trajectory would therefore been revised at T=0s, T=10s, T=20s and T=30s.

Either at T=0s, or T=10s/T=20s, the simulated annealing process will have identified a non-optimal trajectory. This trajectory will not have resulted in the target along the predicted non manoeuvring trajectory to be detectable at some instant in time.

The reliability of the Simulated Annealing algorithm was calculated to be between $88 - 98\%$ at 95% confidence therefore it highly unlikely that these two misses are due to three simulated annealing failures in each case. The most likely explanation is that at one of the update points before T=30s, the simulated annealing process failed once. The intercept probability distribution obtained at later update points is then dependent on the trajectory that the weapon can now fly based on the remaining maximum yaw change. The later trajectory optimisation processes whether simulated annealing or simple search will then have optimised the trajectory based on the possible trajectories that the weapon can now physically fly.

If the trajectory has been incorrectly shaped such that the weapon trajectory cannot be corrected to allow a detection along the non manoeuvring trajectory, the weapon will therefore fail to engage the target.

5.11.2 Manoeuvring Target Fails

Out of the 5 I.B.M misses, only in one engagement did the IMM produce a incorrect behaviour detection. In 2 of the 19 manoeuvring target fails, the IMM produced an incorrect behaviour detection. Therefore the first step in the analysis of the manoeuvring target and I.B.M fails is to consider those trajectories whereby the IMM has not failed. The two aspects of the system which could therefore contributed to the failed intercept would be the simulated annealing and simple search algorithms used in the actual trajectory optimisation process.

Based on the reliability analysis of the simulated annealing algorithm, then it is likely that a failure by this algorithm will have contributed to a target miss in only a small proportion of these failed intercepts.

A failure by the simple search method can be discounted as the algorithm is simple, it calculates the optimal trajectory by considering all possible trajectories through an exhaustive search and simply selects the trajectory which yields the maximum probability of intercept.

Assuming that the trajectory optimisation process has calculated the optimal trajectory successfully in the majority of the failed intercepts, then the first possible failure reason is that the scan area associated with the optimal weapon trajectory, based on the detection of predicted target locations does not include a location on the actual target trajectory at the same scan time. This scenario

is depicted in Figure 5.22

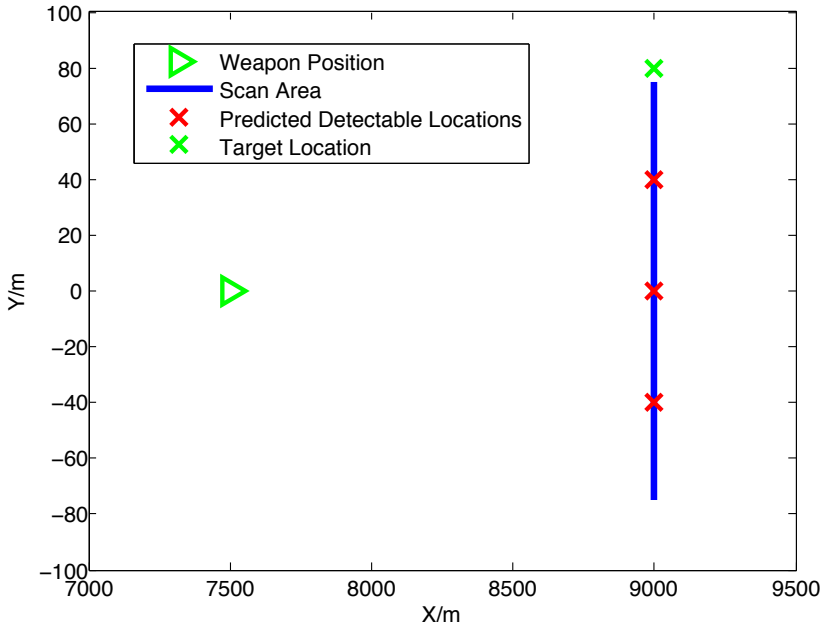

Figure 5.22: S.A.S.S Failure Due to Scan Area Orientation

If this scenario occurred in each case, then though the target has not been detected, the trajectory optimisation process has actually still been proven effective for the majority of the simulated engagement. In every simulation performed including those where the IMM produced a false behaviour detection, the trajectory optimisation process successfully minimised the initial 10000m range to the target to the seeker detection range of 1500m. In essence the difficult part of the weapon guidance has been achieved. In these cases its simply the orientation of the seeker scan area in respect to the target which has resulted in a failure.

An incorrect behaviour detection however will of course impact the probability of achieving a successful target detection. In the I.B.M and manoeuvring target fails, the incorrect detection will have changed the shape of the distribution of the predicted target trajectories as well as the associated probabilities. Each optimisation process performed after the incorrect detection will then optimise the trajectory based on what is now a poor target prediction. It will be unlikely that the trajectory calculated on this incorrect distribution will result in the scan area covering the actual target at any instant in time.

However as demonstrated in engagement 60, an incorrect detection can still result in a successful intercept occurring. In this situation, the trajectory of the target will have brought it back within the scan area associated with the optimal

trajectory calculated on the IMM miss detection.

The successful interception of some late manoeuvring targets using a basic Fire and Forget system raises the question whether there is any benefit in only shaping the trajectory after launch if a manoeuvre is detected. Furthermore can the same performance against manoeuvring targets be achieved, if only the most probable trajectory of the target distribution is considered? Chapter 6 will therefore seek to determine if the performance of the AAAW using an integrated fire control system which focuses on addressing these two questions can be improved against manoeuvring targets.

5.12 Chapter Review

This chapter has discussed the design, implementation and simulation of an integrated fire control system which sought to calculate an optimal weapon trajectory which would maximise the probability of successfully intercepting a potentially manoeuvring target.

The trajectory of the weapon was optimised considering a distribution of possible target trajectories and the probability of intercept that could be obtained from overlapping the scan area of the weapon over the distribution of possible target trajectories.

Shaping the weapon trajectory from different off-boresight combinations, varied the probability of intercept. The integrated fire control system sought to determine the weapon trajectory which would yield the maximum probability of intercept using 4 or more off-boresight angles which are transmitted to the weapon at various points in time.

A performance evaluation of the system, indicated that this system improves the performance of the original AAAW to intercept manoeuvring targets. However it appears that, under certain circumstances, late manoeuvring targets could be intercepted before the manoeuvre can be executed.

Chapter 6

Integrated Systems Two - Most Probable Trajectory (M.P.T)

Within the predicted target trajectory distribution their will be one target trajectory which is more probable than the remaining trajectories. Initially this most probable trajectory will be a non-manoeuvring target as stipulated by the probabilities used in the Markov Chain discussed earlier in this thesis. If no manoeuvres are detected by the IMM, the probability of a non manoeuvring target will naturally increase. However if manoeuvres are detected by the IMM, then the most probable trajectory will change from a non-manoeuvring target trajectory, to a manoeuvring target trajectory.

It is postulated in this chapter that, the performance of the weapon against manoeuvring targets can be improved by shaping the trajectory of the weapon and associated scan area only on the detection of a manoeuvre. The weapon trajectory will be shaped considering only the most probable trajectory of the predicted target trajectory distribution.

As in Chapter 5, the integrated system will be discussed as operating within two phases consisting of Weapon Initialisation and In-flight Trajectory Revision.

6.1 Weapon Initialisation

At T=0s, the distribution of predicted target trajectories will be calculated from an initial target state with components $[x, v_x, y, v_y]'$. The most probable trajectory from the distribution (which is a non-manoeuvring target trajectory) will be isolated from the rest of the distribution.

The same procedure used to calculate the launch off-boresight in the case of the

Fire and Forget system detailed in section 3.9.2 is applied to calculate the launch off-boresight for the integrated system. The maximum absolute yaw change, $|\Delta\psi_{max}|$ which could be applied in subsequent off-boresight commands is reduced instantly. At T=1s, the weapon will achieve separation from the launcher and the initial off-boresight command will be executed.

If no manoeuvre detections occur, the weapon in this integrated system will follow the same trajectory calculated using the Fire and Forget system. The system will not transition to the in-flight retargeting phase. Provided that the target performs 0 manoeuvres, there are 0 false manoeuvre detections, the seeker does not fail or the terminal guidance phase, then this system should always intercept a non-manoeuvring and an I.B.M target.

The integrated tracking and prediction system will continue to reduce the distribution of potential trajectories, the trajectory will not be revised unless a manoeuvre detection occurs.

6.2 In-flight Trajectory Revision

The detection of a manoeuvre will result in the calculation of an updated target prediction just as in the case of the S.A.S.S system. The new most probable trajectory will be isolated from the updated distribution of predicted target trajectories. The future weapon trajectory is determined by considering the range of possible off-boresight commands which can then be transmitted to the weapon. An initial off-boresight angle O_b is calculated as :

$$O_b = \psi - |\Delta\psi_{max}| \tag{6.1}$$

The associated trajectory and seeker scan area are calculated based on the application of this off-boresight command transmitted to the weapon at this update time. The scan area and updated most probable trajectory are compared to determine if a location along the most probable trajectory is detectable by the weapon.

If a detectable location exists, this off-boresight command will be transmitted to the weapon. The maximum absolute yaw change which could be applied in future off-boresight commands would therefore be 0°.

If no intercept exists the off-boresight command is incremented by 1° as:

$$O_b = O_b + 1 \tag{6.2}$$

The check for a detectable location is performed again. This process is repeated until either a detectable location is found or the maximum yaw change is exceeded. An example of the calculation of the updated most probable trajectory and associated off-boresight command is depicted in Figure 6.1

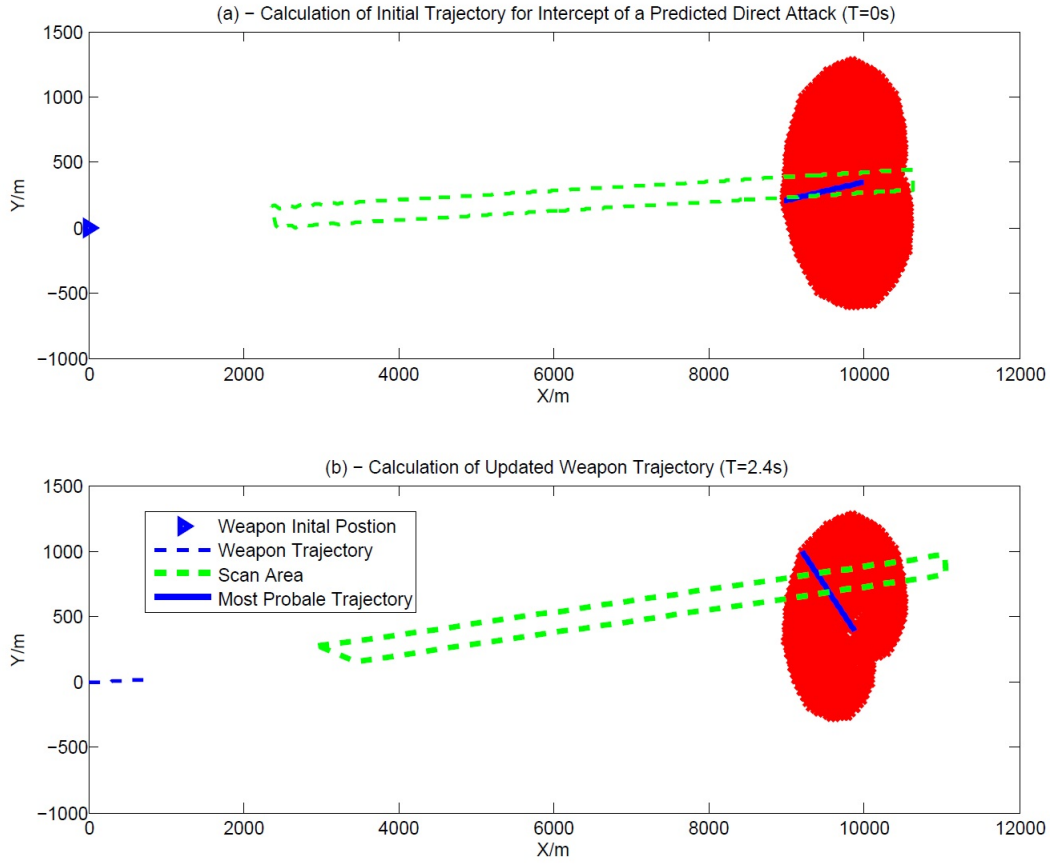

Figure 6.1: Example Calculation of an Updated Target Trajectory in the M.P.T System and Associated Off-boresight Command

In this simulation, an initial off-boresight command of 2° was calculated to create a target detection on the assumption of a non manoeuvring target trajectory. At T=2.4s, a left turn by the target was detected. The distribution of predicted target trajectories was subsequently updated considering an assumed 5s left turn by the target which will occur between T=0s and T=35s. Predicted trajectories which did not feature an initial 5s left turn were eliminated. The distribution is then recalculated based on a 35s prediction from T=5s, to T=40s. The most probable trajectory after the calculation of the updated distribution for the remainder of the weapon flight (i.e between T=5s and T=40s) is then a trajectory with no further manoeuvres. The absolute maximum yaw change available at T=2.4s was 38°.

An off-boresight angle of 5° was calculated to produce a detection along the new most probable target trajectory. This required a yaw change of 3°. The maximum yaw change which would then be available for subsequent trajectory revisions would therefore be 35°.

6.3 Example Engagement

A typical engagement of a manoeuvring target using this integrated system is depicted in Figures 6.2 and 6.3

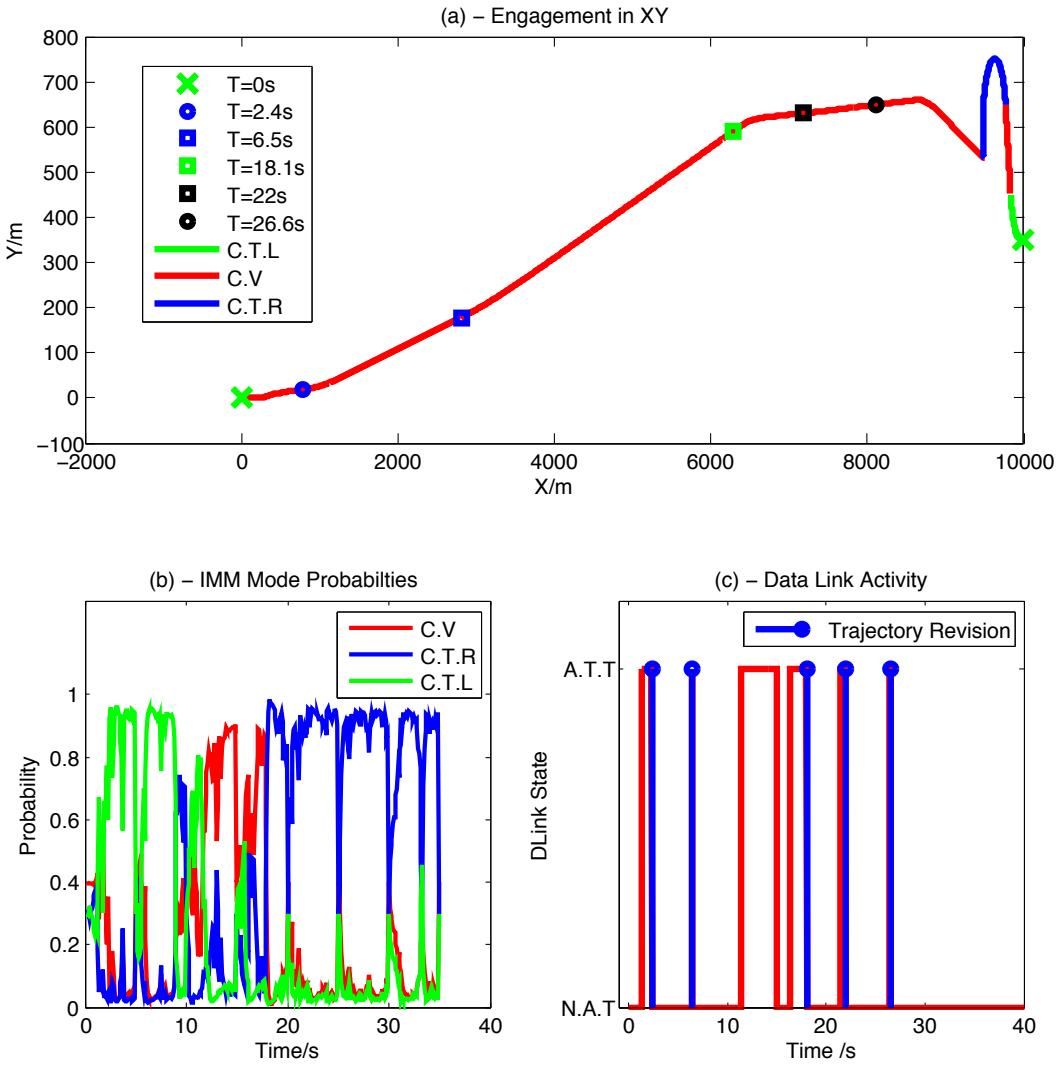

Figure 6.2: Example Engagement of a Manoeuvring Target using the M.P.T Integrated Fire Control System

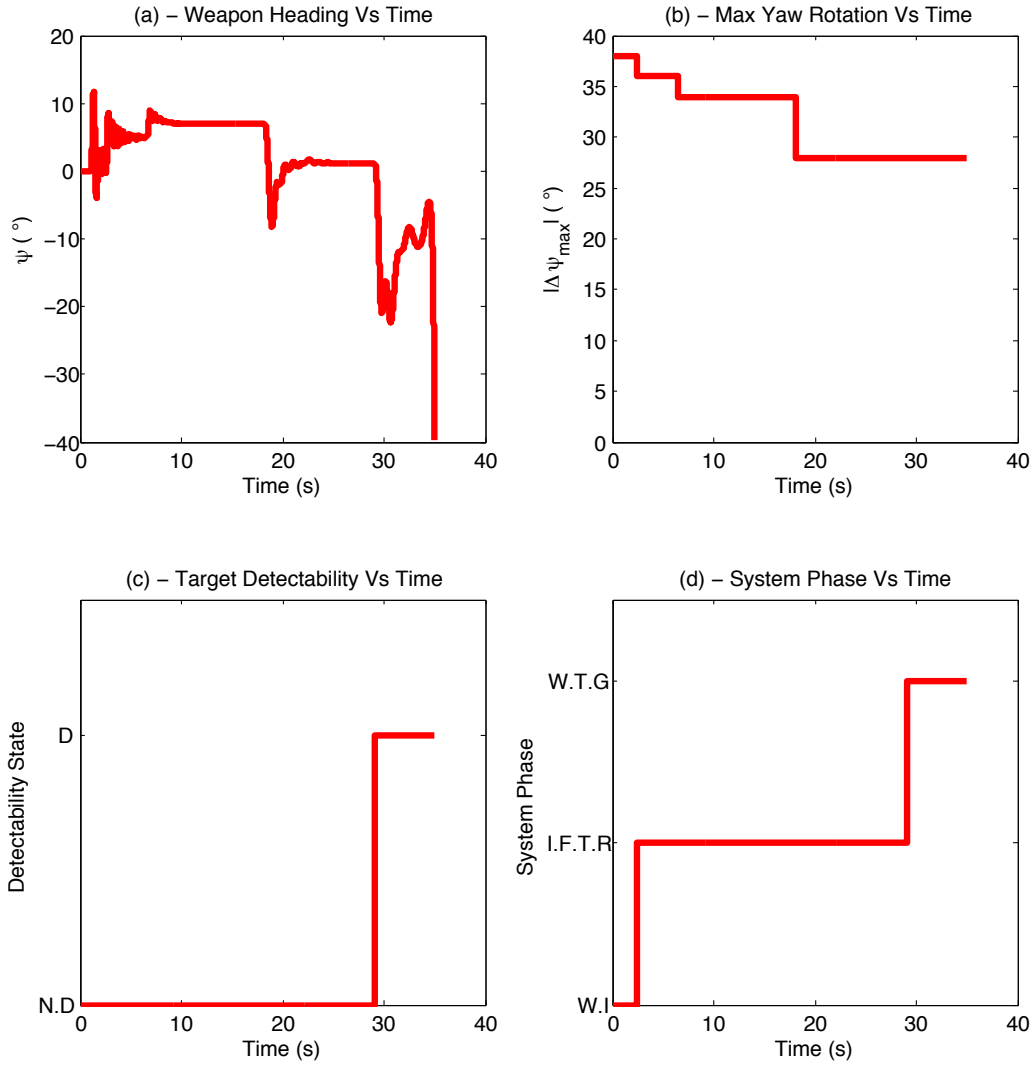

Figure 6.3: Example Engagement of a Manoeuvring Target using the M.P.T Integrated Fire Control System plot set 2

From an initial state of [10000,-26,350,3]', the target began an 8s turn to the left. It continued on the resultant heading until T=16s. It then executed a turn to the right, until interception by the weapon at T=35.035s. Manoeuvre detections occurred at T=2.4s, T=6.5s, T=18.1s, T=22s, T=26.6s. The trajectory of the weapon was updated at each of these time steps by the transmission of an off-boresight command via the data link.

The trajectory of the weapon and the target in the XY plane is depicted in Figure 6.2 (a). The IMM mode probabilities and the activity of the data link including the periods whereby the fire control system was able to transmit off-

boresight commands is shown in Figure 6.2 (b) and (c) respectively. The heading of the weapon and the maximum yaw rotation (change) which can be applied at each point in time during the simulation is depicted in Figure 6.3 (a) and (b).

The target was detected by the weapon seeker at T=29.045s, as can be seen in Figure 6.3 (d), the fire control system transitions to the weapon terminal guidance phase at this time.

The target did not comply with the 5s predicted state transitions. However an intercept has been achieved by shaping the trajectory after launch on the detection of target manoeuvres, considering only the most probable trajectory.

6.4 Performance Evaluation

The Most Probable Trajectory (M.P.T), integrated fire control system was benchmarked against the same 80 random target trajectories used to assess the performance of the Fire and Forget system. The results of which would determine whether an integrated fire control system using this approach would still achieve a performance increase against manoeuvring targets. The results of the simulated engagements are provided in Figure 6.4

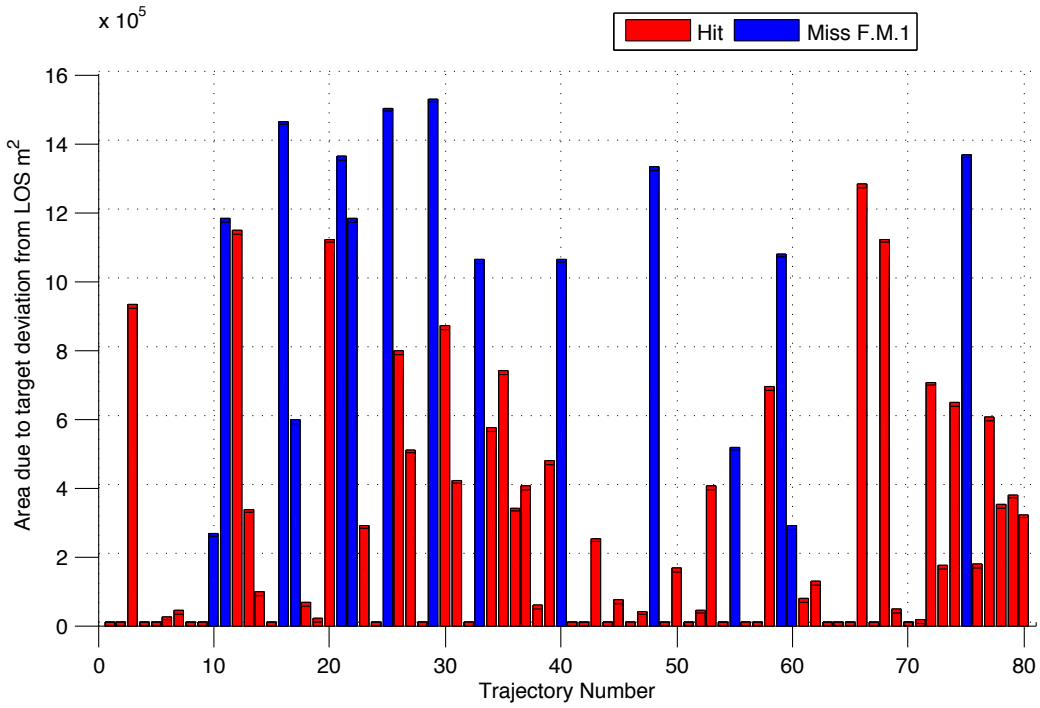

Figure 6.4: M.P.T results

The weapon in the case of the M.P.T system successfully intercepted 65 targets and failed to intercept 15. As in the F.F and S.A.S.S systems the area due to the target deviation in Figure 6.4 has been calculated either using the point of interception or the final location of the target at T=40s. The performance of this system against each of the three types of target trajectory generated by the model is presented in Table 6.1 along with the Fire and Forget (F.F) results obtained in Chapter 3.

System	N.M	I.B.M	M.T
M.PT	14/14	5/6	46/60
F.F	14/14	6/6	27/60

Table 6.1: M.P.T and F.F Results

Each failed intercept in the case of this system is classed as Failure Mode 1. Of the 14 non-manoeuvring trajectories generated by the target model, the weapon in the M.P.T system intercepted all 14 targets. Of the 6 manoeuvring trajectories which could be intercepted before the target performed a manoeuvre, the weapon in this system intercepted 5 targets. One of the 6 trajectories was classed as a manoeuvring target fail.

The weapon in the M.P.T successfully intercepted 24 of the manoeuvring targets, which were also intercepted in the case of the F.F system. Three successful manoeuvring intercepts by the F.F system where missed by the weapon in the M.P.T system.

The weapon in the M.P.T system intercepted 22 targets which the F.F system failed to intercept. The remaining 11 manoeuvring target trajectories generated by the target model where missed by the weapon in both the F.F and M.P.T fire control systems.

The performance of the weapon against non manoeuvring targets using this integrated fire control system remains excellent with all 14 non manoeuvring targets successfully intercepted. The results of the simulated engagements against manoeuvring targets indicate that this system offers superior performance against this type of target. The calculation of the χ^2 value resulted in a probability of 0.002. This value is below that for statistical significance which supports the initial conclusion that this system does improve the performance of the AAAW against manoeuvring targets.

6.5 Failure Analysis

There are 3 possible causes why the M.P.T failed to produce an intercept in the case of 15 simulated engagements .

In the first instance, the IMM does not make any miss detections. Therefore on each manoeuvre detection, the most probable trajectory is successfully updated. On the final manoeuvre detection and therefore most probable trajectory update, the trajectory of the weapon has been suitably shaped such that a location on the most probable target trajectory can be detected within the seeker scan area at a given scan time. However the actual target trajectory places the target at a location outside the scan area at that scan time. Therefore the target will not be detected and the weapon will not be able to attempt an intercept.

The next possible reason for a failure is that considering only the most probable trajectory can commit the weapon to a given target detection along one updated most probable trajectory early in the engagement. When further manoeuvre detections occur triggering the calculation of an updated target trajectory, the trajectory of the weapon cannot be sufficiently shaped in response. The possible overcommitment of the weapon can be explained considering the simulation de-

picted in Figure 6.5

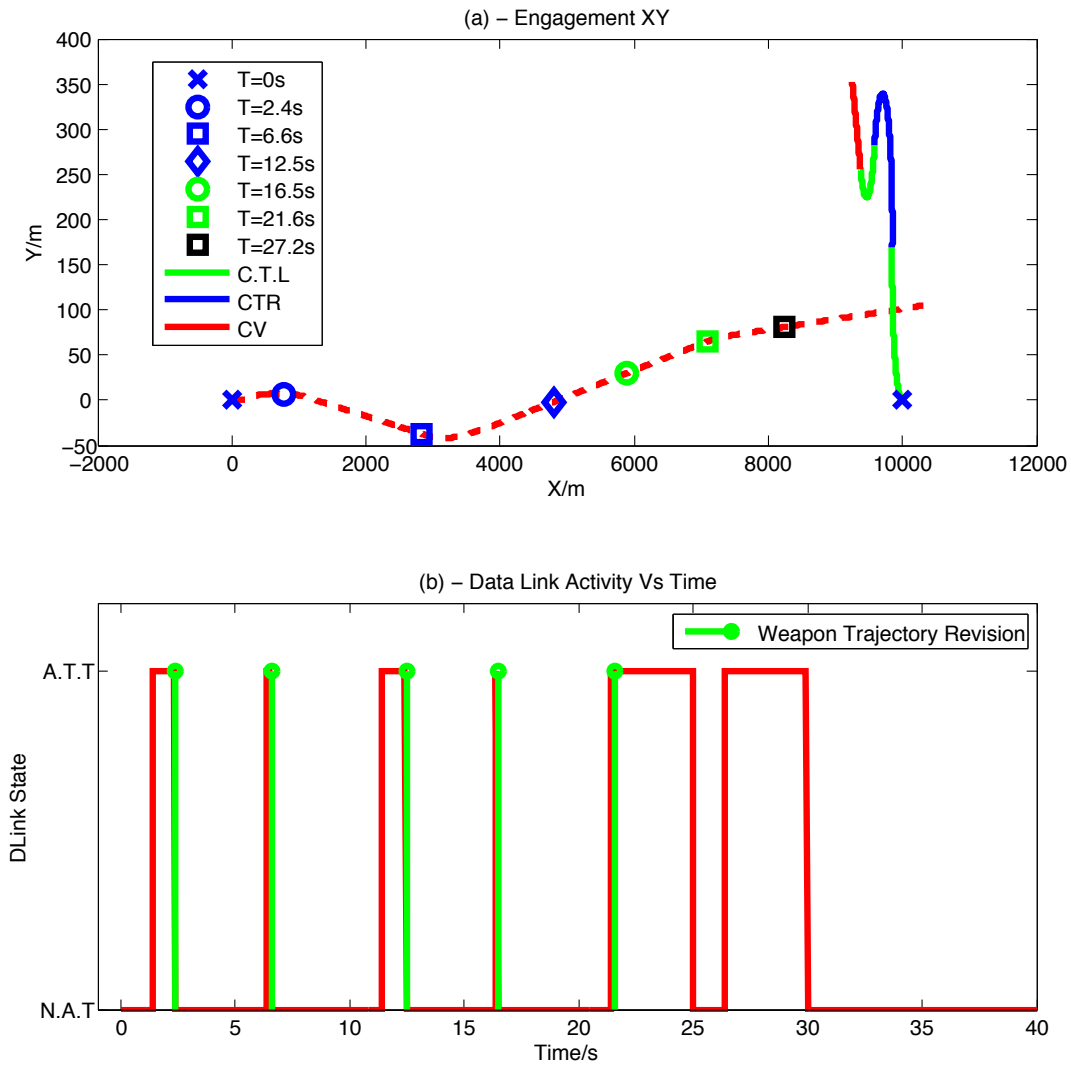

Figure 6.5: Weapon Overcommitment in M.P.T Integrated Fire Control System

From the initial target state at T=0s, the target performed a 10s turn to the left. At T=10s the target began a 25s turn to the right. Between T=25s and T=34s, the target turned to the left. The target continued on the resultant heading until T=40s.

Manoeuvre detections where made at T=2.4s, T=6.6s, T=12.5s, T=16.5s, T=21.6s and T=27.2s.

The trajectory was successfully revised at the first 4 manoeuvre detections as indicated by the data link activity in Figure 6.5 (b). At each of these 4 update points, the target following the updated most probable trajectory would have

been detectable by the weapon seeker. However at T=27.2s, the weapon trajectory could not be updated in response to the updated target trajectory. The weapon had been overcommitted to a detection along the predicted target trajectory defined at T=21.6s.

The final reason why the M.P.T system can fail to produce an intercept is from incorrect behaviour detection by the IMM component of the integrated tracking and prediction system.

This system optimises the trajectory based on only one predicted trajectory, it is therefore reliant on correct behaviour detection. A false positive by the IMM or an incorrect manoeuvre detection (i.e. a right turn detected when the target is actually turning left) will result a poor target trajectory prediction. In each failed engagement, the weapon range to the target had been minimised to the seeker detection range. However by shaping the trajectory on incorrect prediction, the seeker will be oriented away from the actual target trajectory. It will be highly unlikely that the actual target will be successfully detected. As in the S.A.S.S system for a target detection to then occur the target must manoeuvre into this scan area calculated on the incorrect behaviour detection at a later point in the engagement.

The M.P.T system does not utilise a random optimisation process to calculate the weapon trajectory. It is therefore possible to determine which part of the fire control system failed in the case of the 15 misses by the weapon. The system fails are provided in Figure 6.6 where IMM is a system failure due to an incorrect behaviour detection, O.C is an overcommitment by the weapon during the engagement and T.N.I.S.A is that the target is not in the scan area, with no IMM miss detections or overcommitment by the weapon.

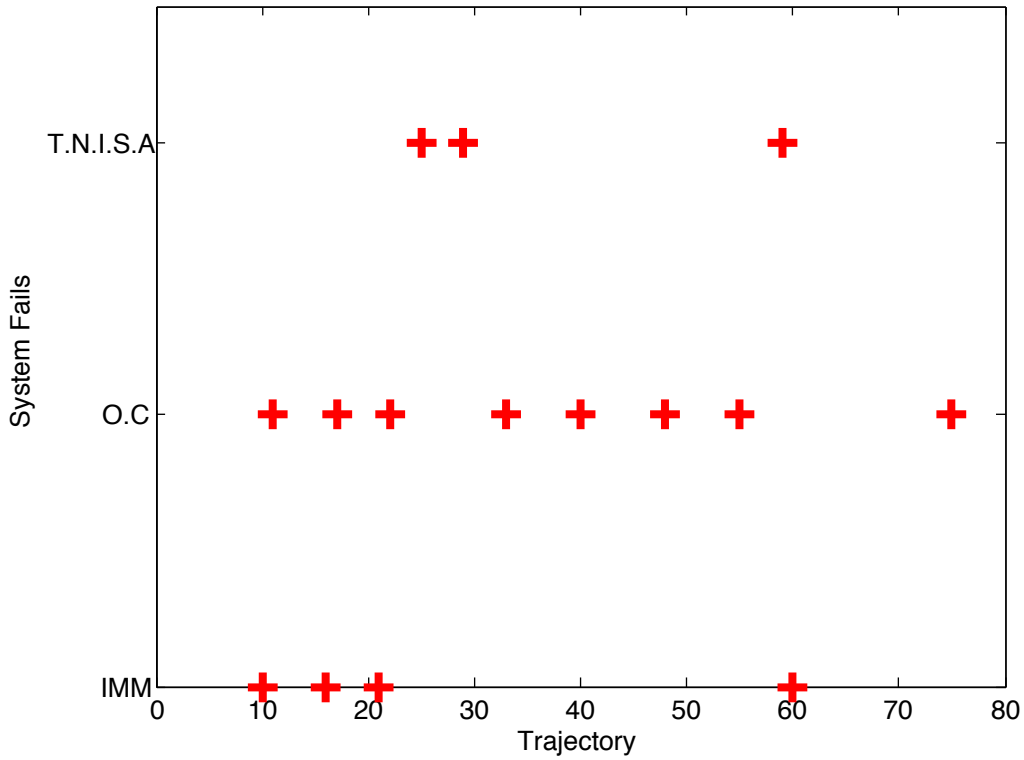

Figure 6.6: M.P.T System Component Fails

In only 3 of the failed engagements, the target was outside the scan area calculated on a correct predicted trajectory. In 8 of the engagements, the weapon had been overcommitted by considering only one possible trajectory. However the 65 successful interceptions would indicate that considering only one possible trajectory within an integrated fire control system is an effective approach to improving the performance of the weapon against manoeuvring targets.

6.6 Chapter Review

This chapter has discussed an integrated fire control system which will shape the trajectory of the weapon after launch only if a manoeuvre is detected by the IMM. The trajectory is shaped after launch considering only the most probable trajectory of the remaining distribution of possible target trajectories. An integrated system utilising this approach was shown to be effective against both non manoeuvring and manoeuvring targets.

Chapter 7

Integrated System Three - Simulated Annealing and Most Probable Trajectory (S.A.M.P.T)

This Chapter seeks to determine whether the performance of the AAAW against manoeuvring targets can be improved utilising a hybrid integrated fire control system. This system will utilise trajectory optimisation using simulated annealing and isolation of the most probable target trajectory. The theory of how both systems optimise the weapon trajectory has been discussed extensively in Chapters 5 and 6. The system will therefore be presented briefly considering the two phases of weapon initialisation and in-flight trajectory revision.

7.1 Weapon Initialisation

The initial trajectory of the weapon is calculated considering 4 off-boresight angles which will initially be assumed to be updated at T=0s, T=10s, T=20s and T=30s. The trajectory is calculated using the simulated annealing algorithm. The calculation of the initial trajectory therefore follows the same procedure as discussed in Section 5.8.

7.2 In-flight Trajectory Revision

The trajectory of the weapon will be revised using the simulated annealing and most probable trajectory algorithms. The use of either algorithm will depend on the number of manoeuvre detections and the time steps at which the detections occur.

7.2.1 In-flight Trajectory Revision 0 Manoeuvre Detections

If no manoeuvres are detected by the IMM, then the trajectory of the weapon will be revised using the simulated annealing algorithm at T=10s and T=20s. At T=30s the most probable trajectory will be isolated from the remaining distribution of possible target trajectories. The off-boresight command required to produce a detection along the isolated most probable trajectory will be calculated using the remaining absolute maximum heading change.

If a detection is found, the off-boresight command 4, determined at T=20s, will be updated and transmitted to the weapon. If no detection is obtained and the maximum heading change has been exhausted, off-boresight command 4 determined at T=20s will be transmitted to the weapon.

7.2.2 In-flight Trajectory Revision Manoeuvres Detected

The trajectory will be revised twice using simulated annealing and one or more times using the most probable trajectory approach. The final number of off-boresight commands used to shape the trajectory will be either 4 or 7.

If a detection occurs between 2 planned SA updates, the latter update will be brought forwards. For example, consider a manoeuvre detection which occurs at T=12.5s. This detection is between off-boresight command 2 at T=10s and off-boresight command 3 at T=20s. The trajectory revision at the latter time step (T=20s) would be completed using a simulated annealing optimisation process. The simulated annealing process performed at T=20s, would now be performed at T=12.5s. If no further manoeuvre detections are made, then the most trajectory approach will be used to fine tune the trajectory at T=30s provided no target detection is made by the seeker.

If further manoeuvre detections are made after the third trajectory revision has been completed using the simulated annealing algorithm, the trajectory will be revised using the most probable trajectory method for each subsequent detection. If no detection occurs between T=25s and T=30s, the trajectory will still be revised using the M.P.T approach at T=30s. If a detection occurs in this time interval, then the most probable trajectory approach will be used to revise the trajectory at the detection point. The data link will subsequently be deactivated.

7.3 Performance Evaluation

The simulated annealing and most probable trajectory (S.A.M.P.T) system was benchmarked against the 80 random target trajectories generated to assess the performance of the F.F, S.A.S.S and M.P.T systems. The results of the simulated engagements are provided in Figure 7.1.

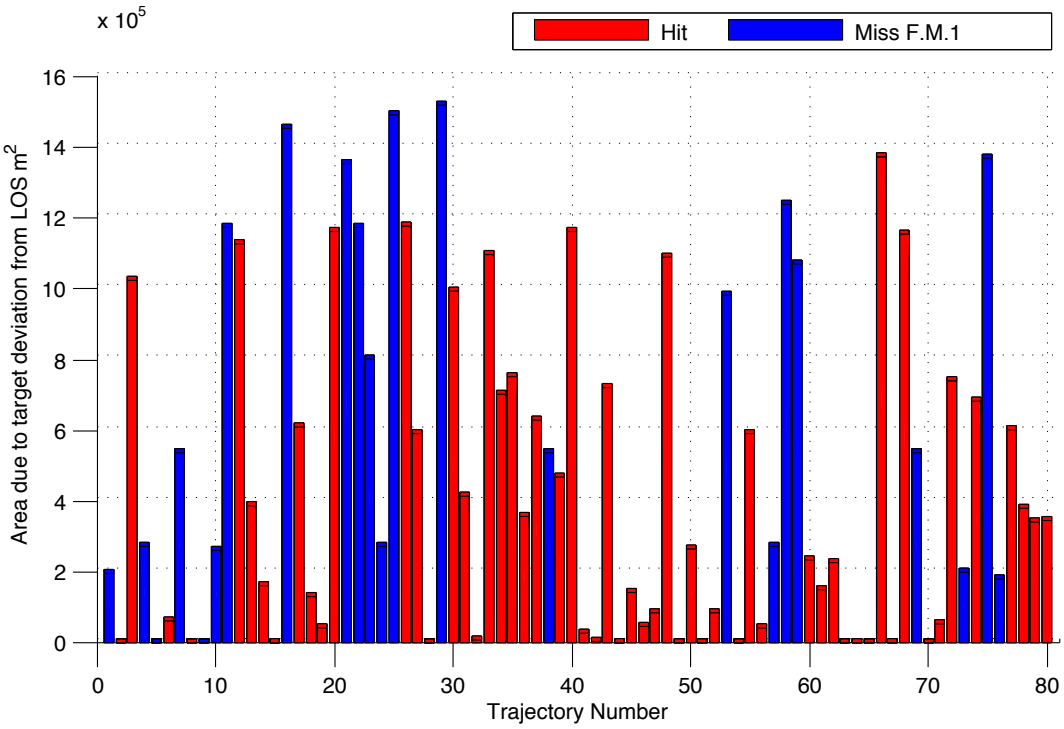

Figure 7.1: S.A.M.P.T results

Of the 80 simulated engagements, the weapon in the S.A.M.P.T system successfully intercepted 54 targets. The performance of the weapon in this system against, non-manoeuvring targets, targets which can be intercepted before manoeuvre (I.B.M) and manoeuvring targets (M.T) is shown alongside the F.F results in Table 7.1

System	N.M	I.B.M	M.T
S.A.M.PT	12/14	1/6	44/60
F.F	14/14	6/6	27/60

Table 7.1: S.A.M.P.T and F.F Results

Of the 44 manoeuvring target intercepts by the S.A.M.P.T system, 20 were also intercepted by the F.F system. Of the 16 failed manoeuvring target intercepts, 9 where missed by the weapon in both the F.F and S.A.M.P.T. The remaining 7

manoeuvring trajectories where intercepted by the weapon in the F.F system and missed using the S.A.M.P.T system. The results of the manoeuvring trajectory intercepts indicate that the performance of the AAAW within the S.A.M.P.T fire control system against manoeuvring attacks is substantially improved over the F.F system.

The calculation of the χ^2 value considering the manoeuvring trajectories, resulted in a probability of 0.002 which is below that of statistical significance. Therefore as in the cases of the other integrated systems, the results of the χ^2 test support the conclusion of superior performance against manoeuvring targets.

7.4 Failure Analysis

In each of the trials using the S.A.M.P.T system, the random trajectory used during the simulated annealing process of the S.A.S.S system was also utilised in the simulated annealing process of the S.A.M.P.T system. This is because the S.A.M.P.T was designed to determine whether using the M.P.T approach after the SA trajectory optimisation component was a superior method to either S.A.S.S or M.P.T. In the case of the 2 non-manoeuvring target fails, the IMM produced 0 false detections.

7.4.1 Non Manoeuvring Target Fails

The reasons why the weapon will have failed to produce an intercept in the case of two non manoeuvring targets are similar to those in the S.A.S.S. Considering the failure analysis provided in Section 5.11.1, the simulated annealing optimisation process would most likely have failed on one occasion. The weapon would then have flown a non optimal trajectory which took it away from the target.

At T=30s, the most probable trajectory process would have been triggered. However the system would not have been able to calculate a trajectory which would produce a detection along the most probable trajectory.

The system would have therefore defaulted to the trajectory calculated at T=20s. The scan area associated with the non optimal weapon trajectory would not have allowed the actual target to be detected at any scan time. Therefore the weapon will have failed to detect and intercept the target.

7.4.2 Manoeuvring Target Failure Analysis

Just as in the S.A.S.S system, out of the 5 I.B.M fails only in one engagement did the IMM produce an incorrect behaviour detection. In 2 of the 16 manoeuvring target fails, the IMM produced an incorrect behaviour detection. In the failed engagements where the IMM has not produced an incorrect behaviour detection, then the trajectory optimisation process using the simulated annealing and most probable trajectory approaches are the only possible system failure sources.

A failure by the most probable trajectory component can be excluded as the system will either find or not find a possible target detection based on the updated most probable trajectory. It will only update the weapon trajectory if a detection is found.

The reliability analysis of the simulated annealing algorithm performed in Chapter 5 would suggest that a failure by this algorithm will have only contributed to a small proportion of the failed intercepts. Assuming that the trajectory optimisation was successful on each occasion, then the failure will be simply due to the orientation of the seeker scan area to the target. The target will not have been detectable within the area, initially calculated on a distribution of possible trajectories and later on in the engagement a single probable trajectory.

The incorrect behaviour detections will affect the performance of the S.A.M.P.T system in the same manor as the S.A.S.S systems.

The incorrect detection will change the shape of the distribution and associated probabilities. Both the simulated annealing and most probable trajectory systems will then optimise the trajectory on a poor prediction which is far more likely to orientate the seeker scan area away from the target. In the failures where the IMM produced an incorrect detection, the trajectory of the weapon would have been shaped by both processes such that the target would not lie within the scan area. In each of the failed intercepts the S.A.M.P.T had successfully minimised the weapon range to the target to within the seeker detection range. Considering the fails without incorrect detections by the IMM, then this integrated system has been proven to be an effective method for improving the performance of the AAAW against manoeuvring targets.

7.5 Chapter Review

This chapter has the discussed the development and implementation of the third and final integrated fire control system to be discussed in this thesis. An integrated fire control system which considers multiple target trajectories initially and then only the most probable trajectory later on in the engagement is proven to be an effective method of improving the performance of the AAAW against manoeuvring targets. This is apparent from a comparison of the number of manoeuvring targets intercepted by the AAAW in this system and the F.F. system. However the weapon in this integrated system did not successfully intercept all of the 60 manoeuvring targets generated by the target model.

The potential reasons why the S.A.M.P.T system fails to intercept 2 non manoeuvring and a number of manoeuvring targets have been outlined. The results indicate that the hybrid system does not offer a further performance increase over the S.A.S.S system and M.P.T systems.

Chapter 8

Summary and Conclusions

This chapter firstly presents a summary of the research discussed in this thesis. A number of conclusions about the results obtained from the three systems developed are then provided. The thesis then concludes with recommendations for further work.

8.1 Summary

It was demonstrated that the addition of a data link to the AAAW will allow the trajectory of the weapon to be shaped in flight by the transmission of one or more off-boresight commands after the weapon has been launched. Each off-boresight command is comprised of the current weapon heading and a required heading change. The constraints of the original weapon design specified that the absolute sum of the heading changes associated with n transmitted off-boresight commands are limited to 40°.

It was proposed that the ability to shape the trajectory of the weapon after launch could improve the performance of the AAAW against manoeuvring targets, notably a small agile surface vessel which was representative of a small boat threat.

In order to achieve the maximum performance increase of the AAAW against manoeuvring targets, the limited retargeting (trajectory shaping) capability would have to be efficiently utilised over the course of a potential 40s engagement. It was postulated that this could be accomplished through the use of an integrated fire control system which would seek to calculate an optimal shaped weapon trajectory. A fundamental component of the integrated fire system would be an integrated tracking and target prediction system.

The tracking system was comprised of a pulsed radar model as the sensor input and a Kalman filter based IMM Estimator.

The prediction component calculates the possible trajectories that the target could follow over a maximum 40s weapon flight period. A Markov chain is used to calculate the probability of the target following each predicted trajectory.

The two components were integrated such that as the IMM detected different target behaviours, possible target trajectories could be eliminated. The distribution of target trajectories becomes a better prediction of the possible target behaviour as the engagement progresses.

Three integrated fire control systems where developed which, sought to calculate the optimal trajectory considering the distribution of possible target trajectories under different criteria.

In each of the three integrated systems, the AAAW demonstrated a substantial performance increase against manoeuvring targets in respect of the initial Fire and Forget system discussed in Chapter 3 of the thesis.

8.2 Overall Conclusions

It can be concluded that utilising an integrated fire control system will improve the average performance of a data linked AAAW against manoeuvring targets. The statistical analysis of the results of each system, consisting of a series of χ^2 tests, support this conclusion.

The results of the three integrated systems suggest that the M.P.T system offers the greatest performance increase. This is because, the AAAW in this system successfully intercepted the highest number of manoeuvring targets. However, considering only one possible trajectory can over commit the weapon to a particular detection location.

In theory, the S.A.S.S system should offer the greatest performance increase as the weapon trajectory is optimised, to allow the weapon to detect the target along more than one possible trajectory. The issue with the S.A.S.S system is that the simulated annealing process is computationally heavy, which for implementation in an operational system would potentially require a significant level of computing power to achieve real time trajectory calculation.

No further benefit was obtained in using a hybrid system when comparing the performance against the M.P.T and S.A.S.S systems.

Though the integrated systems presented in this thesis have been developed around the problem of an AAAW which is to intercept a small boat. The systems could be easily modified to consider other types of weapon and target, in particular the original data link demonstrator ePavewayII which is an INS/GPS guided weapon.

Instead of considering a seeker area, the reachable set of the bomb defined by the INS guidance would simply be considering in the trajectory optimisation process of each system.

8.3 Recommendations for Further Work

In each of the failed intercepts by all three integrated systems, the fire control system had successfully minimised the weapon range to target to within the seeker detection range. The failure was due to the orientation of the seeker to the target.

If this research is to be taken further, then the primary focus should be to determine whether the estimated target position and velocity obtained from the IMM can be integrated into the trajectory optimisation process. In such a way that, once the target is within the seeker detection range a final trajectory optimisation step can be used to steer the weapon onto the target.

Consideration should also be given to exploring different off-boresight update times as well as an increased number of off-boresight commands in the initial trajectory calculation of the S.A.S.S system. This will allow greater trajectory variation and may yield a more optimal weapon trajectory, further improving the performance of the AAAW in this system against manoeuvring targets.

It would also be worth exploring a method of recording the state of the integrated fire control system at each time step. This would allow a more in depth failure analysis to be conduced for each system, especially in the case of the S.A.S.S and S.A.M.P.T systems.

Appendix A

	Constant	α	β	δ_p	δ_q	δ_r	δ_x	α^2	β^2	δ_{p^2}	δ_{q^2}	δ_{r^2}	δ_{x^2}	$\dot{\alpha}$	$\dot{\beta}$	P	Q	R
C_D	C_{D_0}	0	0	0	0	0	0	0	0	$C_{D_{\delta_{P^2}}}$	$C_{D_{\delta_{q^2}}}$	$C_{D_{\delta_{r^2}}}$	$C_{D_{\delta_{x^2}}}$	0	0	0	0	0
C_Y	0	0	C_{Y_β}	0	0	$C_{Y_{\delta_r}}$	0	0	$C_{Y_{\beta^2}}$	0	0	0	0	0	0	0	0	0
C_L	0	C_{L_α}	0	0	$C_{L_{\delta_q}}$	0	0	$C_{L_{\alpha^2}}$	0	0	0	0	0	0	0	0	0	0
C_m	0	0	0	$C_{m_{\delta_p}}$	0	0	0	0	0	0	0	0	0	0	0	C_{m_P}	0	0
C_n	0	C_{n_α}	0	0	$C_{n_{\delta_q}}$	0	0	$C_{n_{\alpha^2}}$	0	0	0	0	0	$C_{n_{\dot{\alpha}}}$	0	0	C_{n_Q}	0
C_l	0	0	C_{l_β}	0	$C_{l_{\delta_q}}$	0	0	0	$C_{l_{\beta^2}}$	0	0	0	0	0	$C_{l_{\dot{\beta}}}$	0	0	C_{n_R}

Table 1 Aerodynamic Coefficients for AAAW model

Appendix B

Processor	Intel I7 CPU 87- @2.93GHz
Memory	16.0 GB
Graphics	NVIDIA GeForce GTS450
Hard drive SSD	120 GB
Operating System	Windows 8 64 Bit
Matlab Version	R 2011b

Appendix C

Appendix D

Bibliography

[1] Fritz X Guided Bomb. http://airandspace.si.edu/collections/artifact.cfm?id=A19710760000, April 2013.

[2] Rigby, K.A. *Aircraft Systems Integration of Air-Launched Weapons*. John Wiley and Sons, 2013.

[3] 'UK Apache, Storm Shadow strikes during Libyan operations detailed'. *Jane's defence weekley*, 48, November 2011.

[4] Seawolf vs Exocet-test detailed. http://www.flightglobal.com/pdfarchive/view/1983/1983%20-%202230.html, April 2013.

[5] Think Defence. The Brimstone Missile. http://www.thinkdefence.co.uk/2012/03/the-brimstone-missile/, April 2013.

[6] National Research Council (U.S) and Commitee on Network-Centric Naval Forces. *Network-Centric Naval Forces: A Transition Strategy for Enhancing Operational Capabilites*. National Academic Press, 2000.

[7] Office of Inspector General. 'Small Vessel Security Strategy'. Technical report, Department of Homeland Security, United States, April 2008.

[8] Raytheon Demonstrates Enhanced Paveway II Data Link Capability. http://investor.raytheon.com/phoenix.zhtml?c=84193&p=irol-newsArticle_print&ID=883205&highlight=, April 2013.

[9] Dual Mode Brimstone (DMB) and SPEAR (United Kingdom), Air-to-Surface missiles - Direct Attack. *Jane's Air-Launched Weapons*, August 2011.

[10] Chuter, A. 'MBDA Offers Brimestone Missile as the Answer to Swarm Boats'. *DefenceNews*, July 2012.

[11] Siouris, G.M. *Missile Guidance and Control Systems*. Springer, New York, 2004.

[12] 'UK changes JSF configuration for ASRAAM'. *Defense Security Intelligence and Analysis*, 2008.

[13] Gorecki, R.M. 'A Baseline 6 Degree of Freedom (DoF) Mathematical Model of a Generic Missile'. Technical report, Defence Science and Technology, 2003.

[14] Brochu, R and Lestage, R. 'Three degrees of freedom (DoF) missile trajectory simulation and comparative study with a high fidelity 6DoF model'. Technical Report 056, Deference R D Canada, 2003.

[15] Strickland, J. *Missile Flight Simulation*. Lulu Inc, 1st edition, 2011.

[16] Gurfil, P. and Hector, R. 'Partial Aircraft State Estimation from Visual Motion Using the Subspace Constraints Approach'. *Guidance Control and Dynamics*, 24(5):1016–1028, 2001.

[17] Talay, T.A. *Introduction to the Aerodynamics of Flight*. Scientific and Technical Information Office, National Aeronautics and Space Administration, Washington DC, 1975.

[18] Blakelock J.H. *Automatic Control of Aircraft and Missiles*. Wiley Interscience, 2nd edition, 1991.

[19] Freeman, E.L. *Tactical Missile Design*. American Institute of Aeronautics and Astronautics (AIAA), Reston VA, 2001.

[20] Stroud, K.A and Booth, J. *Advanced Engineering Mathematics*. Palgrave Macmillan, N.Y, 4th edition, 2003.

[21] Vesantera, P.J. and Celier, F.E. 'Building intelligence into an autopilot using qualitative simulation to support global decision making'. *Simulation*, 52(3):111–121, March 1989.

[22] US Navy Training Publications Center under direction of the Bureau of Naval Personnel. *Principles of Guided Missiles and Nuclear Weapons*. Bureau of Naval Personnel, 1959.

[23] USA Army. Grenades and Pyrotechnic Signals. `http://armypubs.army.mil/doctrine/DR_pubs/dr_a/pdf/fm3_23x30.pdf`, April 2013.

[24] Ward, T.A. *Aerospace Propulsion Systems*. John Wiley and Sons, Asia, 2010.

[25] Jerger, J.J. *Principles of Guided Missile Design*. Van Nostrand, Princeton, 1960.

[26] Filipoo, N. *Introduction to Electronic Defense Systems*. SciTech Publishing, USA, 2nd edition, 2006.

[27] Yanushevsky, R. . *Modern Missile Guidance*. CRC Press, Boca Raton, FL, 2008.

[28] Ralph, J.F and Davies, J. 'Semi-Active Guidance using Event Driven Tracking'. In *Proceedings of the 14th International Conference on Information Fusion*, Chicago, 2011.

[29] Novatel. UIMU-LN200. `http://www.novatel.com/assets/Documents/Papers/LN200.pdf`, April 2013.

[30] army technology.com. Brimestone Adavanced Anti-Armour Missile, United Kingdom. `http://www.army-technology.com/projects/brimstone/`, April 2013.

[31] armedforces.co.uk. The HOUSEHOLD CAVALRY ROYAL ARMOURED CORPS. `http://www.armedforces.co.uk/army/listings/l0024.html`, April 2013.

[32] Bar-Shalom, Y. and Li X.R and Kirubarjan T. *Estimation with Application to Tracking and Navigation Theory Algorithms and Software*. Wiley, Canada, 2001.

[33] Scott.R. MBDA targets Brimstone at anti-FIAC role. `http://www.janes.com/events/exhibitions/farnborough-2012/news/july-11/MBDA-targets-Brimstone-anti-FIAC-role.aspx`, April 2013.

[34] Office of Inspector General. 'dhs' strategy and plans to counter small vessel threats need improvement'. Technical Report OIC-09-100, Department of Homeland Security, Washington DC, 2009.

[35] Tiwari, A. 'Small Boat and Swarm Defence: A Gap Study'. Master's thesis, Naval Postgraduate School, September 2008.

[36] Royal navy. `www.royalnavy.mod.uk`, July 2012.

[37] J. Garamone. Small Boats Provide Links to Local Maritime Community. `http://www.defense.gov/News/NewsArticle.aspx?ID=15895`, April 2013.

[38] Chuch, R.R. and Lowe, A.W. *The Law of The Sea*. Manchester University Press, UK, 1983.

[39] Nee, T.W. and Nee, S.F. 'Shipboard Infrared Circular Polarization Sensor for Sea-Skimming Missile Detection'. Technical report, Naval Air Warfare Center Weapons Division, CA, December 1999.

[40] Skolnik, M. *Radar Handbook*. McGraw-Hill Professional, 3rd edition, March 2008.

[41] Kingsley, S. and Quegan, S. *Understanding Radar Systems*. McGraw-Hill, Europe, 1999.

[42] Richard, G. *Radar Essentials - A Concise Handbook for Radar Design and Performance Analysis*. SciTech Publishing, 2011.

[43] Baker, C.J and Trimmer, B.D. 'short-range-surveillance radar systems'. *Electronics and Communications Engineering*, pages 181–191, August 2000.

[44] Briggs, J. *Target Detection by Marine Radar*. IET, 2004.

[45] Raju, G.S.N. *Radar Engineering*. I.K.International Pvt Ltd, 2008.

[46] Lockheed Martin. System elements. `http://www.lockheedmartin.co.uk/us/products/aegis/system-elements.html`, April 2013.

[47] Welch G and Bishop G. 'Course 8 - An Introduction to the Kalman filter'. ACM SIGGRAPH 2001, California, August 2001.

[48] Simon, D. *Optimial State Estimation Kalman filter and Non Linear approaches*. Wiley, USA, 2006.

[49] Goldenstien, S. 'A Gentle Introduction to Predictive Filters. *Informatica Teorica e Aplicada (RITA)*, XI(1):61–89, October 2004.

[50] Mayback, P.S. *Stochastic Models, Estimation and Control*, volume 1. Academic Press Inc, 1979.

[51] Ralph. J.F. *Target Tracking in Encyclopedia of Aerospace Engineering, Dynamics and Control*, volume 5, chapter 251, pages 3017–3030. John Wiley and Sons, 2010.

[52] St-Pierre, M. 'Comparison between the unscented Kalman filter and the extended Kalman filter for the position estimation module of an integrated navigation information system'. In *IEEE Symposium on Intelligent Vehicles*, pages 831–835, Canada, 2004.

[53] Liu, C. 'Unscented extended Kalman filter for target tracking'. *Journal of Systems Engineering and Electronics*, 22, April 2011.

[54] Watson A. and Mihavlova, L. and Vorlev, D. 'Challenges with Bearings Only Tracking for Missile Guidance Systems and How to cope with them'. In *MCM-ITP Conference*, pages 63–71, Manchester UK, October 2010.

[55] Kalman R. E. 'A new approach to linear filtering and prediction problems. *Journal of Basic Engineering*, 82D:35–45, March 1960.

[56] Cheah L.H. Zainudin, Arsad H. H. 'Causal Relationship between Stock Price and Macroeconomic variables in Malaysia'. In *Proceedings of the 2nd IMT-GT Regional Conference on Mathematics Statistics and Applications*, number 2, pages 1–8, Universiti Sains Malaysia Penang, June 2006.

[57] Grewal, M.S. *Kalman Filtering Theory and Practice Using Matlab.* N.J. WILEY, 3rd edition, 2008.

[58] Gershenfeld N. *'The Nature of Mathematical Modelling'*, chapter 14. Cambridge Press, 1999.

[59] du Plessis R.M. 'Poor man's explantion of Kalman Filters or How I stopped worrying and learned to love matrix inversion'. Technical report, Rockwell International Technical Note (Taygeta Scientific Incorparated), 1997.

[60] Bar-Shalom, Y. and Blair W.D. *Multitarget-Multisensor Tracking: Applications and Advances*, volume 3. AIAA, Artech House, Boston, 2000.

[61] Bar-Shalom, Y. and Daum, F. and Hunag, J. 'The Probabilistic Data Association Filter : Estimation in the presence of measurement origin uncertainty', 2009.

[62] Ferrero, A. and Salicone, S. 'Decision Making in the Presence of Measurement Uncertainity: an Approach in Terms of the Theory of Evidence'. In *International Conference on Probabilistic Methods Applied to Power Systems*, pages 1–6, Stockholm, June 2006.

[63] McAulay, R.J and Denlinger, E.J. 'A decision-directed adaptive tracker. *IEEE Transactions on Aerospace and Electronic Systems*, AES-9:229–236, March 1973.

[64] Li, X.R. 'A Survey of Manuevering Target Tracking - Part IV: Decision-Based Methods'. In *Proccedings of SPIE Conference on Signal and Data Processing of Small Targets*, pages 4728–4760, Orlando FL, USA, April

2002. Proceedings of SPIE Conference on Signal and Data Processing of Small Targets.

[65] Farina A. and F.A Studer. *Radar Data Processing Vol. I : Introducion and Tracking Vol.II : Advanced Topics and Applications*. Research Studies Press, Letchworth Hertfordshire, England, 1985.

[66] Blackman, S.S. *Multiple Target Tracking with Radar Applications*. Artech House, Norwoord, MA, 1986.

[67] Bar-Shalom, Y. and Fortmann, F.E. *Tracking and Data Association*. Academic Press, New York, 1988.

[68] Blackman, S. and Popolo R. *Design and Analysis of Modern Tracking Systems*. Artech House, MA, 1999.

[69] Bogler, P.L. *Radar Principles with Applications to Tracking Systems*. Wiley, 1990.

[70] Li, X.R and Bar-Shalon Y. *Estimation and Tracking : Principles, Techniques and Software*. YBS Publishing, 1998.

[71] Bekir, E. 'Adaptive Kalman Filter for Tracking Maneuvering Targets'. *AIAA Journal of Guidance*, 6(5):414–416, September-October 1983.

[72] Woolfson, M.M. *Everyday Probability and Statistics : Health, Elections and War*. Imperial College Press, 2008.

[73] Cloutier, J.R. and Lin, C.F. and Yang, C. 'Maneuvering Target Tracking via Smoothing and Filtering Through Measurement Concatenation'. *AIAA Journal of Guidance, Control and Dynamics*, 16(2):377–384, March-April 1993.

[74] Koteswararo, S. and Arun, A. and Neelima, P. 'Application of Kalman Filter and Input Estimation for Underwater Target Tracking'. In *Intelligent Sensing and Information Processing 2005, Proceedings of 2005 International Conference on*, pages 100–103, India, January 2005.

[75] Young, H.P and Seo, J.H and LEE, J.G. 'Tracking using the variable dimension filter with input estimation'. *IEEE Transactions on Aerospace and Electronic Systems*, 31(1):399–408, 1995.

[76] Farooq, M. Comments on "Tracking a maneuevering target using input estimation". *IEEE Transactions on Aerospace and Electronic Systems*, 25:300–302, March 1989.

[77] Slocumb, B.J. and West, P.D. and Shirley, T.N and Kamen, E.W. 'Tracking a maneuvering target in the presence of false returns and ECM using a variable state dimension Kalman filter'. In *Proceedings of the American Control Conference*, volume 4, pages 2611–2615, Seattle W.A, June 1995.

[78] Bar-Shalom, Y. 'Variable dimension filter for manuevering target tracking'. *IEEE Transactions on Aerospace and Electronic Systems*, AES-18:621–629, September 1982.

[79] A. Munir. 'Maneuvring target tracking using different turn rate models in the interacting multiple model algorithm'. In *Proceedings of the 34th IEEE Conference on Decision and Control*, volume 3, pages 2747–3751, New Orleans, LA, December 1995.

[80] Arulampalam, M.S. and Gordon, N. and Orton, M. and Ristic, B. 'A variable structure multiple model particle filter for GMTI tracking'. In *Proceedings of the 2002 International Conference on Information Fusion*, volume 2, pages 927–934, Annapolis, MD, USA, July 2002.

[81] Averbuch, A. and Itzikowitz, S. and Kapon, T. 'Parallel implementation of multiple model model tracking algorithms'. *IEEE Transactions on Parallel and Distributed Systems*, 2(2):242–252, April 1991.

[82] Berketis, K. and Katsikas, S.K. and Likothanassis, S.D. 'Multimodel partitioning filters and genetic algorithms'. *Nonlinear Analysis, Theory, Methods and Applications*, 30(4):2421–2427, 1997.

[83] Blackman, S. and Busch, S. and Popoli, R.F. 'IMM/MHT tracking and data association for benchmark tracking problem'. In *Proceedings of the 1995 American Control Conference*, volume 4, pages 2606–2610, Seattle W.A, June 1995.

[84] Blair, W.D and Watson, G.A. 'IMM algorithm for solution to benchmark problem for tracking maneuvering targets'. In *Proceedings of the SPIE Symposium on Acquistion,Tracking and Pointing*, volume 2221, pages 476–488, Orlando FL, USA, 1994.

[85] Busch, M. and Blackman, S. 'Evaluation of IMM filtering for an air defence system application'. In *Proceedings of the 1995 SPIE Conference on Signal and Data Processing of small targets*, volume 2561, pages 435–447, San Diego, CA, July 1995.

[86] Driessen, J.N and Boers, Y. 'A multiple model multiple hypothesis filter for tracking maneuvering targets'. In *Proceedings of the 2001 SPIE Conference on Signal and Data Processing of Small Targets*, volume 4473, pages 279–288, California, 2001.

[87] Hutchins, R.G and San Jose, A. 'IMM Tracking of a theater ballistic missile during boost phase'. In *Proceedings of 1998 SPIE Conference on Signal and Data Processing of Small Targets*, volume 3373, pages 528–531, Orlando FL, USA, April 1998.

[88] Kameda H and Tsujimichi, S. and Kosuge, Y. 'Target tracking for maneuvering reentry vehicles using multiple maneuvering models'. In *Proceedings of the 36th SICE (Society of Instrument and Control Engineers) Annual Conference*, pages 1031–1036, Japan, July 1997.

[89] LI, X.R. 'Multiple-model estimation with variable structure: Some theoretical considerations'. In *Proceedings of the 33rd IEEE Conference on Decision and Control*, volume 2, pages 1194–1204, Orlando FL, USA, December 1994.

[90] Li, X.R. 'Multiple-model estimation with variable structure -Part II: Model-set adaption'. *IEEE Transactions on Automatic Control*, 45(11):2047–2060, November 2000.

[91] Sworder, D. and Boyd, J. 'Enhanced multiple model algorithms'. *Automatica*, 2000.

[92] Watson, G.A and Blair, W.D. 'Tracking targets with multiple sensors using the interacting multiple model algorithm'. In *Proceedings of the 1993 SPIE Conference on Signal and Data Processing of Small Targets*, Orlando FL, USA, April 1993.

[93] WU. W. and Cheng, P. 'A nonlinear IMM algorithm for maneuvering target tracking. *IEEE Transactions on Aerospace and Electronic Systems*, 30(3):875–885, July 1994.

[94] Blom, H.A.P and Bar-Shalom, Y. 'The Interacting Multiple Model Algorithm for Systems With Markovian Switching Coefficients'. *IEEE Transactions on Automatic Control*, AC-33:780–783, August 1988.

[95] Li, X.R and Jilkov, V.P. 'Survey of maneuvering target tracking. Part V Multiple Model Methods'. *IEEE Transactions on Aerospace and Electronic Systems*, 41(4):1255–1321, April 2005.

[96] Davies J, and Ralph, J. and Oxtoby, N. 'Tracking System to Maximize the Engagement Envelope of a Data Linked Weapon'. In *Proceedings of SPIE Conference, Signal Processing, Sensor Fusion and Target Recognition XX*, volume 8050, Orlando FL, USA, April 2011.

[97] Crassidis, J. and Junkins, J. *Optimal Estimation of Dynamic Systems*. CRC Press, 2 edition, 2011.

[98] I.Simeonova. and T.Semerdjiev. 'About the Specifics of IMM Algorithm Design'. In *Proceeding NMA '02 Revised Papers from the 5th International Conference on Numerical Methods and Applications'*, pages 333–341, 2002.

[99] X.R. Li. 'Survey of maneuvering target tracking. Part I. Dynamic models'. *IEEE Transactions on Aerospace and Electronic Systems*, 39:1333–1364, October 2003.

[100] Challa, S. and Morelande M. and Musicki, D. and Evans,R. *Fundamentals of Object Tracking*. Cambridge University Press, 2011.

[101] Lerro, D. and Bar-Shalom, Y. 'Tracking with Debiased Consistent Converted Measurements Vs EKF'. *IEEE Transactions on Aerospace and Electronic Systems*, 29(3):1015–1022, July 1993.

[102] Farina, A. and Benvenuti, D. and Ristic, B. 'Estimation accuaracy of a landing point of a ballistic target'. In *Proceedings of the Fifth International Conference on Information Fusion*, volume 1, pages 2–9, Maryland, USA, 2002.

[103] Green, D.M and Swets, J.A. *Signal detection theory and psychophysics*. John Wiley and Sons, 1966.

[104] Boyd, S.P. and Vandenberghe, L. *Convex Optimisation*. Cambridge University Press, Cambridge, 2004.

[105] Geem, Z.W. and Kim, J.H and Loganathan, G.V. 'A new heuristic optimization: Harmony search'. *Simulation*, 76:60–68, 2001.

[106] Kennedy, J. and Eberhart, R.C. 'Particle swarm optimization'. In *Proceedings of the IEEE International Conference on Neural Networks*, volume 6, pages 1942–1948, Piscataway NJ, November 1995.

[107] Slawomir, K. and Yang, X.S. *Computational Optimization, Methods and Algorithms*. Springer, 2011.

[108] Yang X.S and Koziel S. *Computational Optimization and Applications in Engineering and Industry*. Springer, 2011.

[109] Carroll T.B and Linton R.F. *Computational Optimization : New Research Developments*. Nova Science Publishers, 2010.

[110] Cox, M.G and Forbes, A.B. and Harris, P.M. 'Discrete Modelling, SSFM Best Practice Guide'. Technical Report 4, National Physical Laboratory, UK, 2002.

[111] Matthews, C. and Wright, L. and Yang, X.S. 'Senstivity Analysis, Optimization and Sampling Methods Applied to Continous Models'. Technical report, National Physical Laboratory, UK, 2009.

[112] Chong, E.K.P and Zak, S.H. *An Introduction To Optimization*. Wiley Interscience, USA, 2001.

[113] Hooke, R. and Jeeves, T.A. 'Direct search solution of numerical and statisitical problems'. *J.Assoc.Comput*, 8:212–229, 1961.

[114] Kirkpatrick, S. and Gelatt, C.D and Veechi, M.P. 'Optimization by Simulated Annealing'. *Science*, 220(4598):671–680, 1983.

[115] Metropolis, N. and Rosenbluth, A.W and Rosenbluth, M.N and Teller, A.H and Teller, E. 'Equation of State Calculation by Fast Computing Machines'. *J.of Chem. Phys*, 21, 1953.

[116] De Jong, K.A. *'An Analysis of the Behavour of a Class of Genetic Adaptive Systems'*. PhD thesis, University of Michigan, 1975.

[117] Digalakis, J.G and Margaritis, G. 'AN EXPERIMENTAL STUDY OF BENCHMARKING FUNCTIONS FOR GENETIC ALGORITHMS. *International Journal of Computer Mathematics*, 79(4):403–416, 2002.

[118] Mann, J.W and Smith, G.D. *Modern Heuristic Search Methods*. John Wiley and Sons, 1996.